

SEISMIC RESPONSE OF TELECOMMUNICATIONS EQUIPMENT  
SUPPORTED ON ACCESS FLOORS

by

CHI MING WONG

A Thesis

Submitted to the School of Graduate Studies  
in Partial Fulfilment of the Requirements  
for the Degree  
Doctor of Philosophy

McMaster University

April 1990

© Copyright by Chi Ming Wong, 1990

**SEISMIC RESPONSE OF TELECOMMUNICATIONS EQUIPMENT  
SUPPORTED ON ACCESS FLOORS**

DOCTOR OF PHILOSOPHY (1990)  
(Civil Engineering and Engineering Mechanics)

McMASTER UNIVERSITY  
Hamilton, Ontario

TITLE: Seismic Response of Telecommunications Equipment  
Supported on Access Floors

AUTHOR: Chi Ming Wong, B.A.SC. (University of Toronto)  
M.Eng. (McMaster University)

SUPERVISOR: Professor W.K. Tso

NUMBER OF PAGES: xxii, 194

## ABSTRACT

Access floor systems have been widely used to support equipment in telecommunications central offices. In this thesis, the seismic response of equipment supported on access floors in telecommunications central offices is studied. There are two major issues for equipment supported on access floor under seismic condition. First, the access floor tends to amplify the motions from the building floor; as a result, the equipment supported on it is subjected to a more severe shaking than if it were supported directly on a building floor. Second, most access floor systems are designed for gravity load only. Their seismic performance depends on their lateral stiffness and strength. Such information is not generally available. The objective of the study is to address the first issue and to provide guidelines for the seismic analysis, design and qualification of equipment installed on access floors. This is achieved by a systematic study on the dynamic response of combined equipment-access floor systems by experimental and analytical approaches.

The experimental work is carried out using commercial access floors of two different floor heights and a typical switching equipment unit commonly used in telecommunications central offices as test specimens. There are three phases involved in the experimental work. First, static tests are performed to investigate the stiffness and strength properties of the access floors. Second, dynamic exploratory

tests are carried out to study the dynamic characteristics of the access floors, the telecommunications equipment and the combined equipment-access floor systems. Lastly, seismic tests are performed for the equipment alone and the combined equipment-access floor systems to evaluate the effect of the access floor on the seismic response of the equipment.

Based on the observations and results of the experiment, an analytical model is developed. The reliability of the model to predict the dynamic properties and the seismic response of combined equipment-access floor systems is checked by experimental results. A parametric study is then carried out using this model to provide insight into the dynamic properties of equipment-access floor systems. The model is also used to study the seismic response of equipment supported on access floors in telecommunications central offices. Finally, design spectra for telecommunications equipment supported on access floors are generated for the purposes of seismic analysis, design and qualification.

## ACKNOWLEDGEMENT

I wish to expressed my gratitude to my research supervisor, Professor W.K. Tso, for his guidance, encouragement and friendship throughout the course of my graduate study. I am grateful to his dedication and the countless number of hours that he spent with me on this research. His ability to discern the essential points of complex problems was of great value to this research. It has been a great privilege and pleasure for me to be his student.

I am indebted to my supervisor committee members, Professors A. Ghobarah, D.S. Weaver, and J.C. Wilson for their valuable comments and suggestions on my research and also their time in reviewing this thesis.

The help of Dr. N. Naumoski in processing the experiment data, his encouragement and friendship are greatly appreciated. The ADL technicians, Dave Parrett who assisted me in the experiment, Peter Koudys and Ross McAndrew who fabricated the testing fixtures, deserve much credit to the success of the experiment. I am thankful to my fellow student T.J. Zhu for his friendship and his time in discussing with me the problems I encountered in this research.

The generosity of DONN Canada Ltd. in providing the test specimens for this research is greatly appreciated. Thanks are also due to Paul Farrauto, Graeme Gee and Mits Sumiya of Donn Canada Ltd. and Steven Cline of USG Interiors, Inc. for their help in arranging the delivery of the test specimens. Their co-operation, comments and suggestions have been

valuable toward this research. I also wish to thank Rich McDonald of Bell-Northern Research for providing the telecommunications equipment frame and for permitting the publication of the test data.

I wish to acknowledge the NSERC and McMaster University for awarding me scholarships and teaching assistantship to support my graduate study.

My mother and my late father have steadfastly guided, nurtured, loved and supported me. It is through their examples that I become truly educated and taught the meaning of humanity. I am thankful to my two wonderful sisters, Monica and Chris who have brought much happiness to my life. I am also grateful to my friends in Toronto Chinese Baptist Church who have given me constant support and encouragement throughout the years of my graduate study.

Finally, I am grateful to my wife Ruth who has shared the ups and downs with me and has supported me without any reservation during the course of my graduate study. Her understanding, companionship and help were essential for the completion of this thesis. I dedicate this thesis to her with my love and devotion.

## TABLE OF CONTENTS

	<u>PAGE</u>
ABSTRACT . . . . .	iv
ACKNOWLEDGEMENT . . . . .	vi
TABLE OF CONTENTS . . . . .	viii
LIST OF TABLES . . . . .	xii
LIST OF FIGURES . . . . .	xiv
LIST OF SYMBOLS . . . . .	xx
CHAPTER 1 INTRODUCTION . . . . .	1
1.1 Background . . . . .	1
1.2 Review of Pertinent Work . . . . .	3
1.3 Objectives and Scope . . . . .	6
CHAPTER 2 STATIC TESTS . . . . .	9
2.1 Description of Access Floor systems . . . . .	9
2.2 Experimental Setup and Procedures for Static Tests . . . . .	10
2.3 Observations and Results . . . . .	12
2.4 Summary . . . . .	13
CHAPTER 3 EXPLORATORY TESTS . . . . .	20
3.1 Introduction . . . . .	20
3.2 Test Preliminaries . . . . .	20
3.2.1 Shake Table Testing Facilities . . . . .	21
3.2.2 Selection of Testing Method . . . . .	22

**Table of Contents (cont'd)**

3.2.3	Principles of Random Excitation Testing Technique . . . . .	23
3.2.4	Generation of Random Excitation Time History . . . . .	25
3.2.5	Determination of Dynamic Properties from Transfer functions . . . . .	26
3.3	Determination of the Dynamic Properties of the Access Floor Systems . . . . .	28
3.3.1	Experimental Setup and procedures . . . . .	29
3.3.2	Observations and Results . . . . .	30
3.3.3	Comparison of Experimental and Analytical Results . . . . .	32
3.4	Determination of the Dynamic Properties of the Equipment . . . . .	34
3.4.1	Experimental Setup and procedures . . . . .	35
3.4.2	Observations and Results . . . . .	36
3.5	Determination of the Dynamic Properties of the Combined Equipment-access Floor Systems . . . . .	39
3.5.1	Experimental Setup and procedures . . . . .	39
3.5.2	Observations and Results . . . . .	42
3.6	Summary and Conclusions . . . . .	45
CHAPTER 4	SEISMIC TESTS . . . . .	79
4.1	Introduction . . . . .	79
4.2	Excitation Time History . . . . .	79
4.3	Seismic Tests of the Equipment Supported on a Concrete Slab . . . . .	82
4.3.1	Experimental Setup . . . . .	82
4.3.2	Observations and Results . . . . .	83
4.4	Seismic Tests of the Equipment Supported on Access Floors . . . . .	86

Table of Contents (cont'd)

	4.4.1 Experimental Setup . . . . .	86
	4.4.2 Observation and Results . . . . .	87
	4.4.2.1 Equipment on D12 Access Floor . . . . .	88
	4.4.2.2 Equipment on D20 Access Floor . . . . .	93
	4.4.3 Comparison of the Seismic Responses of the Equipment on a Concrete Slab and on Access Floors . . . . .	94
	4.4.4 Ultimate Behaviour of the Equipment-access Floor Systems Subjected to NEBS Excitation . . . . .	95
	4.5 Summary and Conclusions . . . . .	98
CHAPTER 5	ANALYTICAL MODEL FOR EQUIPMENT-ACCESS FLOOR SYSTEMS . . . . .	132
	5.1 Introduction . . . . .	132
	5.2 Development of the Analytical Model . . . . .	132
	5.3 Equations of Motion . . . . .	134
	5.4 Undamped Free Vibration Response . . . . .	136
	5.5 Parametric Study . . . . .	138
	5.6 Comparison of Analytical and Experimental Results . . . . .	144
	5.7 Summary and Conclusions . . . . .	149
CHAPTER 6	CONSTRUCTION OF ACCESS FLOOR RESPONSE SPECTRA FOR EQUIPMENT IN TELECOMMUNICATIONS CENTRAL OFFICES . . . . .	163
	6.1 Introduction . . . . .	163
	6.2 Selection of Parameter Ranges . . . . .	163
	6.3 Parametric Study for the Seismic Response of Equipment Supported on Access Floors . . . . .	165
	6.4 Access Floor Response Spectra for Equipment in Telecommunications Central Offices . . . . .	170
	6.6 Summary and Conclusions . . . . .	173
CHAPTER 7	CONCLUSIONS . . . . .	187

**Table of Contents (cont'd)**

APPENDIX I . . . . .	190
APPENDIX II . . . . .	191
REFERENCES . . . . .	193

## List of Tables

<u>Table</u>		<u>Page</u>
2.1	Static tests results	14
3.1	Access floor configurations for random excitation tests	47
3.2	Resonant frequencies and damping ratios for various access floor configurations	48
3.3	Comparison between experimental and analytically predicted resonant frequencies: a.) D12 access floor and b.) D20 access floor	49
3.4	Equipment frequencies and damping ratios	50
3.5	Equipment mode shapes: a.) side-to-side and b.) back-to-front	50
3.6	Frequencies and damping ratios computed from transfer functions obtained at different locations on the equipment	51
3.7	Nomenclature for combined equipment-access floor test setups	51
3.8	Resonant frequencies and damping ratios for equipment on D20 access floor	52
3.9	Mode shapes for D20SS-B test setup, equipment side-to-side on D20 floor system with bolted panels: a.) first mode and b.) second mode	52
3.10	Mode shapes for D20BF-B test setup, equipment back-to-front on D20 floor system with bolted panels: a.) first mode and b.) second mode	53
3.11	Resonant frequencies and damping ratios for equipment on D12 access floor	54
4.1	Maximum response values for equipment in back-to-front orientation under different levels of NEBS excitation	100

List of Tables (cont'd)

<u>Table</u>		<u>Page</u>
4.2	Maximum response values for equipment in side-to-side orientation under different levels of NEBS excitation	100
4.3	Test configurations for equipment-access floor systems	100
4.4	Maximum response values for D12SS tests, a.) acceleration and b.) displacement	101
4.5	Maximum response values for D12BF tests, a.) acceleration and b.) displacement	101
5.1	Model parameters for the various equipment-access floor systems tested	151
5.2	Experimental and theoretical modal frequencies and mode shapes	151

## List of Figures

<u>Figure</u>		<u>Page</u>
1.1	Typical telecommunications network distribution configuration	8
1.2	Typical access floor	8
2.1	Access floor used in this study	15
2.2	Static test set up	16
2.3	Anchorage arrangement for pedestals	17
2.4	Load train and instrumentation for static test	18
2.5	Access floor load-deflection curves: a.) D12 access floor b.) D20 access floor	19
3.1	Single input and single output system	55
3.2	Band-passed filter for the random acceleration time history	55
3.3	Fourier spectra of random acceleration measured on the shake table	56
3.4	Re[H(f)] for different damping ratios	57
3.5	A typical setup of a 3 panel by 3 panel access floor on shake table	58
3.6	Instrumentation for a 3 panel by 3 panel access floor test setup	59
3.7	Transfer function for D12-11M test setup	60
3.8	Resonant frequencies obtained for various access floor configuration: a.) D12 access floor and b.) D20 access floor	61
3.9	Damping ratios obtained for various access floor configuration, a.) D12 access floor and b.) D20 access floor	62

List of Figures (cont'd)

<u>Figure</u>	<u>Page</u>
3.10 Correlation between experimental and analytically predicted resonant frequencies: a.) D12 access floor and b.) D20 access floor	63
3.11 Simulated equipment used in this study	64
3.12 Added mass distribution for the simulated equipment	65
3.13 Equipment anchor locations	66
3.14 Locations of accelerometers on equipment	67
3.15 Transfer function obtained for equipment in SS orientation on slab under a 2.5% span random excitation	68
3.16 Dynamic characteristics of equipment: a.) frequencies and b.) damping ratios	69
3.17 Equipment mode shapes	70
3.18 Experimental setup for equipment on access floor	71
3.19 Through-bolt equipment mounting arrangement	72
3.20 Equipment layout on access floor	73
3.21 Transfer function for the D20SS-B equipment-access floor system under a 2.5% span random excitation	74
3.22 Mode shapes for equipment on D20 floor system with bolted panels: a.) side-to-side and b.) back-to-front	75
3.23 Modal frequencies for equipment on D12 access floor: a.) first mode and b.) second mode	76
3.24 Modal damping ratios for equipment on D12 access floor: a.) first mode and b.) second mode	77
3.25 Mode shapes for equipment on D12 access floor with bolted panels: a.) side-to-side and b.) back-to-front	78
4.1 NEBS spectra criteria (after Bell Communications Research)	102
4.2 Excitation time histories compatible with the NEBS 2% damped spectrum: a.) acceleration and b.) displacement	103

List of Figures (cont'd)

<u>Figure</u>		<u>Page</u>
4.3	2% damped response spectra computed for accelerograms recorded for shake table motions of different levels of NEBS excitation	104
4.4	Instrumentation for equipment on concrete slab	105
4.5	Time histories for equipment in back-to-front orientation under full NEBS excitation	106
4.6	2% damped response spectra for acceleration time histories obtained for equipment in back-to-front orientation under full NEBS excitation	107
4.7	Time histories for equipment in side-to-side orientation under full NEBS excitation	108
4.8	2% damped response spectra for acceleration time histories obtained for equipment in side-to-side orientation under full NEBS excitation	109
4.9	Seismic test instrumentation for equipment on access floor	110
4.10	Acceleration time histories for D12SS50 test (equipment side-to-side, D12 drop-in panels and 50% NEBS excitation)	111
4.11	Acceleration time histories for D12SS50B test (equipment side-to-side, D12 bolted panels and 50% NEBS excitation)	112
4.12	Displacement time histories for D12SS50 test (equipment side-to-side, D12 drop-in panels and 50% NEBS excitation)	113
4.13	Displacement time histories for D12SS50B test (equipment side-to-side, D12 bolted panels and 50% NEBS excitation)	114
4.14	2% damped acceleration response spectra for D12SS50 test (equipment side-to-side, D12 drop-in panels and 50% NEBS excitation)	115
4.15	2% damped acceleration response spectra for D12SS50B test (equipment side-to-side, D12 bolted panels and 50% NEBS excitation)	115

## List of Figures (cont'd)

<u>Figure</u>		<u>Page</u>
4.16	Acceleration time histories for D12BF50 test (equipment back-to-front, D12 drop-in panels and 50% NEBS excitation)	116
4.17	Acceleration time histories for D12BF50B test (equipment back-to-front, D12 bolted panels and 50% NEBS excitation)	117
4.18	Displacement time histories for D12BF50 test (equipment back-to-front, D12 drop-in panels and 50% NEBS excitation)	118
4.19	Displacement time histories for D12BF50B test (equipment back-to-front, D12 bolted panels and 50% NEBS excitation)	119
4.20	2% damped acceleration response spectra for D12BF50 test (equipment back-to-front, D12 drop-in panels and 50% NEBS excitation)	120
4.21	2% damped acceleration response spectra for D12BF50B test (equipment back-to-front, D12 bolted panels and 50% NEBS excitation)	120
4.22	Acceleration time histories for D20SS25B test (equipment side-to-side, D20 bolted panels and 25% NEBS excitation)	121
4.23	Displacement time histories for D20SS25B test (equipment side-to-side, D20 drop-in panels and 25% NEBS excitation)	122
4.24	2% damped acceleration response spectra for D20SS25B test (equipment side to side, D20 bolted panels and 25% NEBS excitation)	123
4.25	Acceleration response time histories for equipment in side-to-side orientation supported on slab, D12 and D20 access floor, 25% NEBS excitation	124
4.26	Displacement response time histories for equipment in side-to-side orientation supported on slab, D12 and D20 access floor, 25% NEBS excitation	125
4.27	Acceleration time histories for D12BF100B test (equipment back-to-front, D12 bolted panels and 100% NEBS excitation)	126

## List of Figures (cont'd)

<u>Figure</u>		<u>Page</u>
4.28	Displacement time histories for D12BF100B test (equipment back-to-front, D12 bolted panels and 100% NEBS excitation)	127
4.29	Correlation between dynamic and static load-deflection behaviour for D12 access floor, equipment back-to-front	128
4.30	Acceleration time histories for D20SS50B test (equipment side-to-side, D20 bolted panels and 50% NEBS excitation)	129
4.31	Displacement time histories for D20SS50B test (equipment side-to-side, D20 drop-in panels and 50% NEBS excitation)	130
4.32	Correlation between dynamic and static load-deflection behaviour for D20 access floor, equipment side-to-side	131
5.1	Analytical model for the combined equipment-access floor system	153
5.2	Typical telecommunications equipment framework	154
5.3	Typical vibrational shapes for equipment in a side-to-side orientation	154
5.4	Modal frequencies ratios for equipment-access floor systems with different equipment shape functions: a.) $\mu=0.9$ and b.) $\mu=0.1$	155
5.5	Mode shapes for equipment-access floor systems with different equipment shape function: a.) $\mu=0.9$ and b.) $\mu=0.1$	156
5.6	Modal frequencies ratios for equipment-access floor systems with different mass ratios	157
5.7	Mode shapes for equipment-access floor systems with different mass ratios	158
5.8	Experimental and theoretical acceleration response time histories for D20SS10B test	159
5.9	Experimental and theoretical response spectra for D20SS10B test: a.) equipment top acceleration and b.) access floor acceleration	160

## List of Figures (cont'd)

<u>Figure</u>		<u>Page</u>
5.10	Experimental and theoretical acceleration response time histories for D12SS25B test	161
5.11	Experimental and theoretical response spectra for D12SS25B test	162
6.1	Equipment floor plan in typical telecommunications central offices	175
6.2	Two typical telecommunications equipment lineup arrangements and their equipment tributary area	176
6.3	Artificially generated NEBS 2% damped spectrum compatible acceleration time history	177
6.4	Ensemble average 2% damped response spectrum for the artificially generated time histories	178
6.5	Ensemble average 2% damped access floor response spectrum, $\mu=0.8$ , $\omega_f=6\text{Hz}$ and $\xi_f=2\%$	179
6.6	Ensemble average 2% damped access floor response spectra for different mass ratios, $\xi_f=2\%$ : a.) $\omega_f=3\text{Hz}$ and b.) $\omega_f=9\text{Hz}$	180
6.7	Ensemble average 2% damped access floor response spectra for different access floor damping ratios, $\xi_c=2\%$ : a.) $\omega_f=3\text{Hz}$ , b.) $\omega_f=9\text{Hz}$ and c.) $\omega_f=12\text{Hz}$	181
6.8	Ensemble average 2% damped access floor response spectra for different effective floor frequencies, $\xi_f=2\%$ and $\mu=0.8$	182
6.9	Average and average plus one standard deviation spectral envelopes, $\xi_f=2\%$ and $\mu=0.8$	183
6.10	Upper bound design spectra for equipment on access floor in telecommunications central offices	184
6.11	Access floor amplification curves for different equipment damping ratios: a.) $\omega_f=6\text{Hz}$ , b.) $\omega_f=9\text{Hz}$ , c.) $\omega_f=12\text{Hz}$ and d.) $\omega_f=15\text{Hz}$	185
6.12	Straight line approximation of amplification curves for different effective floor frequencies	186

## LIST OF SYMBOLS

$a_f$	Access floor amplification factor
$C_f$	Access floor damping constant
$C^{\dagger}$	Generalized damping of Equipment
[C]	Damping matrix for equipment-access floor system
$f$	Frequency
$f_n$	Natural frequency
$f_1, f_r$	Frequencies at the peaks of the real part of the transfer function between the absolute acceleration response and the excitation acceleration of a linear system
$g$	Acceleration due to gravity
$G_{xx}$	Input power spectrum
$G_{xy}$	Cross spectrum between input and output
$\hat{G}_{xx}$	Estimate of $G_{xx}$
$\hat{G}_{xy}$	Estimate of $G_{xy}$
$H(f)$	Transfer function
$H_a(f)$	Transfer function between absolute acceleration response and excitation acceleration
$H_r(f)$	Transfer function between relative acceleration response and excitation acceleration
$K_f$	Access floor stiffness
$K^{\dagger}$	Generalized stiffness of equipment
[K]	Stiffness matrix for equipment-access floor system
$g$	Self-adjoint linear operator

List of Symbols (cont'd)

L	Height of equipment
$m(x)$	Mass of equipment per unit length
$M_t$	Total mass of equipment-access floor system
$M_e$	Mass of equipment
$M_f$	Mass of access floor
$M^{\dagger}$	Generalized mass of equipment
[M]	Mass matrix for equipment-access floor system
$S_1, S_1^{\dagger}$	First mode equipment-access floor system mode shape coordinate
$S_2, S_2^{\dagger}$	Second mode equipment-access floor system mode shape coordinate
t	time
$u_e$	Equipment top displacement
$u_f$	Access floor displacement
{u}	Displacement vector for equipment-access floor system
{u}	Velocity vector for equipment-access floor system
{ü}	Acceleration vector for equipment-access floor system
$\ddot{u}_g$	Base acceleration
$W_e$	Weight of equipment
$x(t)$	Input for single input and single output linear system
$x_1$	Distance measured from the equipment base such that $\phi(x_1)=1/\gamma$
$X_t(f, T)$	Finite Fourier transform for $x(t)$ where $(k-1)T \leq t \leq kT$
$y(t)$	Output for single input and single output linear system
$Y_t(f, T)$	Finite Fourier transform for $Y(t)$ where $(k-1)T \leq t \leq kT$
$z(x, t)$	Equipment displacement at a distance x from the base
$\alpha$	Generalized mass coefficient
$\beta$	Frequency ratio $f/f_1$

List of Symbols (cont'd)

$\gamma$	Equipment shape function parameter
$\mu$	Mass ratio
$\xi_e$	Generalized damping ratio for equipment
$\xi_f$	Effective damping ratio for access floor
$\rho_e$	Distribution of equipment mass per unit area
$\rho_f$	Distribution of access floor mass per unit area
$\sigma$	Standard deviation
$\phi(x)$	Equipment shape function
$\{\phi\}^t$	Mode shape vector for equipment-access floor system
$\omega_e$	Equipment natural frequency
$\omega_f$	Effective frequency of access floor
$\Omega_1, \Omega_2$	Modal frequency ratios
$\Omega_e$	Equipment frequency ratio

## CHAPTER 1

### INTRODUCTION

#### 1.1 Background

Within the last two decades, telecommunications have become a vital part of the modern industrial and business world. Coupling with electronic data processing facilities, the role of telecommunications today has expanded much beyond the traditional role of providing voice communications and into data communications. Major business corporations rely heavily on telecommunications facilities to carry out daily activities such as business transactions, payroll and credit verification. The importance of telecommunications in the business world can be vividly seen in the recent disruption of long distance telephone services in the U.S. where millions of dollars of business loss was resulted in a short period of nine hours<sup>1</sup>.

In the field of earthquake engineering, telecommunications networks are classified as a lifeline because their damage in a destructive earthquake not only would inflict heavy economic loss to businesses, but also would hamper rescue efforts during the aftermath of the earthquake. A typical telecommunications network configuration is

---

<sup>1</sup> Time, Vol 135, No.5, Jan 29, 1990, pp. 34-35.

shown in Fig. 1.1. The network consists of circuits that range from major trunks such as high capacity toll transmission paths linking cities, to very minor lines (loop) that interconnect individual telephone subscribers through their local telephone central offices. Each line or trunk path terminates at a central office where switching operations are performed loop-to-loop, loop-to-trunk or trunk-to-trunk by switching equipment. The central office switching equipment, due to its vital roles in the network, are required to be seismically qualified before it can be installed in areas of high seismic risk. In North America, the NEBS (Network Equipment Building System) criteria (Bell Communication Research, 1988) are the most commonly adopted industry standard to evaluate the seismic performance of such equipment.

Ever since the advance in digital electronic technology, there has been an industry-wide transformation from electromechanical relays used in traditional switching equipment to digital electronic switches controlled by microprocessors. Modern telecommunications equipment is in fact like a computer, and in order to function properly, it requires constant circulation of cool air to provide proper temperature and humidity control. Access floors can accommodate the many utility connections and circulation of cooling air beneath the floor; as a result, they are often used in telecommunications central offices to support switching equipment. The typical access floor used today consists of a nominal 2' by 2' modular system which is composed of removable floor panels, stringers and pedestals as shown in Fig.1.2.

Although access floors have been used widely in modern telecommunications central offices, there is little information on the

seismic behaviour of telecommunications equipment supported by them. Since the NEBS criteria used in the industry are derived for equipment supported directly on building floors, it is not clear whether equipment which has passed the seismic performance criteria defined by NEBS would function during and after a destructive earthquake if it were supported on an access floor. To address these issues, a systematic study is carried out to provide information on the seismic behaviour of telecommunications equipment supported on access floors.

## 1.2 Review of Pertinent Work

Although access floors have been used extensively to support electronic data processing (EDP) equipment in buildings located in active seismic regions, only recently building codes have started to address the seismic design of access floors. The 1985 Uniform Building Code (UBC, 1985) specifies guidelines to determine the seismic forces for access floors as a percentage of the weight of the equipment supported on the access floor. The percentage is expressed in terms of a lateral force coefficient and the seismic zone in which the building is located. Although the method is simple, many factors such as the location of the access floor in a building, the stiffness of the access floor and the interaction of the supported equipment and the access floor are not taken into account. Furthermore, the code only deals with the design of access floors, but does not address the modified seismic environment that equipment may be exposed to when it is supported on access floors.

As an outgrowth of the concern with the implications of a catastrophic earthquake on the banking industry in California, the

Committee on Finance, Insurance and Monetary Services (FIMS) was formed in 1981. A document entitled "Data Processing Facilities : Guidelines for Earthquake Hazard Mitigation" (FIMS, 1987) was published by the committee. This document contains valuable guidelines pertaining to the seismic resistant design of electronic data processing (EDP) facilities. Since most of the modern EDP equipment is supported on access floors, a full section of the document is devoted to the design of new access floors and evaluation and retrofitting of existing access floors. Behaviour of access floors during actual earthquakes is also reported in the document. Of special interest is the 1984 Morgan Hill Magnitude 6.5 earthquake where the motions were recorded on the building floor, the access floor and at the top of a piece of computer equipment. It was found that the amplification of the building floor motions was two times on the access floor and three times at the top of the computer equipment. The document also points out some of the research areas needed to be addressed, such as, the interaction of the supported equipment and the access floor, energy dissipation and resonant frequency characteristics and the response under dynamic seismic loading.

Experimental study was carried out by Heidebrecht and Tso (Heidebrecht and Tso, 1983) on the seismic behaviour of a typical commercial access floor system supporting heavy telecommunications switching equipment. The equipment was placed on a 3 panel by 3 panel size access floor in both symmetrical and asymmetrical configurations. The tests were carried out on a shake table, and both sinusoidal and artificially generated earthquake excitation were used in the testing. Some conclusions of interest from this study are: 1. torsional effect due

to asymmetric location of equipment was not significant compared to the lateral response; 2. in the side-to-side shaking direction the fundamental frequency of the combined equipment-access floor system was identical to the fundamental frequency of the equipment on a fixed base due to the relatively flexible equipment used as compared to the access floor; and 3. Under artificial earthquake excitation, up to 1.5 times amplification of the shake table motion was observed on the access floor and up to 4 times amplification was observed at the top of the equipment.

Mehrain, et al (Mehrain, et al, 1988) carried out cyclic static tests on several commonly available types of access floor pedestals and concluded that they did not have the required strength and stiffness to survive a major earthquake without damage. Foss and Nikolakipoulou (Foss and Nikolakipoulou, 1980) proposed a scheme which uses a toggle bar to provide restraint for low height/width ratio computer equipment supported on access floor. Experimental and analytical study were carried out to demonstrate the effectiveness of the this scheme. Chang, et al (Chang, et al, 1986) gave a general survey on some commonly used access floor systems, and pointed out the factors which affected their seismic performance. They also proposed a base isolation concept for the entire access floor in a building. Experimental work was carried out to show the feasibility of the base isolation concept. Forell (Forell, 1983) pointed out the inadequacy of the existing U.S. building code provisions in addressing the design of access floor and EDP equipment. He discussed several engineering considerations which were essential to the seismic performance of access floors under seismic condition, such as, positive anchorage of the access floor pedestals to the building floor and the need

of a stringer system to transmit the earthquake-induced lateral load uniformly to the access floor pedestals.

As seen from the literature review, very few studies have been done to address directly to the area of the seismic behaviour of equipment on access floors. Particularly, there has not been any systematic experimental or analytical study on the subject.

### 1.3 Objectives and Scope

The objective of this research is to provide guidelines for the seismic analysis, design and qualification of equipment supported on access floors in telecommunications central offices. To achieve this objective a systematic study is carried out using experimental and analytical approaches. The experimental work is carried out using two different commercial access floors and a switching equipment frame commonly used in telecommunications central offices as test specimens. There are three phases involved in the experimental work. First, static tests are performed to obtain the stiffness and strength properties of the access floors. Second, dynamic exploratory testing is carried out to study the dynamic characteristics of the access floors, the telecommunications equipment and finally the combined equipment-access floor systems. Lastly, dynamic tests using artificially generated earthquake time history are performed for the equipment alone and the combined equipment-access floor systems. Based on the exploratory testing results, an analytical model is developed for the combined equipment-access floor system. The adequacy of this model in predicting the dynamic properties and seismic response of equipment-access floor systems is checked against experimental results. A

parametric study is carried out using this model to provide insight into the dynamic characteristics and the interaction of equipment and access floor. The model is also used to study the seismic response of equipment supported on access floors in a telecommunications central office setting. Based on the calculated equipment response to the upper bound in-building excitations, design spectra for telecommunications equipment supported on access floors are generated. These spectra provide a basis for seismic analysis, design and qualification of equipment on access floors.

In this thesis, the experimental work is described in chapters 2 to 4, and the analytical work is presented in chapters 5 and 6. The static tests for the access floor are discussed in chapter 2. The dynamic tests carried out to determine the dynamic properties of the access floors, the equipment and the combined equipment-access floor systems are discussed in chapter 3. In chapter 4, the seismic tests performed for the equipment and the combined equipment-access floor systems are described. An analytical model of combined equipment-access floor systems is developed in chapter 5. The results of a parametric study for this model are also discussed in this chapter. Finally, in chapter 6, the seismic response of equipment supported on access floors in telecommunications central offices is studied using the analytical model. Based on the computed seismic response, access floor response spectra are generated. The major findings and conclusions reached in this study are summarized in chapter 7.

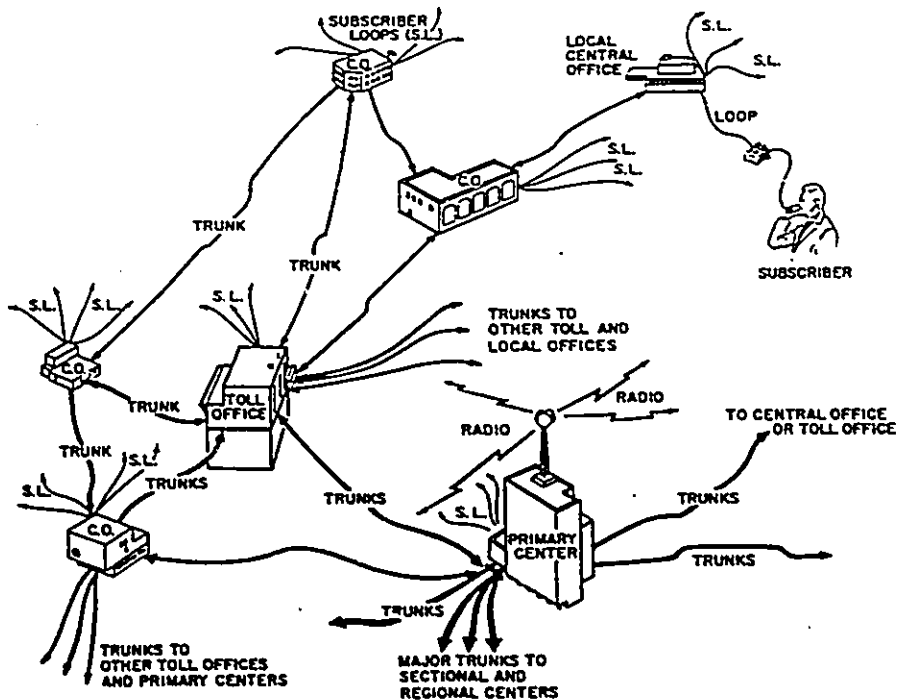


Fig. 1.1 Typical telecommunications network distribution configuration (after Foss and Scobee, 1980)

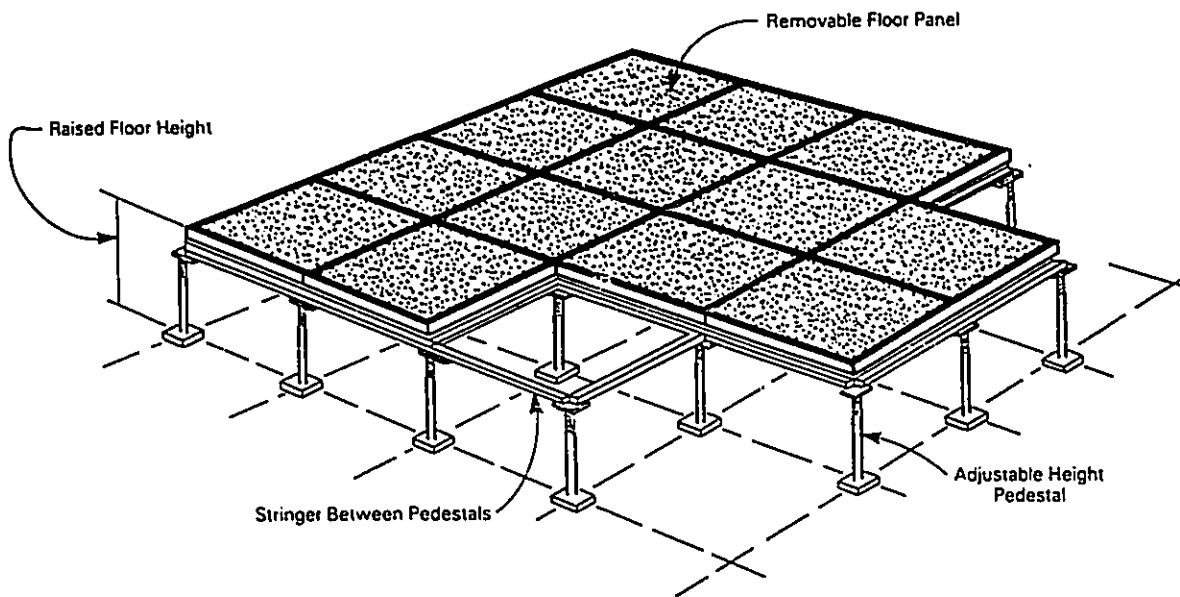


Fig. 1.2 Typical access floor

## CHAPTER 2

### STATIC TESTS FOR ACCESS FLOOR SYSTEMS

#### 2.1 Description of Access Floor Systems

The access floor systems chosen for this study are commercially available and listed in manufacturer's catalogues. The floor systems consist of floor panels and understructures which are composed of stringers and pedestals arranged in a standardized 2' (0.61m) square grid pattern. The floor panels are made of steel and are formed by welding a top sheet to a waffle bottom pan. Each floor panel is supported along its perimeter by stringers. The panels can be attached to the understructure of the access floor by bolts at their four corners or simply be held in place by gravity. These two panel attachment methods will hereafter be referred to as "bolted" and "drop-in" panel attachment, respectively. The stringers are 4' (1.22m) in length and are fastened onto the pedestals by screws in a basketweave pattern as shown in Fig.2.1a. The pedestal shown in Fig.2.1b consists of a pedestal head and a pedestal base. The pedestal head is formed by welding together a thread stud and a steel plate. The pedestal base is made of an 1" (2.54cm) diameter tube welded to a 4x4x1/8" (10.2x10.2x0.32cm) base plate. There is no positive connection between the pedestal head and the tube of the pedestal base. The completed

tube. A levelling nut is used for height adjustment and to transfer the gravity load from the pedestal head to the pedestal base.

A 12" (30.5cm) and a 20" (50.8cm) finish floor height (FFH) access floor are used in the experiment, and they are designated as "D12" and "D20", respectively, hereafter in the discussion. The two access floors are essentially identical except the D20 access floor has a longer tube in the pedestal base.

## 2.2 Experimental Setup and Procedures of Static Tests

One of the major aims in this study is to investigate the possibility of predicting the dynamic properties of a multi-panel access floor based on the stiffness properties obtained from static tests. To achieve this aim, static tests were carried out to obtain the load-deflection characteristics of the D12 and the D20 access floor system. The tests were performed using one-panel access floor modules. The quantities of interest which include stiffness, ultimate strength, ultimate displacement and failure mechanism are determined from the load-deflection curves.

An overview of the experimental setup for the static tests is shown in Fig.(2.2). The test specimens was a one panel access floor module consisting of four pedestals, four 2' stringers and one floor panel. The stringers were fastened to the pedestals by means of screws. The panel was attached to the access floor understructure using the drop-in panel attachment. The anchorage arrangement for the access floor pedestals is shown in Fig.(2.3). The pedestal base-plates were secured to the webs of two 6" (15cm) base channels which ran parallel to the direction of

two 6" (15cm) base channels which ran parallel to the direction of loading. Each pedestal base-plates were clamped onto the web of the base channel by a collar plate which was in turn clamped down by a pair of steel channels arranged in a back-to-back fashion running parallel to the direction of loading. The two steel channels were secured by an arrangement of dog-plates and bolts. The bolts were welded onto the web of the base channels. The two base channels were fastened to the test floor of the laboratory by means of expansion anchors. Such anchorage arrangement provided complete fixity to the base-plates of the pedestals to the test floor.

The lateral load was applied through a load train reacting against a spacer column which in turn reacting against a reaction wall as shown in Fig.2.4. The load train consisted of a hydraulic jack, a 20 kips (89kN) load cell and a ball joint. The lateral load was applied on a spreader beam which distributed the load to the access floor.

Also shown in Fig.2.4 is the instrumentation for the tests. It consists of a load cell for measurement of the applied load and two string LVDT's (Linear variable differential transducer) for measuring the access floor lateral displacements at the two edges. The outputs of the load cell and the LVDT's were fed into an A/D (analog to digital) converter. The analog outputs were digitized and then stored in the hard disk of a computer.

The loading history applied to the specimens comprised in the beginning of a few cycles of loading, unloading and reloading at a load below 2kN. Subsequently, a monotonically increasing load was applied until failure occurred. The three instruments were scanned at a rate typically

every 0.1kN load increment during loading and at every 0.5kN decrement during unloading.

### 2.3 Observations and Results

The static behaviour of both the D12 and the D20 access floor was very similar. A small load (50N) was needed to be applied to the access floor in order to fully mobilize the stiffness of the access floor. This was due to the fact that some of the components of the access floors, such as the pedestal heads and the pedestal bases, were not positively connected but loosely fitted together. The small lateral load was needed to make these components to come into full contact with each other. The lateral load-deflection curves are shown in Figs.(2.5a) and (2.5b) for the D12 and the D20 access floor, respectively. The lateral displacement was taken to be the average of the displacements at the two edges of the access floor. It can be seen that both specimens exhibit a nonlinear softening load-deflection behaviour where the stiffness decreases as the displacement or load increases. The loading and unloading paths do not coincide with each other. Some permanent displacements are resulted upon unloading even at small load. No distinct yield point can be found on the load-deflection curves. Both the D12 and D20 specimens failed by cracking of the welds at the connections between the tube and the base-plate of the pedestals. Once the failure was initiated, both specimens were not capable of resisting any additional load. A significant amount of torsional displacement occurred after the failure of the first weld due to the unbalanced resistance in the two lines of pedestals. Additional cracked welds occurred at the base upon further loading. The D12 specimen failed

in a brittle manner with very little yielding. The D20 specimen behaved in a more ductile manner where the load-deflection curve became almost flat at the onset of failure. Except for the failure of the welded connections at the pedestal bases, no other damage was observed for in either specimen.

Some of the quantities of interest denoted on the load-deflection curves in Figs.(2.5a) and (2.5b) are summarized in Table 2.1. The values of the lateral initial stiffness for both specimens are taken as the slope of a straight line which gives a best fit to the data within a loading ranged from zero to 10% of the ultimate load. The initial stiffness of the D12 access floor is approximately 4.5 times that of the D20 access floor. For practical purposes, the ultimate load for the D12 specimen is taken as 4.2kN at a displacement of 1.4cm. For the D20 system, the ultimate load is 2.85kN at a displacement of 4.0cm. The pedestal stiffness  $k_p$  is taken as the overall initial stiffness divided by the number of pedestals.

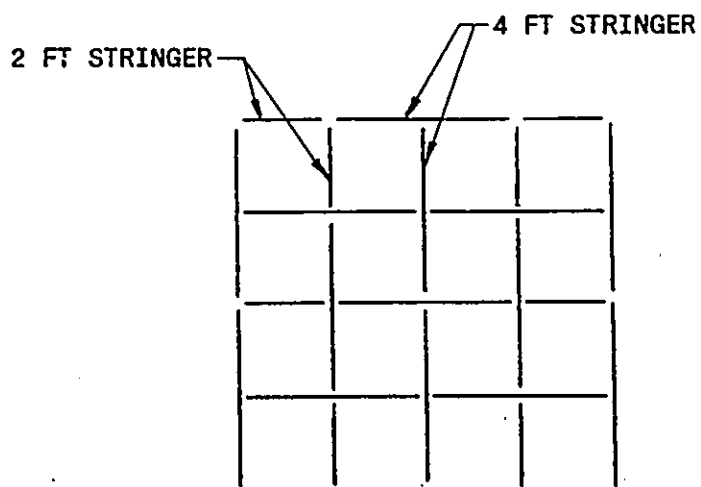
#### 2.4 Summary

In this chapter the experimental results of the static tests carried out for access floor systems of two different heights were presented. It was found that even at a small loading range, the load-deflection curves of both access floors tested exhibited a slightly inelastic behaviour. At the ultimate limited state, the access floors tested exhibited a brittle behaviour. The weakest links were the welds which connects the tubes and the base-plates of the pedestals together. The failure of these welds at the ultimate load was the cause of the brittle behaviour.

Table 2.1 Static Test Results

	Access	Floor
	D12	D20
Stiffness (kN/cm)	7.18	1.64
Pedestal stiff. $k_p$ (kN/cm)	1.80	0.41
Ultimate load (kN)	4.20	2.85
Ultimate disp.(cm)	1.40	4.00

## a.) Basketweave Stringer Arrangement



## b.) Typical Access Floor Pedestal

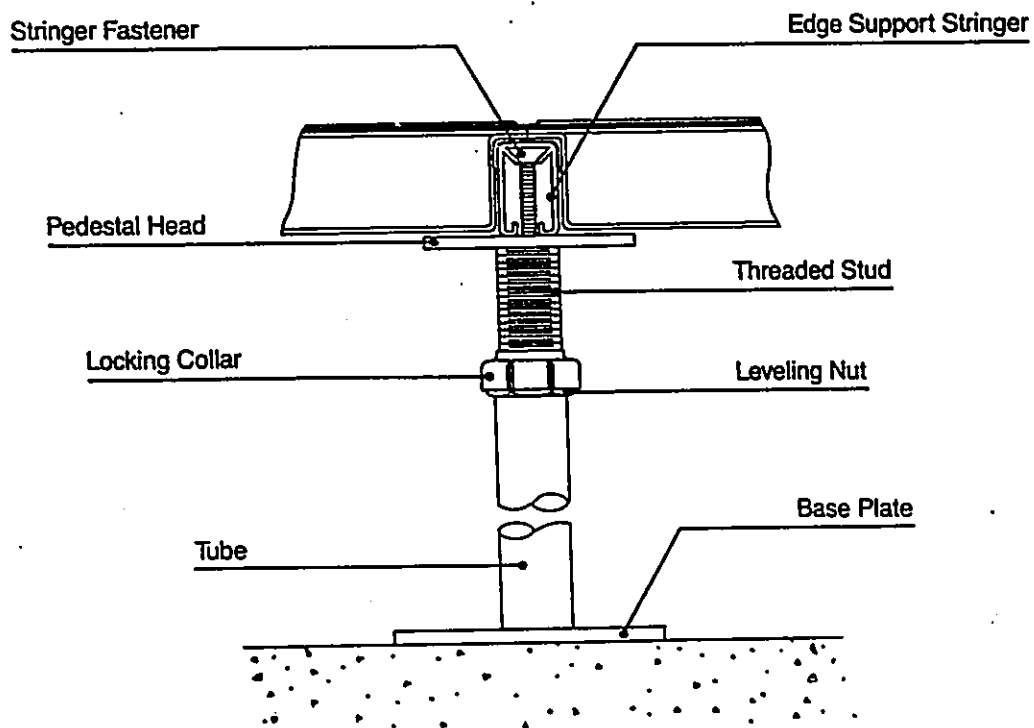


Fig. 2.1 Access floor used in this study

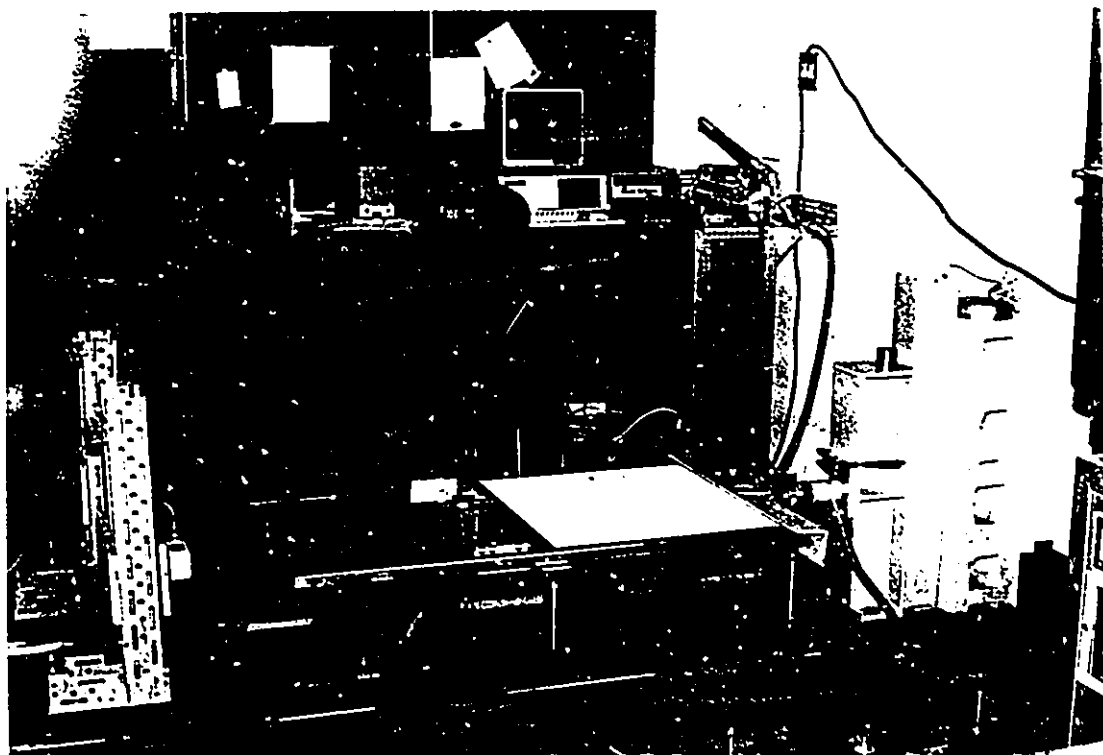


Fig. 2.2 Static test set up

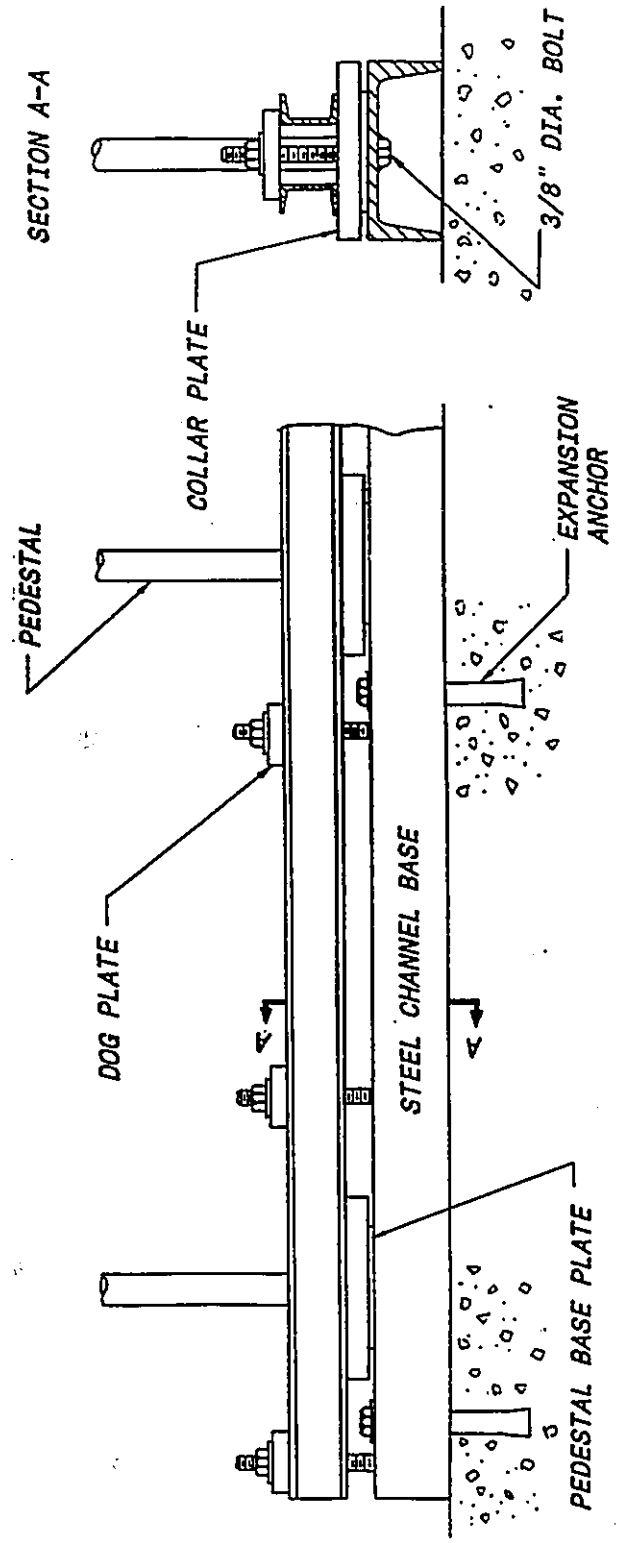


Fig. 2.3 Anchorage arrangement for pedestals

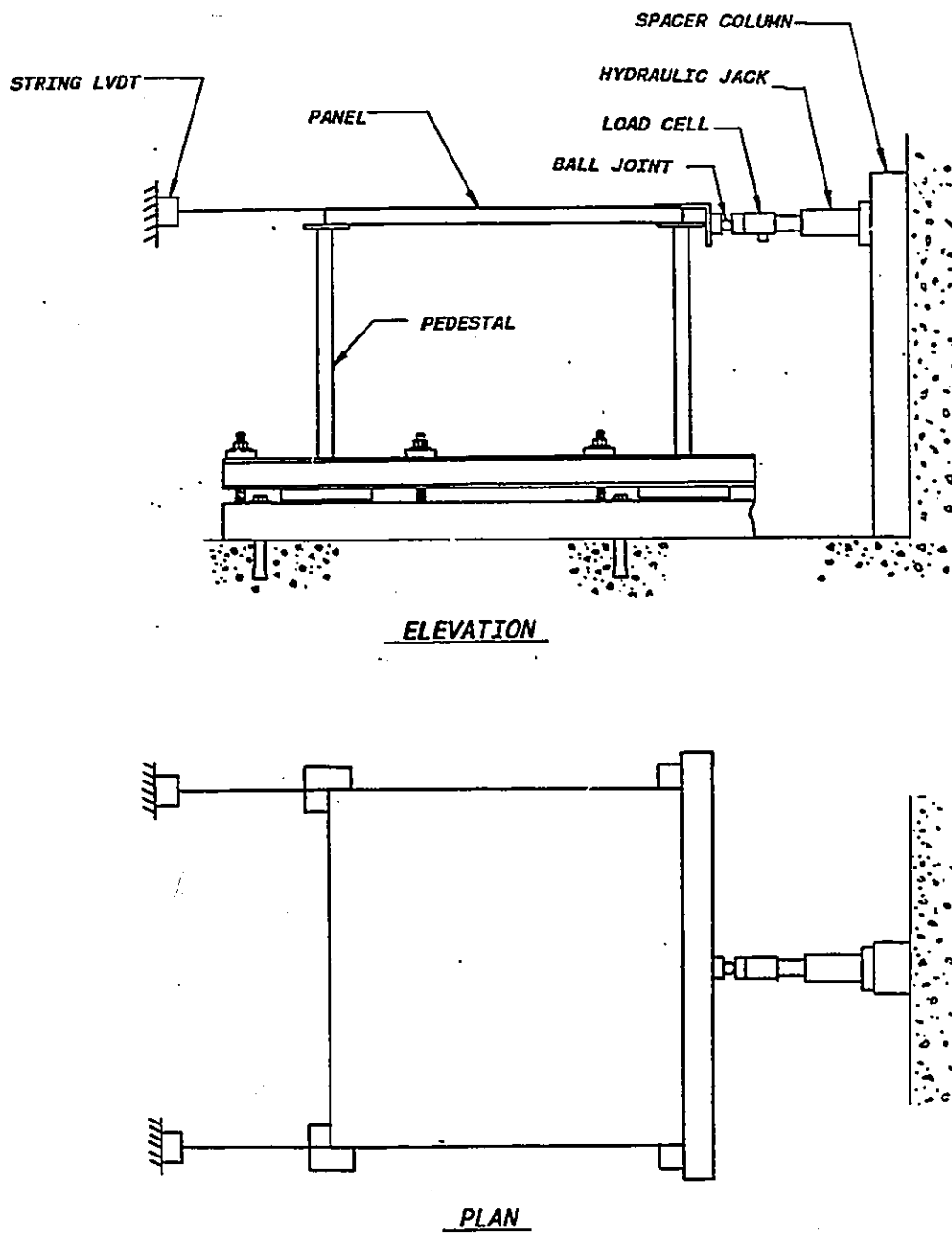
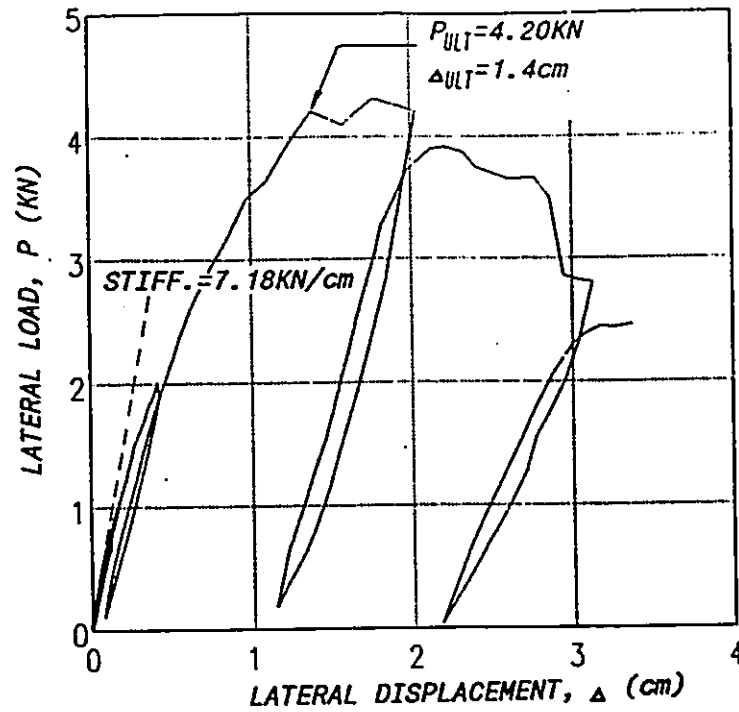


Fig. 2.4 Load train and instrumentation for static test

a.) D12 Access Floor



b.) D20 Access Floor

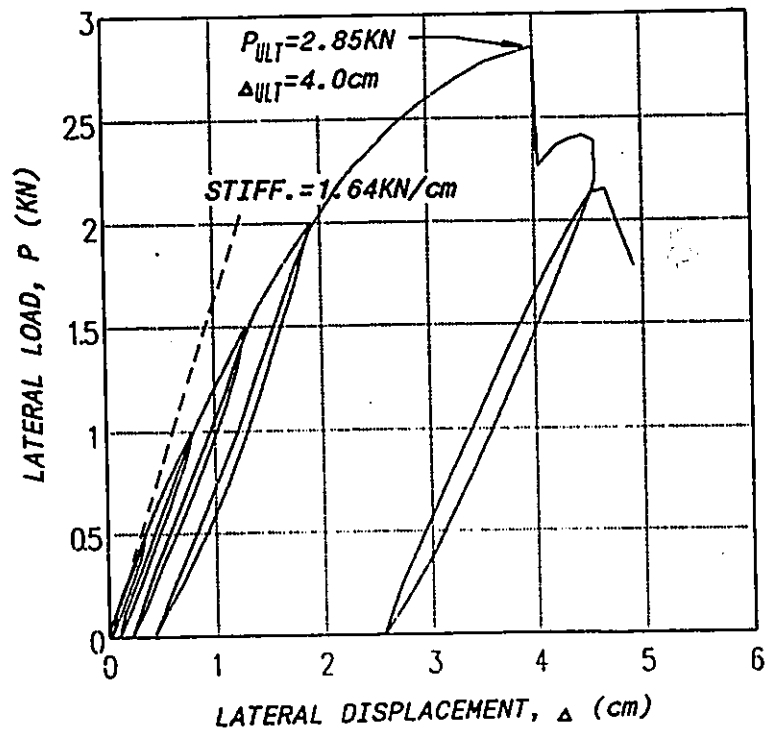


Fig. 2.5 Access floor load-deflection curves: a.) D12 access floor, b.) D20 access floor

## CHAPTER 3

### EXPLORATORY TESTING

#### 3.1 Introduction

The purposes of the exploratory testing are twofold. First, it is to study the dynamic properties (i.e. frequencies, damping ratios and mode shapes) of the access floors, the equipment and the combined equipment-access floor systems. Such information is necessary for a systematic understanding of the dynamic response of the combined equipment-access floor systems. The information will also be needed later to calibrate an analytical model of equipment-access floor systems. The second purpose of the exploratory testing is to investigate the possibility of predicting the frequency of a multi-panel access floor configuration from the stiffness properties obtained from the static test of an one-panel access floor module.

#### 3.2 Test Preliminaries

The essence of the exploratory testing is to determine the transfer function of a test specimen from which the dynamic characteristics of the test specimen can be determined. The transfer functions for the access floors, the equipment and the combined equipment-

access floor systems were determined using a random excitation testing technique on a shake table. In this section, some of the test preliminaries are discussed.

### 3.2.1 Shake Table Test Facilities

The exploratory tests as well as the subsequently discussed seismic tests were carried out on the shake table facilities at McMaster University. The shake table used is a single axis 6x7' (2x2.1m) horizontal table driven by a 20kip (106kN) hydraulic actuator. The actuator is capable of providing a 10" (25cm) peak to peak table displacement. The table is controlled by an MTS controller which can drive the table either in an acceleration or a displacement control mode. From past experience, the displacement mode has been a more stable control mode than the acceleration mode. Hence, the shake table was driven under the displacement control mode for all the tests in this study. Under the displacement control mode, the shake table can operate in a  $\pm 1$ " (2.5cm) or a  $\pm 5$ " (12.5cm) displacement range. For exploratory testing purposes where the required excitation is small, the  $\pm 1$ " displacement range was used. The types of input command signals for the shake table controller can be periodic or random signals generated by waveform generators or arbitrary waveform generated by converting digital data using a microcomputer equipped with a D/A (digital to analog) converter.

Accelerometers and displacement transducers (LVDT) are used to monitor the motions of the test specimen and the shake table during testing. The sensor signals are amplified (or attenuated) and filtered using signal conditioners. A dual-channel Spectral Dynamics spectrum

analyzer is used to process the signal in real time during testing. The output signals of the signal conditioners can be plotted on a strip chart recorder or digitized by a microcomputer based data acquisition system.

### 3.2.2 Selection of Testing Method

There are several types of input excitation which may be employed to obtain the transfer function of a test specimen. The merits of the particular type of excitation chosen for this study are discussed here. Three types of excitation, namely, sinusoidal excitation, random excitation and impulsive excitation, are commonly used for exploratory testing purposes. Since the tests were conducted on a shake table, the impulsive excitation testing technique, which is carried out by using a instrumented hammer, was not considered. The choice between the sinusoidal excitation and the random excitation was made based on some preliminary tests.

Preliminary tests had shown that there were two major drawbacks associate with the sinusoidal excitation technique. First, the weight of the combined equipment-access floor system was very massive compared to the weight of the shake table (of the order of two times the weight of the shake table). As a result, when the frequency of the sinusoidal excitation approached the resonant frequency of the test specimen, a significant amount of specimen vibration, which was at the specimen's resonant frequency, was fed back to the shake table. Instead of sinusoidal motion, the actual table motion became a series of sine beats which resulted from the superposition of two sine-waves of close frequencies; one corresponded to the prescribed frequency of the shake table motion and the

other corresponded to the resonant frequency of the test specimen. Because of the sine beats, it was difficult to determine accurately the resonant frequency of the test specimen. Second, when the excitation frequency was close to the resonant frequency of the test specimen, the response build-up caused excessive shaking on the specimen, and this could damage the specimen prematurely.

Preliminary tests using random excitation input had shown that the major drawbacks pertaining to the sinusoidal excitation input did not exist. In addition, random excitation input has the advantage that all the vibration modes of a test specimen within the frequency bandwidth of the excitation are excited simultaneously. With a dual-channel spectrum analyzer, the transfer function of the test specimen can be readily obtained using this testing technique. In view of its merits, random excitation was chosen to be used to excite the test specimens in this study.

### 3.2.3 Principles of Random Excitation Testing Technique

For any constant parameter linear system which is stable, the dynamic characteristics of the system can be described by a transfer function  $H(f)$  in the frequency domain. For a single input  $x(t)$  and a single output  $y(t)$  system as shown in Fig.3.1, the system transfer function  $H(f)$  can be written in terms of the input/output cross spectrum  $G_{xy}(f)$  and the input power spectrum  $G_{xx}(f)$  as

$$H(f) = G_{xy}(f)/G_{xx}(f)$$

Given that  $x(t)$  is a stationary Gaussian random process,  $G_{xx}(f)$  and  $G_{xy}(f)$

can be estimated from a collection of  $n$  records,  $x_k(t)$  and  $y_k(t)$ ;  $(k-1)T \leq t \leq kT$ ;  $k=1,2,\dots,n$ , taken from  $x(t)$  and  $y(t)$  by

$$\hat{G}_{xx}(f) = \frac{2}{nT} \sum_{k=1}^n |X_k(f,T)|^2$$

and

$$\hat{G}_{yy}(f) = \frac{2}{nT} \sum_{k=1}^n X_k^*(f,T)Y_k(f,T)$$

where  $X_k(f,T)$  and  $Y_k(f,T)$  are the finite Fourier transforms of  $x_k(t)$  and  $y_k(t)$  of time duration  $T$ ,  $X_k^*(f,T)$  is the complex conjugate of  $X_k(f,T)$ , and  $\hat{G}_{xx}(f)$  and  $\hat{G}_{yy}(f)$  denote the estimates of  $G_{xx}(f)$  and  $G_{yy}(f)$ , respectively. The above derivation for the estimation of  $H(f)$  is given in detail by Bendat and Piersol (Bendat and Piersol, 1980).

In this study,  $H(f)$  was determined by exciting the specimen with an excitation derived from a stationary Gaussian random process. Using the dual channel spectrum analyzer with appropriate settings,  $H(f)$  was computed based on the above estimations of  $G_{xx}(f)$  and  $G_{yy}(f)$  during the test using the real time signals of  $x(t)$  and  $y(t)$ .

The coherence function  $\gamma_{xy}^2$  defined as

$$\gamma_{xy}^2 = \frac{|G_{xy}(f)|^2}{G_{xx}(f)G_{yy}(f)}$$

which is a measured of linear cause/effect relationship between  $x(t)$  and  $y(t)$  was also determined using the spectrum analyzer in the experiment. For ideal situation where the system is linear and there is no extraneous noise involved in the measurements of  $x(t)$  and  $y(t)$ ,  $\gamma_{xy}^2$  has a value of unity. For system with non-linearities or the measurements of  $x(t)$  and  $y(t)$

are corrupted by extraneous noise,  $\gamma_{xy}^2$  takes on a value between 0 and unity. The coherence functions obtained for all the random excitation tests conducted in this study were found to be close (within 5%) to unity.

#### 3.2.4 Generation of Random Excitation Time History

Using the displacement, the velocity and the acceleration of the excitation and of the response of a test specimen, the transfer function of the test specimen may be expressed in six different ways (e.g., displacement/velocity and acceleration/displacement). Considering the simplicity of instrumentation required for the experiment, the transfer function between the absolute acceleration of the test specimen and the input base acceleration is the most suitable. To obtain such a transfer function, an excitation acceleration time history is derived from a Gaussian random process as follows. First, a sequence of random numbers having a Gaussian distribution was generated by using a random number generation subroutine in a computer. This sequence of random numbers consisted of 180,000 numbers and was sufficient for providing 15 minutes of random excitation with a D/A (digital to analog) conversion rate of 200 samples/sec. In order to meet the requirement of the shake table control system, the time history data was first passed through a band-pass filter having a shape as shown in Fig.3.2. This band-pass filter has a high-pass cut-off frequency of 2 Hz and low-pass cut-off frequency of 30 Hz. The filtered data was then integrated twice to obtain a displacement time history. The displacement time history was scaled such that the maximum value in the time history would produce a 1 inch maximum displacement on the shake table under the  $\pm 1$ " displacement control mode. With such

scaling, the shaking intensity could be varied by adjusting the span control of the shake table control console where a 100% span setting would produce a table motion with an 1" maximum displacement. The random displacement time history data was stored in the hard-disk of a microcomputer equipped with a D/A converter. During a random excitation test, the time history was continuously streamlined from the hard-disk through the D/A converter to the shake table control console.

Two averaged Fourier spectra of the shake table acceleration generated by the random displacement time history data are shown in Fig.3.3. The acceleration was measured by an accelerometer mounted on the shake table, and its Fourier spectra were obtained by a spectrum analyzer. The top spectrum shown in Fig.3.3 was obtained for a frequency range from 0 to 25 Hz, and the bottom spectrum for frequency range between 0 and 50 Hz. It can be seen from the spectra that the cut-off frequency is at about 2 Hz at the lower ends of the spectra. Between 2 and 15 Hz the spectra are relatively flat. The amplitude of the spectrum increases with frequency between 15 and 25 Hz, levels off between 25 and 30Hz and decreases with the increase of frequency beyond 30 Hz. The Fourier spectra for the measured random acceleration is different from its ideal shape as shown in Fig.3.2. The differences were caused by the shake table's oil column resonance which occurred in a frequency region between 25 to 30 Hz depending on the amount of mass attached to the table.

### 3.2.5 Determination of Dynamic Properties from Transfer Functions

Given the transfer function of a test specimen, the resonant frequencies can be obtained by noting the frequencies at which the peaks

of the magnitude of the transfer function occur. The method of determining the damping ratios of a test specimens from its transfer function is discussed below.

The transfer function  $H(f)$  for the absolute acceleration response of a single degree of freedom system having a natural frequency of  $f_1$  and a damping ratio of  $\xi$  subjected to a base acceleration can be expressed in the frequency domain as

$$H(f) = 1 - \frac{(f/f_1)^2}{(f/f_1)^2 - 1 + 2j\xi f/f_1} \quad \text{and } j = \sqrt{-1}$$

The derivation of  $H(f)$  is given by Bendat and Piersol (Bendat and Piersol, 1966).  $H(f)$  is a complex function, and the real part of  $H(f)$  expressed in terms of the frequency ratio  $\beta=f/f_1$  can be written as follows:

$$\text{Re}[H(\beta)] = 1 - \frac{\beta^2(\beta^2-1)}{(\beta^2-1)^2 + (2\xi\beta)^2}$$

The plot of  $\text{Re}[H(\beta)]$  against  $\beta$  for a range of damping ratios  $\xi$  is shown in Fig.3.4. The  $\text{Re}[H(\beta)]$  trace exhibits two peaks where one occurs at  $\beta_1$  (to the left of  $\beta=1$ ) and the other at  $\beta_2$  (to the right of  $\beta=1$ ). It also can be seen from Fig.3.4 that as the damping ratio  $\xi$  increases, the two peaks in  $\text{Re}[H(\beta)]$  spread further away from each other. The above observations on the transfer function indicate that if the transfer function of a test specimen is obtained, its damping ratio can be determined based on the spread of  $\beta_1$  and  $\beta_2$  on  $\text{Re}[H(\beta)]$ .

The expression which relates the damping ratio  $\xi$  to  $\beta_1$  and  $\beta_r$  can be written as

$$\xi = \frac{1}{2} \cdot \frac{(\beta_r/\beta_1)^2 - 1}{(\beta_r/\beta_1)^2 + 1}$$

This expression is derived in Appendix I. Letting  $\beta_1 = f_1/f_n$  and  $\beta_r = f_r/f_n$ , the above equation becomes

$$\xi = \frac{1}{2} \cdot \frac{(f_r/f_1)^2 - 1}{(f_r/f_1)^2 + 1} \quad (3.1)$$

where  $f_1$  and  $f_r$  correspond to the frequencies at which the peaks of to the left and to the right of the resonant frequency occur, respectively. Eqn.(3.1) is derived for single degree of freedom systems, but it is also applicable to determine the modal damping ratios for multi-degree of freedom systems provided the modal frequencies are not closely spaced. Since the modal frequencies of all the test specimens in this study are well separated, the above equation is used to determine the damping ratios of the test specimens.

### 3.3 Determination of the Dynamic Properties of the Access Floor Systems

The random excitation technique discussed in the previous section was applied in the experiment to determine the frequencies and damping ratios of a variety of configurations of the D12 and the D20 access floors. The configurations considered ranged from a 1-panel (1x1) to a 9-

panel (3x3) set up. Some configurations were tested with added mass attached on the panels. All except one test were carried out using drop-in floor panel attachment. In order to examine the effect of bolting down of the floor panels, one test configuration was conducted with all the panels bolted to the access floor understructure. The experimentally obtained resonant frequencies are compared with frequencies predicted from a theoretical model using the stiffness properties determined from the static tests of 1-panel access floor modules.

### 3.3.1 Experimental Setup and Procedures

The setup for the dynamic tests of access floor systems was similar to the static test set-up. The only difference was that the mounting fixtures were installed on a shake table instead of a concrete floor, and provisions were made for larger test specimens such as a 9-panel (3x3) floor system. A typical 9-panel test setup can be seen in Fig.(3.5).

A summary of the access floor configurations tested are listed in table(3.1). There were a total of 11 tests carried out for the D12 and the D20 floor system. Three access floor configurations were tested for each system, namely, a 1 panel (1x1), a 4 panels (2x2) and a 9 panels (3x3) configuration. For the D12 systems, all three configurations were also tested with added mass attached on the panels. For the D20 systems, only the 1-panel configuration was tested with added mass. The mass attached ranged from 70 Kg for the 1-panel configuration to 500 Kg for the 9-panel configuration. The 9-panel configuration of the D20 systems was also tested with all the floor panels bolted to the understructure of the

access floor. The stringer system used for the 4-panel and 9-panel configurations had the basketweave pattern shown in Fig.2.1a.

The instrumentation for a 3 panel by 3 panel setup can be seen in Fig.3.6. The motion of the shake table was monitored by an accelerometer. The response motion of the access floor was measured by an accelerometer mounted on the access floor as shown. During the experiment, the signals from the two accelerometers were fed into signal conditioners where the signals were amplified and filtered. The filtered signals of the access floor and shake table accelerations were fed into the dual channel spectrum analyzer for the determination of the transfer function.

Four random excitation levels were used to excite each of the access floor configurations. The maximum table displacements associated with these levels of excitations were 0.025, 0.05, 0.1 and 0.2", which corresponded to a table span setting of 2.5%, 5%, 10% and 20%, respectively.

### 3.3.2 Observations and Results

Two typical transfer functions are shown in Fig.3.7. The two graphs plotted in this figure are the real part (top) and the imaginary part (bottom) of the transfer function of the 1-panel D12 floor system with added mass attached. The solid trace corresponds to the transfer function obtained using a 2.5% span excitation, and the dotted line, using a 10% span excitation. The resonant frequencies can be identified by noting the frequencies at which the peaks of the imaginary part of the transfer function occur, and they are 16.4Hz for a

2.5% span excitation and 15.9Hz for a 10% span excitation. To determine the damping ratio of the access floor under a 10% span random excitation, the frequencies  $f_r$  and  $f_1$  are identified to be 16.6 and 15.2Hz. Using Eqn.(3.1) a damping ratio of 4.6% is obtained. For the 2.5% span excitation, the damping ratio is 2.5%. The resonant frequencies and damping ratios obtained for all the test setups are summarized in Table 3.2.

The resonant frequencies are plotted against the excitation span in Fig.3.8a and 3.8b for the D12 and D20 floor systems, respectively. As excitation span increases, the resonant frequency decreases slightly. The decrease of resonant frequency was due to the reduction of the stiffness of the access floor systems as the excitation intensity increases. This observation is consistent with the static test results where the lateral stiffness of the access floor decreases with the increase of lateral displacement.

The damping ratios of the two access floors are plotted in Fig.3.9a and 3.9b against the excitation span. In general the damping ratio increases with the excitation span. Based on the experimental observations, three sources of damping mechanism can be identified, namely, hysteretic damping, friction and impact. The hysteretic damping contribution can be inferred from the load-deflection curve of the static test where the loading and unloading paths do not coincide even at relatively small load. The damping mechanism due to friction and impact was evident from the noise generated during the shaking, particularly at high shaking intensity of 10 and 20% spans. Energy dissipation due to friction and impact is resulted from the relative motions between the

loosely fitted parts of the access floors, such as, between the floor panels and the stringers and between the pedestal heads and the pedestal bases.

The effect of bolting down of the floor panels is seen in the 9-panel configuration test for the D20 system. The resonant frequency of the bolted panel system is slightly higher than that of the drop-in panel system. The increase of resonant frequency was due to the extra restraint provided by the connections between the panels and the understructure. The damping ratio decreased substantially at all levels of excitation when the floor panels were bolted down. The decrease in damping ratios was due to the fact that sliding and impacting between the panel and the stringer were eliminated when the panels were being bolted to the understructure of the access floor.

### 3.3.3 Comparison of Experimental and Analytical Results

One of the objectives of testing the access floor systems by themselves is to validate a simple theoretical model in predicting the natural frequency of a multi-panel access-floor configuration from the results of a 1-panel static test. To establish this model, it is necessary to identify the various sources of contribution to the lateral stiffness of the access floor. There are two major sources of stiffness for the type of access floor systems considered in this study. First, it is the lateral stiffness of the individual pedestals. Second, the pedestals are coupled by means of stringers and panels, and this coupling will provide additional lateral stiffness to the system. Since the stringers are 4' (1.22m) in length and span over three pedestals, it is believed that

irrespective of the size of the access floor, this coupling effect tends to be localized. A theoretical model is set up which assumes that the total lateral stiffness of an access floor system can be obtained by summing up the effective lateral stiffness  $k_p$  of the individual pedestals. The effective pedestal stiffness is determined by finding the lateral stiffness of an 1-panel access floor and dividing it by four (i.e. the number of pedestals in an 1-panel configuration). Once  $k_p$  is determined, the overall lateral stiffness of an access floor consists of  $n$  pedestals is taken as  $nk_p$  in the proposed model.

Since the mass of an access floor is always concentrated on the panels, the access floor would behave as a single degree of freedom lumped mass system. Therefore, the frequency of an access floor  $f$  with  $n$  pedestals can be expressed as

$$f = \sqrt{(nk_p/M)} \quad (3.2)$$

where  $n$  is the number pedestals,  $k_p$  is the effective stiffness of a single pedestal obtained from the 1-panel static test and  $M$  is the total mass of the panels plus the added mass attached on the panels.

The frequencies of all the access floor configurations tested were determined using Eqn.(3.2), and they are listed along with the experimentally obtained frequencies in table (3.3a) for the D12 floor systems and (3.3b) for the D20 floor systems. The values of the pedestal stiffness used in the calculations were obtained from static tests. The masses  $M$  used in the computation are listed in table(3.1). Correlation plots of the predicted frequencies against the experimentally determined resonant frequencies for the D12 and D20 floor systems are presented in

Fig.3.10a and 3.10b, respectively. The data points in both figures lie closely to the 45 degree correlation line. The discrepancies between the predicted and observed resonant frequency are generally within  $\pm 10\%$  of the observed values for both the D12 and the D20 access floor. It is concluded, therefore, that the proposed model using the effective lateral stiffness of the individual pedestals obtained from the static test of 1-panel access floor module may be used to estimate the frequency of a multi-panel access floor with reasonable accuracy.

#### 3.4 Determination of the Dynamic Properties of the Equipment

Random excitation tests were carried out to determine the dynamic properties of the equipment-frame used in this study. This equipment-frame was created by substituting the electronic components of an actual digital switching equipment commonly used in telecommunications central offices with an equivalent amount of mass. The actual equipment-frame consists of a steel frame inside which are housed four shelves of electronic cards, a massive network of wires and cables and a fan cooling unit at the bottom of the frame. In actual installation, a cable trough is mounted at the top of the frame to accommodate electrical wires and cables running to and from other equipment. The overall dimensions of the frame are 42x26" (107x66cm) and 6' (1.83m) in height. The footprint of the frame is 42x23" (107x58cm). For the simulated equipment-frame shown in Fig.3.11, only the top shelf is filled with electronic cards. The rest of the mass of the electronics and the electrical wires and cables as well as the cable trough at the top and the fan units at the bottom are simulated by mounting steel plates of equivalent mass on the frame and in the shelves.

The distribution of the added mass is shown in Fig.3.12. The mass of the entire equipment-frame amounts to 1660lb (756Kg). This simulated equipment-frame will be referred to as the equipment in the subsequent discussions.

The results of the random excitation tests of the equipment are presented below. For the ease of discussion, the side-to-side and back-to-front orientations of the equipment relative to the direction of shaking are referred to as SS and BF orientations, respectively.

#### 3.4.1 Experimental Setup and Procedures

The equipment was mounted on a 50 x 35" (127 x 89cm) by 6" (15 cm) thick concrete slab which in turn was mounted on the shake table. The equipment was anchored to the concrete slab by four 0.5" (12mm) diameter expansion anchors. The anchors were set by the specified 65ft-lb (88N-m) torque. The locations of the anchors in the equipment footprint are shown in Fig.3.13. Both the SS and BF orientations were considered in the testing. The change of test orientation was accomplished by turning the entire concrete slab and equipment assembly 90 degrees.

Accelerometers were used to monitor the motions of the equipment and the shake table. The locations of the accelerometers are identified in Fig.3.14. The accelerometer signals were amplified and filtered by signal conditioners. To determine the resonant frequencies and the damping ratios, four levels of random excitation - 2.5%, 5%, 10% and 20% of an 1" table span - were used to obtain the transfer functions of the equipment. The transfer functions were taken between the response acceleration at the top of the equipment and the input acceleration of the

shake table. To determine the mode shapes, transfer functions were taken between the response acceleration measured at each of the accelerometer locations on the equipment and the input acceleration of the table. A 2.5% span random excitation was used to obtain the transfer functions.

#### 3.4.2 Observations and Results

Preliminary tests were first performed to obtain the transfer functions of the equipment in both orientations for a frequency range between 0 and 40 Hz. This was done to provide a broad survey of all the vibration modes within this frequency range. It was found that for both orientations the second lateral and first torsional modes were beyond 25 Hz. Since these response modes were outside the frequency range of interest in this study, the focus of the investigation was placed on the fundamental lateral mode of vibration.

A typical transfer function for the equipment tested in the SS orientation is shown in Fig.3.15. The transfer function was taken between the acceleration at the top of the equipment and the acceleration of the shake table under a random excitation of 2.5% span. The resonant frequency as indicated by the peak of the imaginary part of the transfer function is 8.9Hz. The corresponding damping ratio as indicated by the real part of the transfer function was determined to be 0.7%. Similar plots were obtained for excitation levels of 5%, 10% and 20% span. The fundamental frequencies and damping ratios obtained for both test orientations are summarized in Table 3.4 and graphically shown in Fig.3.16a and 3.16b. The equipment has a higher frequency in the BF orientation than in the SS orientation. The fundamental frequencies range

from 8.6 to 8.9Hz for the SS orientation and from 12.5 to 13.2Hz for the BF orientation. The damping ratios range from 0.7% to 1.8% for the SS orientation and 1.2% to 4.2% for the BF orientation. The equipment's fundamental frequencies decrease slightly and the damping ratios increase as the excitation amplitude increases.

It is worthwhile at this point to compare the resonant frequencies of the simulated equipment tested with that of the actual equipment furnished with full electronics and other accessories. A test for the actual equipment was performed in 1986 for the purpose of seismic qualification (Tso, 1986). The fundamental frequencies of the actual equipment as determined by the sine-sweep test were 9.2 and 12.5Hz for the SS and the BF orientation, respectively. These values compared favourably with those obtained for the simulated equipment presented here. Therefore, the simulated equipment is considered to be a good representation in the dynamic sense of the actual telecommunications equipment.

In order to determine the mode shapes of the equipment, it is necessary to obtain the transfer function for the relative response motions along the height of the equipment with respect to the equipment base. However, due to the limitation of the instrumentation, only the transfer function for the absolute response motion can be monitored directly. For this reason, it is necessary to compute the relative response transfer function from the absolute response transfer function analytically. The computation is done by subtracting a value of unity from the absolute response transfer functions obtained from the tests. In the form of an equation, the relative response transfer function  $H_r(f)$  is written in terms of the absolute response transfer function  $H_a(f)$  as

$$H_r(f) = H_a(f) - 1 \quad (3.3)$$

The mode shapes of the equipment in the SS orientation was determined by monitoring the response motions at three center-line locations (at the mid-height, at the 3/4-height and at the top) along the height of the equipment. The acceleration at the top of the equipment was taken as the average of the accelerations measured at the two top corners. For the B-F orientation, two locations (at approximately the mid-height and at the top) along the height of one of the uprights of the equipment were chosen for the determination of the mode shape.

Using Eqn.(3.3) the value of the relative acceleration response transfer functions at the fundamental frequencies were determined for both equipment orientations. These values are expressed as magnitudes and phase angles as shown in Table 3.5a and 3.5b. The mode shape coordinates of the equipment were obtained by normalizing the transfer function values with respect to that for top of the equipment, and they are summarized also in Table 3.5a and 3.5b. The phase angles of all the mode shapes coordinates were close to zero. This means that the motions of the equipment at the specified locations were in phase with each other as can be expected for the fundamental mode of vibration. The fundamental mode shapes of the equipment in the two orientations are depicted graphically in Fig.3.17. The mode shape for the SS orientation exhibits a slight double curvatures. The mode shape for the equipment in the BF orientation is essentially linear. For practical purposes, both mode shapes may be approximated by a linear shape.

Since the transfer functions used to determined the mode shades were taken using measurements obtained at different locations on the

equipment, it is worthwhile to check the consistency of the frequencies and damping ratios determined from these transfer functions. Theoretically, the damping ratios and frequencies obtained from these transfer functions should be identical. As seen from Table 3.6, the fundamental frequencies obtained from the different transfer functions are the same. The four damping ratios obtained for the SS equipment orientation has an average of 0.94% and a standard deviation of 0.11%. For the BF orientation, the average damping ratio is 1.27%, and the corresponding standard deviation is 0.01%. The above results indicate that the method employed to determine the resonant frequencies and damping ratios of the test specimens leads to consistent results.

### 3.5 Determination of the Dynamic Properties of the Combined Equipment-Access Floor Systems

The resonant frequencies, damping ratios, and mode shapes of the combined equipment-access floor systems were also determined using the random excitation testing techniques. The various equipment and access floor system combinations considered are summarized in Table 3.7. The nomenclatures in Table 3.7 will be used in the discussions to refer to the different equipment and access floor combinations.

#### 3.5.1 Experimental Setup and Procedures

A typical experimental setup for the equipment supported on an access floor is shown in Fig.3.18. The equipment was mounted on a 9-panels (3x3) access floor system using a through-bolt arrangement. The

details of the through-bolt arrangement can be seen in Fig.3.19. The equipment was bolted to the shake table by four 0.5" (12mm) diameter threaded steel rods which extended downward to the shake table through holes pre-drilled on the floor panels. Two sets of anchoring fixtures were devised to provide the reactions for the four rods. As seen in Fig.3.19, each sets of anchoring fixtures consisted of a pair of steel channels arranged back-to-back running perpendicular to the four pairs of channels used to secure the access floor pedestals. These two pairs of channels were clamped to the shake table by threaded rods and dog plates. Two through-bolting rods were anchored on each pair of channels.

The equipment was tied down at the base-plate by tightening the nuts of the four threaded rods. Due to the flexibility of the floor panels, only a limited amount of torque could be applied to the equipment base-plate without causing excessive floor panel deflection. The torque applied to tighten the rods was approximately 15ft-lb (20N-m). This corresponds to only 25% of the torque applied to the expansion anchors when the equipment was mounted on slab. The torque of each through-bolting rod was always checked before and after each test.

The locations of the equipment in the SS and the BF orientations on a 9-panel access floor can be seen in Fig.3.20. To facilitate the discussion later on, the 9-panel access floor is subdivided into three strips along the direction of shaking, namely, the center strip and the two side strips. In the SS orientation the equipment occupies only the center strip of panels whereas in the BF orientation, the equipment overlaps all three strips of panels.

The instrumentation for the equipment-access floor systems in the

SS and the BF orientation can also be seen in Fig.3.20. The accelerations at the top of the equipment were monitored by two accelerometers mounted at the two front corners (designated as E1 and E2). Two accelerometers were also placed at the two front corners of the access floor (designated as F1 and F2). An accelerometer was also used to measure the shake table motion. The accelerometer signals were fed into signal conditioners which amplified and filtered the signals. The transfer function between the acceleration measured by each of the accelerometer on the equipment-access floor system and the acceleration of the shake table were determined in turn by a spectrum analyzer.

The frequencies and damping ratios of the various test setups were determined based on transfer functions obtained between the response acceleration at the top right corner of the equipment (E1) and the table acceleration. For the case where the equipment was mounted on the D12 floor system, four levels of random excitation which correspond to 2.5%, 5%, 10% and 20% of 1" table span were used. Both the bolted and drop-in panel attachment were considered for this floor system. For the D20 equipment-access floor system, only the first three levels of random excitation were used to avoid premature damage of the D20 access floor. Only the bolted panel attachment was considered for this system. The mode shapes were computed from the transfer functions between the acceleration response measured by each of the four accelerometers at the specified locations on the test specimen and the acceleration of the shake table. The random excitation level used for the determination of the mode shapes was 2.5% of 1" table span.

### 3.5.2 Observations and Results

#### *i. Equipment on D20 access floor*

A typical transfer function obtained from the random excitation test for the equipment in the SS orientation on the D20 access floor is shown in Fig.3.21. Two dominant response modes at a frequency of 4.7 Hz and 15.1 Hz can be seen. These two modes correspond to the first and second lateral mode of the system. The damping ratio for the first lateral mode is 1.6% and for the second mode 1.0%. For the case where the equipment is in the BF orientation, two dominant modes of similar frequencies were also observed. The frequencies and damping ratios of all the tests are summarized in Table 3.8.

For the range of excitation spans considered (2.5%, 5.0% and 10%), the first mode frequency varies between 4.6 to 4.7Hz for the equipment in the SS orientation, and between 4.56 to 4.65Hz for the equipment in the BF orientation. Between the two equipment orientations, the first mode frequencies are almost the same despite the fact that the equipment on the concrete slab is much stiffer in the BF than in the SS orientation. This is because in either orientation the equipment is much stiffer than the access floor, hence, it behaves as a rigid body on the access floor in both orientations. It is significant to note that first mode frequency of the combined equipment-access floor system (4.7Hz) is much lower than both the frequency of the access floor alone (14Hz from table (3.2)) and of the equipment alone (8.9Hz for the SS orientation). In the SS orientation, the second mode frequency varies between 14.7 to 15.1Hz, and in the BF orientation between 17.1 to 17.3Hz.

The first mode damping ratios range from 1.6% to 2.2% for the SS

orientation, and from 1.7% to 2.7% for the BF orientation. The second mode damping ratios range from 1.0% to 1.5% for the SS orientation, and from 0.9% to 1.4% for the BF orientation. The damping ratios in general increase as the excitation amplitude increases.

The mode shapes for the D20SS-B and the D20BF-B system were determined based on the transfer functions between the table acceleration and the relative response acceleration at each of the four specified locations on the test specimen. The values of these transfer functions at the corresponding fundamental frequencies are summarized in Table 3.9 and 3.10. The mode shape coordinates at the four locations are also summarized in the same tables for both response modes. The mode shape coordinates were computed by normalizing the transfer function values with the one obtained for the E1 location. The phase angle of the mode shape coordinates are denoted as "+" for in phase and "-" for out of phase depending on whether the phase angles are close to 0 or 180 degrees. The phase angles and the values of the mode shape coordinates at the two sides of the equipment-access floor system imply that the two modes identified are translational modes. The two mode shapes are shown graphically in Fig.3.22a for the D20SS-B system and in Fig.3.22b for the D20BF-B system. The values of the mode shape coordinates plotted are the average values for the two sides of the equipment-access floor systems. As seen from the two figures, the response motions at the access floor level and at the top of the equipment are in phase for the first mode and out of phase for the second mode. For the first mode response, the deformation between the access floor and the shake table is larger than that between the top of the equipment and the access floor.

*ii. Equipment on D12 access floor*

There are a total of four D12 equipment-access floor setups tested. Since these tests were carried out essentially in the same fashion as those for the D20 equipment-access floor systems, only the final results are presented and discussed here.

Two dominant response modes were observed in each of the four tests. The modal frequencies and damping ratios for each test are summarized in Table 3.11. The first and second mode frequencies are plotted against the excitation span in Fig.3.23a and 3.23b, respectively. Despite the variations in the type of access floor panel attachment and orientation of the equipment, the modal frequencies for the four different test setups are similar to each other. Both modal frequencies are higher for the case where the floor panels are bolted to the understructure of the access floor. The differences are particularly significant when the equipment is mounted in the SS orientation. The reason for such differences can be understood by examining the layout of the equipment on the access floor as shown in Fig.3.20. In the SS orientation, the equipment footprint occupied only the middle strip of the three strips of floor panels; consequently, bolting down of the floor panels enhances the rigid diaphragm action of the access floor to mobilize the stiffness of the two outer row pedestals. In the BF orientation, the equipment footprint overlapped all three strips of the access floor, hence, the stiffness of the two outer rows of pedestals is mobilized regardless of whether the panels are bolted down to the understructure or not. As a result, the effect of bolting down of the panels to the understructure is less pronounced in this case.

The damping ratios corresponding to the two response modes obtained for each test are summarized in Table 3.11 and plotted against the excitation span in Fig.3.24a and 3.24b. The damping ratios of the bolted panel systems in general are smaller than those of the drop-in panel system. Such differences in damping ratios are due to the fact that the panels were free to slide when they were not bolted down. As a result, energy was dissipated by friction and impact when the panels were sliding on the stringers. The differences in damping ratios between the bolted panel and drop-in panel arrangement are more prominent for the equipment in the SS orientation as compared to the equipment in the BF orientation.

The mode shapes for the two dominant response modes of the D12SS-B and D12BF-B equipment-access floor system are shown in Fig.3.25. The distortion of the access floor relative to the shake table in the first mode is less as compared to the mode shapes of the D20 equipment-access floor systems shown in Fig.3.22.

### 3.6 Summary and Conclusions

In this chapter, the dynamic characteristics of the access floors, the equipment, and the combined equipment-access floor systems were determined using the random excitation testing technique. Several conclusions are drawn from the study:

1. Under lateral excitation, the natural frequency of a multi-panels access floor can be predicted with reasonable accuracy (within  $\pm 10\%$ ) using a SDOF lumped mass model. The stiffness of this model can be computed based on the effective pedestal stiffness determined from the static test of a single panel access floor module.

2. An access floor is slightly stiffer and has less damping when its panels are bolted to the understructure.

3. In both the side-to-side and the back-to-front orientation, the equipment on the concrete slab has only one dominant mode of response in the frequency range of seismic excitation (less than 15Hz).

4. Two lateral vibration modes were identified for all the equipment-access floor systems tested.

5. The first mode frequencies of the combined equipment-access floor systems tested are substantially smaller than either the frequency of the access floor alone or that of the equipment alone.

6. The frequencies and damping ratios of the access floors, the equipment and the combined equipment-access floor systems are excitation amplitude dependent. In general, the frequencies decrease and the damping ratios increase as the excitation amplitude increases.

Table 3.1 Access floor configurations for random excitation testing

Test ID	Access Floor	Floor Config.	# of pedestal	Panel Mass,kg	Added Mass, kg
D12-11	D12	1x1 drop-in panel	4	14.1	-
D12-22	D12	2x2 drop-in panel	9	48.7	-
D12-33	D12	3x3 drop-in panel	16	107.6	-
D12-11M	D12	1x1 drop-in panel	4	14.1	68.6
D12-22M	D12	2x2 drop-in panel	9	48.7	271.3
D12-33M	D12	3x3 drop-in panel	16	107.6	511.5
D20-11	D20	1x1 drop-in panel	4	14.1	--
D20-22	D20	2x2 drop-in panel	9	48.8	-
D20-33	D20	3x3 drop-in panel	16	107.6	-
D20-11M	D20	1x1 drop-in panel	4	14.1	48.5
D20-33B	D20	3x3 bolted panel	16	107.6	-

Table 3.2 Resonant frequencies and damping ratios for various access floor configurations

Test ID	2.5% span		5.0% span		10% span		20% span	
	Freq (Hz)	Damp (%)						
D12-11	38.5	1.7	-	-	37.9	2.7	-	-
D12-22	31.2	1.4	29.8	4.2	29.7	4.5	28.9	5.6
D12-33	26.3	4.4	25.2	5.2	24.5	10.1	22.9	14.2
D1211-M	16.4	2.5	-	-	15.9	4.6	-	-
D12-22M	12.0	4.6	11.8	5.5	11.3	6.5	10.7	11.0
D12-33M	10.9	3.5	10.4	5.1	10.0	7.3	9.3	9.1
D20-11	17.4	1.7	17.1	3.1	16.9	4.3	16.3	7.9
D20-22	15.0	1.2	14.8	2.1	14.6	3.9	14.2	3.9
D20-33	13.2	2.2	12.8	2.9	12.7	3.4	12.3	5.4
D20-11M	8.7	2.2	8.6	3.5	8.3	4.5	8.0	6.1
D20-33B	14.0	1.1	13.9	1.2	13.6	1.5	13.4	2.4

Table 3.3 Comparison between experimental and analytically predicted resonant frequencies

a.) D12 access floor

Test ID	Analy. predicted	2.5% span	5.0% span	10% span	20% span
	Freq, Hz	Freq, Hz	Freq, Hz	Freq, Hz	Freq, Hz
D12-11	35.95	38.5 (-6.6) <sup>1</sup>	-	37.9 (-5.3)	-
D12-22	28.97	31.2 (-7.1)	29.8 (-2.8)	29.7 (-2.4)	28.9 (0.3)
D12-33	26.00	26.3 (-1.2)	25.2 (3.1)	24.5 (6.2)	22.9 (13.8)
D1211-M	14.83	16.4 (-9.6)	-	15.9 (-6.7)	-
D12-22M	11.31	12.0 (-5.8)	11.8 (-3.8)	11.3 (0.1)	10.7 (5.4)
D12-33M	10.84	10.9 (-0.8)	10.4 (3.7)	10.0 (8.4)	9.3 (17.2)

b.) D20 access floor

Test ID	Analy. predicted	2.5% span	5.0% span	10% span	20% span
	Freq, Hz	Freq, Hz	Freq, Hz	Freq, Hz	Freq, Hz
D20-11	17.17	17.4 (-1.6) <sup>1</sup>	17.1 (0.1)	16.9 (1.8)	16.3 (5.5)
D20-22	13.85	15.0 (-7.8)	14.8 (-6.2)	14.6 (-5.0)	14.2 (-2.3)
D20-33	12.43	13.2 (-5.5)	12.8 (-2.9)	12.7 (-1.8)	12.3 (1.4)
D20-11M	8.15	8.7 (-6.7)	8.6 (-5.6)	8.3 (-2.2)	8.0 (1.8)

<sup>1</sup> Values in brackets are discrepancies in % of experimental value.

Table 3.4 Equipment frequencies and damping ratios

Test ID	2.5% span		5.0% span		10% span		20% span	
	Freq (Hz)	Damp (%)						
Frame SS	8.91	0.70	8.82	0.92	8.71	1.22	8.55	1.82
Frame BF	13.2	1.23	13.1	2.40	12.9	3.60	12.5	4.21

Table 3.5 Equipment mode shapes

a.) side-to-side

Locations	Transfer function		Mode shape coordinate
	$ H(f_c) $	Phase, °	
Top	73.8	-102.3	1.00
3/4 height	60.0	-97.2	0.81
Mid height	31.8	-91.0	0.43

b.) back-to-front

Locations	Transfer function		Mode shape coordinate
	$ H(f_c) $	Phase, °	
Top	27.8	-90.9	1.00
Mid height	17.6	-83.6	0.63

Table 3.6 Frequencies and damping ratios computed from transfer functions obtained at different locations on the equipment

Location	side - to - side		Back - to - front	
	Freq., Hz	Damp., %	Freq., Hz	Damp., %
Top right	8.91	0.85	13.2	1.34
Top left	8.91	0.99	13.2	1.23
3/4 height	8.91	0.85	-	-
Mid height	8.91	1.06	13.2	1.24
Average	8.91	0.94	13.2	1.27
S.D., $\sigma$	0.0	0.11	0.0	.06

Table 3.7 Nomenclature for combined equipment-access floor test setups

Test ID	Access floor	Equipment-frame orientation
D12SS	D12 drop-in panel	Side to side
D12SS-B	D12 bolted panel	Side to side
D12BF	D12 drop-in panel	Back to front
D12BF-B	D12 bolted panel	Back to front
D20SSB	D20 bolted panel	Side to side
D20BF-B	D20 bolted panel	Back to front

Table 3.8 Resonant frequencies and damping ratios for equipment on D20 access floor

Test ID	2.5% span		5.0% span		10% span	
	Freq (Hz)	Damp (%)	Freq (Hz)	Damp (%)	Freq (Hz)	Damp (%)
D20SS-B	4.70 <sup>1</sup>	1.6	4.65	2.2	4.60	2.2
	15.1 <sup>2</sup>	1.0	14.9	1.3	14.7	1.5
D20BF-B	4.69	1.7	4.66	1.7	4.56	2.7
	17.3	0.9	17.2	0.8	17.1	1.4

Table 3.9 Mode shape for D20SS-B test setup, equipment side-to-side on D20 floor system with bolted panels

a.) First mode

Locations	Freq, Hz	Transfer function		Mode shape coordinate
		$ H(f_c) $	Phase, °	
Right frame	4.70	46.2	-74.0	1.00
Left frame	4.70	45.0	-88.2	0.97
Right floor	4.70	25.1	-96.0	0.54
Left floor	4.70	31.1	-86.6	0.67

b.) Second mode

Locations	Freq, Hz	Transfer function		Mode shape coordinate
		$ H(f_c) $	Phase, °	
Right frame	15.1	12.2	98.2	1.00
Left frame	15.1	12.1	84.7	0.99
Right floor	15.1	11.1	-97.4	-0.91
Left floor	15.1	11.5	-88.4	-0.94

<sup>1</sup> First mode

<sup>2</sup> Second mode

Table 3.10 Mode shape for D20BF-B test setup, equipment back-to-front on D20 floor system with bolted panels

a.) First mode

Locations	Freq,Hz	Transfer function		Mode shape coordinate
		$ H(f) $	Phase, °	
Right frame	4.69	40.6	-67.0	1.00
Left frame	4.69	41.7	-85.5	1.01
Right floor	4.69	30.1	-83.7	0.74
Left floor	4.69	23.7	-82.0	0.58

b.) Second mode

Locations	Freq,Hz	Transfer function		Mode shape coordinate
		$ H(f) $	Phase, °	
Right frame	17.3	10.2	86.6	1.00
Left frame	17.3	8.3	84.9	0.81
Right floor	17.3	11.8	-97.3	-1.15
Left floor	17.3	11.8	-97.4	-1.15

Table 3.11 Resonant frequencies and damping ratios for equipment on D12 access floor

Test ID	2.5% span		5.0% span		10% span		20% span	
	Freq (Hz)	Damp (%)	Freq (Hz)	Damp (%)	Freq (Hz)	Damp (%)	Freq (Hz)	Damp (%)
D12SS	6.25 <sup>1</sup>	4.0	6.05	2.88	6.65	3.75	6.45	4.2
	19.1 <sup>2</sup>	1.9	18.3	3.24	18.0	2.5	17.6	3.0
D12SS-B	6.70	1.1	6.65	1.5	6.55	1.92	6.40	2.3
	19.5	0.8	19.4	1.8	19.0	1.6	18.5	2.5
D12BF	6.80	2.2	6.75	2.2	6.65	3.75	6.45	1.2
	20.5	1.1	20.3	1.8	20.1	1.8	19.6	-
D12BF-B	7.00	1.8	6.85	2.6	6.70	2.3	6.45	3.5
	21.0	1.3	20.8	1.9	20.1	-	19.6	-

<sup>1</sup> First mode

<sup>2</sup> Second mode

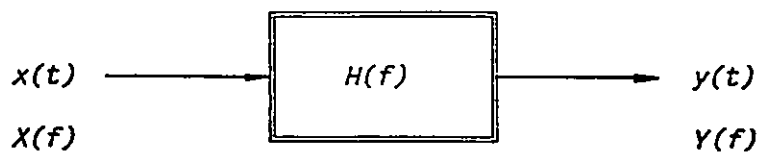


Fig. 3.1 Single input and single output system

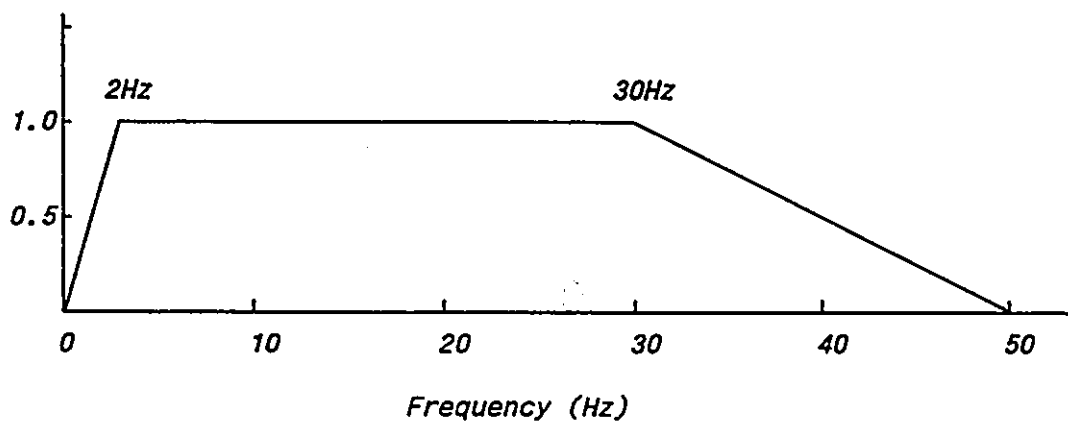


Fig. 3.2 Band passed filter for random acceleration time history

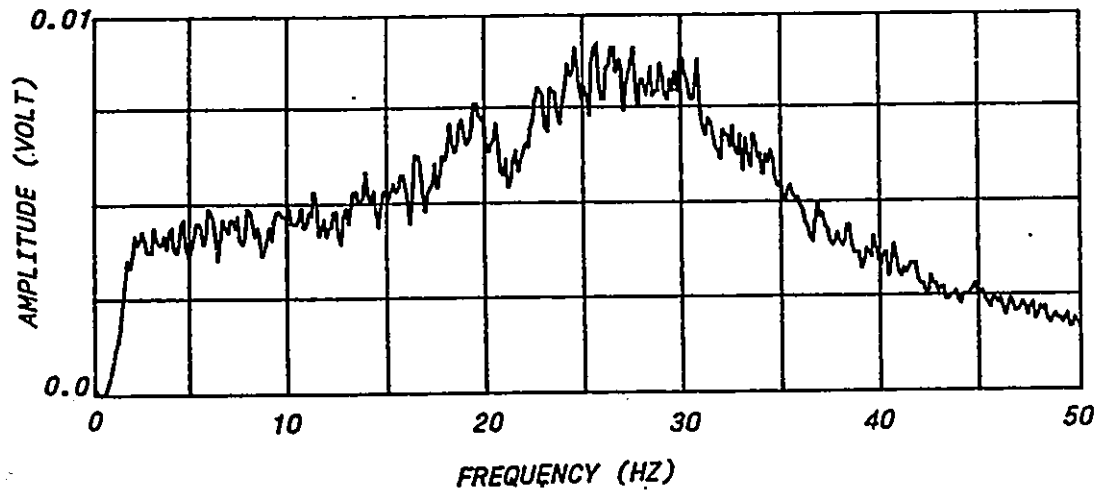
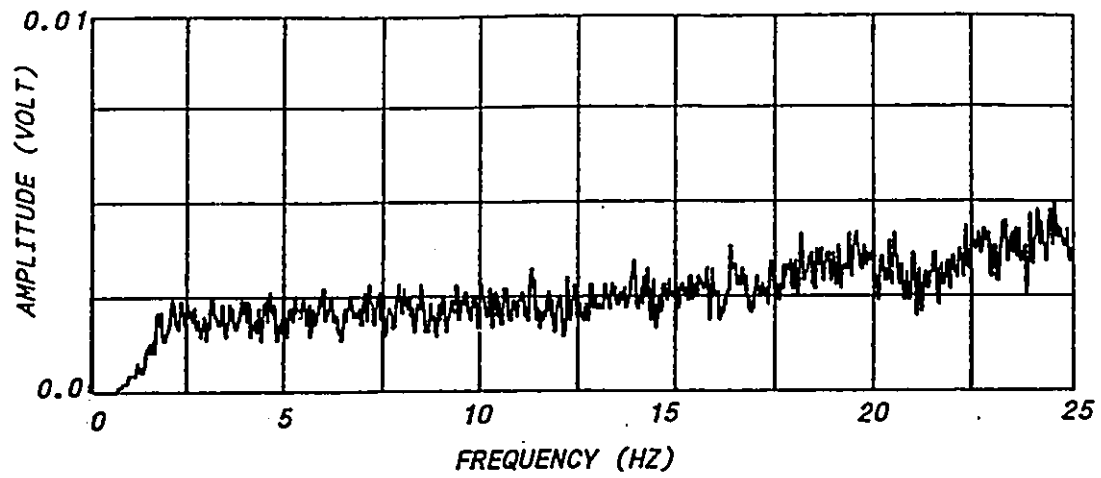


Fig. 3.3 Fourier spectra of random acceleration measured on the shake table

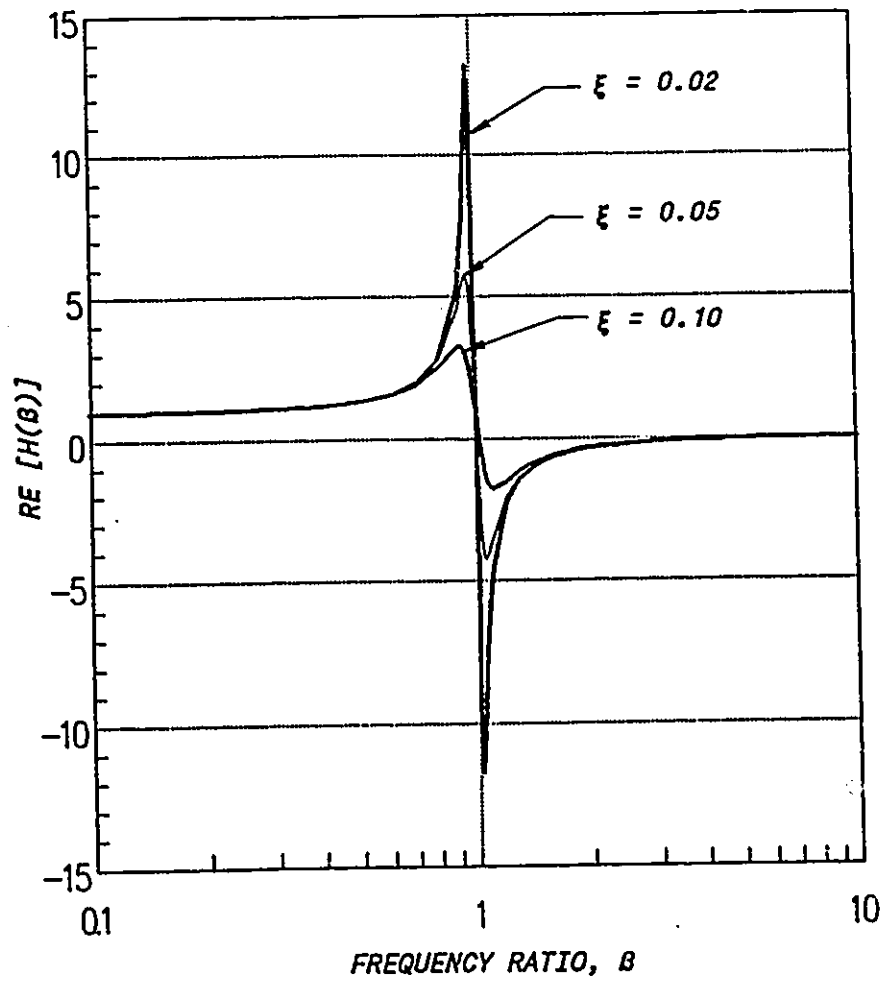


Fig. 3.4  $Re[H(f)]$  for different damping ratios

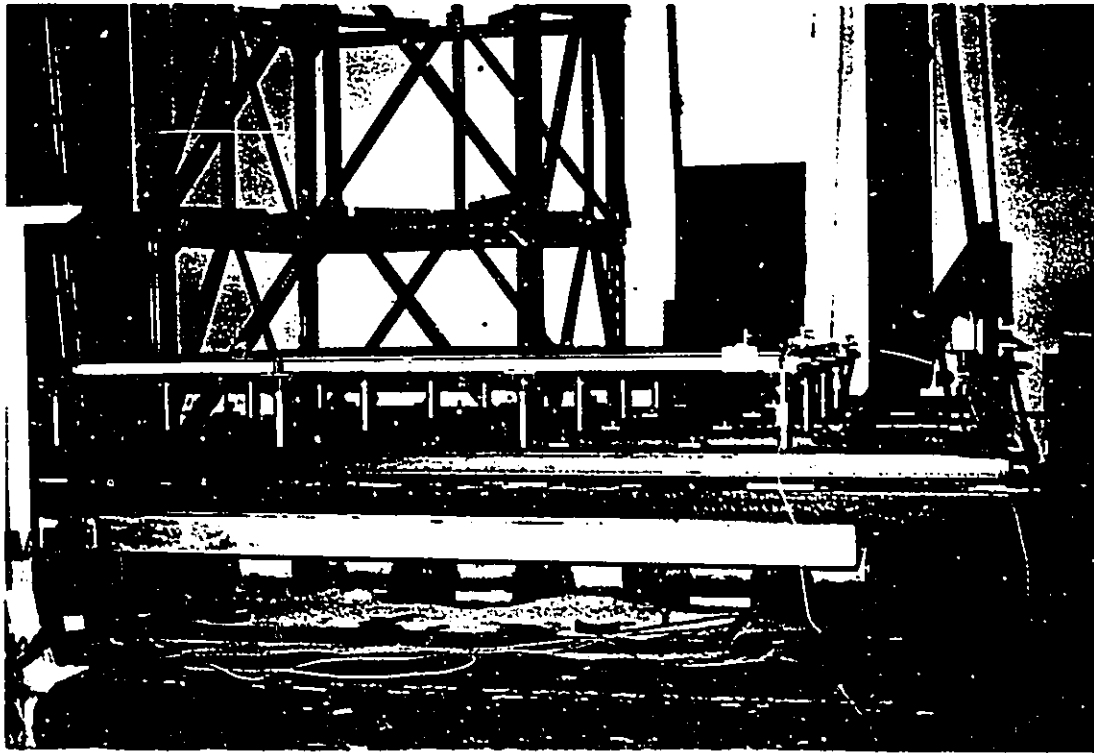


Fig. 3.5 A typical setup of a 3 panel by 3 panel access floor on shake table

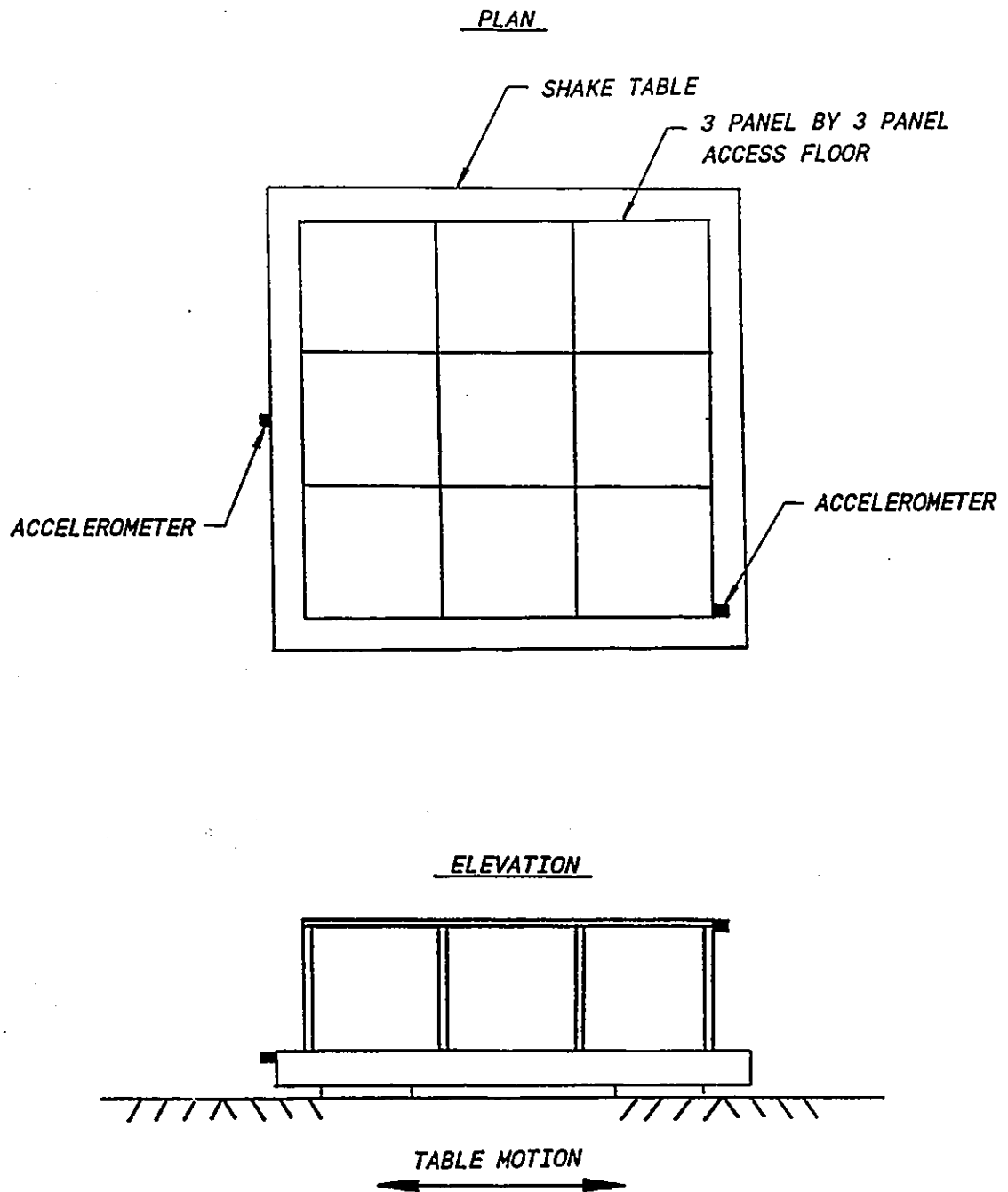


Fig. 3.6 Instrumentation for a 3 panel by 3 panel access floor test setup

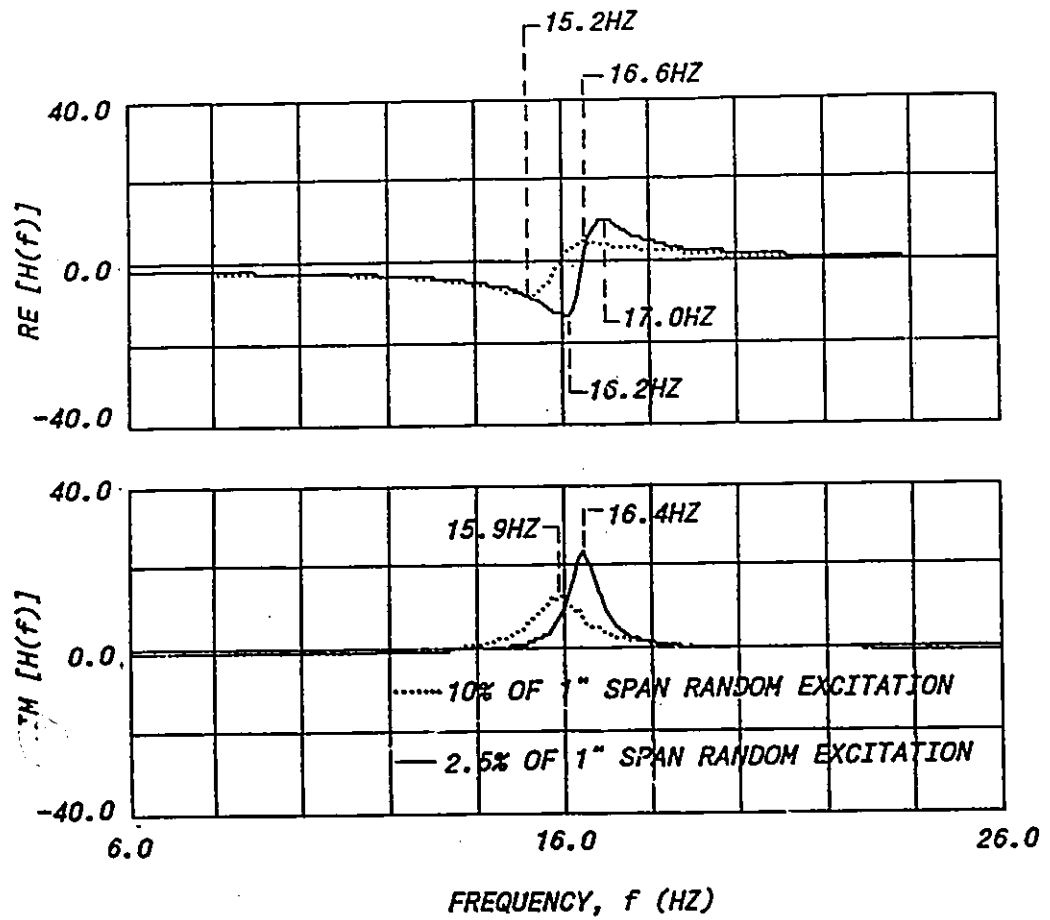
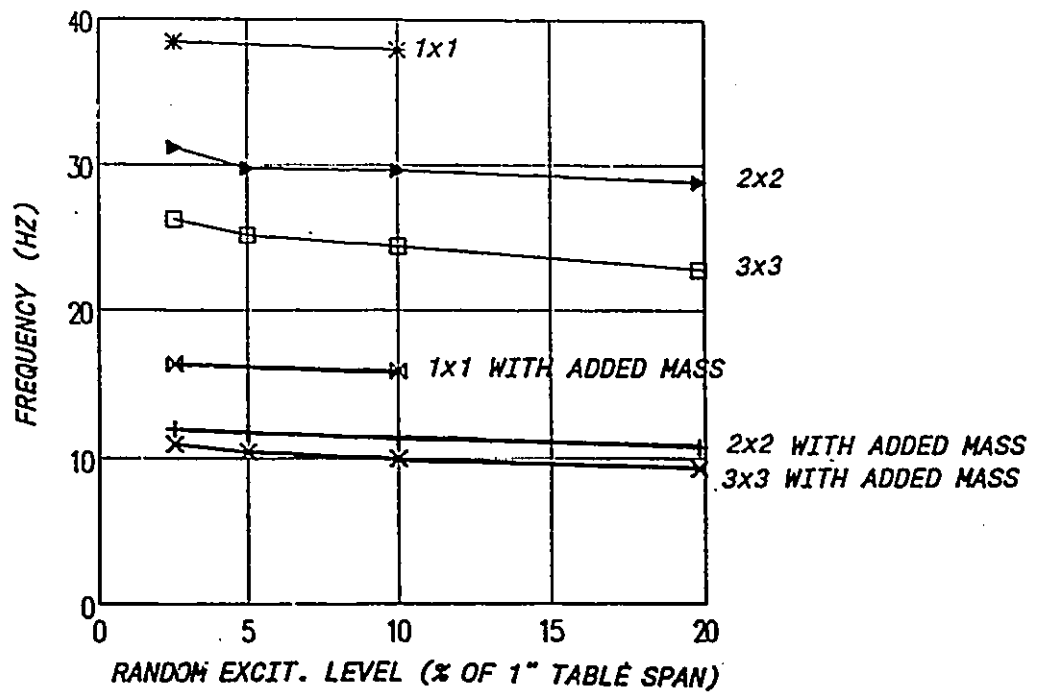


Fig. 3.7 Transfer function for D12-11M test setup

## a.) D12 Access Floor

PANEL ATTACHMENT: DROP-IN UNLESS SHOWN OTHERWISE



## b.) D20 Access Floor

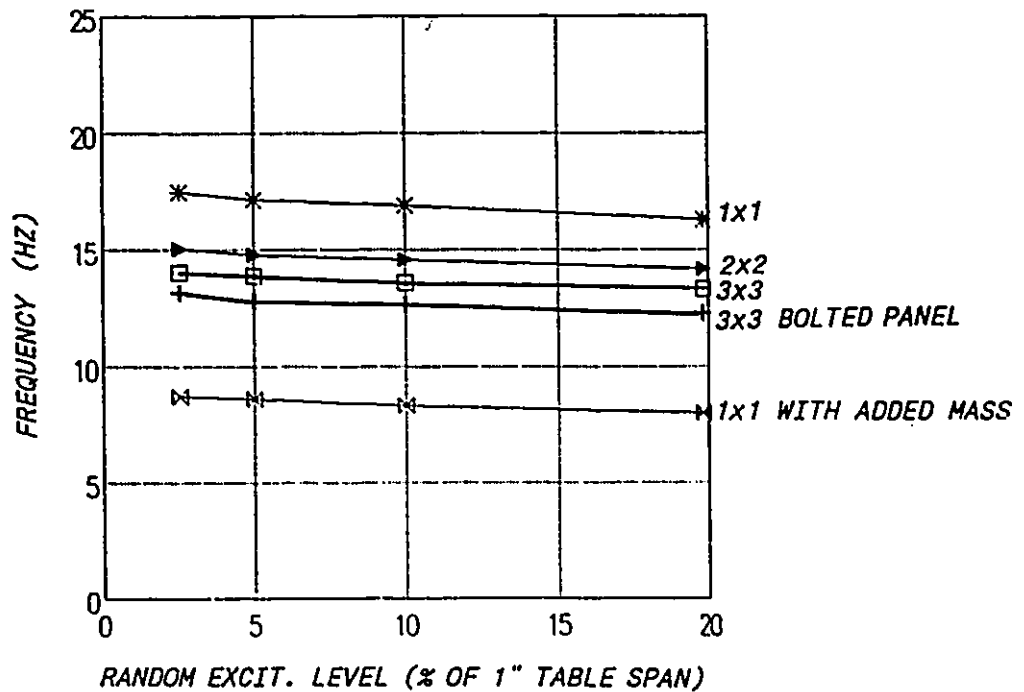
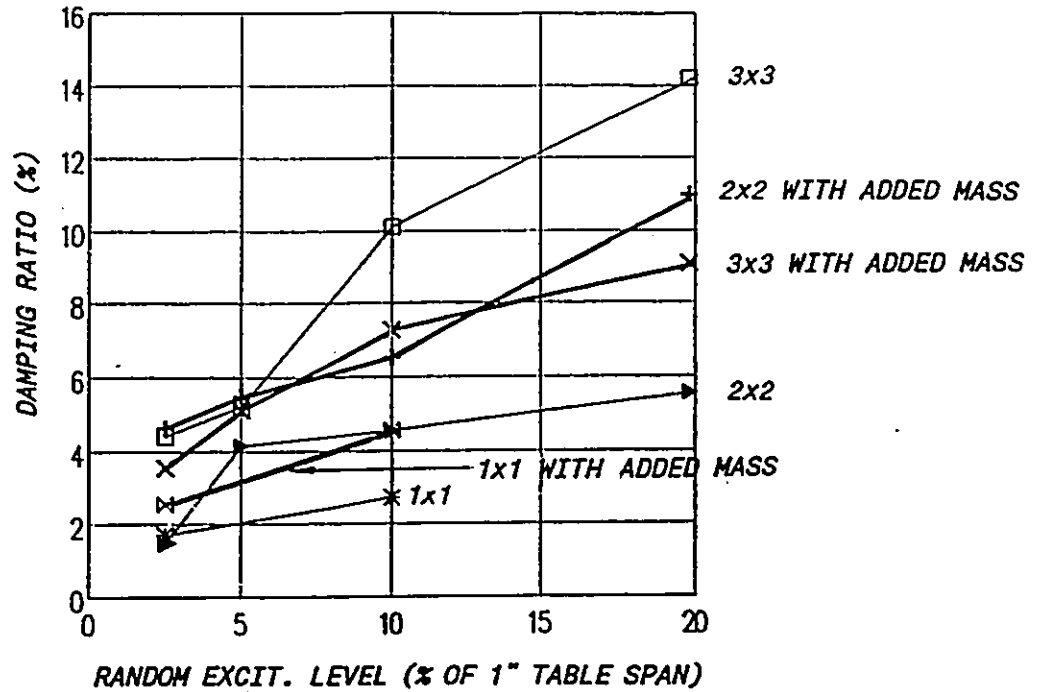


Fig. 3.8 Resonant frequencies obtained from random excitation tests for various access floor configuration: a.) D12 access floor and b.) D20 access floor

PANEL ATTACHMENT: DROP-IN UNLESS SHOWN OTHERWISE

a.) D12 Access Floor



b.) D20 Access Floor

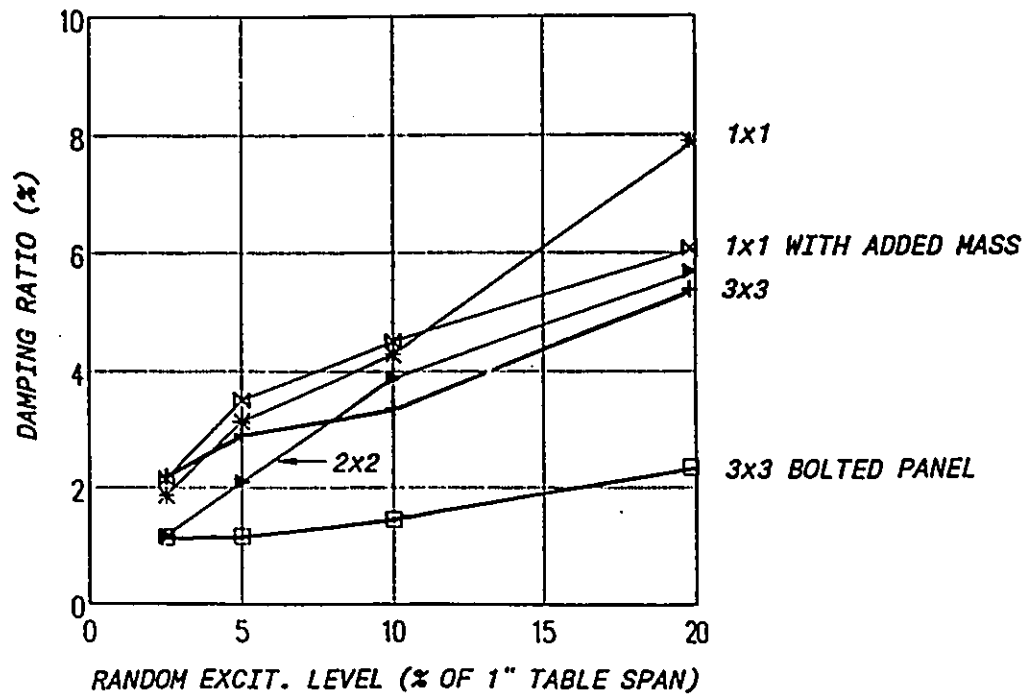
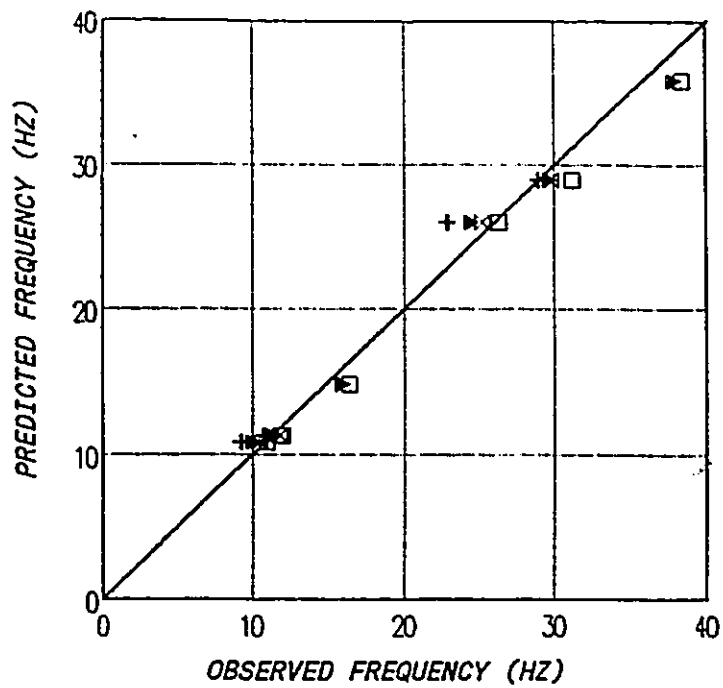


Fig. 3.9 Damping ratios obtained from random excitation tests for various access floor configuration: a.) D12 access floor and b.) D20 access floor

a.) D12 Access Floor



b.) D20 Access Floor

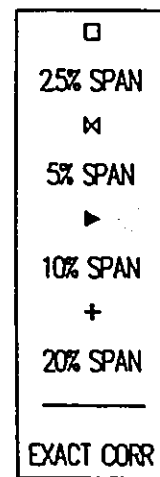
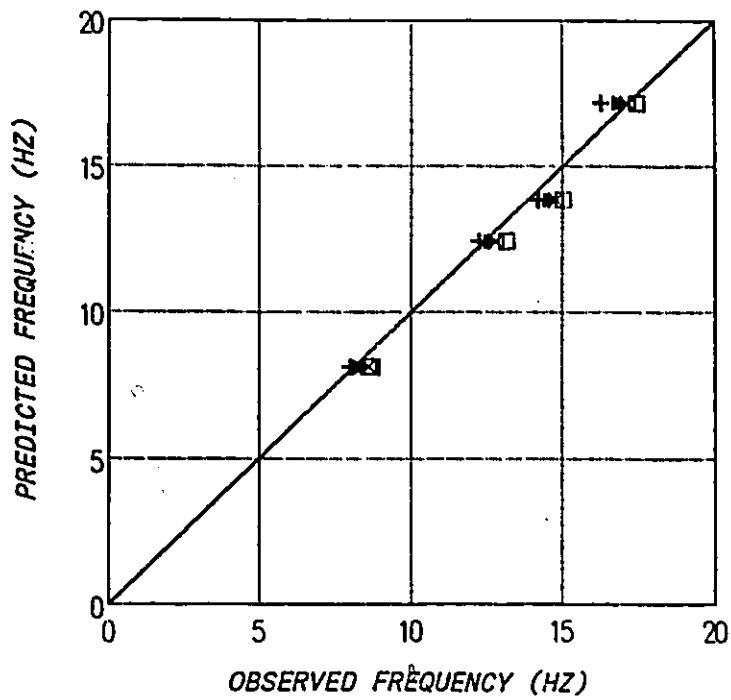


Fig. 3.10 Correlation between experimental and analytically predicted resonant frequencies: a.) D12 access floor and b.) D20 access floor

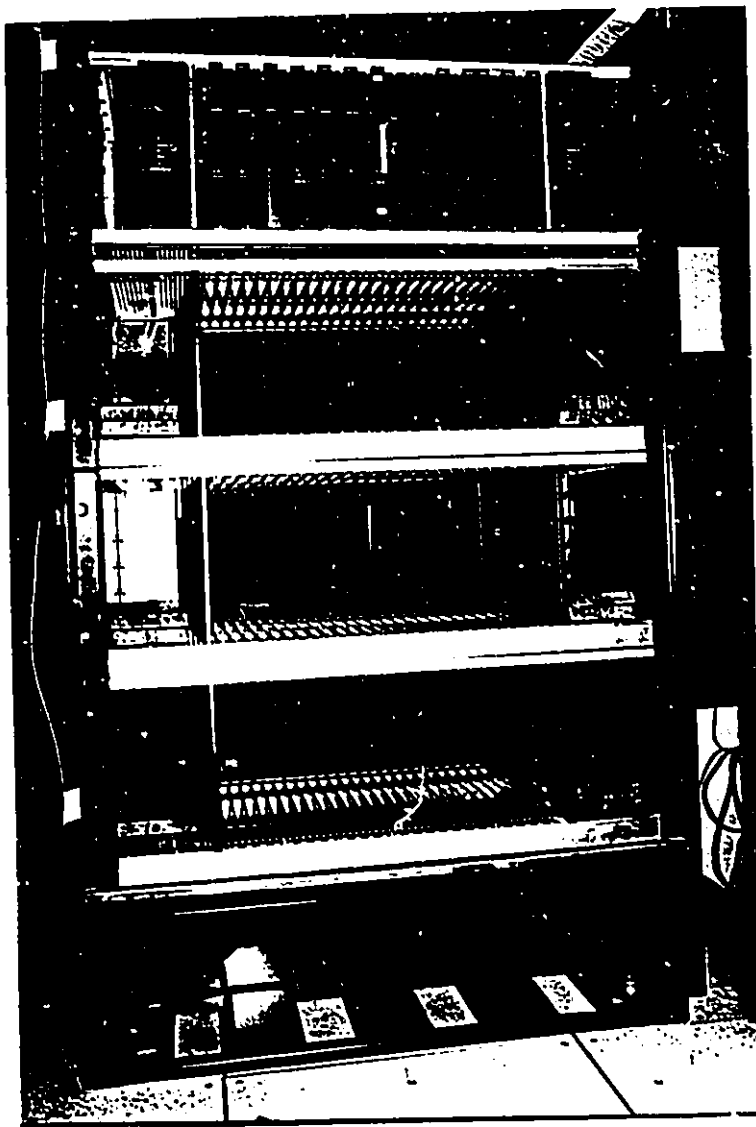


Fig. 3.11 Equipment used in this study

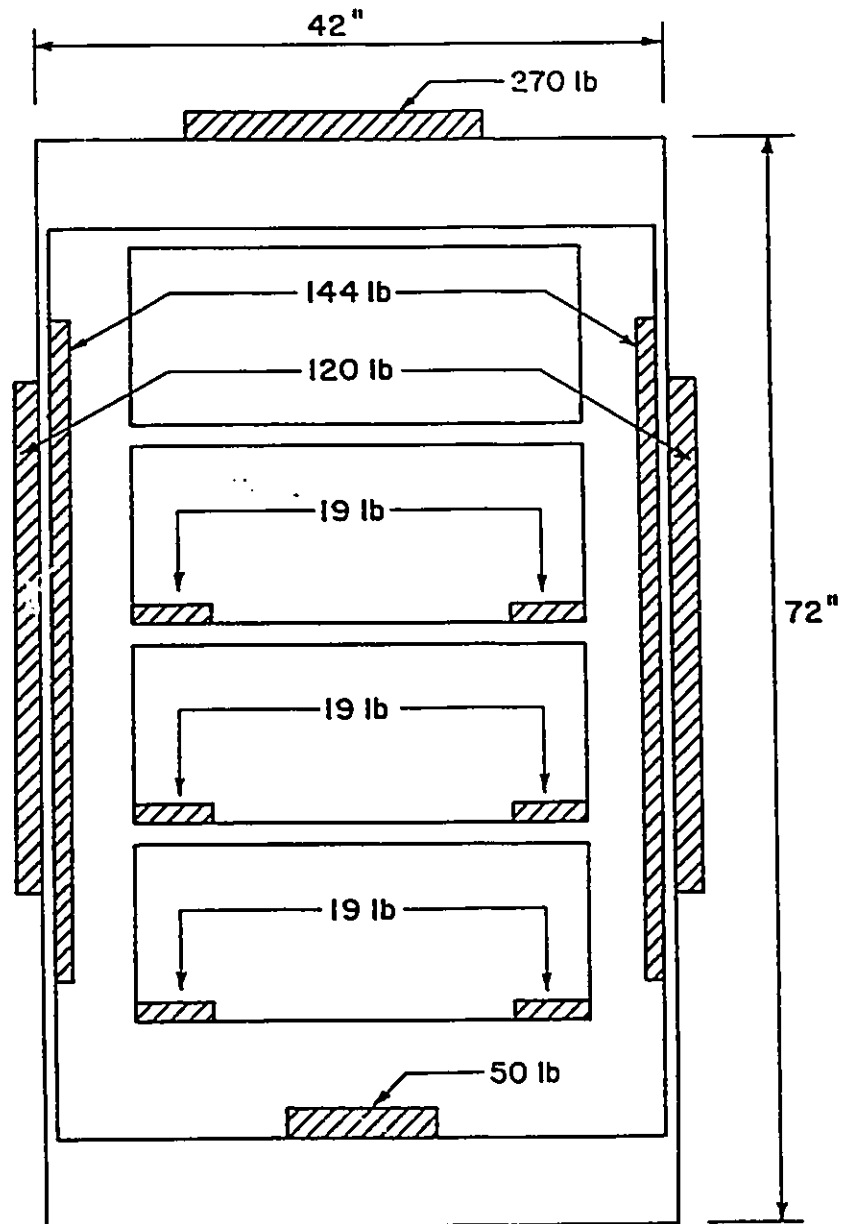


Fig. 3.12 Added mass distribution for the simulated equipment

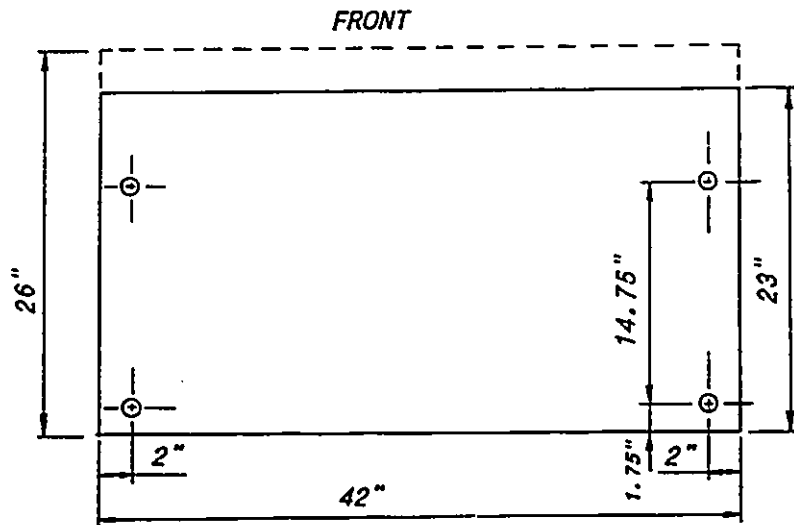


Fig. 3.13 Equipment anchor locations

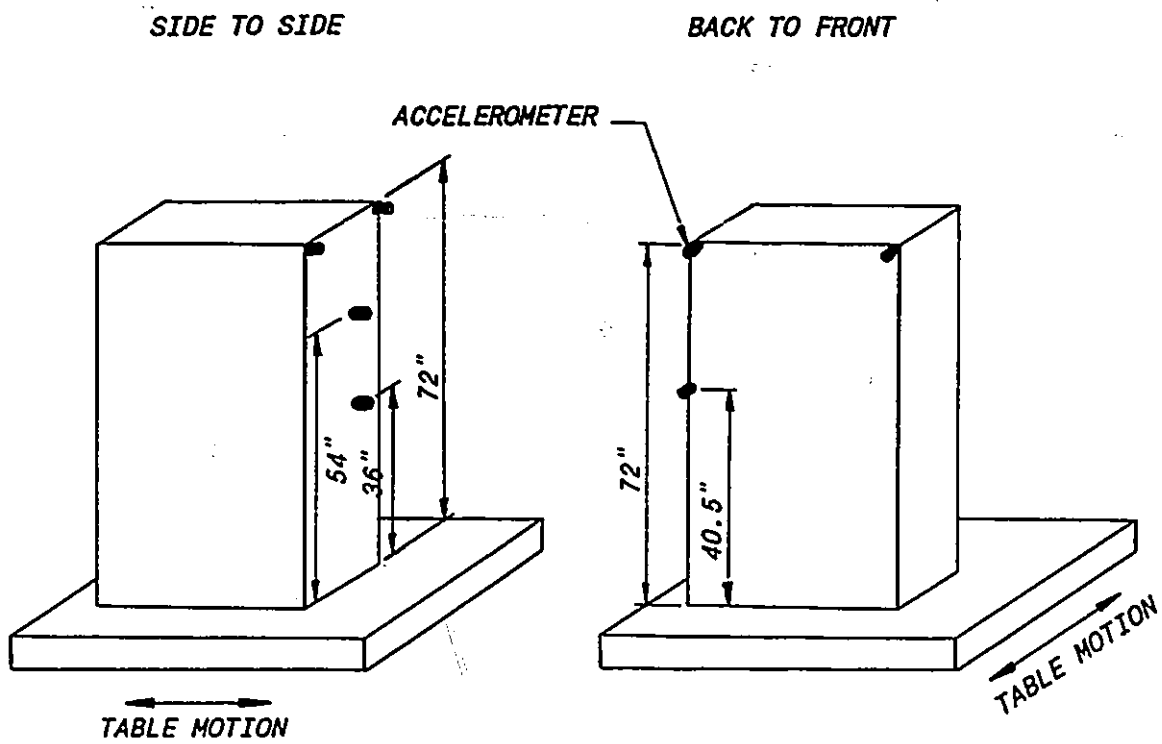


Fig. 3.14 Locations of accelerometers on equipment

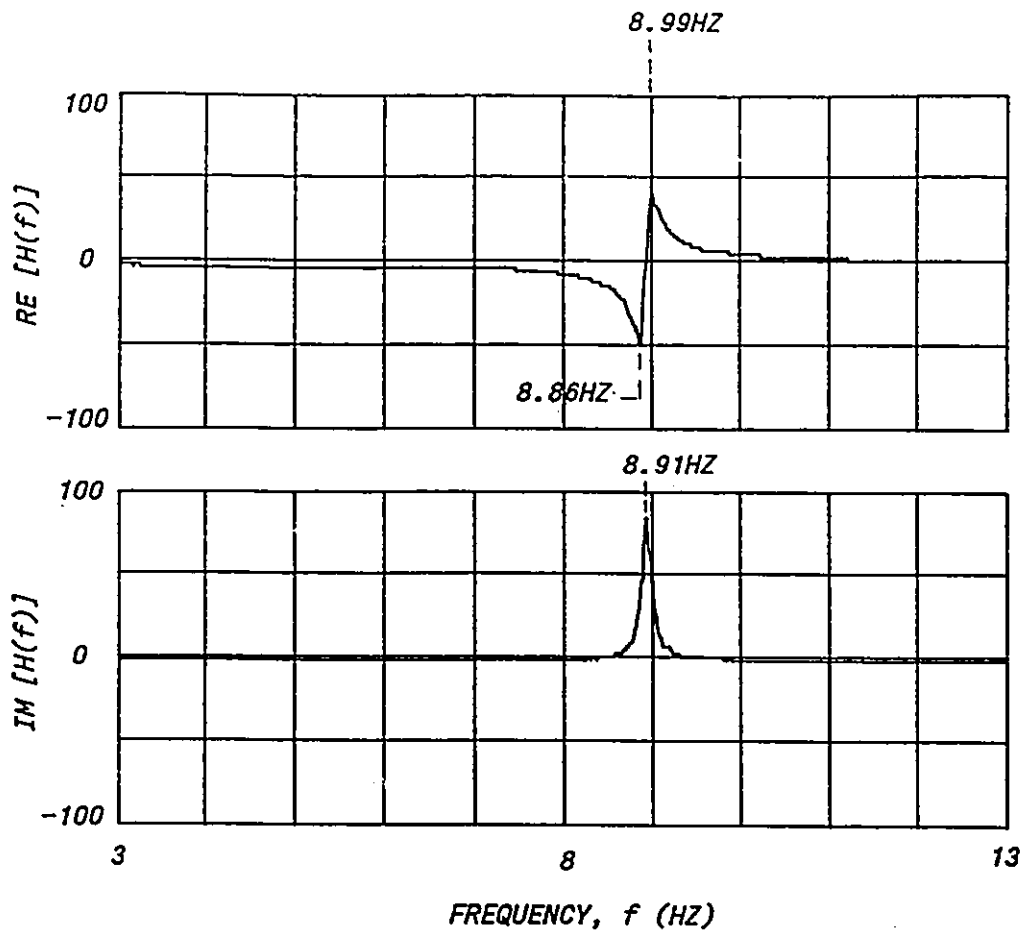
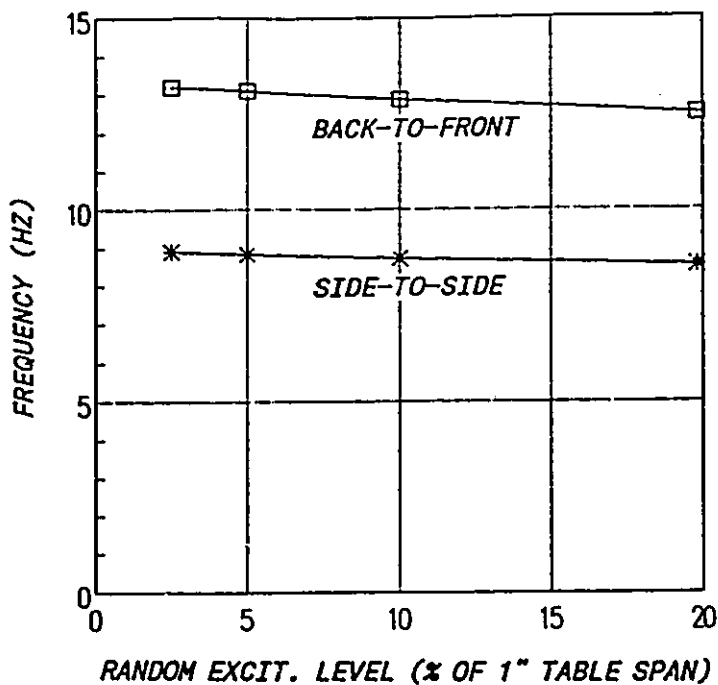


Fig. 3.15 Transfer function obtained for equipment in SS orientation on slab under a 2.5% span random excitation

## a.) FREQUENCY



## b.) DAMPING RATIO

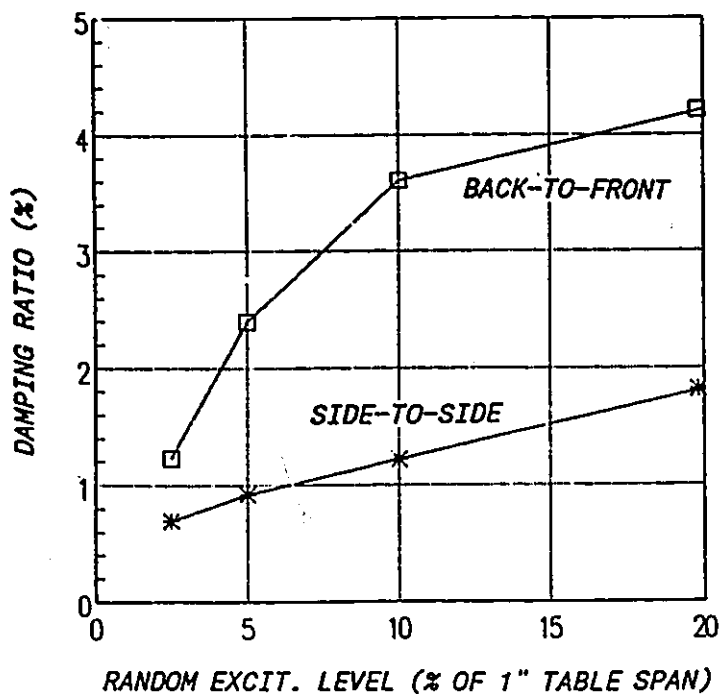


Fig. 3.16 Dynamic characteristics of equipment determined from random excitation tests: a.) frequencies and b.) damping ratios

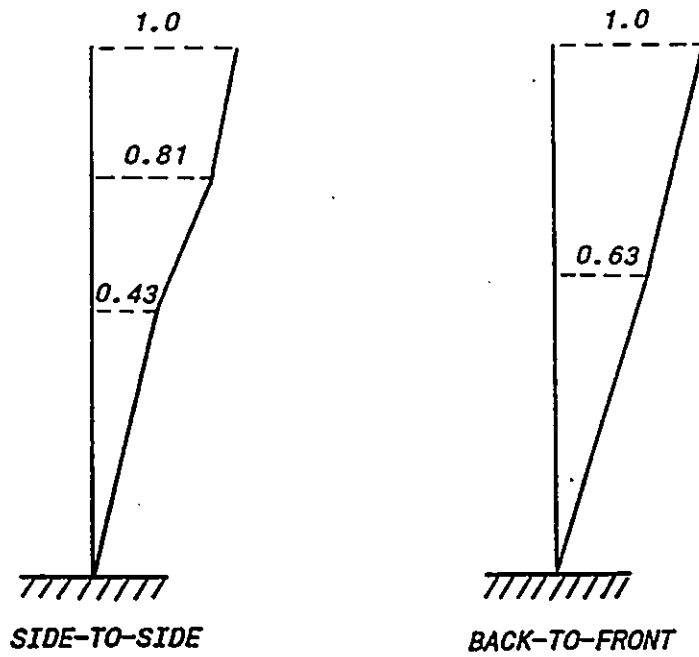


Fig. 3.17 Equipment mode shapes

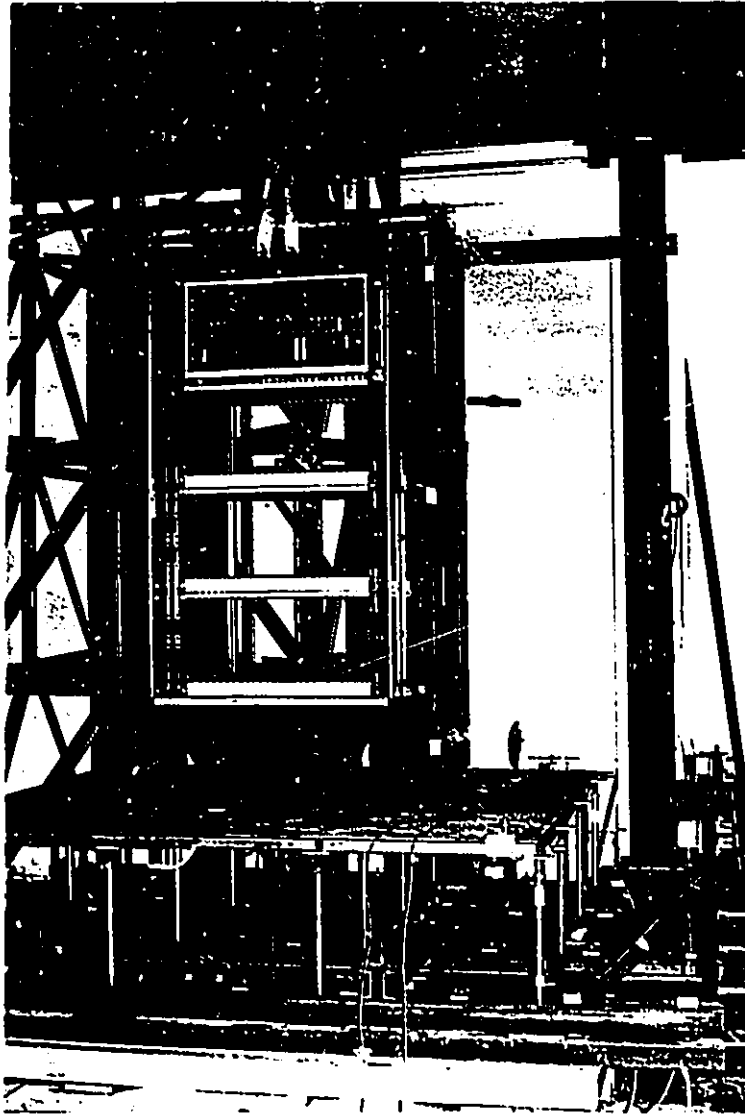


Fig. 3.18 Experimental setup for equipment on access floor

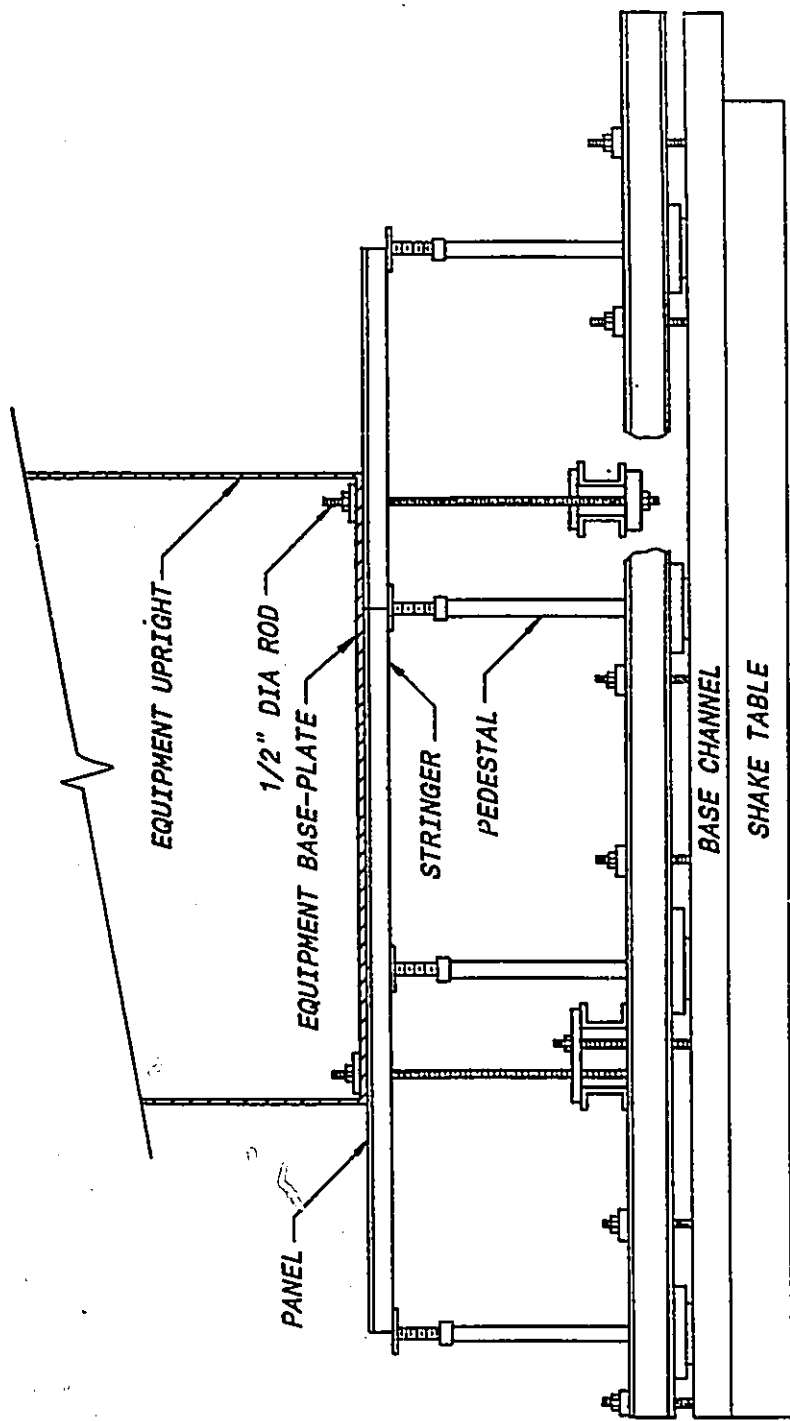


Fig. 3.19 Through-bolt equipment mounting arrangement

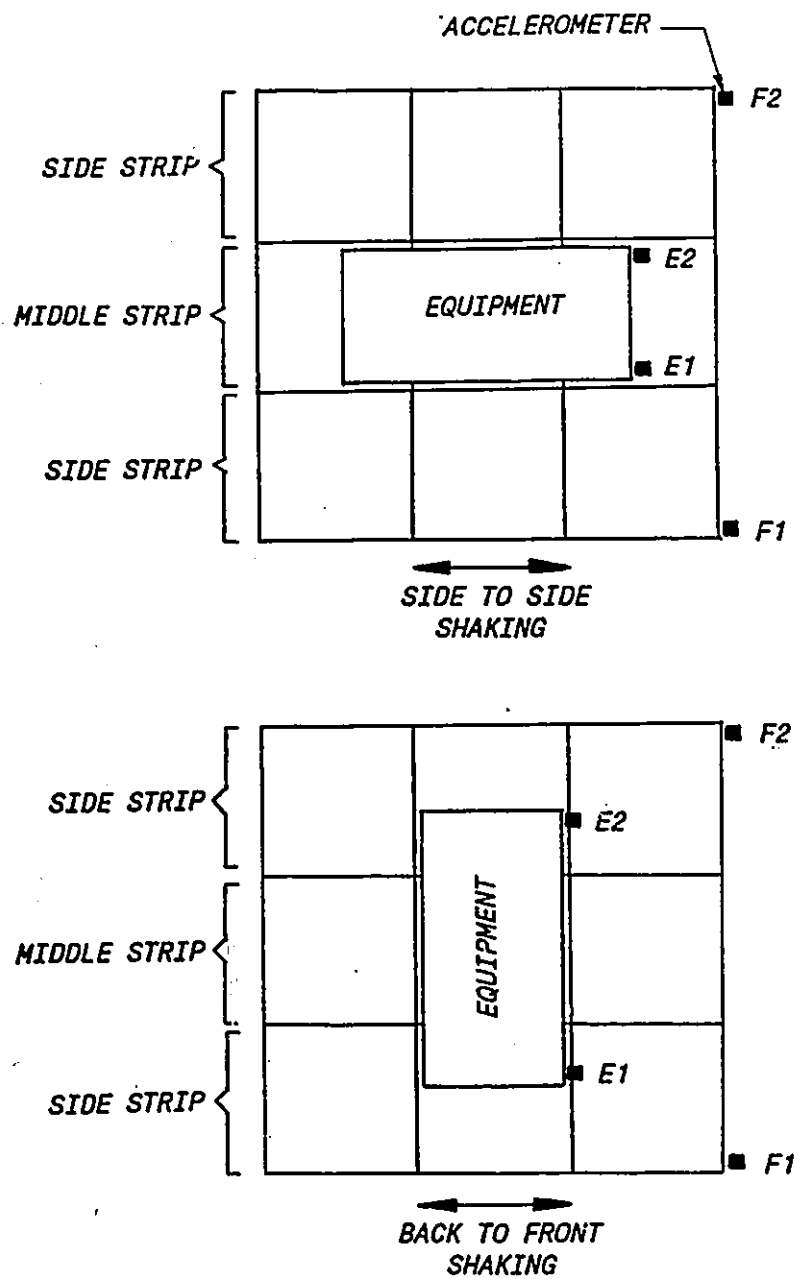


Fig. 3.20 Equipment layout on access floor

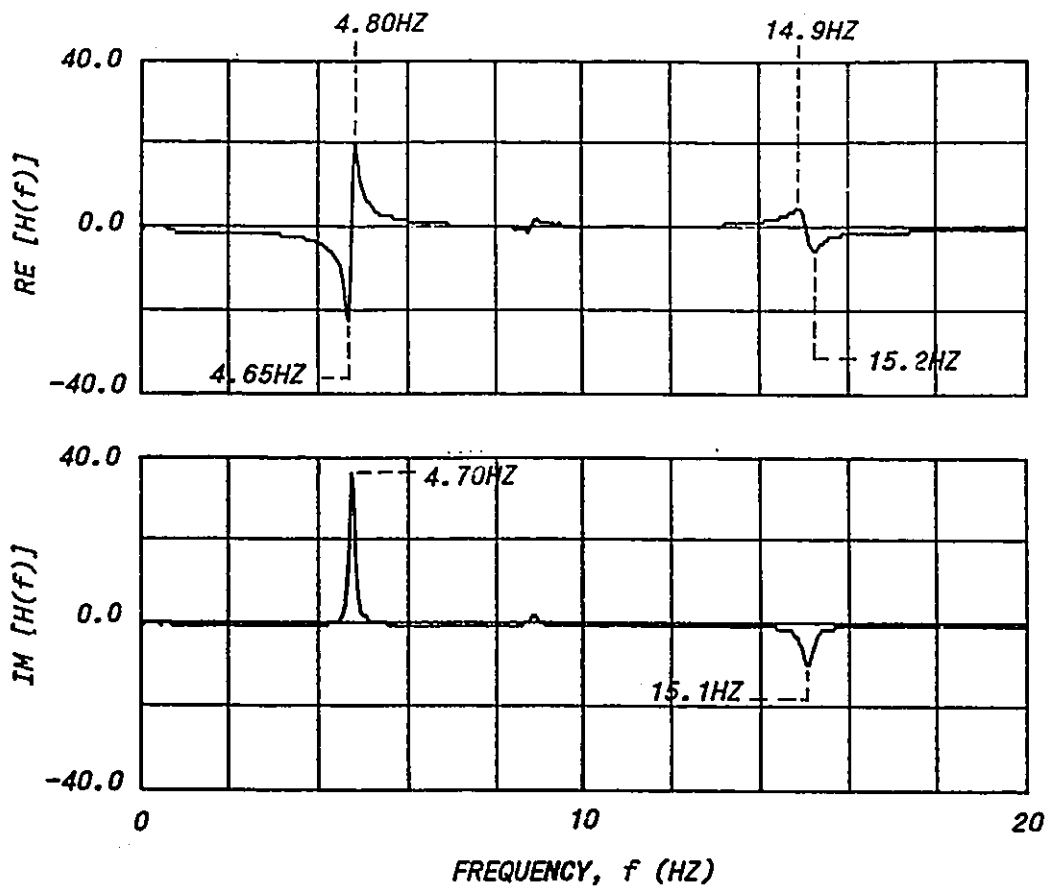
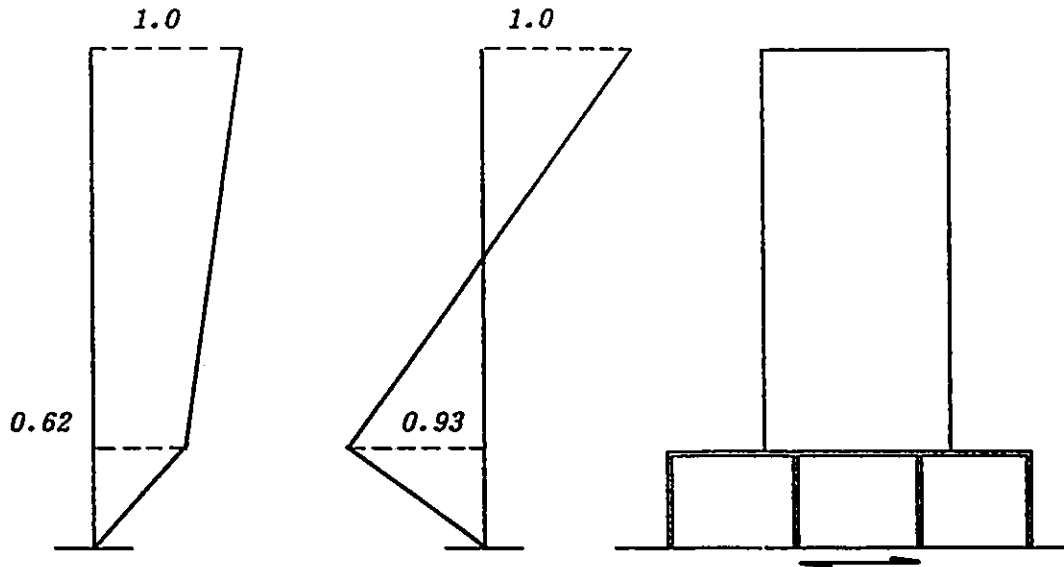


Fig. 3.21 Transfer function for the D20SS-B equipment-access floor system under a 2.5% span random excitation

## a.) SIDE-TO-SIDE EQUIPMENT ORIENTATION



## b.) BACK-TO-FRONT EQUIPMENT ORIENTATION

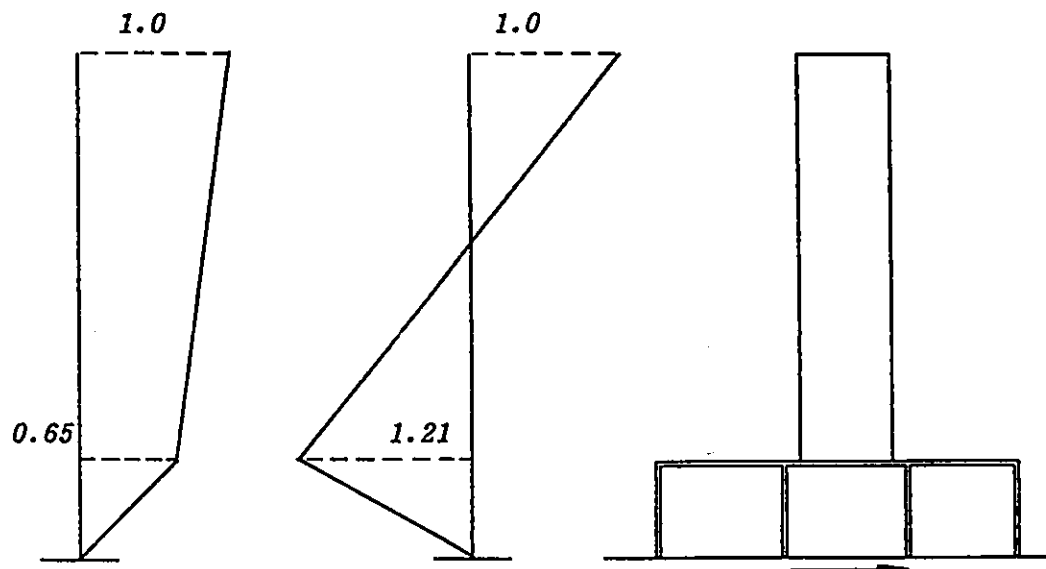
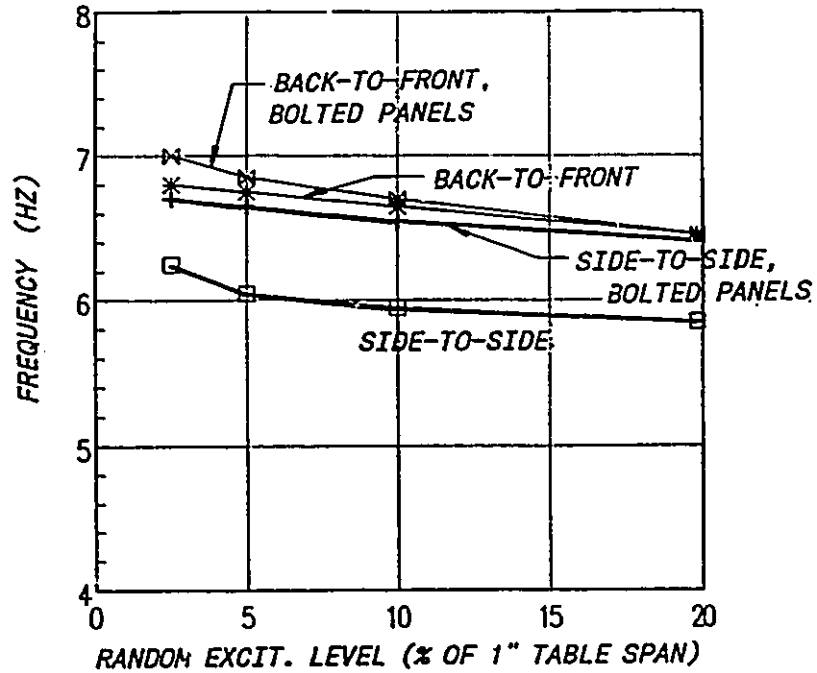


Fig. 3.22 Mode shapes for equipment on D20 floor system: a.) side-to-side and b.) back-to-front

## a.) First Mode



## b.) Second Mode

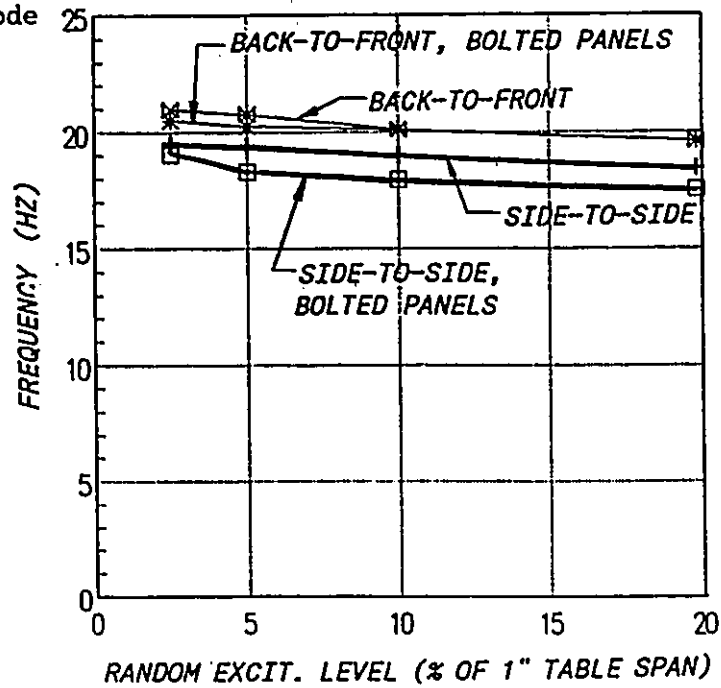
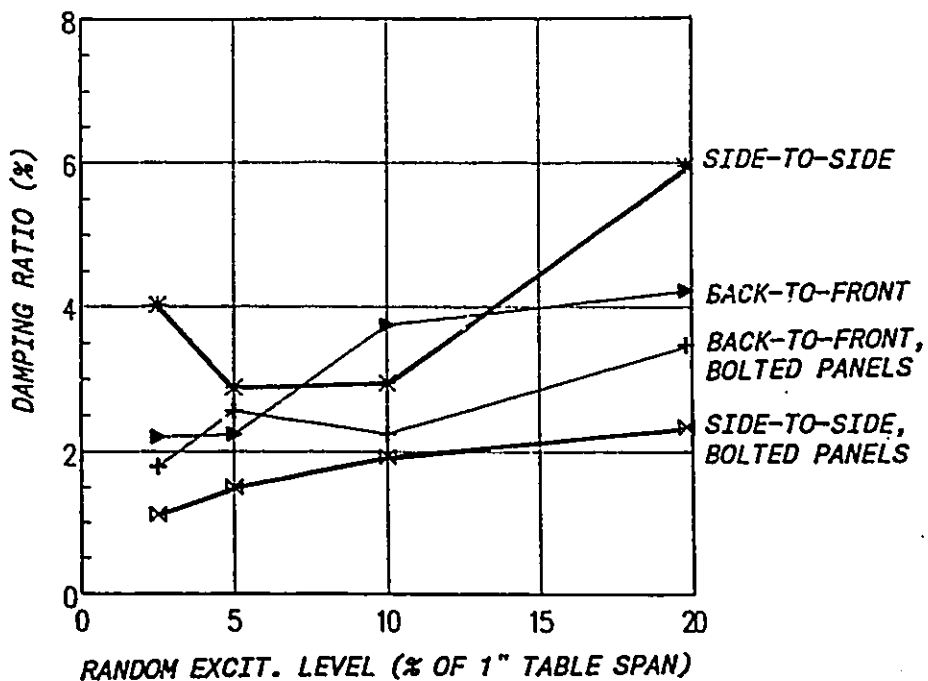


Fig. 3.23 Modal frequencies for equipment on D12 access floor: a.) first mode and b.) second mode

## a.) First Mode



## b.) Second Mode

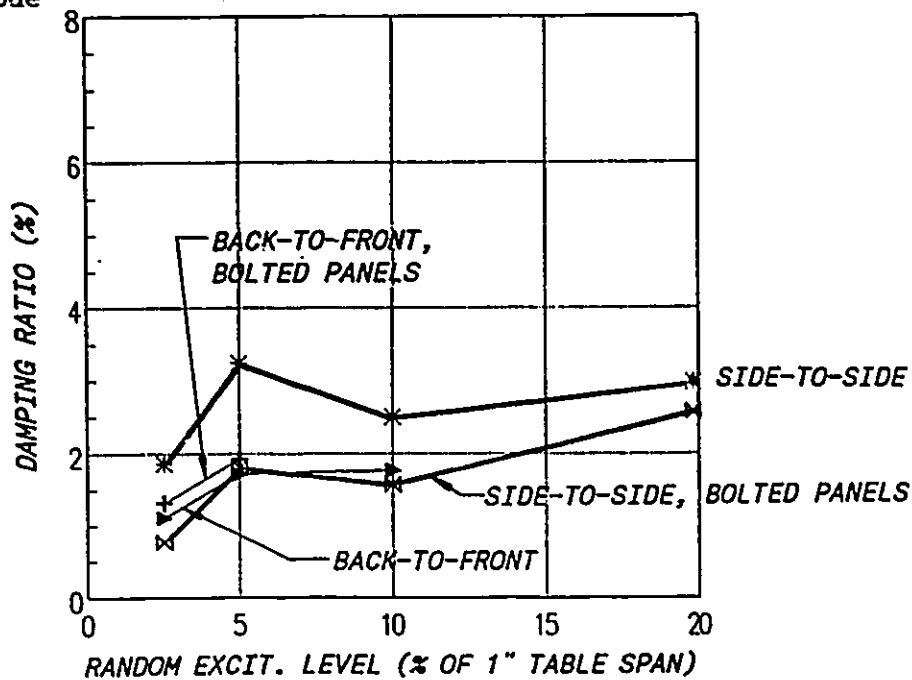
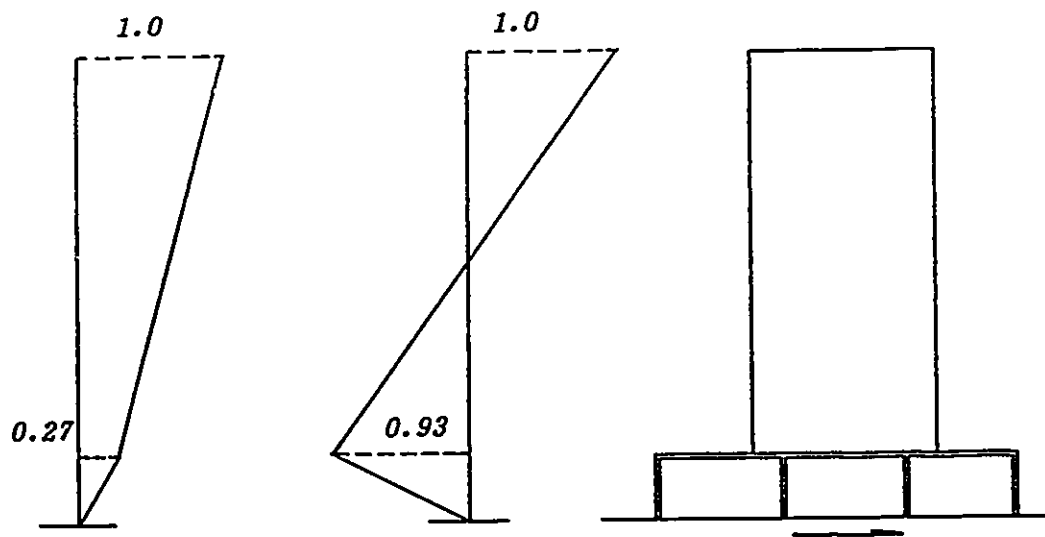


Fig. 3.24 Modal damping ratios for equipment on D12 access floor: a.) first mode and b.) second mode

## a.) SIDE-TO-SIDE EQUIPMENT ORIENTATION



## b.) BACK-TO-FRONT EQUIPMENT ORIENTATION

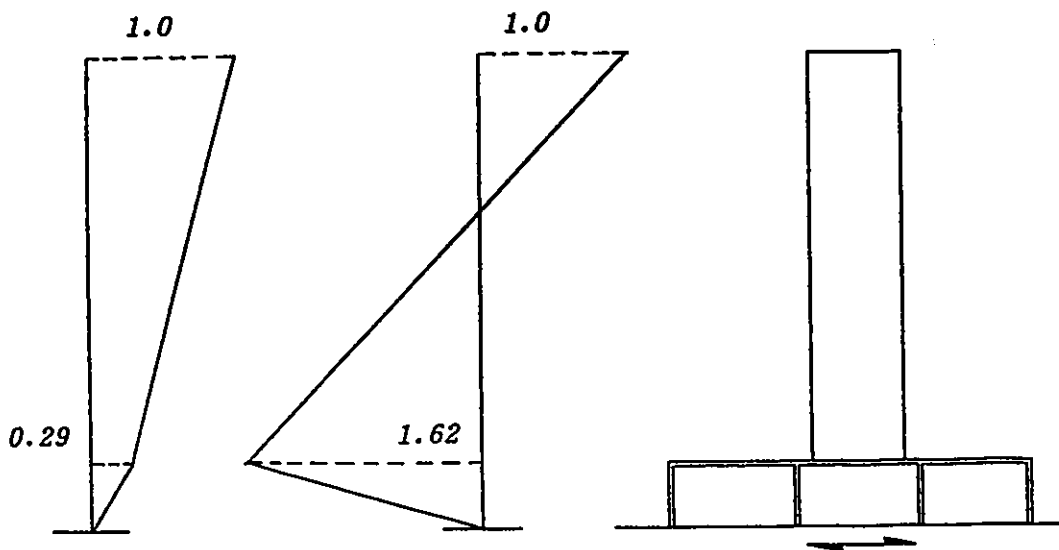


Fig. 3.25 Mode shapes for equipment on D12 access floor with bolted panels: a.) side-to-side and b.) back-to-front

## CHAPTER 4

### SEISMIC TESTING

#### 4.1 Introduction

The small amplitude random excitation tests described in the previous chapter have provided useful information on the dynamic properties of the access floors, the equipment, and the combined equipment-access floor systems. However, in order to understand the dynamic behaviour of equipment-access floor systems under earthquake induced-shaking, seismic tests are needed to be carried out. In this chapter, the seismic tests conducted for the equipment mounted on access floors as well as on a concrete floor slab are described. The primary objectives are to study the dynamic behaviour of the equipment on different access floor systems under earthquake conditions and to evaluate the differences between the dynamic response of the equipment installed on access floors and that on a fixed base.

#### 4.2 Excitation Time History

A suitable time history for seismic testing of equipment housed in buildings needs to reflect the potential floor motions of the buildings during earthquakes. In the telecommunications industry, an upper bound in-building floor excitation is characterized by the response spectra shown

in Fig.4.1. These floor response spectra are given in the Bell Communications Research Document entitled "Network Equipment-Building Systems-General Equipment Requirement" (Bell Communications Research, 1988), hereafter will be referred to as NEBS. They represent the upper bound floor motions which telecommunications equipment would experience in an earthquake of moderate to large intensity ( $V \leq \text{MMI} \leq X$ ). A brief summary of the rationale in deriving these floor response spectra is given here.

Telecommunications equipment in buildings are generally very light compared to the weight of the buildings. It is, therefore, reasonable to treat the building and the equipment as uncoupled systems where the in-building equipment response is dependent only on the motions of the attachment points of the equipment to the building. The attachment point motions are in turn dependent on several factors:

1. the locations of the attachment points along the height of the building;
2. the stiffness, mass distribution and energy dissipation characteristics of the building;
3. soil interaction at the foundation of the building; and
4. the seismic environment of the region where the building is located.

In many cases, the cost effectiveness of manufacturing mass-produced, interchangeable hardware, such as equipment frames, rules out the possibility of equipment design for a specific situation. As a result, the equipment must be designed such that it is capable to survive the upper-bound in-building floor motions induced by earthquake. The NEBS floor

response spectra were developed to represent such upper bound in-building floor motions. The derivation of the floor response spectra was given by Liu et al (Liu, et al, 1977), and the rationale behind it was discussed by Foss and Scobee (Foss and Scobee, 1980).

An acceleration time history compatible with the 2% damped floor response spectrum was given in the NEBS specification. This time history was modified to suit the requirements of the shake table control system. First, a high-pass filter with transition ramp between 0.4 and 0.5 Hz was used to remove the low frequency components associated with large displacements motions. The filtered acceleration time history is shown in Fig.4.2a. This time history was then numerically integrated to obtain the displacement time history shown in Fig.4.2b. This displacement time history was used as input to the shake table system. The time history has a 31 sec duration, a maximum displacement of 3.5" (8.9cm) and is capable of producing a maximum acceleration of 1g. It is discretized at 0.01 second intervals. This time history will be referred to as the NEBS time history in this thesis.

The discretized NEBS displacement time history was stored in the hard disk of the laboratory microcomputer. During a seismic test, the time history data were converted into analog form by the microcomputer and fed into the shake table control console to drive the shake table. The intensity of the shaking was controlled by the span setting on the shake table control console. A 70% span setting in the  $\pm 5"$  (12.7cm) stroke range would yield the full NEBS motion on the shake table.

The 2% damped response spectra computed from the measured accelerograms for the shake table motions of several different levels of

NEBS excitation are shown in Fig.4.3. The response spectra computed from these measured accelerograms conform to the target spectrum quite well in the frequency range between 2 and 10Hz which encompasses the natural frequency range of most telecommunications equipment.

#### 4.3 Seismic Tests of the Equipment Supported on a Concrete Slab

Seismic tests were carried out for the equipment mounted on a concrete slab. The objective for these tests was to establish a basis with which the seismic response of the equipment mounted on access floors is compared. The tests were carried out for both the SS and the BF equipment orientation using different levels of shaking.

##### 4.3.1 Experimental Setup

The experimental setup for the seismic tests was essentially the same as the random excitation tests except for the data acquisition arrangement. The instrumentation for the equipment tested in the SS and the BF orientation is shown in Fig.4.4. For both test orientations three accelerometers were mounted on the equipment to monitor the accelerations at the two top corners and the acceleration at the mid-height of the equipment. A  $\pm 20$ " range LVDT was used to measure the absolute displacement at the top of the equipment. An accelerometer and a LVDT were used to monitor the table motion. The two LVDT's used were string type LVDT's. Each LVDT was installed by mounting it on a fixed point along the axis of motion and attaching its string to the moving part whose displacement with respect to the fixed point was to be measured.

The signals of the four accelerometers were amplified and filtered by signal conditioners. The accelerometer signals and the LVDT signals were digitized by a microcomputer equipped with an analog to digital (A/D) converter. The digitized signals were stored in the hard disk of the microcomputer for processing.

The equipment was shaken for both SS and BF orientations with several levels of excitation ranging from 10% to full NEBS specified intensity. Prior to each test, the expansion anchors which tied the equipment to the slab were torqued to the specified 65 ft-lb (88 N-m) torque. After each test the torque of the anchors was checked. The LVDT at the top of the equipment frame was also checked for residual displacement.

#### 4.3.2 Observations and Results

There was no significant loss of torque in the four anchors for all of the tests performed. The residual displacements at the top of the equipment were also negligible. No equipment damage could be observed for all the tests carried out.

The digital data recorded in each test were processed and plotted. For each test, the relative displacement between the top of the equipment and the shake table was computed by subtracting the shake table displacement from the absolute displacement measured at the top of the equipment. The average acceleration at the top of the equipment was computed from the accelerations measured at the two corners of the equipment. The results of the tests will be shown and discussed separately for the equipment in the SS and the BF orientation.

*i. Back-to-front (BF) Orientation*

The time history traces obtained for the equipment tested in the BF orientation under full NEBS excitation are shown in Fig.4.5. The maximum accelerations in the acceleration traces measured at the top and at the middle of the equipment are 1.7 and 1.6g, respectively. The mid-height acceleration trace and the top acceleration trace of the equipment are very similar to the table acceleration trace in both frequency content and amplitude. Such behaviour implies that during the shaking the equipment was essentially acting as a rigid body riding on the shake table. This type of behaviour can also be seen from the relative displacement trace between the top of the equipment and the shake table. The maximum relative displacement is in the range of 0.3cm which corresponds to 0.2% of the height of the equipment. It should be noted that the relative displacement trace is only good for qualitative comparison. It was vulnerable to noise because its magnitude was only a fraction of a percent of the dynamic ranges of the LVDT's. The rigid behaviour of the equipment in the BF direction is not surprising since its frequency (12.5Hz from 20% span random excitation test) was well above the frequency range where there is significant energy in the NEBS spectrum (i.e. between 2 and 5Hz). The maximum values of the time histories obtained from the tests using different levels of NEBS excitation are summarized in Table 4.1.

The 2% damped spectra for the acceleration response are shown in Fig.4.6. Below a frequency of 5Hz the spectra for the accelerations at the table, at the mid-height and at the top of the equipment essentially coincide with each other. The natural frequency of the

equipment can be identified by a peak at a frequency between 12Hz and 13Hz. This frequency corresponds well with the frequency of 12.5Hz obtained from the 20% span random excitation test.

ii. *Side to Side (SS) Orientation*

The time histories shown in Fig.4.7 were obtained for the tests performed for the equipment in a side-to-side orientation under an excitation of full NEBS intensity. The acceleration and relative displacement time histories of the equipment are dominated by a frequency component of approximately 8Hz. A maximum acceleration of 2.7g was attained at the top and 2.0g at the middle of the equipment. The corresponding maximum relative displacement of the equipment was 1.3cm. In an overall sense, the acceleration amplitude at the top of the equipment is almost two times that of the table. The maximum values of the time histories traces obtained from the tests using different levels of NEBS excitation are summarized in Table 4.2. Comparing to the maximum acceleration values for the back-to-front orientation in Table 4.1, the equipment experienced a higher acceleration response in the side-to-side orientation.

The 2 % damped response spectra for the response acceleration traces are shown in Fig.4.8. The major peaks of the top acceleration and mid-height acceleration spectra occur at a frequency of approximately 8Hz. This frequency corresponds well to the frequency of 8.5Hz determined by the 20% span random excitation test.

The seismic test results presented so far will form the basis of comparison with the response of the equipment when it is supported on

access floors.

#### 4.4 Seismic Tests of the Equipment Supported on Access Floors

Dynamic tests were carried out to study the seismic behaviour of the equipment mounted on access floors. The tests were carried out with the equipment installed on both D12 and D20 access floor system. In two of the test setups, the level of excitation was increased until the access floors were damaged.

##### 4.4.1 Experimental Setup

The equipment-access floor systems tested were installed on the shake table as described in the random excitation tests. The instrumentation for the equipment-access floor systems with the equipment in the SS and the BF orientation is similar. Four accelerometers and three LVDT's were attached on the equipment-access floor systems as shown in Fig.4.9. At the top of the equipment, two accelerometers were used to measure the acceleration at the two corners, and a LVDT was used to measure the absolute displacement at the center. At the access floor level, one accelerometer and one LVDT were used to monitor the motions at each of the two front corners (R1 and R4) of the access floor. The two LVDT's on the access floor have a measuring range of  $\pm 5$ " (12.7cm). They were mounted on two rigid brackets which were bolted onto the shake table. The strings of the two LVDT's were connected to the access floor. With such arrangement the relative displacements between the access floor and the shake table were measured. For some of the tests, the accelerometer

and the LVDT at the R4 position were moved to the R2 position in order to monitor the center strip motion of the access floor. An accelerometer and an LVDT were again used to measure the motion of the shake table. The signals of these instruments were recorded in a manner similar to the tests carried out for the equipment on the concrete slab.

The equipment was tested in both orientations on the D12 and the D20 access floor system. For the D12 equipment-access floor systems, the tests were conducted for both drop-in and bolted panel attachments. For the D20 equipment-access floor systems, the tests were carried out only for the bolted floor panel attachment. All of the test configurations are summarized in Table 4.3 and they will be referred to by their experiment designation in the subsequent discussions.

Prior to each test, the equipment tie-down rods were checked and re-torqued to approximately 20N.m (15 ft-lb). This relatively small torque was used to avoid causing excessive deformation of the floor panels.

#### 4.4.2 Observations and Results

The observations and results of the tests are discussed separately here for the D12 and D20 equipment-access floor systems. For each access floor system the tests which resulted in no damage to the access floor will be discussed first. The tests which led to partial failure of the access floors are discussed separately in a later section.

#### 4.4.2.1 Equipment on D12 Access-floor

##### *i. D12SS (Side-to-side) tests*

This series of tests was carried out for the equipment in a side-to-side orientation on the D12 access floor. Both the drop-in and the bolted panel attachment were considered. To facilitate the discussions, the equipment-access floor system with the drop-in panel attachment will be referred to as the "drop-in system" and for the system with the bolted panel attachment, as the "bolted panel system".

For all the D12SS tests conducted, no significant loss of torque was observed in the four tie-down rods after a 25% and a 50% NEBS excitation. The acceleration time histories measured under a 50% NEBS excitation are shown in Fig.4.10 and Fig.4.11 for the drop-in panel system and the bolted panel system, respectively. In each figure, the accelerations measured at the table, at the side strip (R1) and the center strip (R2) of the access floor and at the top of the equipment are shown. Since the accelerations measured at the two top corners of the equipment are very similar, only the average of the two is shown here. It can be seen that for both the bolted and the drop-in panel system, the amplitude of the acceleration at the access floor level is about twice that of the table, and the amplitude of the acceleration at the top of the equipment is approximately twice that of the access floor. In other words, the amplitude of the shake table motion was amplified four times at the top of the equipment. Such amplification leads to a maximum acceleration of approximately 2g at the top of the equipment.

For the drop-in panel system, the amplitude of the acceleration

measured at the center strip (R2) of the access-floor is larger than that of the edge strip (R1) as seen in the second and the third trace in Fig.4.10. For the bolted panel system, no such difference is seen between the accelerations at the center strip (R2) and at the edge strip (R1) of the access floor.

The displacement traces for the drop-in panel system are shown in Fig.4.12. Significant difference exists between the displacements at the center strip (R2) and at the side strip (R1) of the access floor. Such large difference in floor displacement for the drop-in panel system was due to the lack of in-plane stiffness or diaphragm action. As a result, the lateral resistance of the pedestals at the two side strips was not mobilized fully, and the major portion of the lateral load was resisted by the two rows of pedestals at the center strip.

The displacement traces for the bolted-panel system are shown in Fig.4.13. The difference between the displacements at the center and the side strip of the access floor are not as pronounced as the drop-in panel system. As implied by the above observations, bolting down of the floor panels to the understructure of the access floor system improves the floor diaphragm action; consequently, the resistance of the outer strip pedestals are better mobilized. The maximum accelerations and displacements of the traces shown in Figs.(4.10) to (4.13) are summarized table (4.4).

Although the displacement response at the access floor is quite different between the bolted panel and the drop-in panel system, the equipment response is insensitive to the panel attachment as seen from the bottom traces in Fig.4.10 and 4.11. Similar observations can also be

made for the displacement response at the top of the equipment relative to the R2 location of the access floor. Intuitively, one would expect that the equipment response would be higher for the drop-in panel system, since the equipment is on a more flexible access floor. However, due to the added damping resulted from the rubbing between adjacent panels of the drop-in panel system, the dynamic response of the equipment-access floor system is decreased. As a result, the dynamic response of the equipment is similar regardless of whether the panels of the access floor system are dropped in or bolted to the understructure.

As shown in the bottom traces in Figs.(4.10) to (4.13), the acceleration and displacement response at the top of the equipment is primarily contributed by the first mode response of the combined equipment-access floor system. This observation is also confirmed by the 2% damped response spectra shown in Fig.4.14 for the drop-in panel system and in Fig.4.15 for the bolted panel system. The three spectra shown in each figure were computed from the acceleration time histories measured at the table, at the center strip (R2) of the access floor and at the top of the equipment. Two major peaks corresponding to the first and the second mode response of the equipment-access floor systems can be identified. The spectral peak corresponding to the first mode response is much higher than that of the second mode. This implies that the response at the top of the equipment is constituted mainly by the first mode response.

The first mode peak of the equipment response spectrum occurs at approximately 5.5Hz for the drop-in panel system (Fig.4.14) and at about 6.3Hz for the bolted panel system (Fig.4.15). These frequencies agree well

with the corresponding first mode frequencies of 5.9 and 6.4Hz obtained from the 20% span random excitation tests for the drop-in and the bolted panel system, respectively.

It can be seen that the equipment response spectrum for the bolted panel system has a higher first mode spectral peak than that of the drop-in panel system. This phenomenon may appear to be contradictory to the previous observation that the amplitudes of the acceleration response time histories at the top of the equipment are similar regardless of the type of panel attachment. However, as a result of having a smaller damping, the frequency content of the time history for the bolted panel system is concentrated to a much narrower band of frequencies than the drop-in panel system. As a result, a larger spectral peak for the bolted panel system is resulted.

#### *ii. D12BF (Back-to-front) tests*

This series of tests was carried out for the equipment in a back-to-front orientation on the D12 access floor system. Both the drop-in and the bolted panel attachment were considered. For the bolted panel system, no significant loss of torque was observed in the four tie-down rods after a 25% and a 50% NEBS excitation. For the drop-in panel system, no loss of torque was observed after the 25% NEBS test; however, approximately 30% of the initial torque was lost in two of the tie-down rods after the 50% NEBS test.

The acceleration time histories recorded for the test carried out using a 50% NEBS excitation are shown in Figs.(4.16) for the drop-in panel system and in Fig.4.17 for the bolted panel system. The traces shown in

each figure were measured at the table, at the R1 and R2 locations of the access floor and at the top of the equipment. These traces are very similar in frequency contents and amplitude as those obtained for the side-to-side equipment orientation. For both the bolted panel and the drop-in panel systems, the maximum acceleration is approximately 2g at the top of the frame and approximately 1g on the access floor. Similar to the tests for the side-to-side equipment orientation, the same amplification factor of two prevails for the acceleration amplitudes between the access floor and the shake table, and between the top of the equipment and the access floor. Also, there is little difference in equipment response between the drop-in panel system and the bolted panel system.

The relative access floor displacement measured at the R2 and the R1 location as well as the equipment displacement relative to the R2 position of the access floor are shown in Figs.(4.18) for the drop-in panel system and in Fig.4.19 for the bolted panel system. For the drop-in panel system, the amplitude of the relative floor displacement at the center strip (R2) is approximately twice of that at the side strip (R1), however, the difference is not as drastic as the case where the equipment is mounted in a side-to-side orientation. The reason for this is that in the BF orientation the equipment straddles over all three panel strips, hence, part of the resistance of the outer strip pedestal is also mobilized regardless of whether the panels are bolted or not. The maximum values for the acceleration and displacement traces shown in Fig.4.16 to 4.19 are summarized in Table 4.5.

The 2% damped response spectra of the acceleration time histories are shown in Fig.4.20 for the drop-in panel system and in Fig.4.21 for the

the bolted panel system. The response spectra for both cases have the major peaks at approximately 6.5 Hz which corresponds to the first translation mode frequency of 6.45 Hz as determined by the 20% span random excitation test. The response spectra as well as the response time histories of the equipment indicate that the response motion of the equipment is primarily contributed by the first mode response.

#### 4.4.2.2 Equipment on D20 Access Floor

The tests carried out for the equipment supported on the D20 access floor are similar to those for the D12 floor system, hence, only the behaviour which is different from the D12 test series will be discussed.

Shown in Fig.(4.22) are the acceleration time histories obtained for the test carried out for the equipment in a side-to-side orientation on bolted floor panels. The excitation used in the test was 25% of the full NEBS excitation. The four acceleration time histories shown in the figure were measured at the shake table, at the B1 and the R4 location of the access floor and at the top of the equipment. The equipment and the access floor acceleration time histories consist mainly of a 4.5Hz frequency component which corresponds to the first mode response of the equipment-access floor system. The amplitude of the acceleration at the access floor is approximately three times that of the shake table, and the acceleration amplitude at the top of the equipment is about one and a half times that of the access floor. In other words, the acceleration at the shake table was amplified almost five times at the top of the equipment. The maximum accelerations in these traces are 1.14g on the access floor

the R1 and R4 accelerations) and 1.64g at the top of the equipment.

Plotted in Fig.4.23 are the displacement time histories measured at the R1 and the R4 position of the access floor, and at the top of the equipment relative to the access floor. The maximum values of the displacement time histories for the R1 and R4 access floor locations are 1.2cm and 1.5cm, respectively. The maximum equipment displacement relative to the access floor is 0.91cm.

The 2% damped response spectra for the acceleration time histories recorded at the shake table, at the access floor and at the top of the equipment are shown in Fig.4.24. There are two major peaks on both the equipment and the access floor spectrum at frequencies of approximately 4.5Hz and 15Hz. These two frequencies agree well to the two translational mode frequencies of 4.6Hz and 14.7Hz determined from the 10% span random excitation test. Once again, both the response spectra and the time history indicate that the response motion at the top of the equipment is primarily contributed by the first mode response.

#### 4.4.3 Comparison of the Seismic Responses of the Equipment mounted on a Concrete Slab and on Access Floors

Shown in Fig.4.25 are three acceleration traces for the response at the top of the equipment. These traces were obtained from the tests carried out for the equipment mounted in a SS orientation on a concrete slab, on a D12 and on a D20 access floor with bolted floor panels. All three acceleration time histories were obtained using an input excitation of 25% NEBS. A similar figure for the equipment relative displacement is shown in Fig.4.26. As seen from both figures, the equipment response on

the access floor was larger than that on a concrete slab. In other words, the equipment response was amplified due to the flexibility of the access floors. The level of amplification depends to a great extent on the fundamental frequency of the system considered. The fundamental frequency for the equipment alone in a SS orientation is 8.5Hz, for the D12 equipment-access floor system is 6.4Hz and for the D20 equipment-access floor system is 4.6Hz. As indicated by the NEBS spectrum which defines the shake table motion, the response of a 4.6Hz system is higher than that of a 6.4Hz system which in turn is higher than that of an 8.5Hz system. As a result, the equipment response is the highest when supported on the D20 access floor and lowest on the concrete slab.

#### **4.4.4 Ultimate Behaviour of the Equipment-access Floor Systems Subjected to NEBS Excitation**

The D12 and the D20 equipment-access floor system were tested until failure occurred. The objectives of these tests are to investigate the ultimate behaviour of the equipment-access floor systems under dynamic loading, and to relate the dynamic ultimate behaviour of the access floor with the behaviour observed in the static tests.

For the D12 access floor, the equipment was tested in a BF orientation on bolted floor panels. The floor was damaged under a 100% NEBS excitation. After the test, the equipment was shifted 2mm in the direction of shaking. Two of the tie-down rods were completely shaken loose, and the two other ones retained only a small portion of the initial torque. One of the panels under one of the corners of the equipment was depressed, and the head plate of the pedestal closest to the depression

was bent. Before the damaged access floor was disassembled, the tie-down rods of the equipment were re-tightened, and a 2.5% span random excitation test was performed to determine the resonant frequencies of the damage system. A fundamental frequency of 5.5Hz was obtained. This is significantly lower than the frequency of 7Hz obtained using the same excitation span prior to the 100% NEBS test. This reduction of frequency corresponds to a 40% decrease in the stiffness of the system. After the equipment and the floor panels had been disassembled, it was found that 11 of the 12 pedestals in rows R2, R3 and R4 were damaged at the welded connections between the pedestal tubes and the pedestal base-plates. One of the pedestal in row R4 was completely severed at the base-plates. All of the pedestals in row R1 were intact.

The acceleration time histories recorded for the test are shown in Fig.4.27. It should be noted that, some of the spikes in the equipment acceleration trace were clipped because the full scale range of the data acquisition system was set too low for the acceleration at the top of the equipment. The actual maximum acceleration at the top of the equipment, therefore, would be larger than what was measured. The maximum acceleration at the access floor level is 2.4g and is over 2.9g at the top of the equipment. The corresponding displacement time histories are shown in Fig.4.28. Some amount of residual displacements can be seen at the end of the shaking on the access floor and at the top of the equipment. The maximum access floor displacement is 1.2cm, and the maximum displacement at the top of the equipment relative to the access floor is 0.92cm.

In order to relate to the results of the static test, the maximum access floor displacements for the tests carried out for the D12BF

equipment-access floor system using different levels of NEBS excitation are indicated on the access floor load-deflection curve shown in Fig.4.29. For excitation levels up to 75% NEBS, the load induced on the pedestals due to the maximum displacement is less than half of the ultimate static load. However, for the full NEBS excitation, the maximum floor displacement induces a load which is very close to the ultimate load on the pedestals.

On the D20 access floor the equipment was tested in a SS orientation on bolted floor panels. The access floor was damaged at 50% NEBS excitation. After the shaking, there was no significant loss of torque in the four tie-down rods. A 2.5% span random excitation test performed on the damaged system indicated that the fundamental frequency had been decreased from 4.7 to 4.0Hz. The decrease of frequency corresponds to about 30% loss in stiffness. Apart from the reduction of frequency there was no visible sign of damage on the access floor panels. However, upon disassembling of the floor panels, it was found that 8 of the 16 pedestals were damaged at the welded connections between the pedestal tubes and the pedestal base-plates. Similar to the D12 system damages, 7 out of the 8 damaged pedestals were concentrated on one side (row R3 and R4).

The acceleration time histories recorded for the test are shown in Fig.4.30. The maximum acceleration is 2.0g on the access floor and 2.3g at the top of the equipment. The displacement traces obtained from the tests are shown in Fig.4.31. The maximum floor displacement is 2.4cm, and the maximum displacement at the top of the equipment relative to the access floor is 1.3cm.

To relate the seismic test results to the static test observations, the maximum floor displacements obtained for the D20SS tests using different levels of NEBS excitation are indicated on the access floor load-deflection curve in Fig.4.32. For a NEBS excitation below 25%, the load induced on the pedestals by the maximum floor displacement is less than 50% of the ultimate static load. For the 50% NEBS test where the access floor failed, the load induced on the pedestals by the floor displacement is at about 80% of the ultimate load. Since the maximum displacements shown here were measured at the corners of the access floor (i.e. R1 and R4 location), it is very likely that the load on the center strip pedestals (R2 and R3 location) was even higher.

#### 4.5 Summary and Conclusions

In this chapter, the results of the seismic tests performed for the equipment on a concrete slab and on different access floors are presented. Several conclusions can be drawn from the experiment:

1. The dynamic response of the equipment on access floors is primarily contributed by the first mode response of the combined equipment-access floor system.

2. The dynamic response of the equipment on access floors is greater than that on a floor slab. The response of the equipment depends very much on the stiffness of the supporting access floor. The equipment response on a flexible access floor is larger than that on a stiff access floor. The above observations imply that equipment which has been seismically qualified to a certain level of NEBS excitation on a concrete slab does not necessarily mean that it is qualified to the same level of

excitation if it were mounted on an access floor. However, it is possible to limit the amplification of the response of the equipment by specifying an access floor with proper stiffness and strength.

3. Rigid diaphragm action cannot be achieved with either the drop-in or bolting method of attaching the floor panels to the access floor understructure. However, by bolting the floor panels to the understructure, the in-plane stiffness of the access floor is increased. As a result, the rows of pedestals which are not directly supporting the equipment are more efficiently mobilized to share the seismic load. This reduces the seismic load imposed on the pedestals directly supporting the equipment. However, the dynamic response of the equipment is relatively insensitive to whether the panels are bolted to the understructure or not. Thus, bolting down of the floor panels does not necessarily reduce the seismic response of the equipment.

4. The seismic load imposed on the access floor pedestals due to the NEBS excitation which causes the access floor pedestals to fail correspond well to the ultimate load observed in the static test. The ultimate load obtained from the static test, therefore, is useful for design purposes in determining the allowable load for an access floor system.

Table 4.1 Maximum response values for equipment in back-to-front orientation under different levels of NEBS excitation

NEBS Level, %	Table Acc., g	Equip mid height acc, g	Equip top acc., g	Equip relative disp. cm
10	0.12	0.20	0.21	0.15
25	0.30	0.44	0.46	0.13
50	0.56	0.69	0.70	0.24
75	0.85	1.09	1.08	0.68
100	1.25	1.61	1.70	0.34

Table 4.2 Maximum response values for equipment in side-to-side orientation under different levels of NEBS excitation

NEBS Level, %	Table Acc., g	Equip mid height acc, g	Equip top acc., g	Equip relative disp. cm
10	0.15	0.30	0.36	0.16
25	0.28	0.88	1.00	0.44
50	0.57	1.17	1.77	0.73
75	0.88	1.69	2.45	1.08
100	1.51	2.05	2.71	1.30

Table 4.3 Test configurations for equipment-access floor systems

Expt. designation	Equip orientation	Access floor system	NEBS excit. level, %
D12SS	Side to side	D12 drop-in panel	25, 50
D12SS-B	Side to side	D12 bolted panel	25, 50
D12BF	Back to front	D12 drop-in panel	25, 50
D12BF-B	Back to front	D12 bolted panel	25, 50, 75, 100
D20SS-B	Side to side	D20 bolted panel	10, 25

Table 4.4 Maximum response values for D12SS tests

## a.) Acceleration

Test ID	Panel Attachment	Table acc, g	Floor Acc., g			Equip acc, g
			R1	R2	R4	
D12SS50	Drop-in	0.50	1.08	1.29	-	1.92
D12SS50B	Bolted	0.58	1.21	1.25	1.29	2.01

## b.) Displacement

Test ID	Panel Attachment	Floor disp. (cm)			Equip acc, cm
		R1	R2	R4	
D12SS50	Drop-in	0.18	0.60	-	0.97
D12SS50B	Bolted	0.30	0.42	0.34	0.92

Table 4.5 Maximum response values for D12BF tests

## a.) Acceleration

Test ID	Panel Attachment	Table acc, g	Floor Acc., g			Equip acc, g
			R1	R2	R4	
D12BF50	Drop-in	0.53	1.10	1.10	0.98	1.91
D12BF50B	Bolted	0.59	1.31	-	1.14	1.64

## b.) Displacement

Test ID	Panel Attachment	Floor disp. (cm)			Equip disp, cm
		R1	R2	R4	
D12BF50	Drop-in	0.28	0.55	0.22	0.83
D12BF50B	Bolted	0.29	-	0.26	1.03

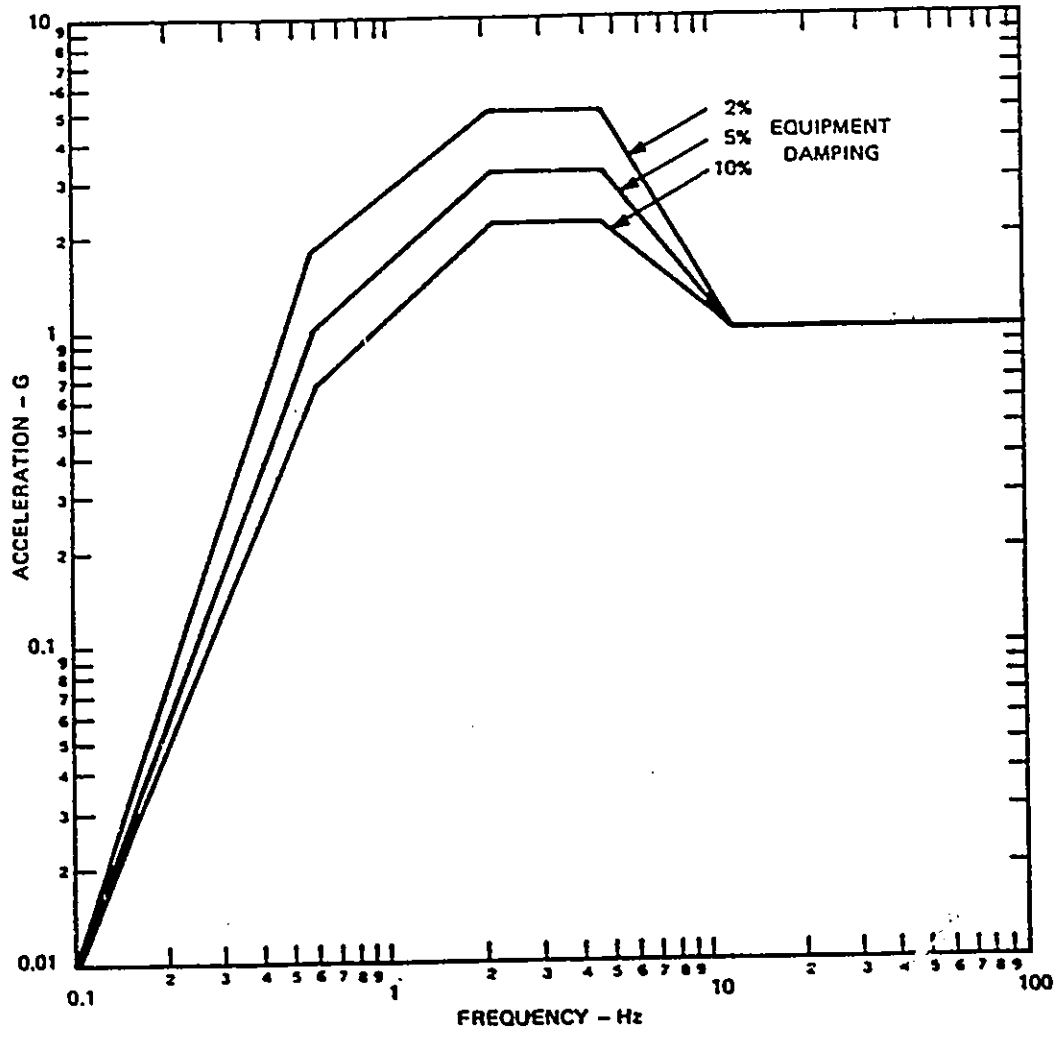


Fig. 4.1 NEBS spectra criteria (after Bell Communications Research, 1988)

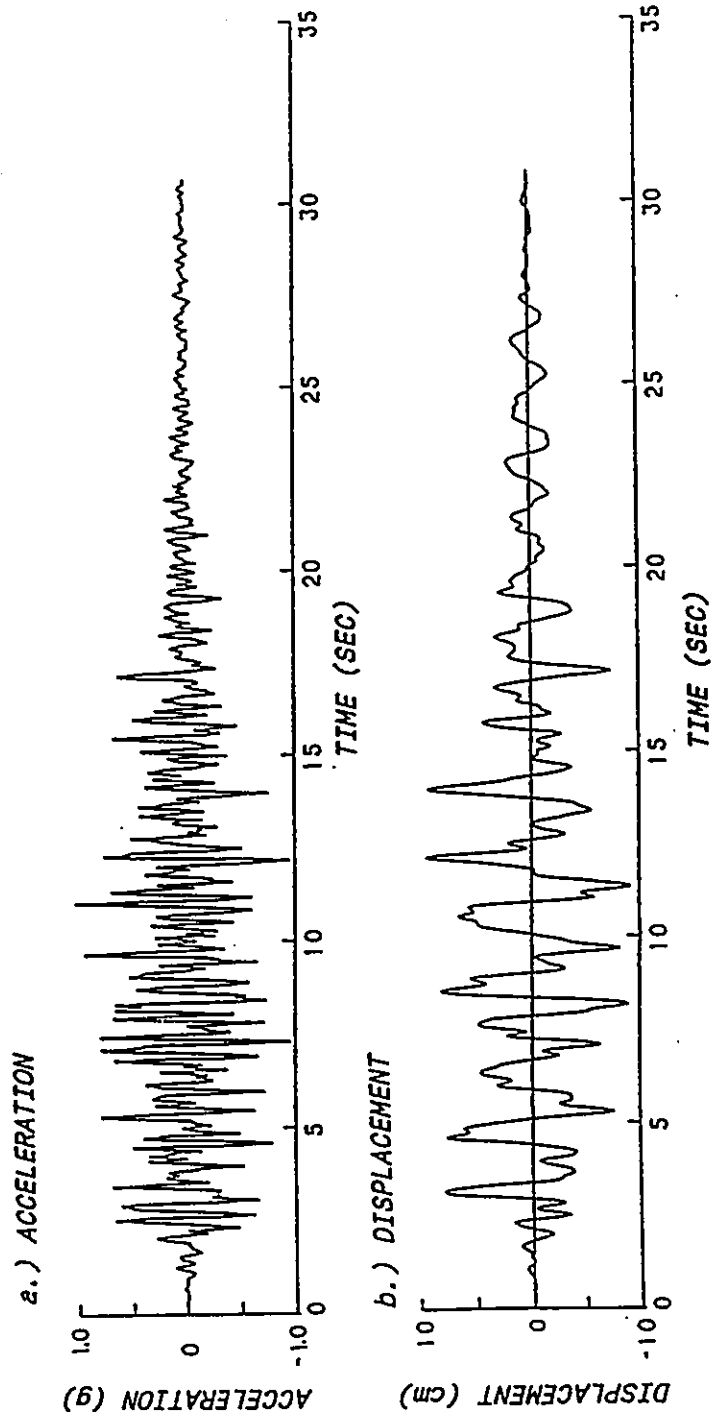


Fig. 4.2 Excitation time histories compatible with the NEBS 2x damped spectrum: a.) acceleration and b.) displacement

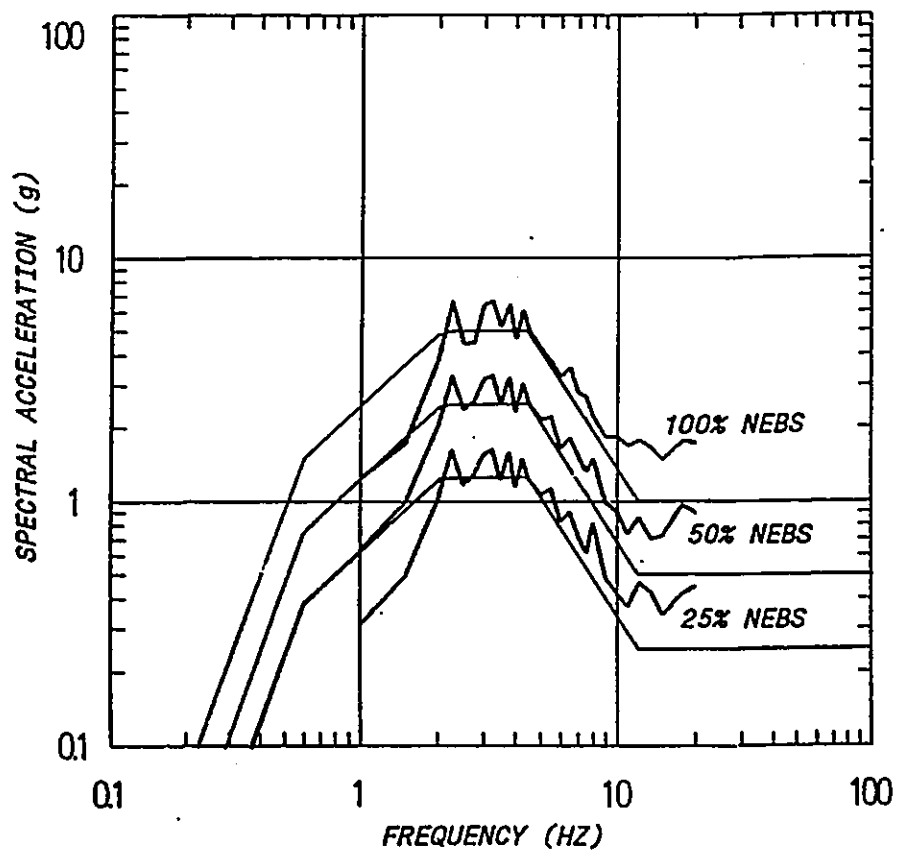


Fig. 4.3 2% damped response spectra computed for accelerograms recorded for shake table motions of different levels of NEBS excitation

a.) SIDE-TO-SIDE EQUIPMENT ORIENTATION

b.) BACK-TO-FRONT EQUIPMENT ORIENTATION

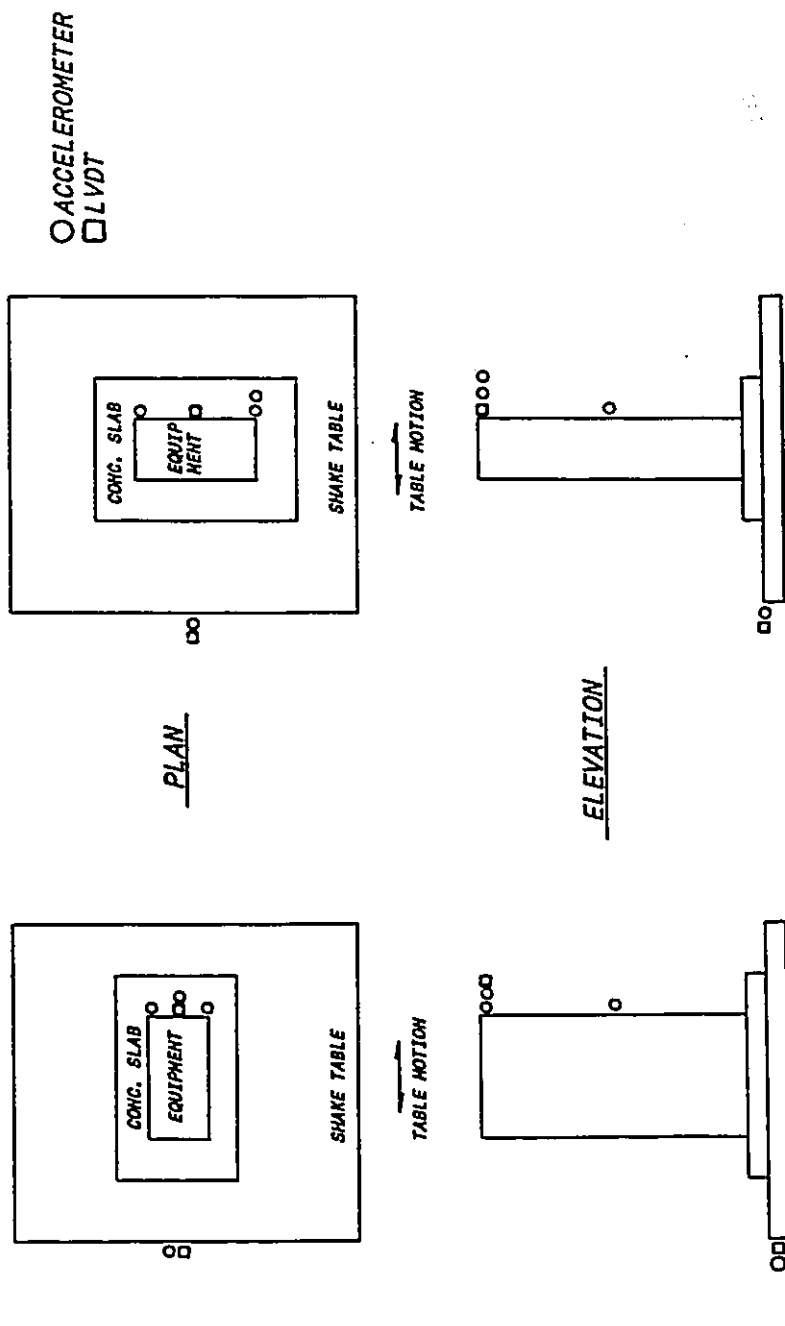


Fig. 4.4 Seismic test instrumentation for equipment on concrete slab

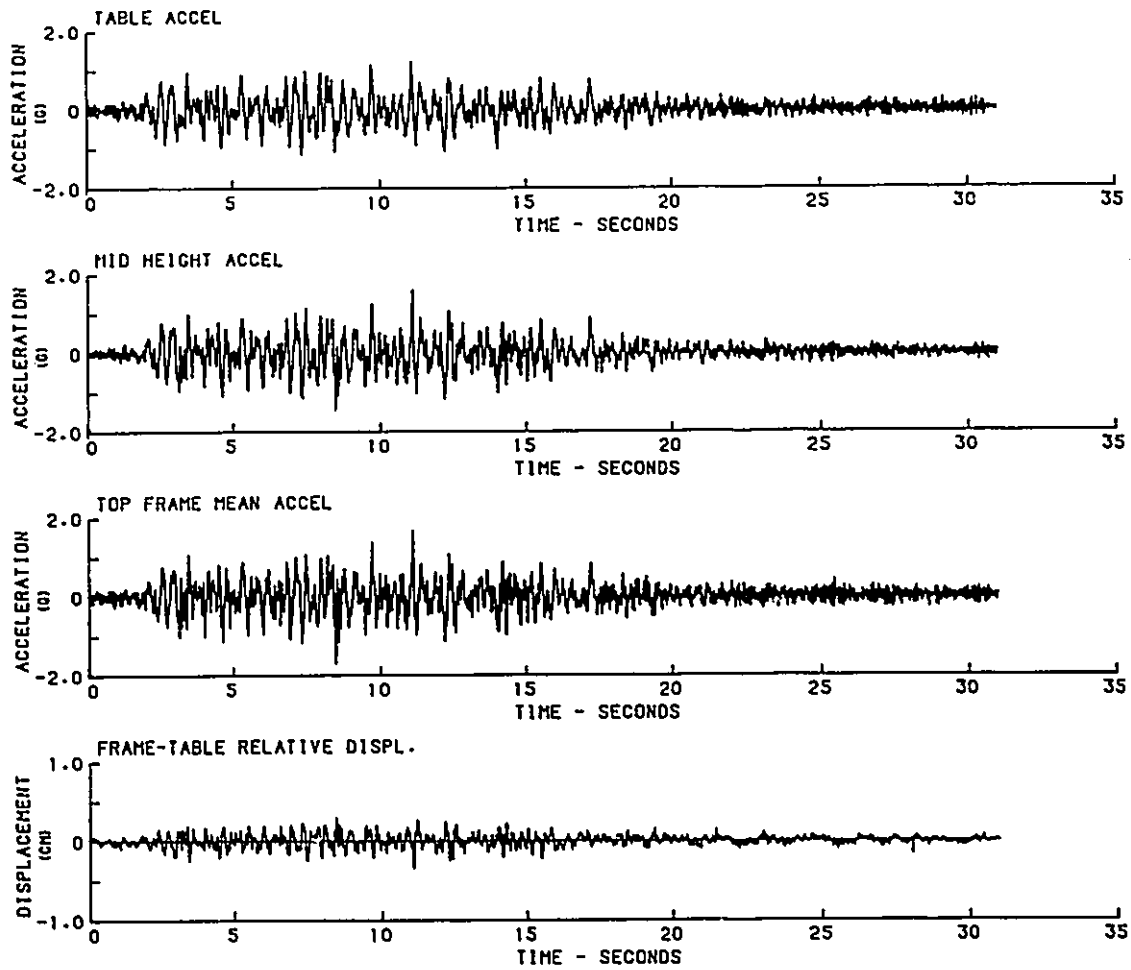


Fig. 4.5 Time histories for equipment in back-to-front orientation under full NEBS excitation

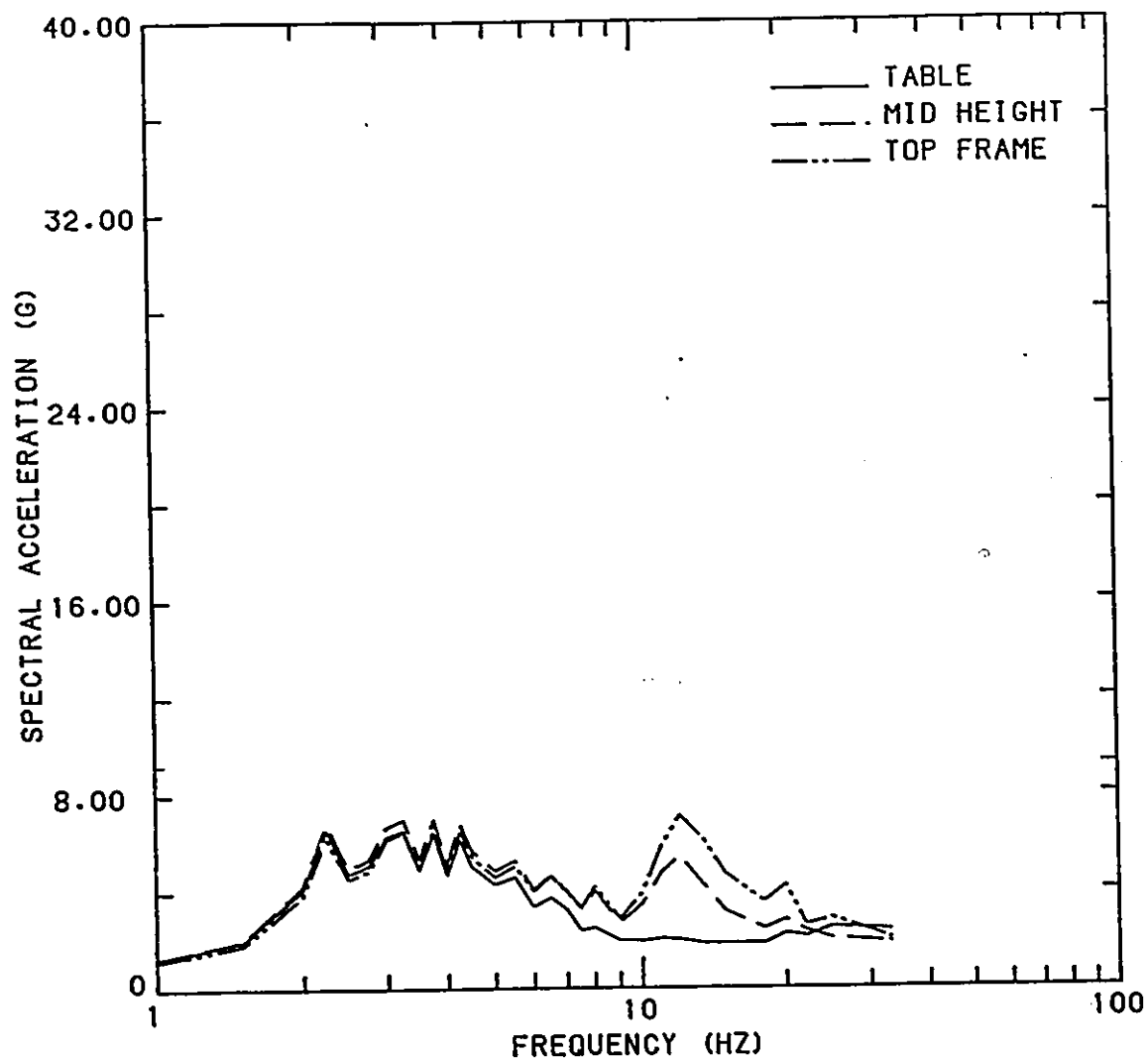


Fig. 4.6 2% damped response spectra of acceleration time histories obtained for equipment in back-to-front orientation under full NEBS excitation

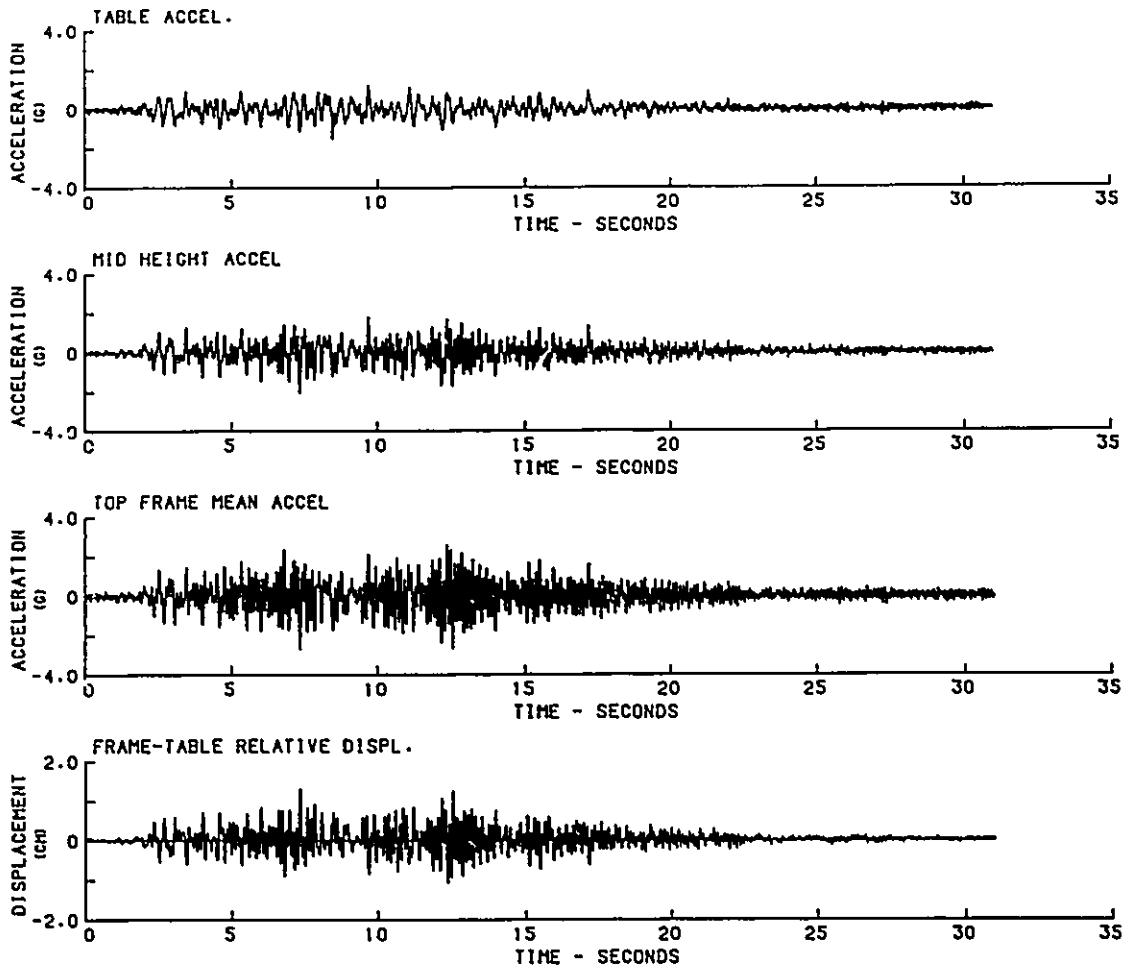


Fig. 4.7 Time histories for equipment in side-to-side orientation under full NEBS excitation

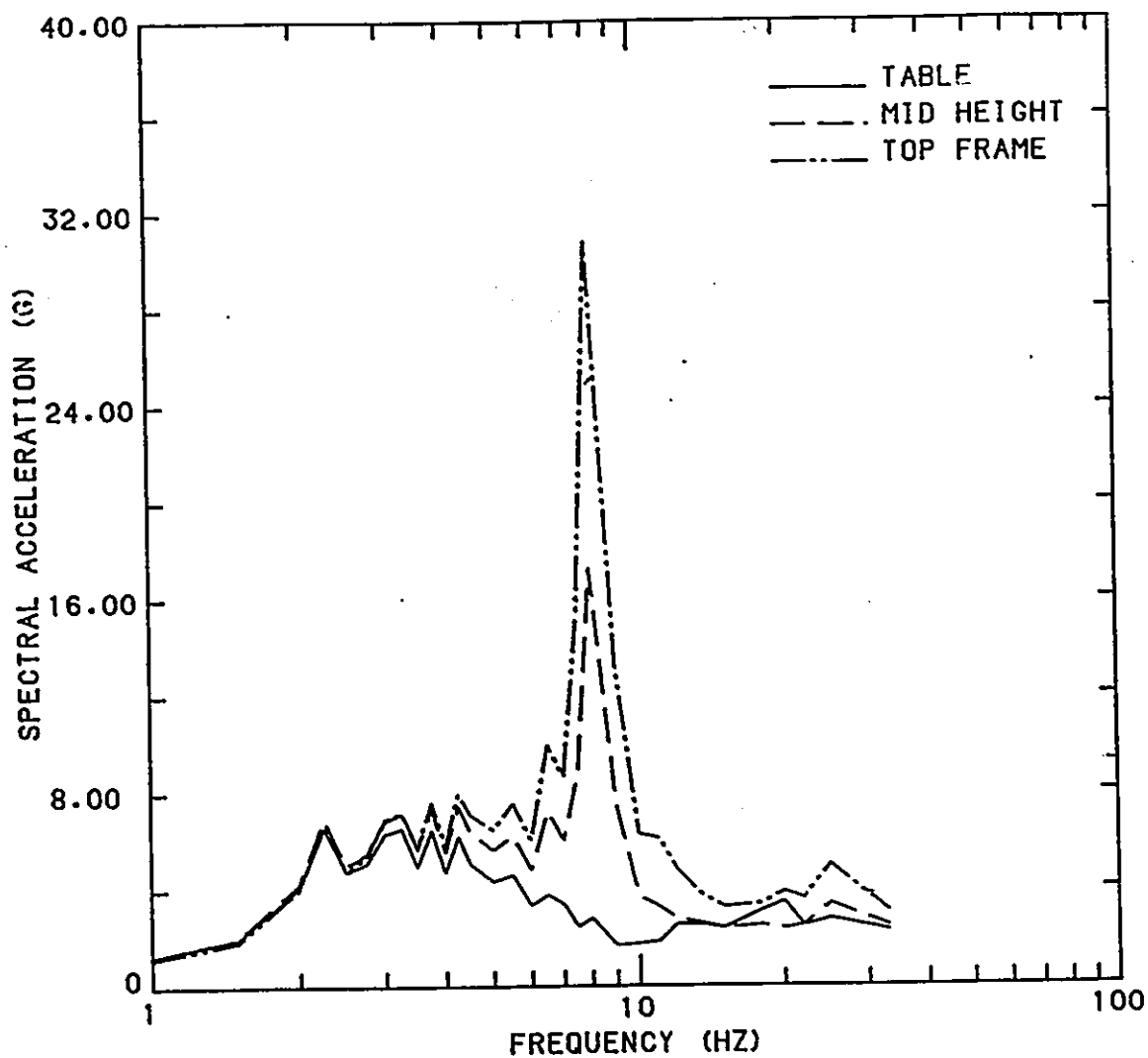
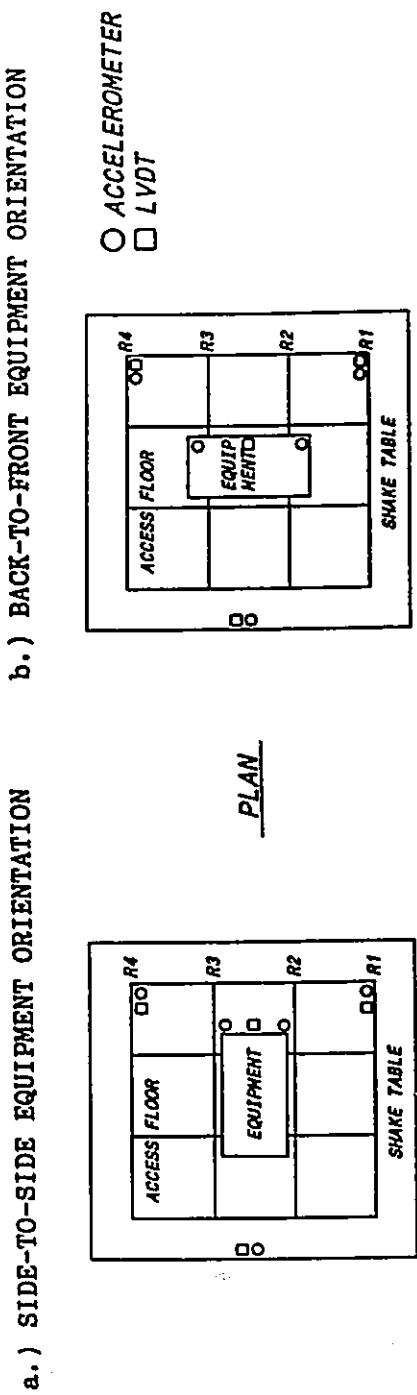


Fig. 4.8 2% damped response spectra of acceleration time histories obtained for equipment in side-to-side orientation under full NEBS excitation



PLAN

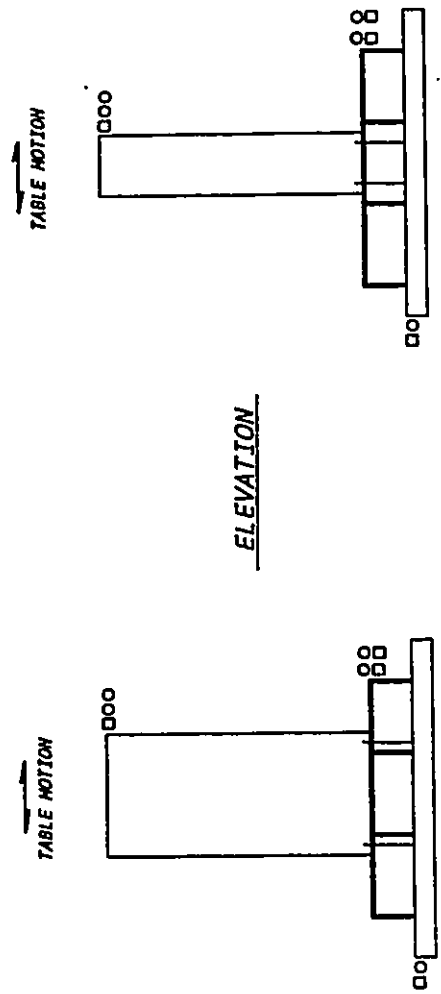


Fig. 4.9 Seismic test instrumentation for equipment on access floor

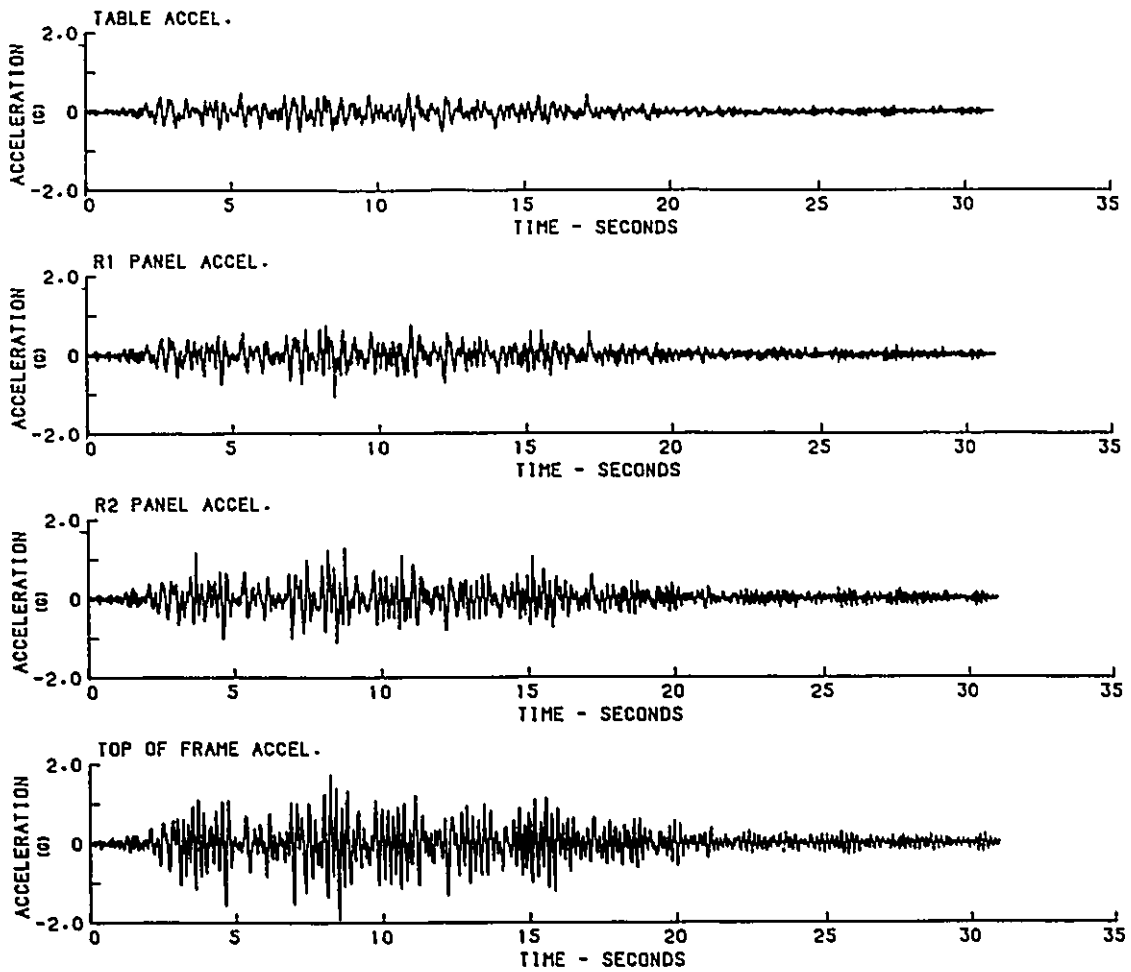


Fig. 4.10 Acceleration time histories for D12SS50 test (equipment side-to-side, D12 drop-in panels and 50% NEBS excitation)

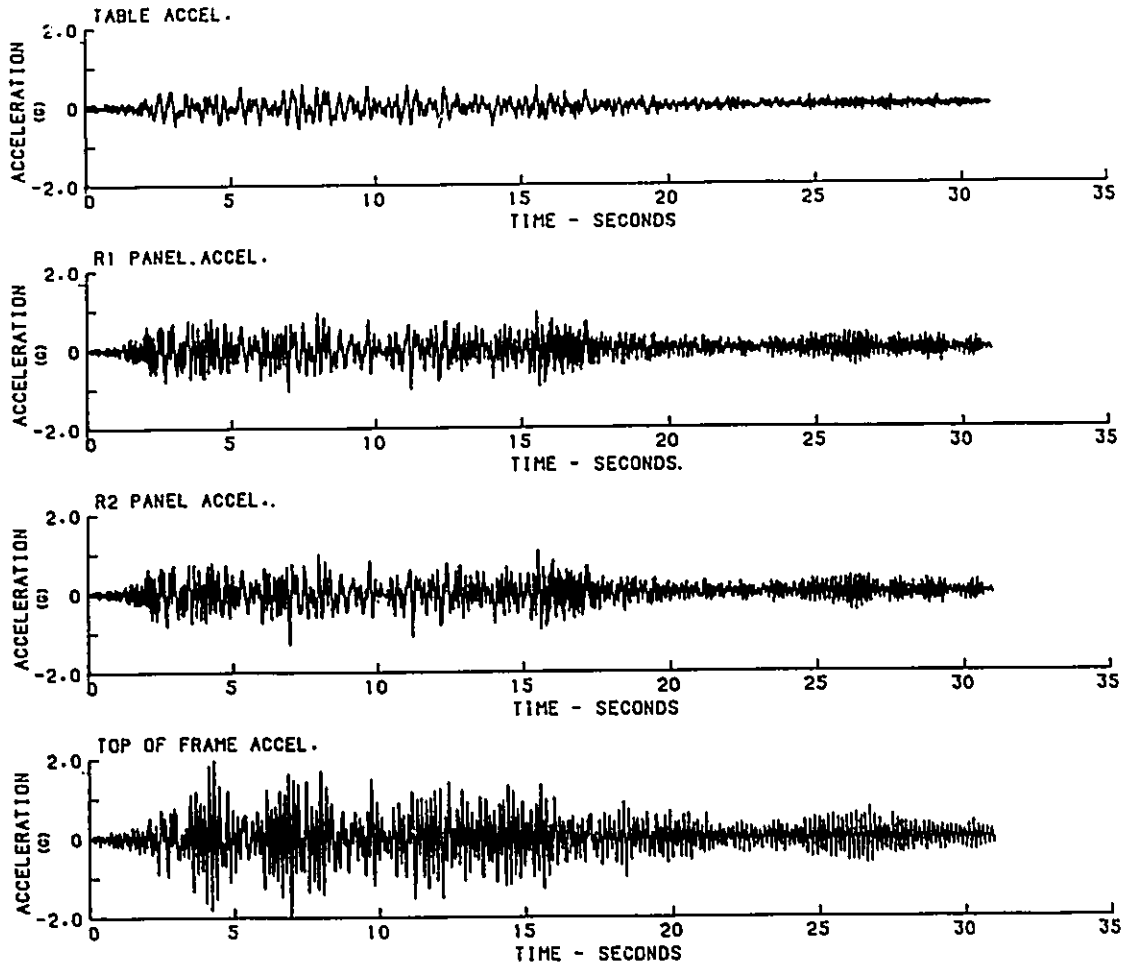


Fig. 4.11 Acceleration time histories for D12SS50B test (equipment side-to-side, D12 bolted panels and 50% NEBS excitation)

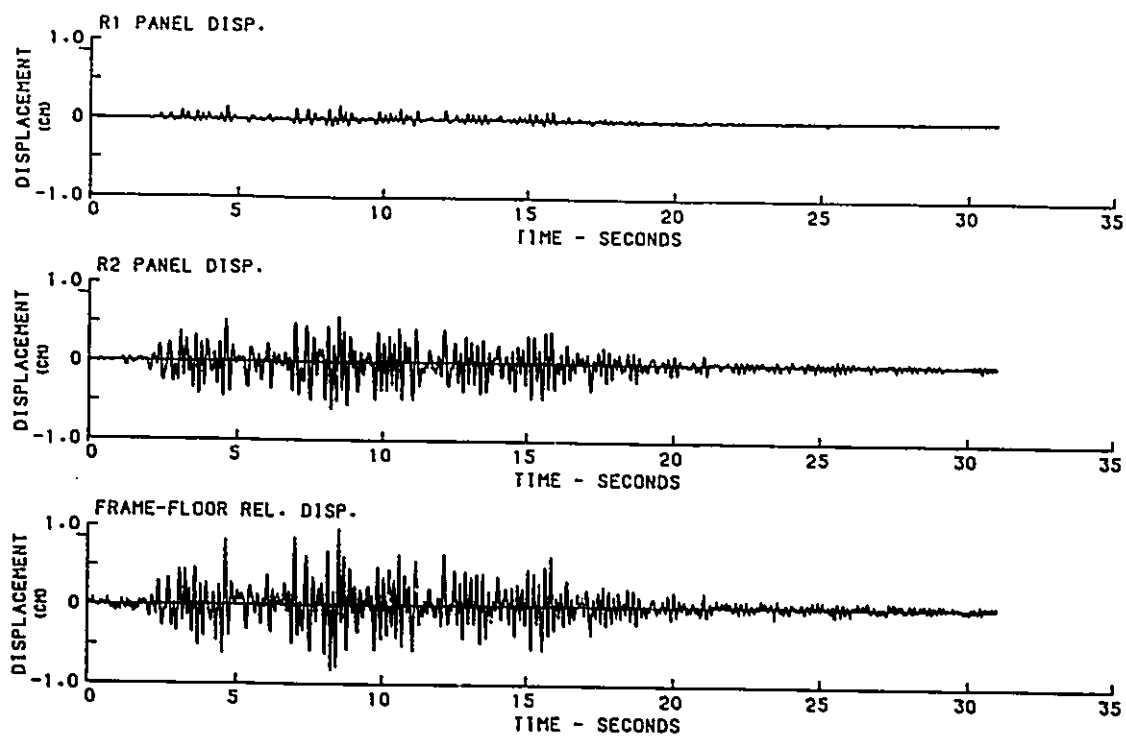


Fig. 4.12 Displacement time histories for D12SS50 test (equipment side-to-side, D12 drop-in panels and 50% NEBS excitation)

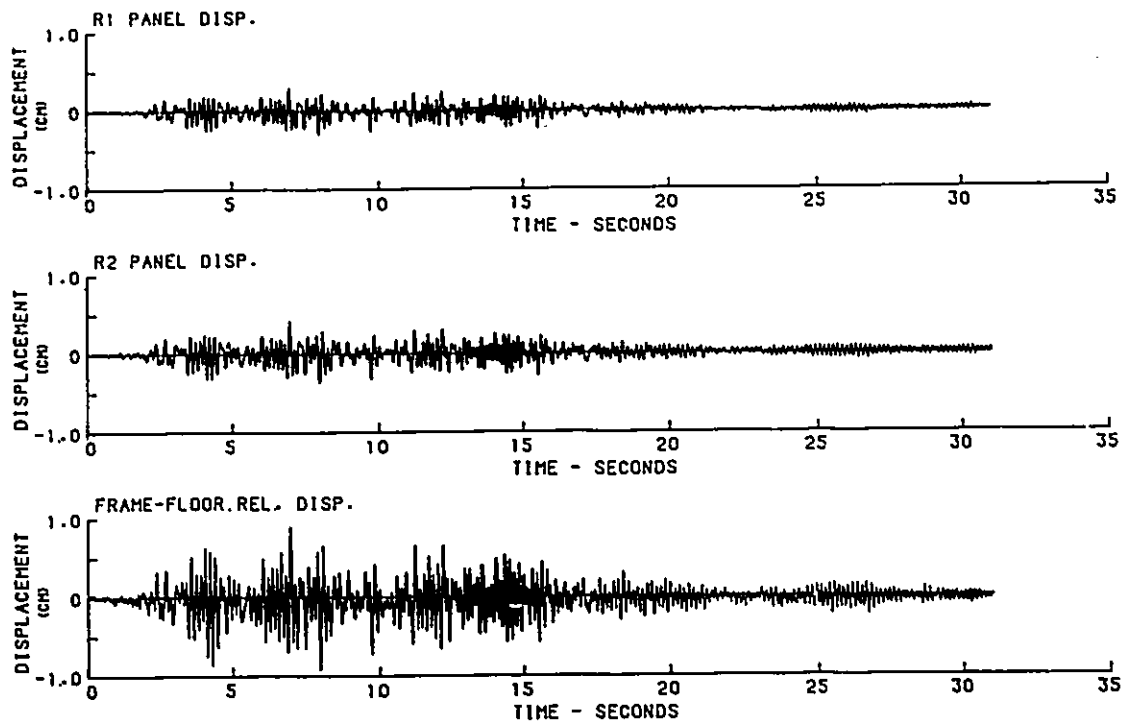


Fig. 4.13 Displacement time histories for D12SS50B test (equipment side-to-side, D12 bolted panels and 50% NEBS excitation)

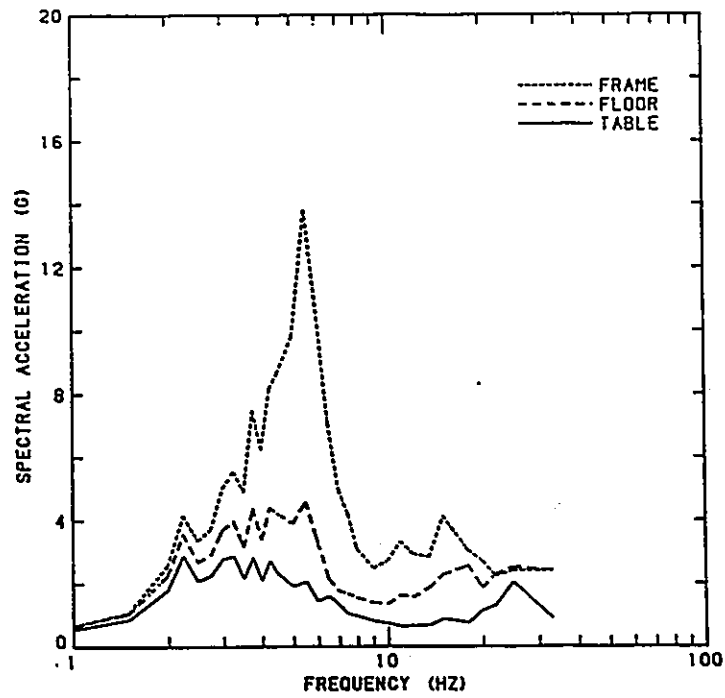


Fig. 4.14 2% damped acceleration response spectra for D12SS50 test

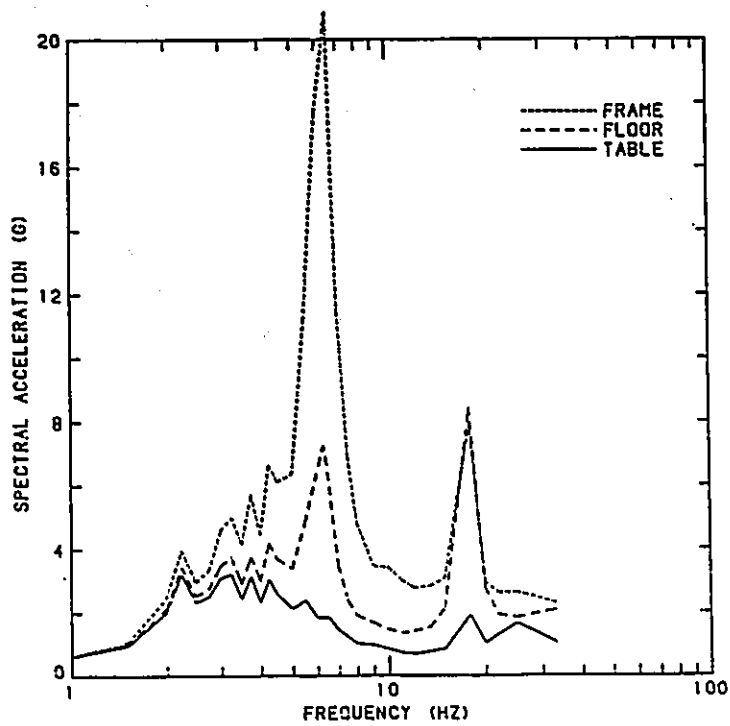


Fig. 4.15 2% damped acceleration response spectra for D12SS50B test

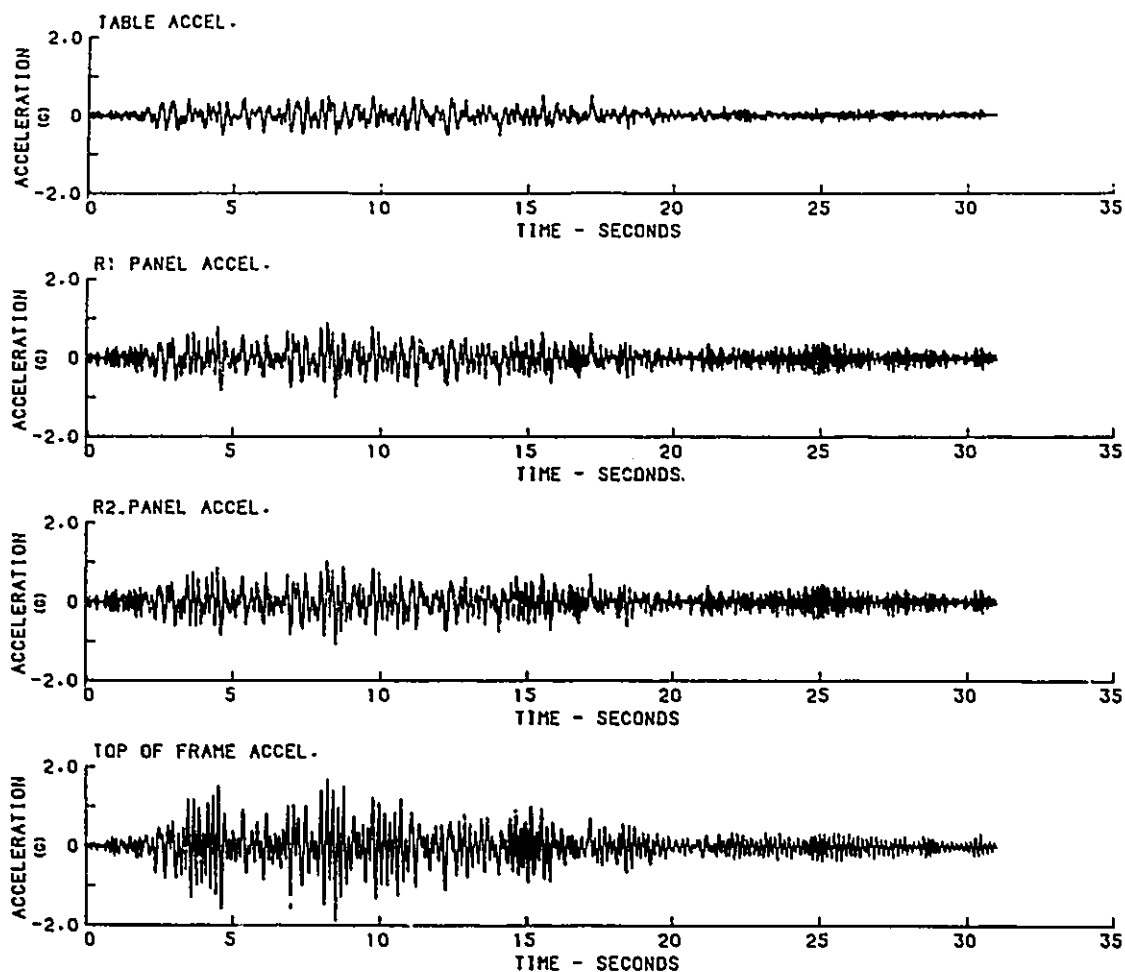


Fig. 4.16 Acceleration time histories for D12BF50 test (equipment back-to-front, D12 drop-in panels and 50% NEBS excitation)

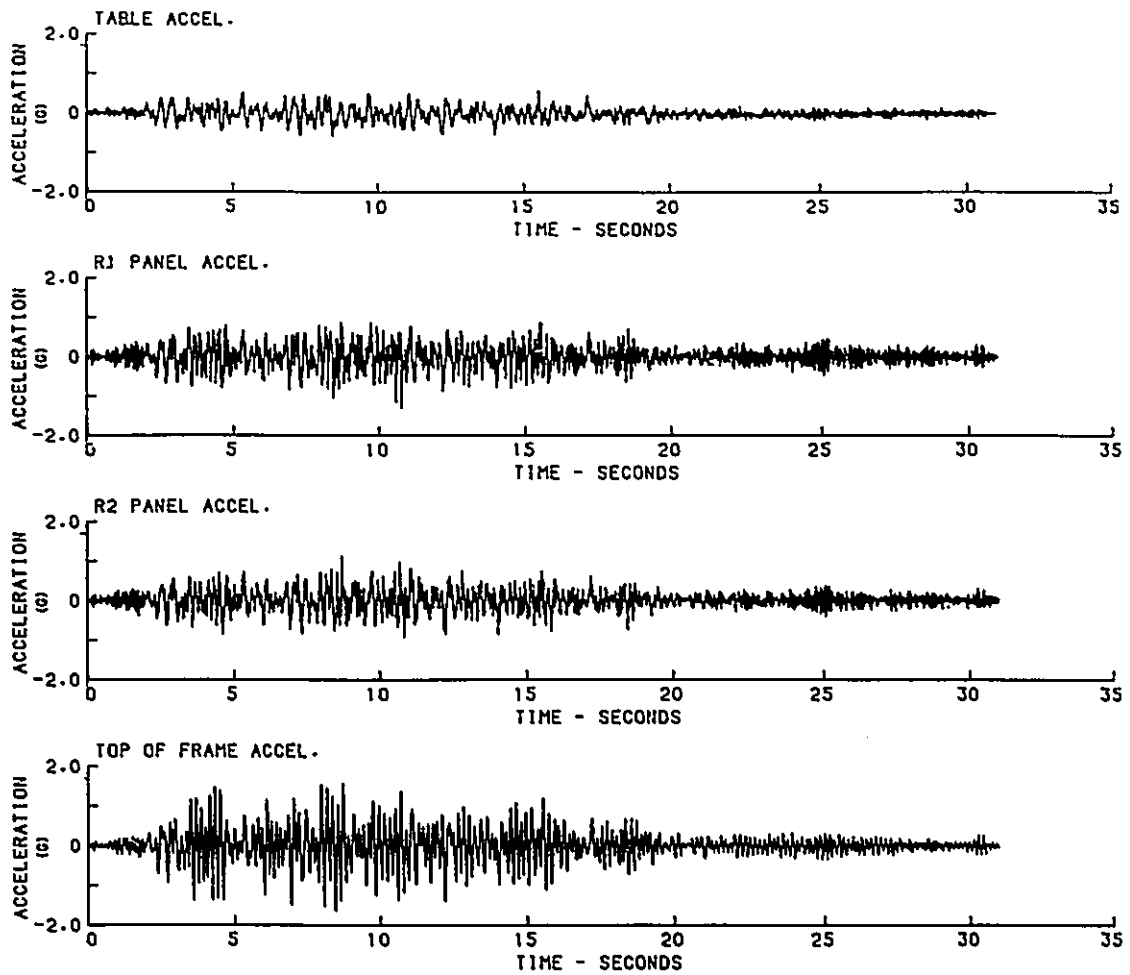


Fig. 4.17 Acceleration time histories for D12BF50B test (equipment back-to-front, D12 bolted panels and 50% NEBS excitation)

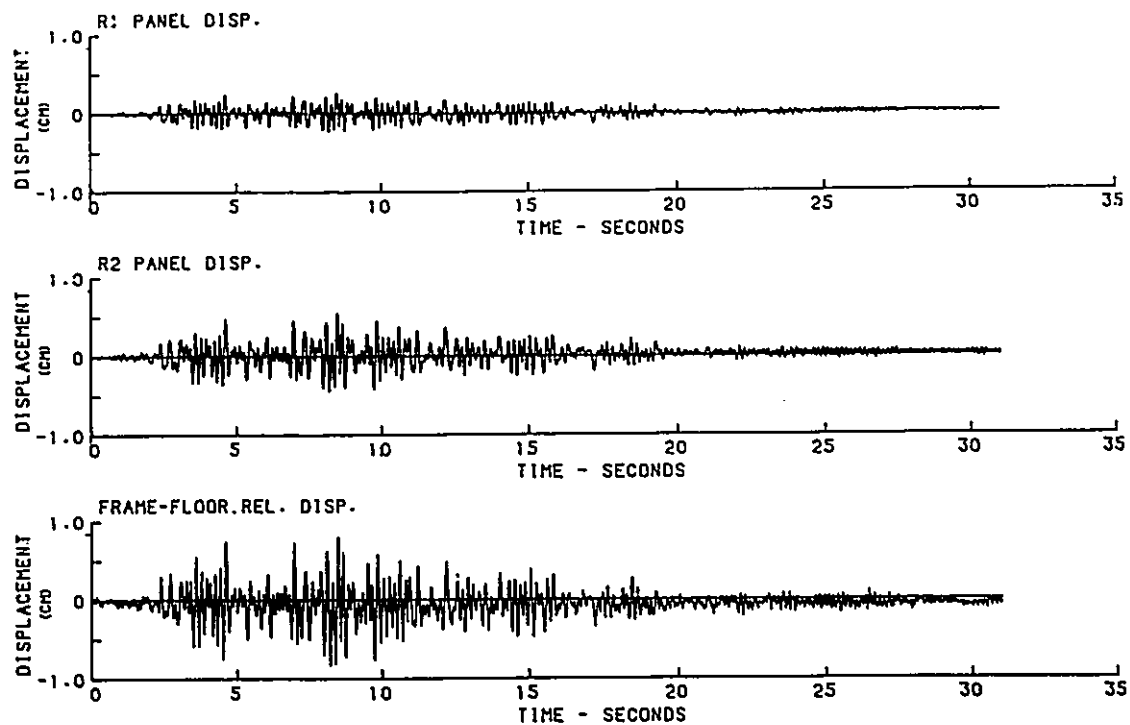


Fig. 4.18 Displacement time histories for D12BF50 test (equipment back-to-front, D12 drop-in panels and 50% NEBS excitation)

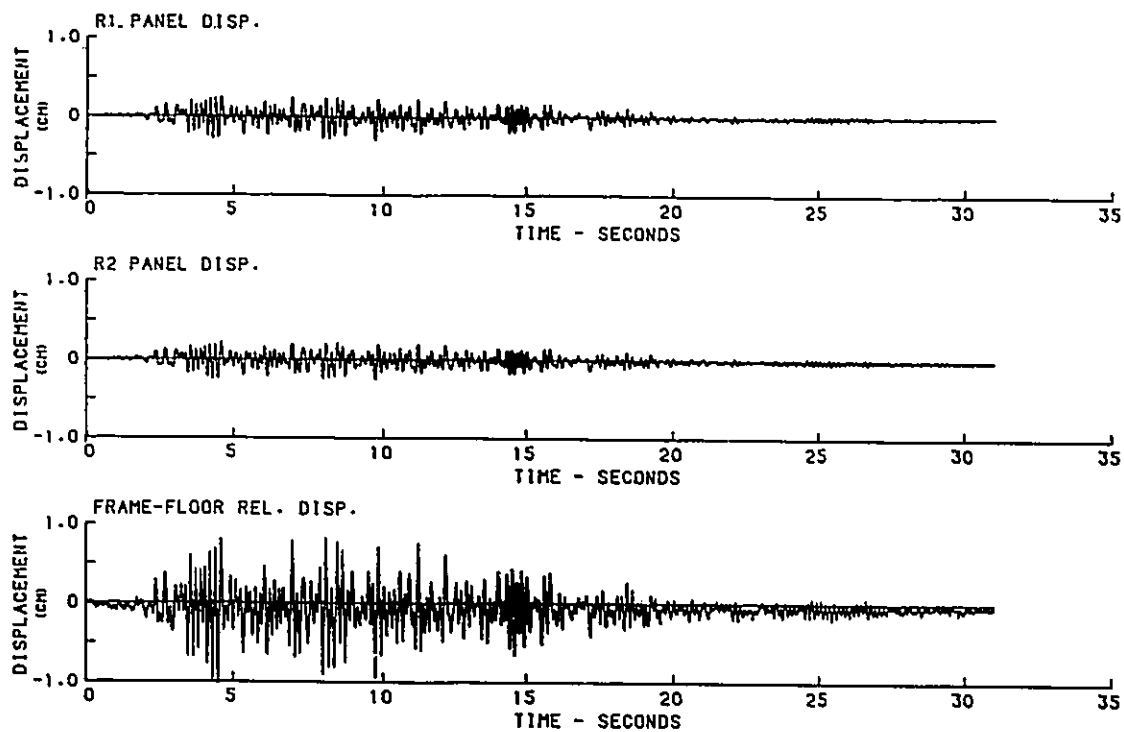


Fig. 4.19 Displacement time histories for D12BF50B test (equipment back-to-front, D12 bolted panels and 50% NEBS excitation) ..

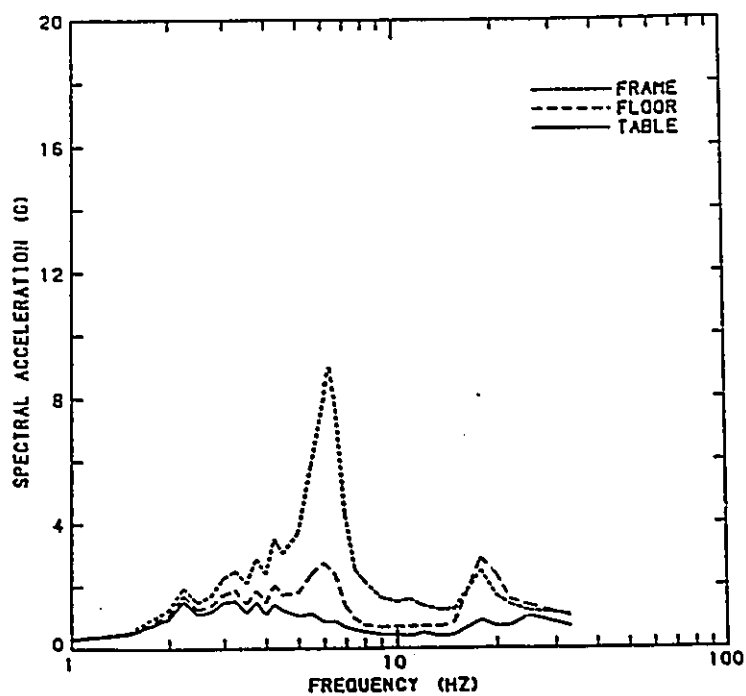


Fig. 4.20 2% damped acceleration response spectra for D12BF50 test

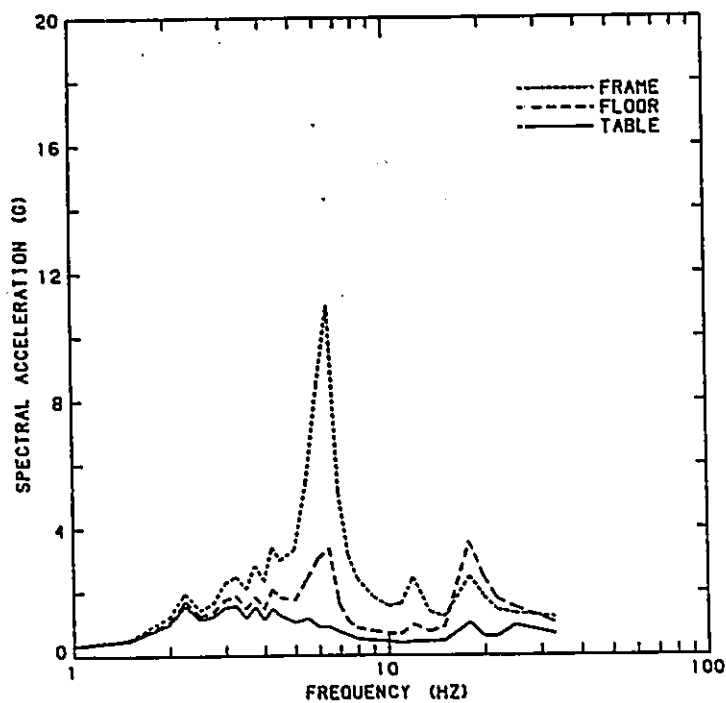


Fig. 4.21 2% damped acceleration response spectra for D12BF50B test

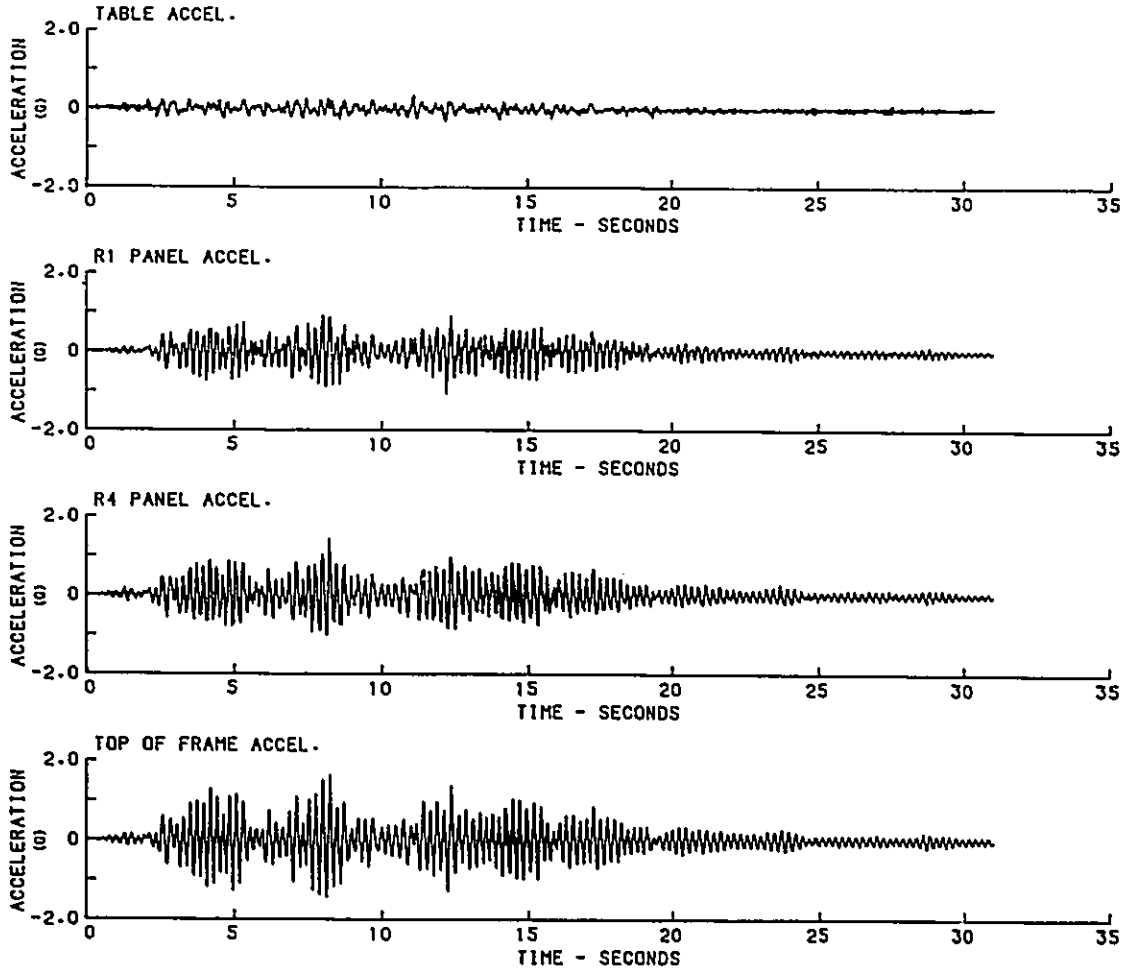


Fig. 4.22 Acceleration time histories for D20SS25B test (equipment side-to-side, D20 bolted panels and 25% NEBS excitation)

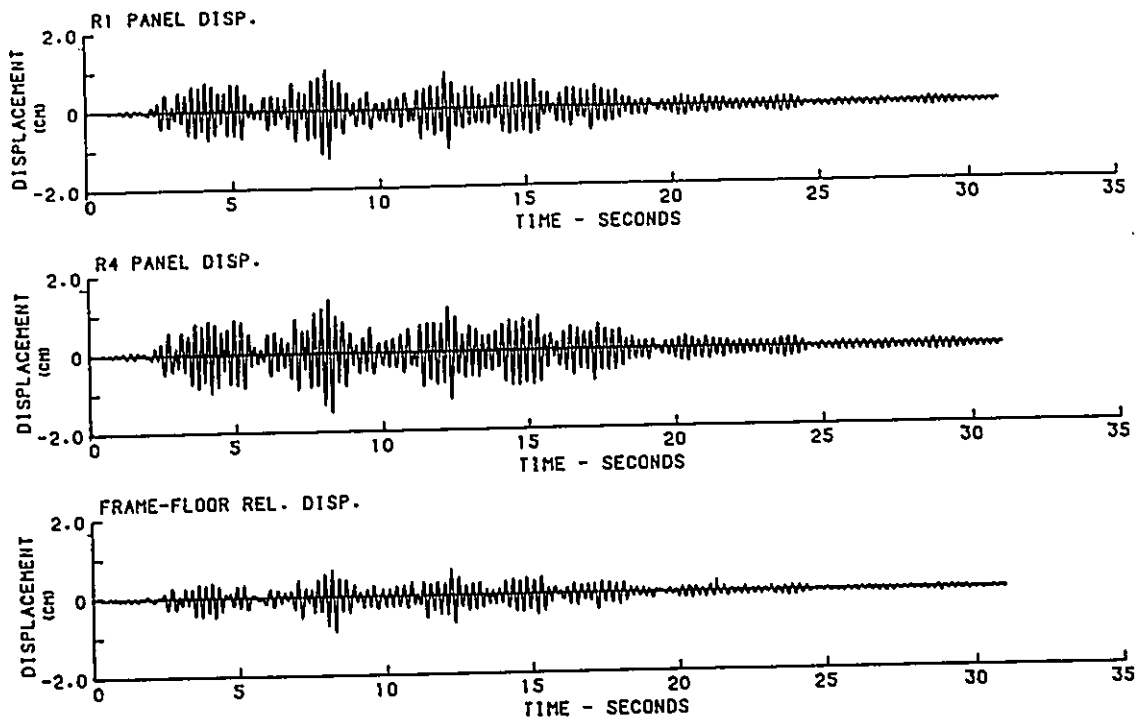


Fig. 4.23 Displacement time histories for D20SS25B test (equipment side-to-side, D20 drop-in panels and 25% NEBS excitation)

DONN SYSTEM-20"  
EXCITATION 25% NEBS. DAMPING = 2%

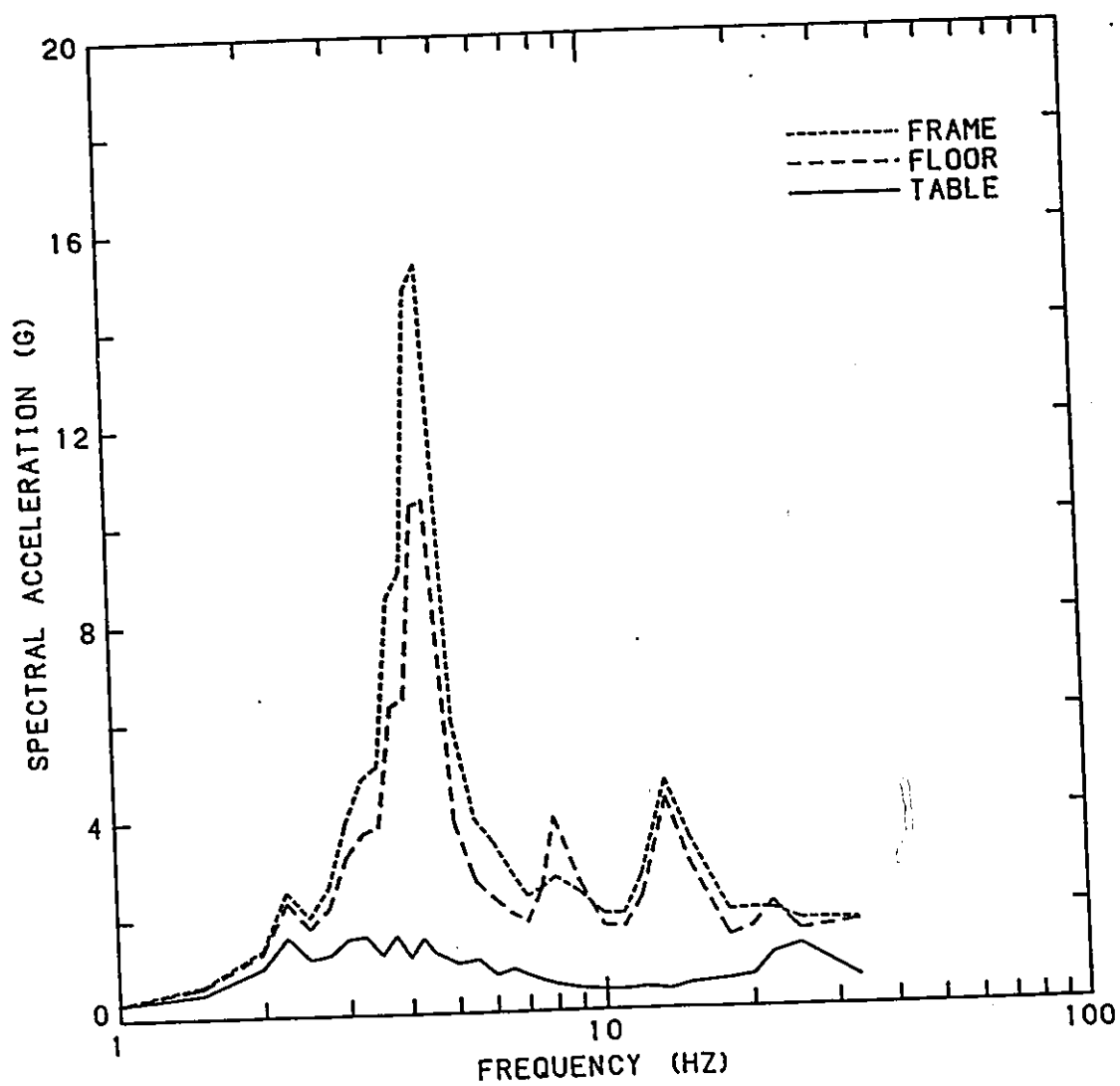


Fig. 4.24 2% damped response spectra of acceleration time histories obtained for D20SS25B test (equipment side-to-side, D20 bolted panels and 25% NEBS excitation)

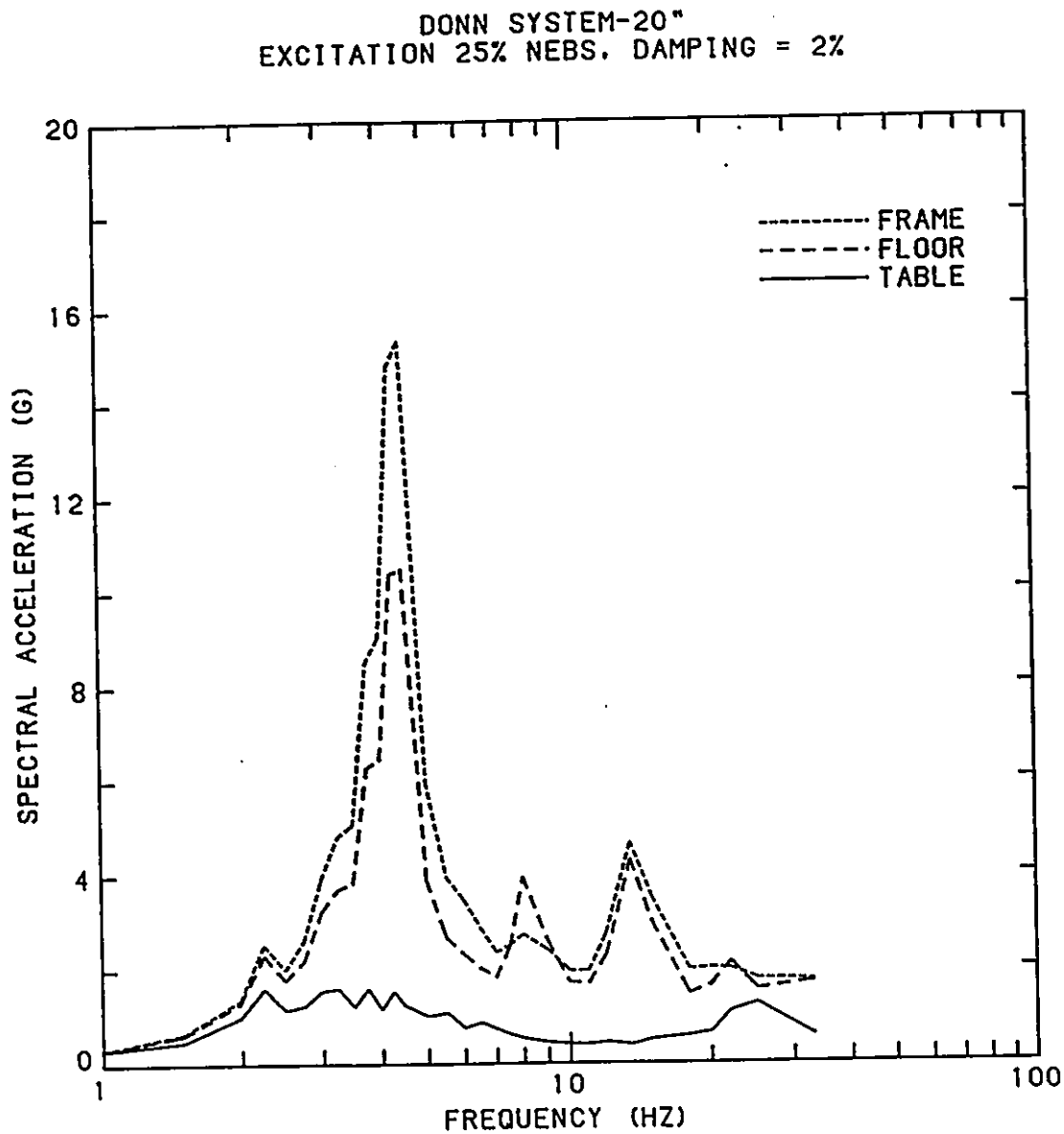
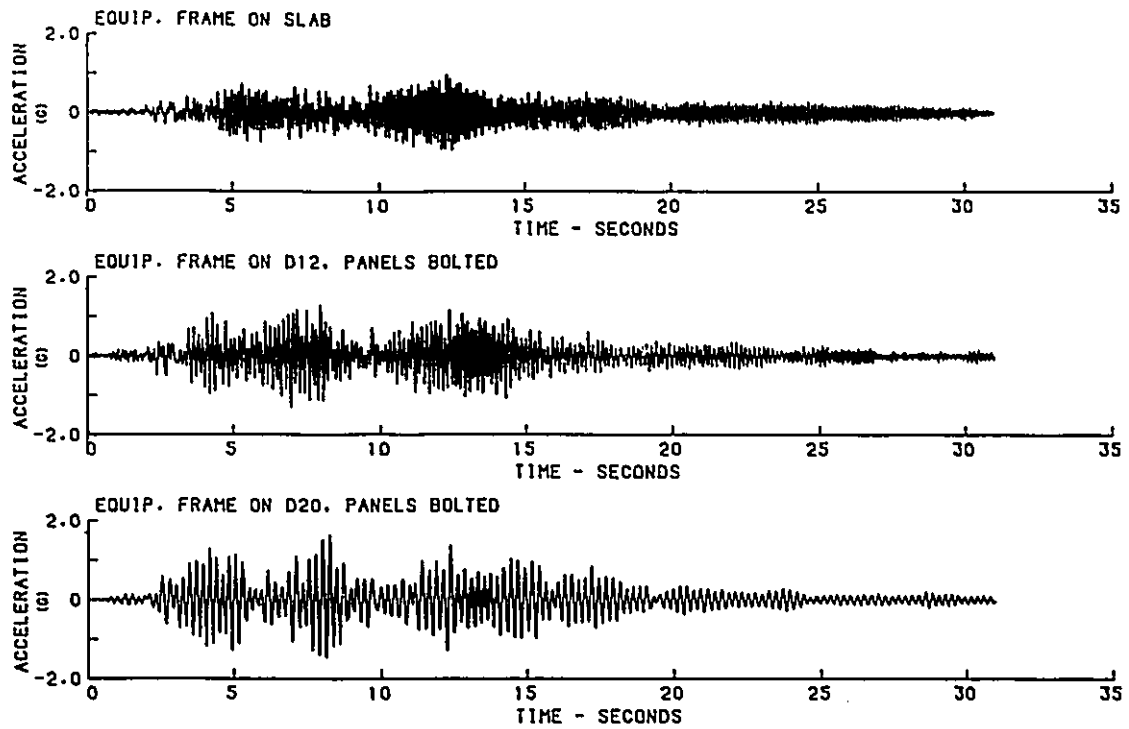
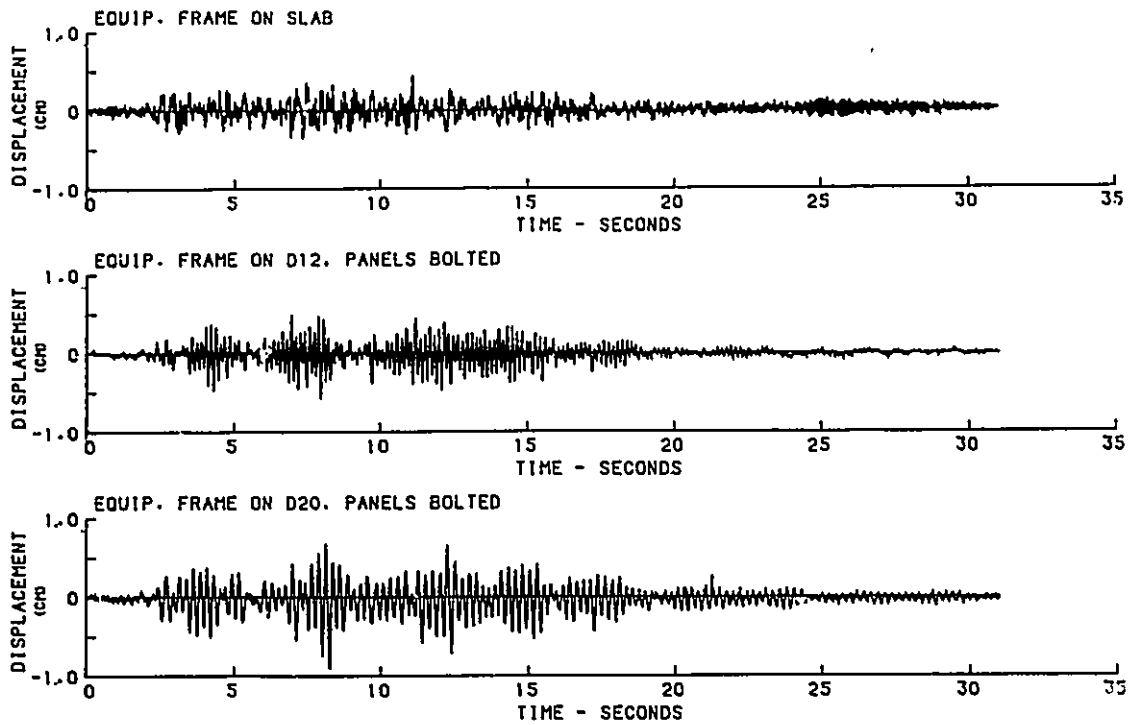


Fig. 4.24 2% damped response spectra of acceleration time histories obtained for D20SS25B test (equipment side-to-side, D20 bolted panels and 25% NEBS excitation)



**Fig. 4.25** Acceleration response time histories for equipment in side-to-side orientation supported on slab, D12 and D20 access floor, 25% NEBS excitation



**Fig. 4.26** Displacement response time histories for equipment in side-to-side orientation supported on slab, D12 and D20 access floor, 25% NEBS excitation

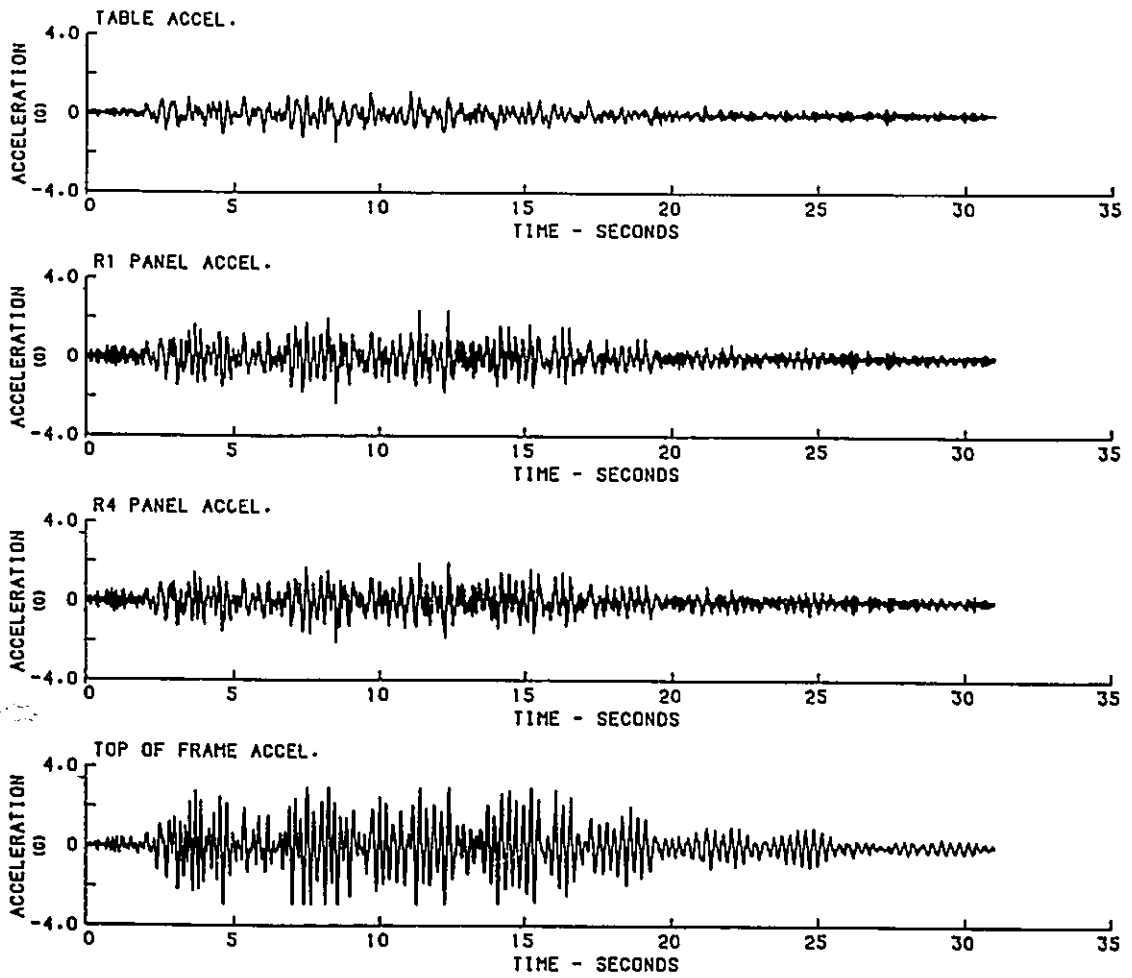


Fig. 4.27 Acceleration time histories for D12BF100B test (equipment back-to-front, D12 bolted panels and 100% NEBS excitation)

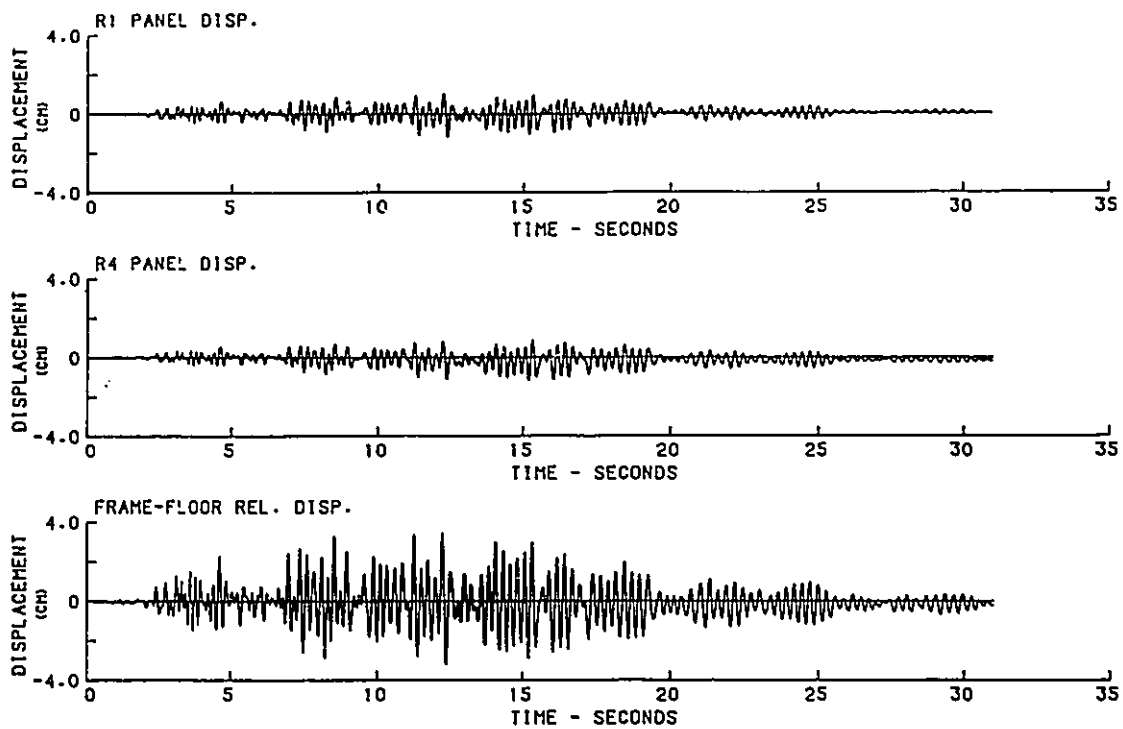


Fig. 4.28 Displacement time histories for D12BF100B test (equipment back-to-front, D12 bolted panels and 100% NEBS excitation)

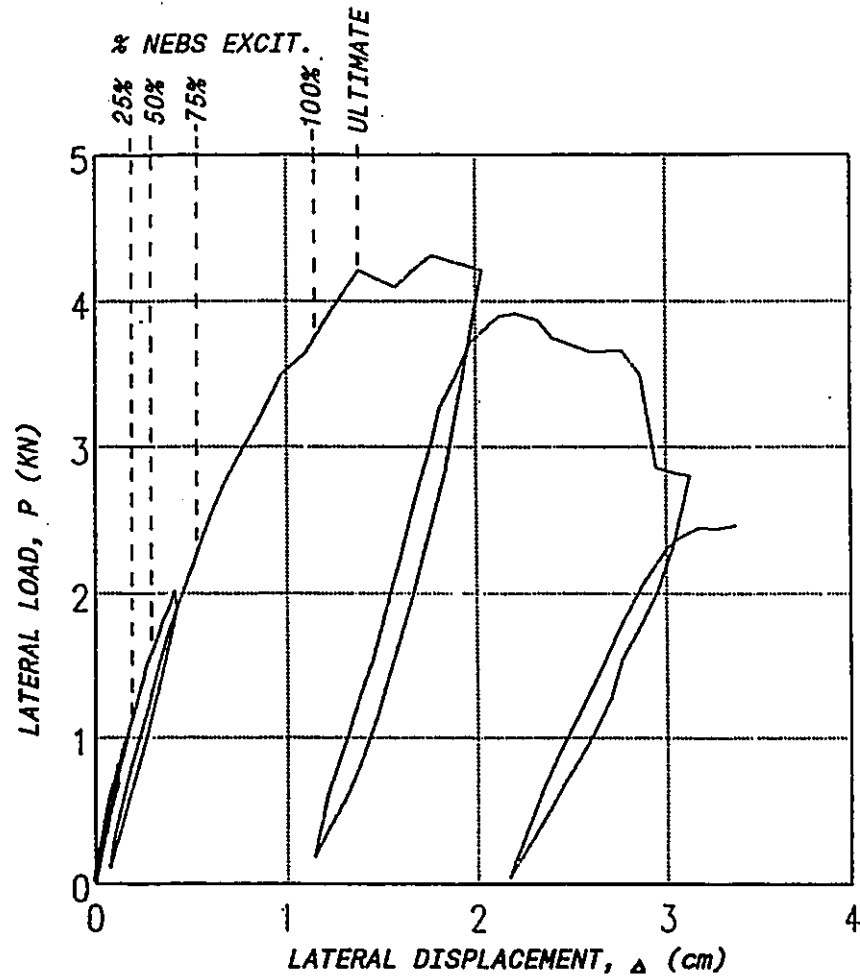


Fig. 4.29 Correlation between dynamic and static load-deflection behaviour for D12 access floor, equipment back-to-front

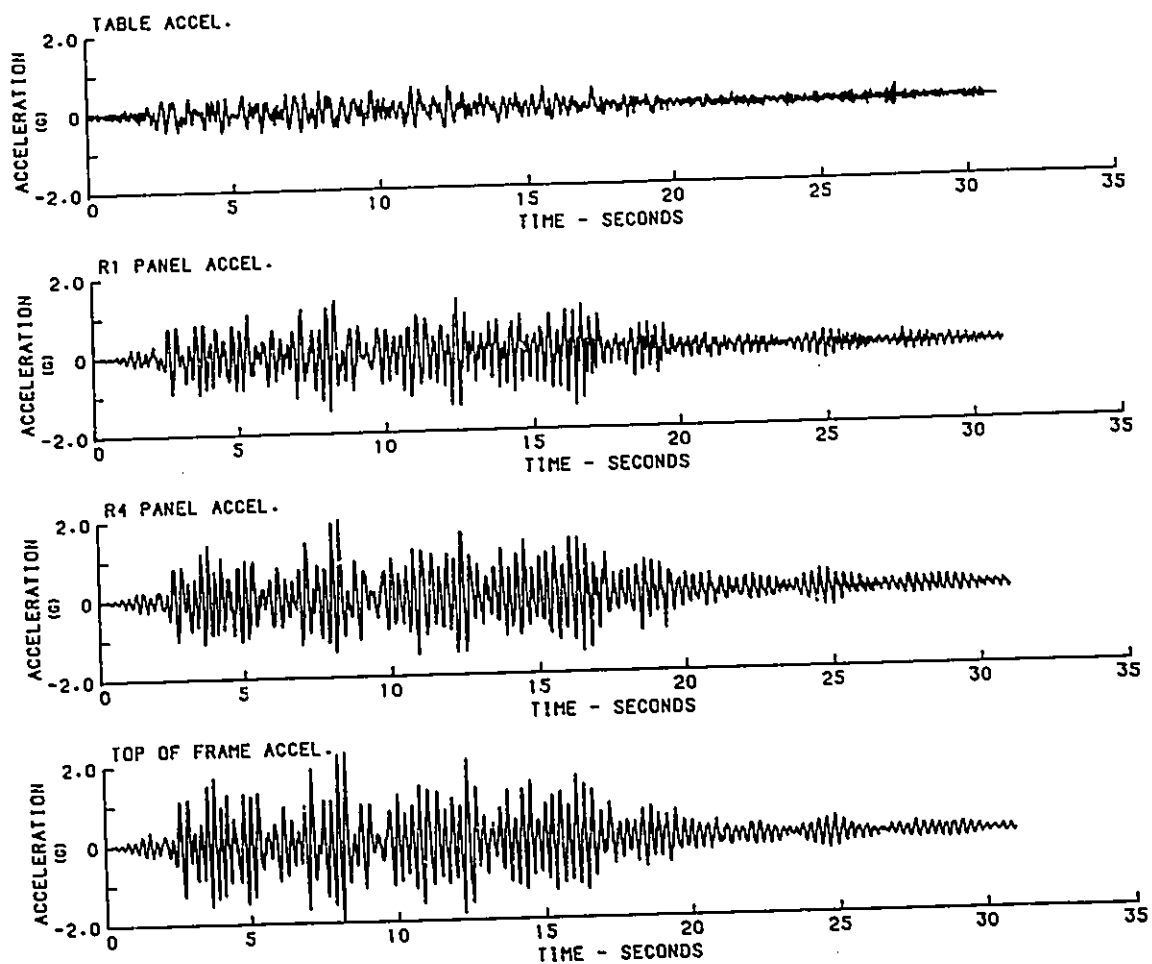


Fig. 4.30 Acceleration time histories for D20SS50B test (equipment side-to-side, D20 bolted panels and 50% NEBS excitation)

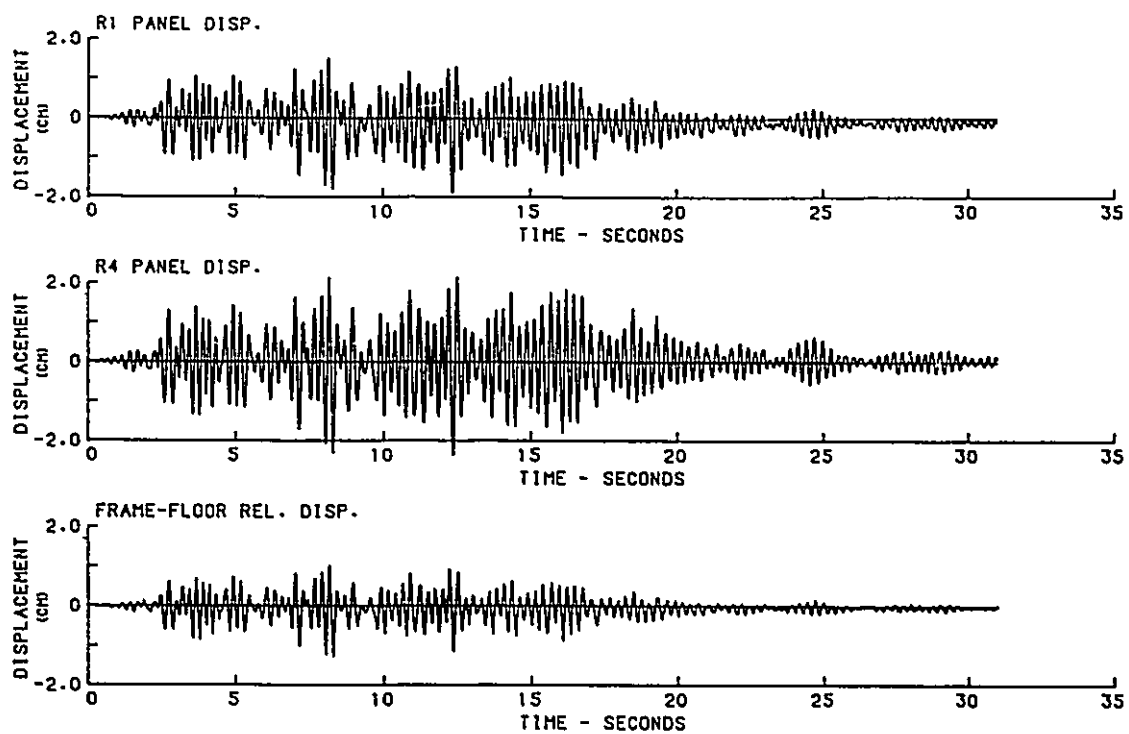


Fig. 4.31 Displacement time histories for D20SS50B test (equipment side-to-side, D20 drop-in panels and 50% NEBS excitation)

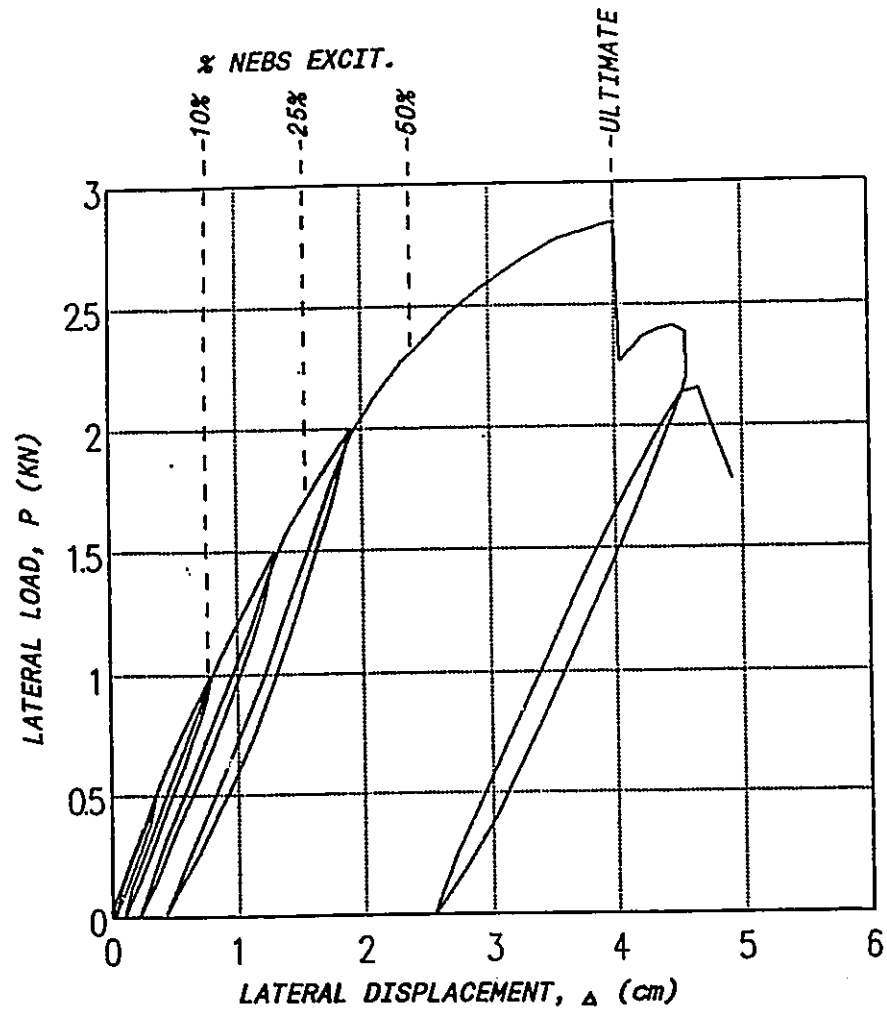


Fig. 4.32 Correlation between dynamic and static load-deflection behaviour for D20 access floor, equipment side-to-side

## CHAPTER 5

### ANALYTICAL MODEL FOR EQUIPMENT-ACCESS FLOOR SYSTEMS

#### 5.1 Introduction

The experimental work presented in the previous three chapters have provided valuable information on the dynamic behaviour of the particular equipment-access floor systems tested. To gain further insight on the dynamics of equipment-access floor systems in general, an analytical study is carried out using an analytical model of equipment-access floor systems. In this chapter, the development of this analytical model is described. The results of a parametric studies using this model are presented. Finally, the experimental results are used to verify the adequacy of the analytical model.

#### 5.2 Development of the Analytical Model

The random excitation tests have shown that the access floor behaves as a single degree of freedom (SDOF) lumped mass system. The natural frequency of this SDOF system is a function of the individual pedestal stiffness, the number of pedestals and the total mass at the floor panel level. Results based on a number of telecommunications equipment installed on fixed bases tested at McMaster University have

shown that only the fundamental mode of the equipment is excited within the frequency range of the seismic excitation specified by the NEBS criteria (Tso and Naumoski, 1990). The equipment can, therefore, be treated as a generalized SDOF system. With these observations in mind, the combined equipment-access floor model shown in Fig.(5.1) is proposed. In this model, the access floor is modelled as a single degree of freedom lumped mass system having a stiffness of  $K_f$ , a mass of  $M_f$  concentrated on the floor panel level, and a viscous damping coefficient of  $C_f$ . The displacement of the access-floor is denoted by  $u_f(t)$ . The equipment has a total mass of  $M_e$  and a mass distribution of  $m(x)$  and a distributed damping coefficient  $c(x)$  where  $x$  is a distance measured from the base of the equipment. The dynamic equilibrium of the equipment in the lateral direction at time  $t$  and at a distance  $x$  from the base is expressed as

$$\mathcal{g}[z(x,t)] + p(x,t) = 0$$

where  $\mathcal{g}$  is a self-adjoint linear differential operator which depends on the elastic properties of the equipment,  $z(x,t)$  is the relative displacement of the equipment with respect to its base, and  $p(x,t)$  represents the lateral loading which includes inertial and damping forces. The equipment is considered to be a generalized SDOF system with a lateral vibration shape defined by the shape function  $\phi(x)$  which satisfies the kinematic boundary conditions. The relative displacement  $z(x,t)$  can, therefore, be written as

$$z(x,t) = \phi(x)u_e(t)$$

where  $u_e(t)$  is the generalized coordinate denoting the displacement at the

top of the equipment relative to the equipment base.

The equipment-access floor model described above is a two degree of freedom system, and its motions are completely defined by  $u_e(t)$  and  $u_f(t)$ .

### 5.3 Equations of Motion

The equations of motion for the model subjected to a base acceleration  $\ddot{u}_g$  are formulated in Appendix II using the principle of virtual work and are written as

$$[M]\{\ddot{u}\} + [C]\{\dot{u}\} + [K]\{u\} = \{P\}\ddot{u}_g \quad (5.1)$$

where the mass matrix  $[M]$ , damping matrix  $[C]$  and stiffness matrix  $[K]$  take the form of

$$[M] = \begin{bmatrix} M_t & \gamma M^{\dagger} \\ \gamma M^{\dagger} & M^{\dagger} \end{bmatrix}, \quad [C] = \begin{bmatrix} C_f & 0 \\ 0 & C^{\dagger} \end{bmatrix}, \quad [K] = \begin{bmatrix} K_f & 0 \\ 0 & K^{\dagger} \end{bmatrix}$$

and the vectors  $\{P\}$  and  $\{u\}$  are expressed as

$$\{P\} = \langle M, \gamma M^{\dagger} \rangle^T,$$

and  $\{u\} = \langle u_f, u_e \rangle^T$

The elements inside the matrices  $[M]$ ,  $[C]$ , and  $[K]$  and the vector  $\{P\}$  are defined as follows

$$M^{\dagger} = \int_0^l m(x) \phi^2(x) dx \quad = \text{the generalized mass of the equipment;}$$

$C^{\dagger} = \int_0^l c(x)\phi(x)^2 dx$  = the generalized damping of the equipment;

$K^{\dagger} = \int_0^l g[\phi(x)]\phi(x) dx$  = the generalized stiffness of the equipment;

$M_t = M_e + M_f$  = the total mass of the equipment-access floor system.

and 
$$\gamma = \frac{\int_0^l m(x)\phi(x) dx}{\int_0^l m(x)\phi^2(x) dx}$$

Dividing Eqn.(5.1) by  $M_t$ , the equation of motion can be written as

$$\begin{bmatrix} 1 & \gamma\alpha\mu \\ \gamma\alpha\mu & \alpha\mu \end{bmatrix} \begin{Bmatrix} \ddot{u}_f \\ \ddot{u}_e \end{Bmatrix} + \begin{bmatrix} 2\xi_f\omega_f & 0 \\ 0 & 2\alpha\mu\xi_e\omega_e \end{bmatrix} \begin{Bmatrix} \dot{u}_f \\ \dot{u}_e \end{Bmatrix} + \begin{bmatrix} \omega_f^2 & 0 \\ 0 & \alpha\mu\omega_e^2 \end{bmatrix} \begin{Bmatrix} u_f \\ u_e \end{Bmatrix} = -\ddot{u}_f \begin{Bmatrix} 1 \\ \gamma\alpha\mu \end{Bmatrix} \quad (5.2)$$

where  $\omega_f = \sqrt{(K_f/M_t)}$  = the effective access floor frequency;  
 $\xi_f = C_f/2M\omega_f$  = the effective access floor damping ratio;  
 $\mu = M_e/M_t$  = the equipment mass ratio;  
 $\omega_e = \sqrt{(K^{\dagger}/M^{\dagger})}$  = the equipment frequency;  
 $\xi_e = C^{\dagger}/2M^{\dagger}\omega_e$  = the equipment damping ratio;  
 and  $\alpha = M^{\dagger}/M_e$  = the generalized mass coefficient.

The equipment mass ratio  $\mu$  is defined as the mass of the equipment divided by the total mass of the equipment-access floor system. Its value is

always less than unity. The effective floor frequency  $\omega_f$  and the effective access floor damping ratio  $\xi_f$  are the frequency and damping ratio of the access floor when a mass equal to the mass of the equipment is being attached to the floor panels. The parameters  $\omega_e$  and  $\xi_e$  are the frequency and the damping ratio of the equipment when it is mounted on a fixed base. The generalized mass ratio  $\alpha$  is the ratio between the generalized mass  $M^*$  and the mass of the equipment  $M_e$ . The parameter  $\gamma$  is a factor dependent on the mass distribution  $m(x)$  and the shape function  $\phi(x)$  of the equipment.

The response of the equipment-access floor model subjected to any arbitrary base excitation  $\ddot{u}_g$  is given by the solutions to Eqn.(5.2).

#### 5.4 Undamped Free Vibration Response

In order to understand its dynamic characteristics, the undamped free vibration of the equipment-access floor model is studied. The solution for the equations of motion is taken in the form of

$$\begin{Bmatrix} u_f \\ u_e \end{Bmatrix} = \{\Phi\} e^{i\omega t}$$

Substituting this assumed solution in Eqn.(5.2) and setting  $\xi_e$ ,  $\xi_f$  and  $\ddot{u}_g$  equal to zero, Eqn.(5.2) becomes

$$[A] \{\Phi\} = \{0\} \quad (5.3)$$

where  $[A] = \begin{bmatrix} (1-\Omega^2)/(\alpha\mu) & -\gamma\Omega^2 \\ \gamma\Omega^2 & \Omega_e^2 - \Omega^2 \end{bmatrix}$

in which  $\Omega_e$  and  $\Omega$  are frequency ratios defined as

$$\Omega_e = \omega_e/\omega_f \quad \text{and} \quad \Omega = \omega/\omega_f.$$

In order to have non-trivial solutions, the determinant of the matrix [A] must vanish which leads to the characteristic equation

$$(1-\gamma^2\alpha\mu)\Omega^4 - (1 + \Omega_e^2)\Omega^2 + \Omega_e^2 = 0 \quad (5.4)$$

The two roots of the characteristic equation are

$$\Omega_1^2 = \frac{1 + \Omega_e^2 - \sqrt{(1 + \Omega_e^2)^2 - 4(1 - \alpha\mu\gamma^2)\Omega_e^2}}{2(1 - \alpha\mu\gamma^2)} \quad (5.5a)$$

$$\text{and} \quad \Omega_2^2 = \frac{1 + \Omega_e^2 + \sqrt{(1 + \Omega_e^2)^2 - 4(1 - \alpha\mu\gamma^2)\Omega_e^2}}{2(1 - \alpha\mu\gamma^2)} \quad (5.5b)$$

Substituting the above two eigenvalues into Eqn.(5.3), the corresponding eigenvectors are expressed as

$$\{ \phi \}_1 = \begin{Bmatrix} S_1 \\ 1 \end{Bmatrix} \quad (5.6a)$$

$$\text{and} \quad \{ \phi \}_2 = \begin{Bmatrix} S_2 \\ 1 \end{Bmatrix} \quad (5.6b)$$

$$\text{where} \quad S_1 = [(\Omega_e/\Omega_1)^2 - 1]/\gamma,$$

$$\text{and} \quad S_2 = [(\Omega_e/\Omega_2)^2 - 1]/\gamma.$$

The free vibration mode shapes expressed in the form given in Eqn.(5.6) may be difficult to visualize since the two coordinates are measured relative to two different points. The degree of freedom at the top of the

equipment is defined relative to the access floor, and the access floor relative to the fixed base. It is more illustrative if the mode shapes are transformed such that both degrees of freedom are relative to the fixed base. The transformed mode shapes  $\{\Phi\}_1^{\dagger}$  and  $\{\Phi\}_2^{\dagger}$  can be written as

$$\{\Phi\}_1^{\dagger} = \begin{Bmatrix} S_1^{\dagger} \\ 1 \end{Bmatrix} \quad (5.7a)$$

and 
$$\{\Phi\}_2^{\dagger} = \begin{Bmatrix} S_2^{\dagger} \\ 1 \end{Bmatrix} \quad (5.7b)$$

where

$$S_1^{\dagger} = \frac{S_1}{1 + S_1} \quad \text{and} \quad S_2^{\dagger} = \frac{S_2}{1 + S_2} \quad (5.7c)$$

Eqns.(5.5) and (5.7) can be used to calculate the modal frequency ratios and the mode shapes for the equipment-access floor model. Although the derivation is for an undamped system, the modal frequencies differ very little for the damped cases since the system is lightly damped.

### 5.5 Parametric Study

As indicated by Eqns.(5.5) and (5.7), the modal frequency ratio and mode shape are functions of the equipment frequency ratio  $\Omega_e$ , the mass ratio  $\mu$ , and the parameter  $\alpha$  and  $\gamma$  which are functions of the equipment shape function and the mass distribution. In this section the effects of these parameters on the frequency ratios and mode shapes are discussed.

Prior to the parametric study, it is necessary to determine the appropriate shape function  $\phi(x)$  for telecommunications equipment.

Telecommunications equipment is usually housed in a steel framework similar to the one shown in Fig.5.2. In the back-to-front (BF) orientation, the frame is in general slender. The lateral stiffness of the frame is derived mainly from its two uprights. The lateral vibrational shape of the equipment in this orientation depends on the relative stiffness among its uprights, its base-plate and its anchorage system. For frames with a base-plate and an anchorage system which are stiff compared to the uprights, a vibrational shape similar to the deflected shape of a cantilever beam can be expected. Where either the base-plate or the anchorage system are relatively flexible compared to the uprights, a linear vibrational shape is expected as the frame tends to rock about its base.

For the side-to-side (SS) orientation, the lateral vibrational shape depends only on how the two uprights are tied together along the height of the frame. For most telecommunications equipment, the uprights are tied together by a cross member at the top and also connected along its height at specified locations by equipment shelves. In this case, the lateral vibrational shape on a fixed base would vary between a single curvature and a double curvature shape depending on the stiffness of the link members as shown in Fig.5.3. The double curvature shape shown in Fig.5.3b may be approximated by a straight line joining the base and the top of the equipment.

Based on the above considerations, two shape functions are taken as representatives of the lateral vibrational shape of the equipment. One shape function corresponds to the mode shape of the first mode vibration of a uniform cantilever beam. The other shape function is a linear

function of the height of the equipment. The mode shape for the first mode vibration of a uniform cantilever beam with a length  $L$  (hereafter referred as cantilever shape function) is expressed as

$$\phi(x) = B \left[ \sin(ax) - \sinh(ax) + \frac{\sin(aL) + \sinh(aL)}{\cos(aL) + \cosh(aL)} (\cosh(ax) - \cos(ax)) \right]$$

where  $aL = 1.875$

and  $B$  is a normalizing constant chosen such that  $\phi(L) = 1$ . The linear shape function is written as

$$\phi(x) = x / L.$$

Given the mass distribution  $m(x)$ , the values of  $a$  and  $\gamma$  for the above two shape functions can be computed. For most telecommunications equipment, the mass distribution can be assumed to be uniform along the height. With this assumption for  $m(x)$ , the value of  $a$  is 0.25 for the cantilever shape function and 0.33 for the linear shape function, and the value of  $\gamma$  is 1.56 for the cantilever shape function and 1.5 for the linear shape function. For comparison purposes, both  $a$  and  $\gamma$  are equal to unity if the equipment is modelled as SDOF lumped mass model.

The range of equipment-access floor frequency ratios  $\Omega_e$  considered in the parametric study is between 0.1 and 10. Any equipment-access floor system whose frequency ratio is outside this range can be treated as a single degree of freedom system in analyses. On one extreme where the frequency ratio is small, the equipment may be treated as mounted directly on a fixed base. On the other extreme where the frequency ratio is large, the equipment may be considered as a rigid body supported on the access floor.

The modal frequency ratios  $\Omega_1$  and  $\Omega_2$  obtained by normalizing with the effective floor frequency  $\omega_f$  are plotted against the equipment-floor frequency ratios  $\Omega_e$  in Fig.5.4. The two graphs shown in this figure correspond to mass ratios  $\mu$  of 0.9 and 0.1. Both the cantilever and the linear equipment shape function are considered. As shown by the figure, the choice of shape function for the equipment essentially has no effect on the first mode frequency ratio of the combined equipment-access floor system. The second mode frequency ratio is more sensitive to the shape function chosen, particularly for large mass ratio.

It can be seen from Fig.5.4 that the first mode frequency ratio  $\Omega_1$  asymptotically approaches a value of unity as  $\Omega_e$  increases, and asymptotically approaches  $\Omega_e$  as  $\Omega_e$  decreases. For a mass ratio of  $\mu=0.9$ , the first mode frequency ratio  $\Omega_1$  can be assumed equal to unity for  $\Omega_e > 4$ . This implies that the first mode frequency is equal to the effective floor frequency  $\omega_f$ . In this case, the equipment is much stiffer than the access floor, therefore the first mode frequency of the combined system can be approximated by treating the equipment as a rigid body attached to the access floor. For  $\Omega_e < 0.5$ , the first mode frequency ratio  $\Omega_1$  can be assumed equal to  $\Omega_e$ . This means that the first mode frequency is the same as the frequency of the equipment. In this case, the access floor is much stiffer than the equipment, hence, the first mode frequency of the combined system can be approximated by treating the access floor as a fixed base. Interaction of the equipment and the access floor becomes significant for  $\Omega_e$  between 0.5 and 4 for large mass ratios of the order of 0.9. The interaction range is reduced to between 0.8 and 1.25 for small mass ratios of the order of 0.1. Within the range of  $\Omega_e$  where the interaction of the

equipment and the access floor is significant, the two degree of freedom model developed here is needed to be used to determine the first mode frequency analytically.

The second mode frequency ratio  $\Omega_2$  asymptotically approaches a constant value which is greater than unity as  $\Omega_e$  decreases. This implies that when the effective floor frequency is larger than the equipment frequency (i.e.  $\Omega_e < 1$ ), the second mode frequency is always larger than the effective floor frequency. When the equipment frequency is larger than the effective floor frequency (i.e.  $\Omega_e > 1$ ), the second mode frequency is always larger than the frequency of the equipment.

In summary, the modal frequency ratio curves in Fig.5.4 imply that the first mode frequency of an equipment-access floor system is always less than the smaller of the equipment frequency or the effective floor frequency. The second mode frequency is always greater than the larger of the equipment frequency or the effective floor frequency.

The mode shapes associated with the modal frequencies are given in Eqn.(5.7) with the top of the equipment displacement coordinate normalized to unity. With such normalization, the values of the first elements in the mode shape vectors  $S_1^\dagger$  and  $S_2^\dagger$  will provide information to describe the actual mode shapes. Hereafter,  $S_1^\dagger$  and  $S_2^\dagger$  as defined by Eqn.(5.7c) will be referred to as the mode shape coordinates at the access floor level. The mode shape coordinates at the access floor level are plotted against the equipment frequency ratios ( $\Omega_e$ ) in Fig.5.5 using a linear and a cantilever equipment shape function. The two graphs shown in this figure correspond to mass ratios of 0.9 and 0.1. Similar to the modal frequency ratios, the first mode shape is indifferent to the choice of

equipment shape function.

It can be seen from Fig.5.5 that  $S_1^f$  asymptotically approaches a value of zero as  $\Omega_e$  decreases, and asymptotically approaches a value of unity as  $\Omega_e$  increases. For a mass ratio of  $\mu=0.9$ , when the access floor is much stiffer than the equipment (i.e.  $\Omega_e < 0.5$ ), the first mode response of the combined equipment-access floor system at the access floor level is negligible compared to the response at the top of the equipment. This implies that the access floor can be treated as a fixed base in the determination of the first mode shape. For the case where the equipment is much stiffer than the access floor (i.e.  $\Omega_e > 4$ ) the first mode response of the combined equipment-access floor system occurs almost entirely at the access floor. The equipment in this case merely rides on the access floor as a rigid body. Within the range of  $\Omega_e$  between 0.5 and 4, interaction of the equipment and the access floor has a significant effect on the first mode shapes. In this range of  $\Omega_e$ , the response of the equipment and the response of the access floor are both significant to the first mode response of the combined system.

The second mode shape coordinate at the access floor level  $S_2^f$  is always negative. This indicates that the second mode response motion at the access floor level is always out of phase with respect to that at the top of the equipment.

To study the effect of the mass ratio on the modal frequencies of the equipment-access floor systems, the two modal frequency ratios are plotted in Fig.5.6 for mass ratios of 0.1, 0.5 and 0.9 using a linear equipment shape function. The first mode frequency ratio is insensitive to the mass ratio outside the range of equipment frequency ratio defined by

$0.5 \leq \Omega_e \leq 4$  where interaction between the equipment and the access floor is significant. Within this range of frequency ratios, the interaction of the equipment and the access floor becomes less significant as the mass ratio decreases. The two modal frequencies are in general widely separated except when both the mass ratio is small ( $\mu \leq 0.1$ ) and  $\Omega_e$  is close to unity.

The mode shape coordinates at the access floor level ( $S_1^{\dagger}$  and  $S_2^{\dagger}$ ) are plotted in Fig.5.7 for mass ratios of 0.1, 0.5 and 0.9 using a linear shape function. The first mode shape is relatively insensitive to the mass ratio except in the range of equipment frequency ratios defined by  $0.5 \leq \Omega_e \leq 4$  where the interaction between the equipment and the access floor is significant. The mass ratio has large effect on the second mode shape, except when  $\Omega_e$  is small (less than 0.1).

In summary, for an equipment-access floor system whose  $\Omega_e$  is outside the range where the interaction of the equipment and the access floor is significant, its first mode dynamic properties can be determined by treating the system as a single degree of freedom system. Within the interaction range defined by  $0.5 \leq \Omega_e \leq 4$ , the two degree of freedom model given here is the simplest model necessary to evaluate the dynamic properties of equipment-access floor systems.

## 5.6 Comparison of Analytical and Experimental Results

To verify the adequacy of the equipment-access floor model developed in this chapter, the model is used first to predict the dynamic properties of some of the equipment-access floor systems tested in the experiment. Second, the model is used to predict the acceleration

response time histories measured in the experiment for two equipment-access floor systems under NEBS time history excitation.

*i. Dynamic properties*

The frequencies and mode shapes of the equipment-access floor systems tested in the experiment can be computed using Eqs.(5.5) and (5.7). The computed values are compared with the experimental values to check the validity of the model. The comparison is carried out for four sets of experimental results corresponding to the equipment on both the D12 and the D20 access floor with bolted panel attachment and in both the SS and the BF orientation. These tests have been designated as D12SS-B, D12BF-B, D20SS-B and D20BF-B in Table 3.7.

The parameters required for the determination of the modal frequencies and mode shapes are tabulated in Table 5.1. The equipment mass ratios  $\mu$  are 0.88 for all four cases. The equipment frequencies are 8.9 and 13.1Hz for the SS and BF orientation, respectively. The effective floor frequencies computed based on the random excitation test data are 9.14Hz for the D12 and 4.87Hz for the D20 access floor system. With these effective floor frequencies, the equipment frequency ratios  $\Omega_e$  range from 0.97 for the D12SS-B system to 2.69 for the D20BF-B system as seen in Table 5.1. Based on the equipment mode shapes determined from random excitation tests, the linear equipment shape function is chosen to be used in the computation for both equipment orientations.

The computed frequencies and mode shapes of the test specimens are summarized in Table 5.2. The discrepancies between the computed values and the experimental values are also shown. It can be seen that the

analytical model gives very good estimates for the first and second mode frequencies when the equipment is in a SS orientation on both access floors. The theoretical values are in general within  $\pm 10\%$  of the experimental values. The predicted first and second mode shapes have larger discrepancies of up to 25% for this equipment orientation.

For the equipment in BF orientation on the D12 and the D20 access floor, the first mode frequency values calculated using the analytical model agree well with the experimental results. The discrepancies are 12% for the D12BF-B system and 1% for the D20BF-B system. For the second mode frequencies the discrepancies are higher.

Collectively, the comparison shows that the analytical model gives better estimates of frequencies and mode shapes for the cases where the equipment is in the SS orientation than in the BF orientation. For the equipment in the BF orientation on both access floor systems, the analytical model always overestimates both modal frequencies. The overestimation is due to the fact that the flexibility of the floor panels which may cause the equipment to rock in the back-to-front orientation is not taken into account by the analytical model.

## *ii Response time histories*

To compute the response time histories of the 2DOF equipment-access floor model under earthquake induced excitation, a computer program was written to numerically integrate Eqn(5.2) using Wilson- $\theta$  numerical integration technique. The parameters which are required by the computer program to completely define the 2DOF model are the effective floor frequency  $\omega_f$ , the effective floor damping ratio  $\xi_f$ , the equipment frequency

$\omega_e$ , the equipment damping ratio  $\xi_e$ , the mass ratio  $\mu$  and the shape function parameters  $\alpha$  and  $\gamma$ . A linear shape function and a uniform equipment mass distribution are assumed in the computations of  $\alpha$  and  $\gamma$ .

Two sets of acceleration response time histories corresponding to the D12SS25B and D20SS10B test setups are considered. The D12SS25B test was carried out for the equipment in a side-to-side orientation on the D12 access floor with bolted panels, and under an excitation of 25% of NEBS. The D20SS10B test was conducted for the equipment in a side-to-side orientation on the D20 access floor with bolted panels and subjected to a 10% NEBS excitation. The parameters used for the computation are taken from the experimental results obtained from random excitation tests. The effective floor frequency  $\omega_f$  is equal to 4.87 and 9.14Hz for the D20 and D12 floor system, respectively. The frequency of the equipment  $\omega_e$  in a side-to-side orientation is 8.91Hz. The mass ratio  $\mu$  is 0.88 for both cases. The random excitation tests have shown that the damping ratios of both the access floor and the equipment are dependent on the amplitude of the excitation. Therefore, a series of damping ratios between 1% to 4% are used for the computations. It was found that the response time histories obtained from the computation were closest to the response time histories obtained from the experiment when both  $\xi_e$  and  $\xi_f$  are taken to be 2%. The actual measured table motions from the experiment are taken as the input excitation for the computation.

The computed acceleration response time histories at the top of the equipment and at the access floor are plotted along with the corresponding experimental time histories in Fig.5.8 for the D20SS10B setup. Excellent agreement in frequency content and amplitude can be seen

between the equipment acceleration time histories obtained from computation and from experiment. The computed access floor response acceleration has a slightly higher amplitude than the experimental response. The 2% damped response spectra for the theoretical and the experimental response time histories are shown in Fig.5.9a for the acceleration at the top of the equipment and Fig.5.9b for the acceleration on the access floor. In both figures, the theoretical and the experimental spectra essentially coincide except at frequencies around the second mode frequency. The theoretical spectra show that the second mode response is not excited by the input motion, but the experimental spectra show that the second mode response was in fact excited in the experiment. However, this subtle difference on the second mode response has almost no effect on the response time histories.

Similar sets of time histories and response spectra for the D12SS25B test are shown in Fig.5.10 and 5.11. The experimental and theoretical acceleration time histories at the top of the equipment in general agree well with each other. The amplitude of the theoretical response is slightly lower than the experimental response at the access floor level. Also, the theoretical response contains less high frequency components than the experimental response. The response spectra of the time histories show that the magnitudes of the second mode peaks for the theoretical response at the top of the equipment and on the access floor are lower than that of the experimental response. Again, although the second mode response may appear to be significant on the spectra, its contribution to the response time histories is insignificant, particularly, for the equipment response.

## 5.7 Summary and Conclusions

In this chapter a two degree of freedom model is developed to study the dynamics of equipment-access floor systems. The model developed is used to perform a parametric study for the modal frequencies and the mode shapes. The first mode frequency and the first mode shape are insensitive to the equipment shape function assumed in the analytical model. A 2DOF representation of equipment-access floor systems is necessary in the determination of the modal frequencies and mode shapes in the interaction range defined by  $0.5 \leq \Omega_p \leq 4$ . Outside this range the equipment-access floor system can be treated as a single degree of freedom system in the determination of the first mode dynamic properties. For  $\Omega_p < 0.5$ , the first mode dynamic properties of the equipment-access floor can be determined by treating the equipment as if it is on a fixed base. For  $\Omega_p > 4$ , the first mode dynamic properties of the equipment-access floor system can be computed by treating the equipment as a rigid body attached on the access floor.

Using the equipment-access floor model, the frequencies and mode shapes for the various equipment-access floor systems tested in the experiment are computed. The analytical results agree well with the experimental values for the fundamental mode properties. The model is less reliable in predicting the second mode properties. The response acceleration time histories of two equipment-access floor systems tested under NEBS time history excitation are computed by numerically integrating the equations of motion derived for the model. The computed response time histories agree very well with the experimentally obtained time histories.

Since the analytical model developed here is capable of predicting

the dynamic properties of the equipment-access floor systems and their response time histories under earthquake-induced excitations, the model will be used in the next chapter to generate access floor response spectra.

Table 5.1 Model parameters for the various equipment-access floor systems tested

	D12SS	D12BF	D20SS	D20BF
Equip. Freq. ( $\omega_e$ ), Hz	8.9	13.1	8.9	13.1
Eff. Floor Freq. ( $\omega_f$ ), Hz	9.14	9.14	4.87	4.87
Mass Ratio ( $\mu$ )	0.88	0.88	0.88	0.88
Freq. Ratio ( $\Omega_e$ )	0.97	1.43	1.83	2.69

Table 5.2 Experimental and theoretical modal frequencies and mode shapes

a). Frame side to side on D12 access floor, D12SSB

	Expt.	Linear model	
		Value	Error, %
$\omega_1$ (Hz)	6.7	6.70	-0.0
$\omega_2$ (Hz)	19.5	20.81	6.7
$s_1^{\dagger}$	0.27	0.34	25.9
$s_2^{\dagger}$	-0.93	-1.20	28.1

b). Frame back to front on D12 access floor, D12BFB

	Expt.	Linear model	
		Value	Error, %
$\omega_1$ (Hz)	7.00	7.82	11.7
$\omega_2$ (Hz)	21.00	26.23	25.2
$s_1^{\dagger}$	0.29	0.55	87.0
$s_2^{\dagger}$	-1.62	-1.00	-38.0

Table (5.2) (cont.)

c). Frame side to side on D20 access floor, D20SSB

	Expt.	Linear model	
		Value	Error, %
$\omega_1$ (Hz)	4.70	4.42	-6.0
$\omega_2$ (Hz)	15.05	16.81	11.7
$s_1^{\dagger}$	0.62	0.67	9.1
$s_2^{\dagger}$	-0.93	-0.92	-0.8

d). Frame back to front on D20 access floor, D20BFB

	Expt.	Linear model	
		Value	Error, %
$\omega_1$ (Hz)	4.69	4.66	0.7
$\omega_2$ (Hz)	17.31	23.49	35.7
$s_1^{\dagger}$	0.65	0.82	-25.7
$s_2^{\dagger}$	-1.21	-0.85	-29.8



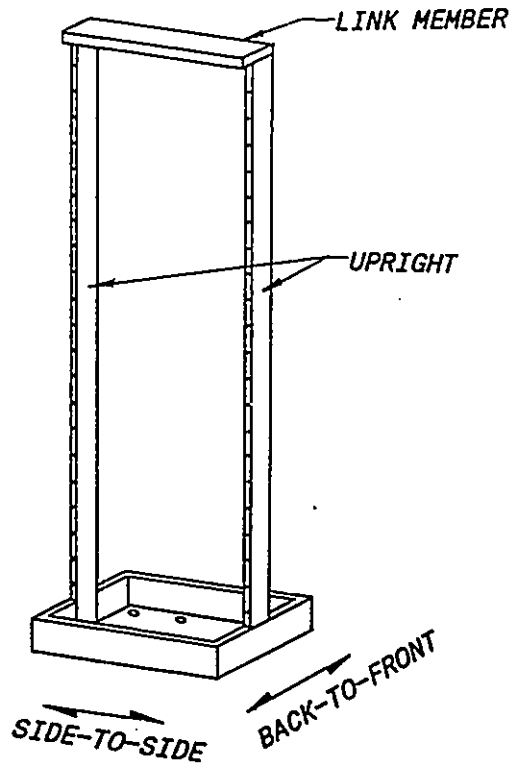


Fig. 5.2 Typical telecommunications equipment framework

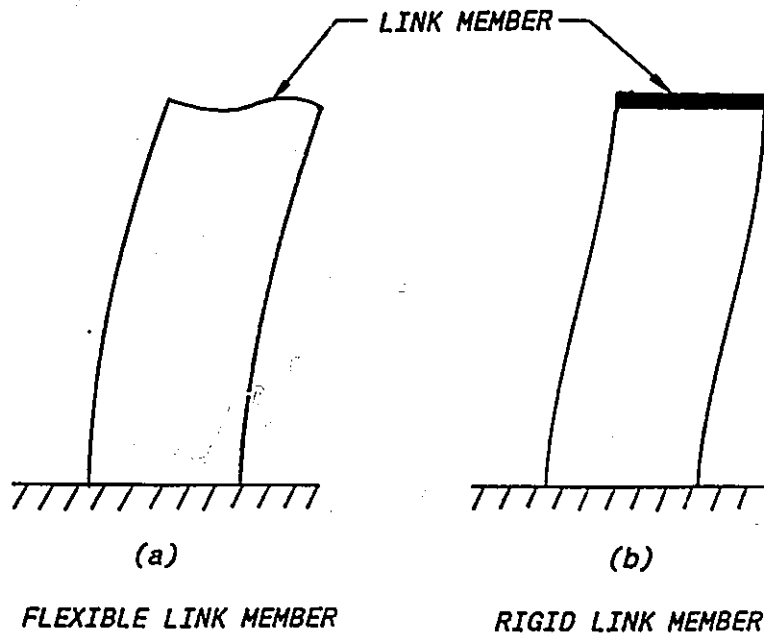


Fig. 5.3 Typical vibrational shapes for equipment in a side-to-side orientation

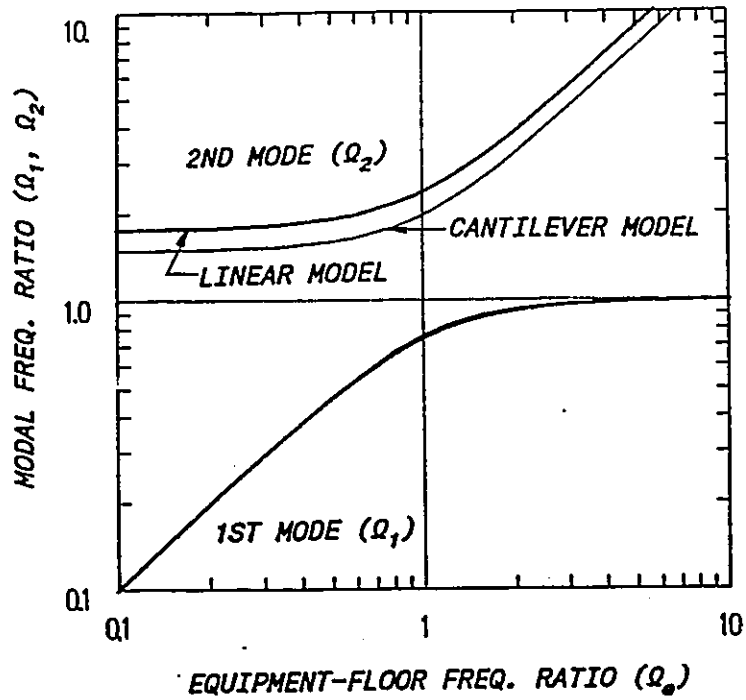
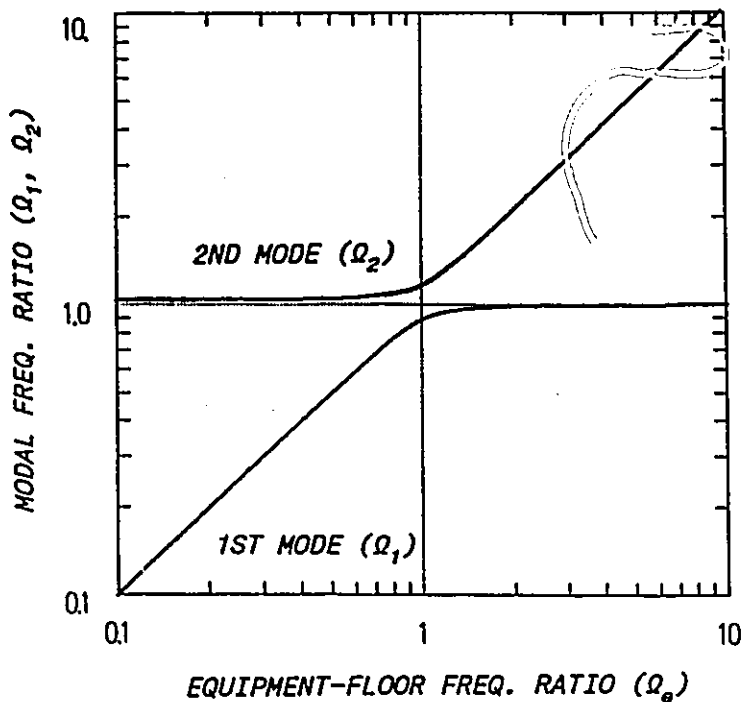
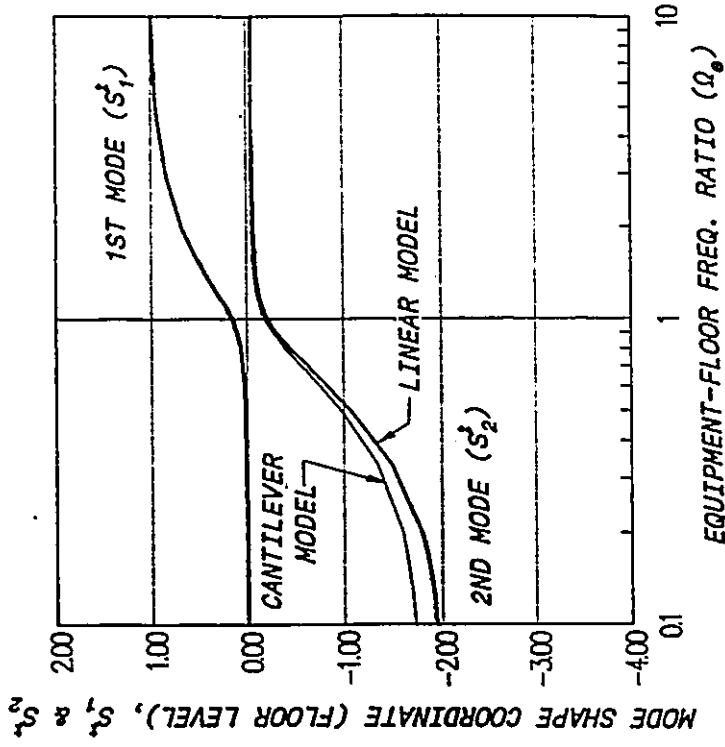
a.)  $\mu = 0.9$ b.)  $\mu = 0.1$ 

Fig. 5.4 Modal frequencies ratios for equipment-access floor systems with different equipment shape functions: a.)  $\mu=0.9$  and b.)  $\mu=0.1$

b.)  $\mu = 0.1$



a.)  $\mu = 0.9$

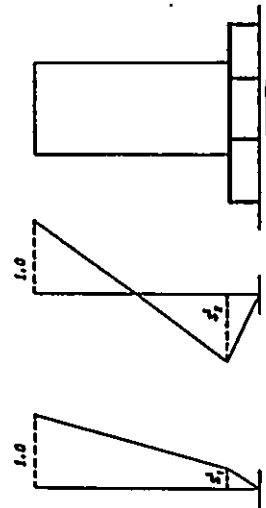
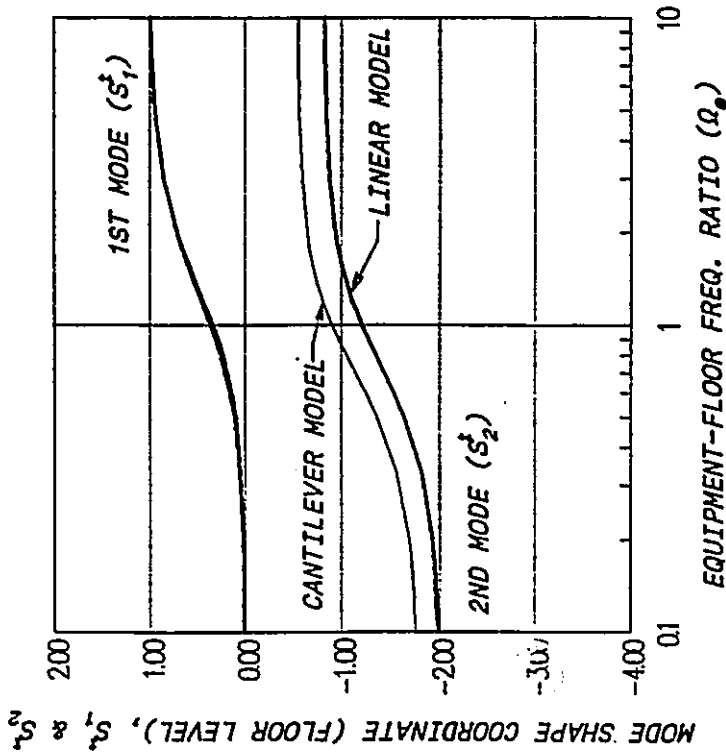


Fig. 5.5 Mode shapes for equipment-access floor systems with different equipment shape function: a.)  $\mu=0.9$  and b.)  $\mu=0.1$

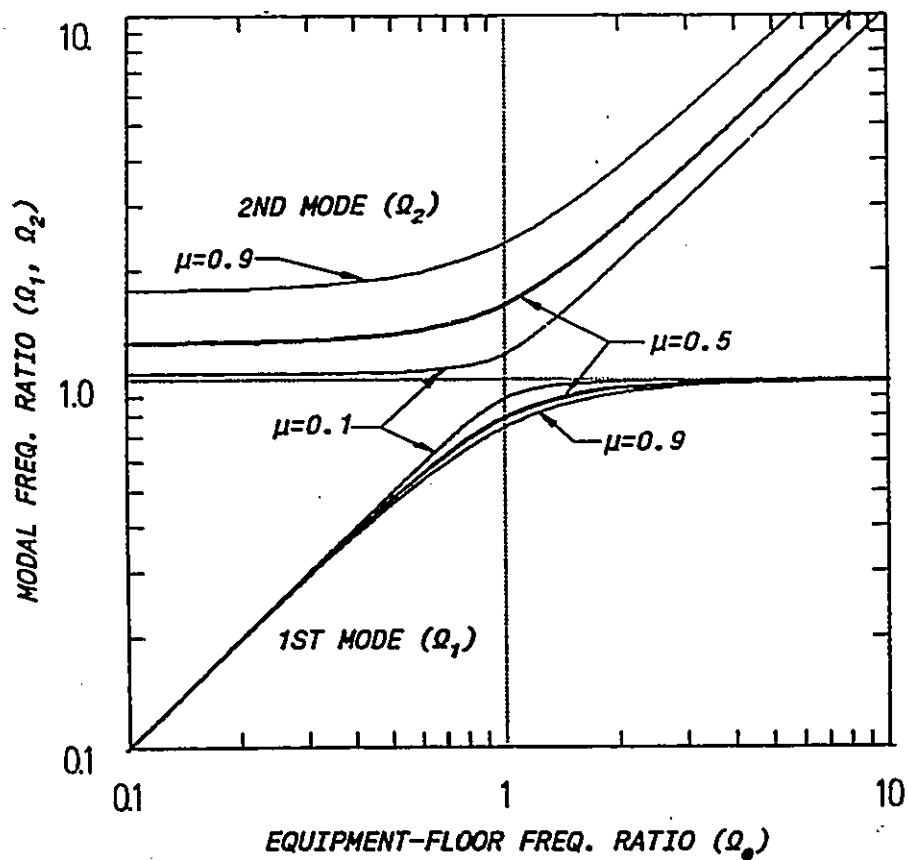


Fig. 5.6. Modal frequencies ratios for equipment-access floor systems with different mass ratios

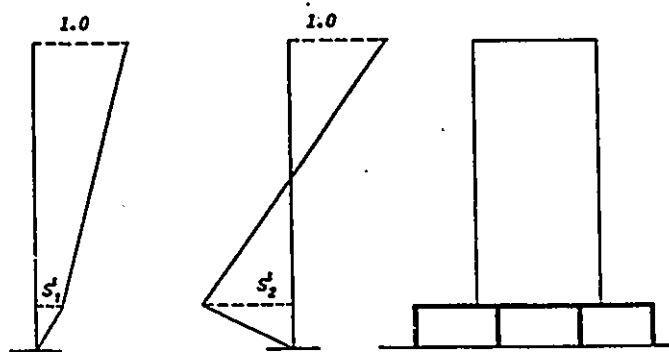
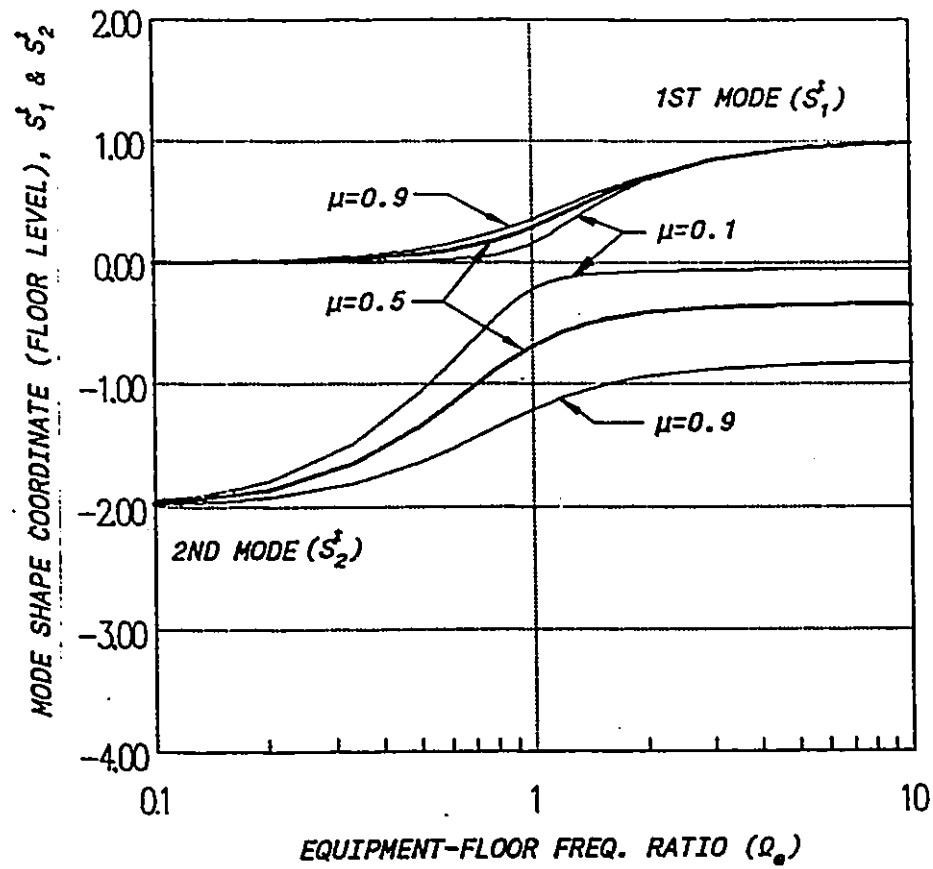


Fig. 5.7 Mode shapes for equipment-access floor systems with different mass ratios

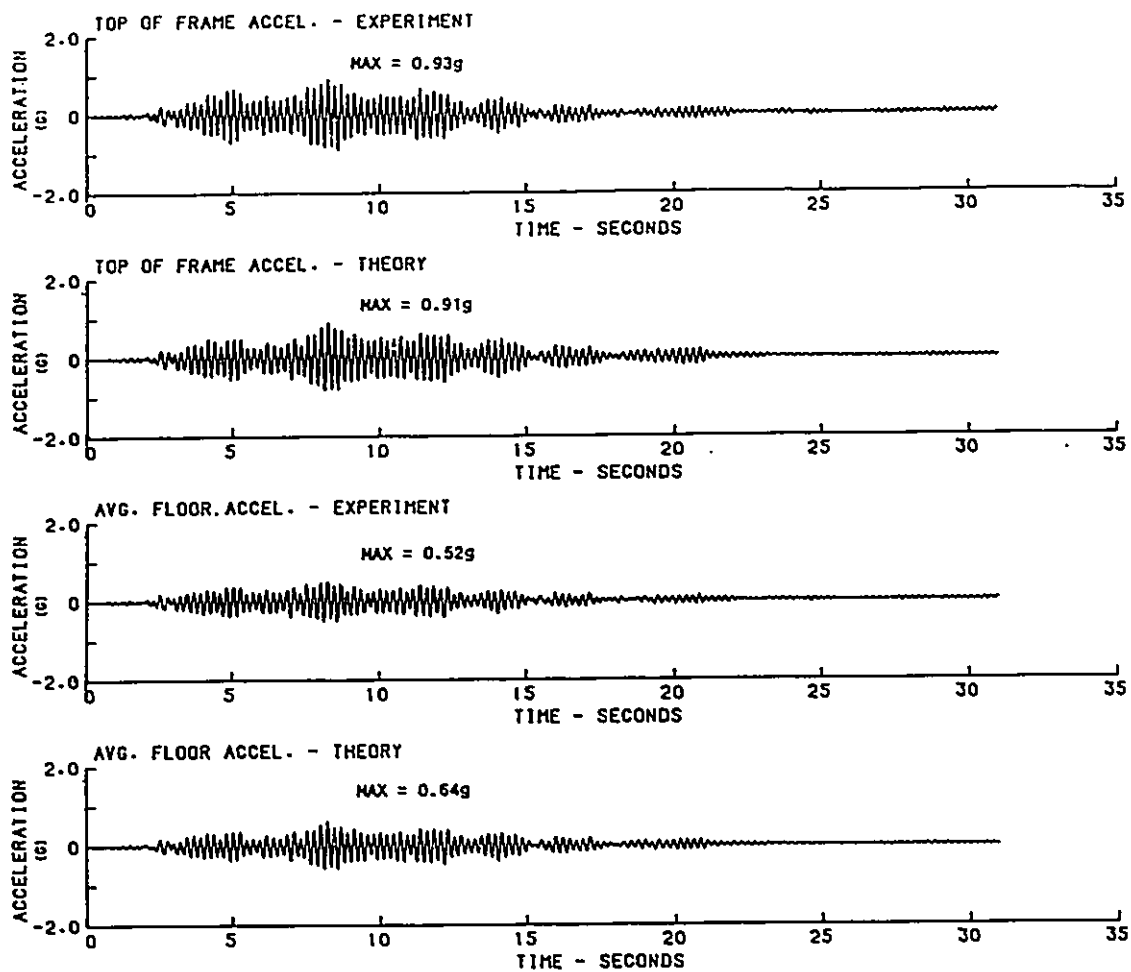
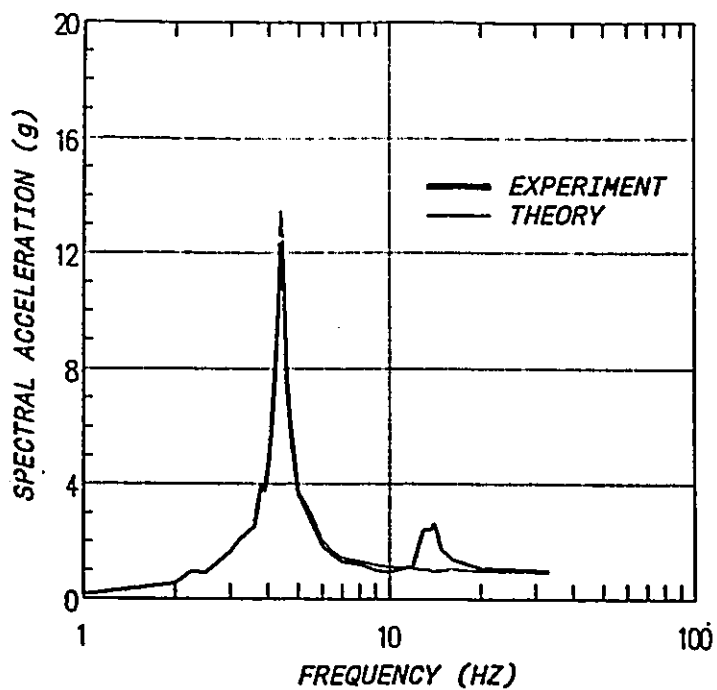


Fig. 5.8 Experimental and theoretical acceleration response time histories for D20SS10B test

## a.) TOP OF EQUIPMENT



## b.) ACCESS FLOOR

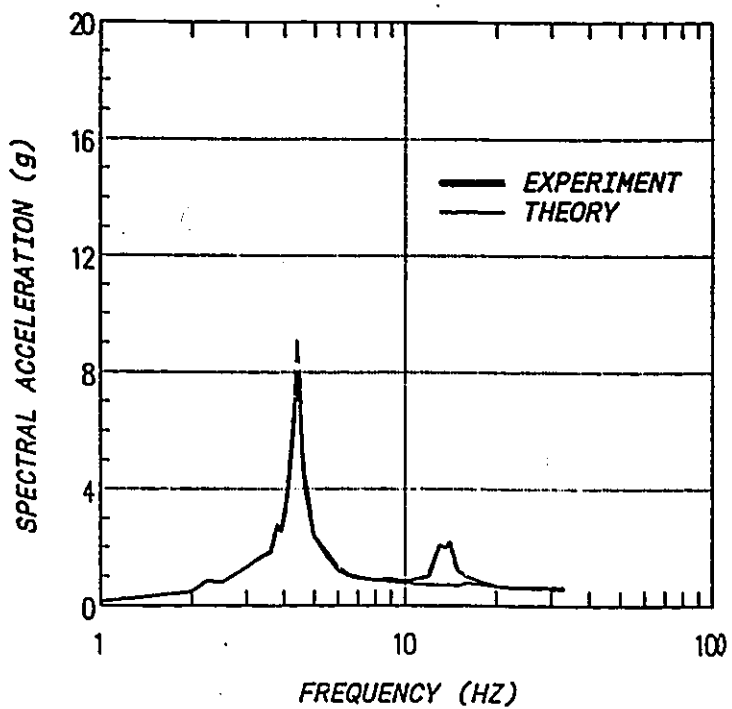


Fig. 5.9 Experimental and theoretical response spectra for D20SS10B test: a.) equipment top acceleration and b.) access floor acceleration

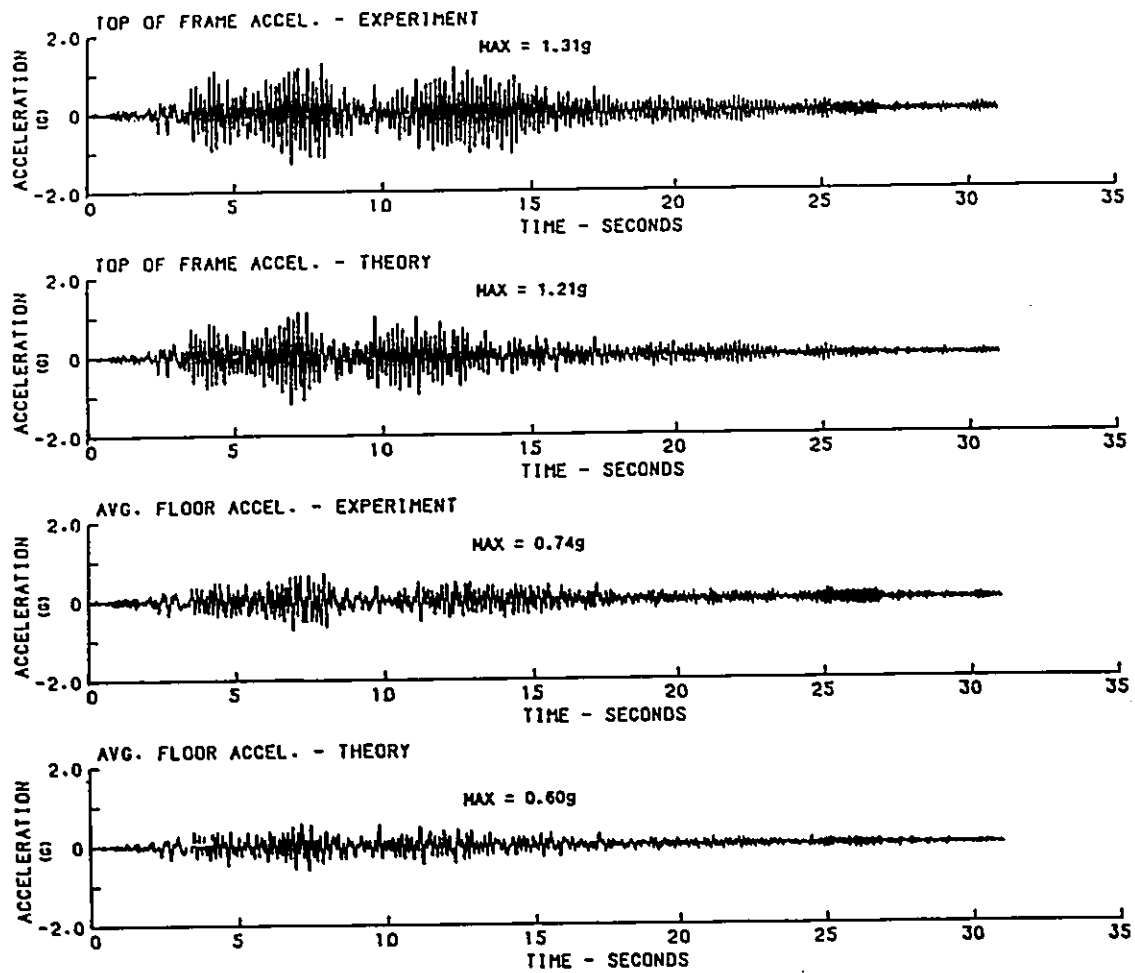


Fig. 5.10 Experimental and theoretical acceleration response time histories for D12SS25B test

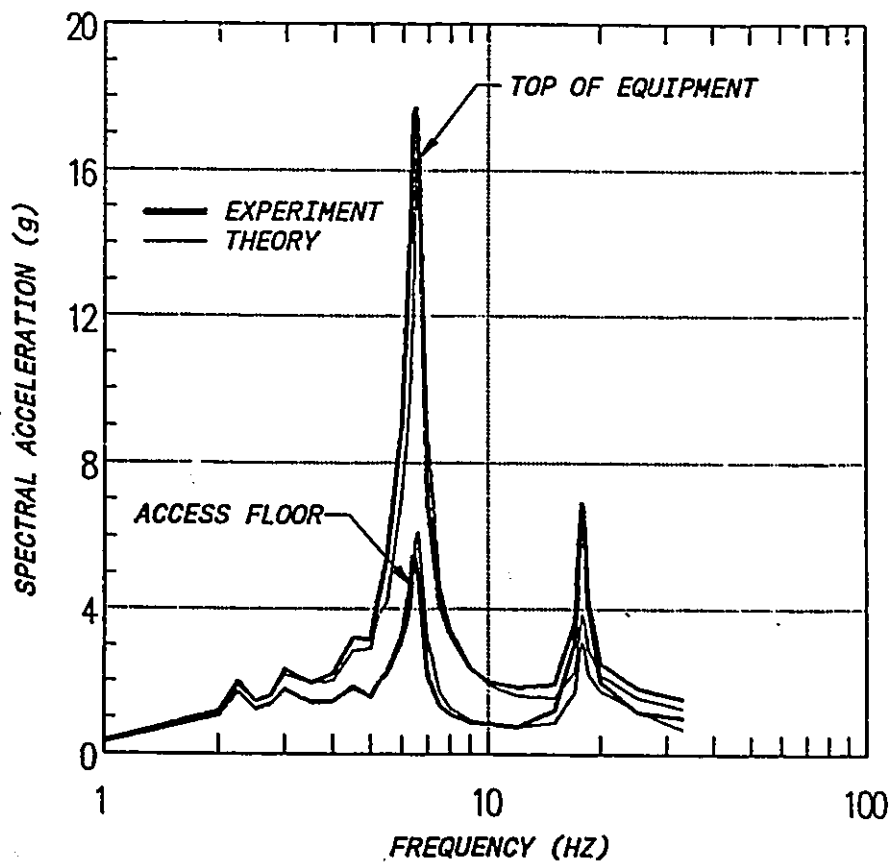


Fig. 5.11 Experimental and theoretical response spectra for D12SS25B test

## CHAPTER 6

### CONSTRUCTION OF ACCESS FLOOR RESPONSE SPECTRA FOR EQUIPMENT IN TELECOMMUNICATIONS CENTRAL OFFICES

#### 6.1 Introduction

The ultimate objective of this study is to provide guidelines for the seismic analysis, design, and qualification of equipment supported on access floors in telecommunications central offices. These guidelines are provided by means of access floor response spectra which are generated in this chapter. To construct such access floor response spectra, the ranges of parameters which characterize the equipment installations in telecommunications central offices are first established. A parametric study is then carried out to investigate the effect of the different parameters within the relevant ranges on the seismic response of equipment supported on access floors. Based on the parametric study, the situations which lead to upper bound equipment response are established. Access floor response spectra are then generated based on these upper bound situations.

#### 6.2 Selection of Parameter Ranges

A typical equipment floor plan for telecommunications central offices is shown in Fig.(6.1). The central office equipment is usually

installed side by side to form equipment lineups. The number of pieces of equipment in a lineup may vary from a minimum of three to as many as twenty. The lineups are separated from each other typically by a front aisle of 36" (91.5cm) and a rear aisle of 24" (61cm). The equipment in each lineup are interconnected by bolts along the height.

To establish the range of mass ratios for equipment installed in lineups on access floor, two typical equipment lineups are considered in Fig.(6.2). One lineup consists of smaller equipment having a footprint of 18" by 27" (46cm by 68.5cm) and a mass between 400 to 800 lb (180Kg to 360Kg). Another lineup consists of larger equipment which is similar to the one tested in the experiment. The equipment has a footprint of 26" by 42" (66cm by 106.5cm) and a mass of 1650 lb (750Kg). The height of the equipment varies between 6' to 7' (1.8m to 2.1m). Their fundamental frequencies are between 2.5Hz to 14Hz (Tso and Naumoski, 1990). Where the units of equipment in all the lineups are identical, it is dynamically equivalent to consider only a single piece of equipment on its tributary access floor area. The 2DOF model which is derived in chapter 5 for a single piece of equipment on its tributary access floor area is, therefore, applicable to model the lineups of identical equipment supported on access floors in telecommunication central offices.

Based on the equipment mass and the equipment tributary area shown in Fig.(6.2), the equipment mass distribution  $\rho_e$  is calculated to be between 40 lb/ft<sup>2</sup> to 100 lb/ft<sup>2</sup> (200Kg/m<sup>2</sup> to 500Kg/m<sup>2</sup>). Based on data obtained for several commonly used access floor systems, the mass distribution of the access floor alone (denoted as  $\rho_f$ ) is between 5.1 lb/ft<sup>2</sup> to 7.2 lb/ft<sup>2</sup> (25Kg/m<sup>2</sup> to 35Kg/m<sup>2</sup>). With  $\rho_f$  and  $\rho_e$  given, the

ratio  $\mu$  can be determined by

$$\mu = \frac{\rho_e}{\rho_e + \rho_f}$$

The range of mass ratio  $\mu$  determined is between 0.85 and 0.95. For the purpose of developing access floor response spectra,  $\mu$  assumes values within a range between 0.8 and 0.95.

Based on the mass distribution of access floors and the stiffness for several other access floor systems of different manufacturers, the relevant range of effective floor frequency considered is between 3 and 15Hz. The effective floor damping considered here is limited within 2 to 5% critical in view of the values determined from the random excitation tests reported earlier.

### 6.3 Parametric Study for the Seismic Response of Equipment Supported on Access Floors

The parametric study is carried out using access floor response spectra for the ranges of parameters described above. An access floor response spectrum is defined by the maximum response of equipment of different frequencies supported on an access floor and subjected to a given building floor excitation. The spectrum represents the shaking environment which a piece of equipment would experience when it is mounted on an access floor. For a given mass ratio  $\mu$ , an effective floor frequency  $\omega_f$ , an effective floor damping ratio  $\xi_f$  and an equipment damping ratio  $\xi_e$ , the access floor response spectrum is expressed as a function of the equipment frequency  $\omega_e$ .

For conventional building floor response spectra (e.g. NEBS), the interaction of the equipment and the building floor can be neglected. Therefore, the response spectra can be computed by using an uncoupled analysis where the building floor motion is used as the input excitation for the equipment, and the equipment is represented by a discrete SDOF oscillator in the computation. However, for equipment supported on an access floor, the interaction of the equipment and the access floor is in general significant. As a result, a 2DOF system representation for the equipment-access floor system is required for the derivation of the access floor response spectra. Furthermore, in order to model the effect of the interaction of the equipment and the access floor correctly, the equipment should be represented as a continuous system. The simplest representation of a continuous system is a generalized SDOF system with a given shape function  $\phi(x)$ .

In order to be consistent with the conventional building floor response spectrum whose spectral values are defined for a discrete SDOF oscillator, the spectral values of the access floor response spectrum are evaluated at a location at a height  $x_a$  from the base of the generalized SDOF equipment system.  $x_a$  is determined such that  $\phi(x_a)=1/\gamma$  where  $\gamma$  is a factor depends on the mass distribution and the shape function of the equipment as defined in chapter 5. The above correspondence between the dynamic response of a discrete SDOF oscillator and that of a generalized SDOF system is discussed in detail by Clough and Penzien (Clough and Penzien, 1975). For a linear shape function and a uniform mass distribution,  $x_a=2L/3$  where  $L$  is the height of the equipment.

The acceleration response of the 2DOF equipment-access floor model

subjected to a base excitation  $\ddot{u}_g$  is computed by numerically integrating Eqn.(5.2). The equipment is assumed to have a uniform mass distribution and to take on a linear shape function in the computation. The absolute acceleration response of the equipment at the location  $x_1=2L/3$  is determined by summing together the fixed base acceleration  $\ddot{u}_g$ , the access floor acceleration relative to the fixed base  $\ddot{u}_f$  and two-thirds of the acceleration at the top of the equipment relative to the access floor  $\ddot{u}_e$ . The maximum values of the acceleration response evaluated at this location constitute the spectral values of the access floor response spectrum.

An ensemble of five time histories which are compatible with the upper bound in-building seismic excitation defined by the 2% damped NEBS spectrum is used as the input excitation. To generate these excitation time histories, an ensemble of five random time histories is first generated from stationary Gaussian white noise. These white noise time histories are then shaped by a deterministic envelope function having a three second initial parabolic build up, followed by 15 seconds of uniform strong shaking and then 13 seconds of an exponential decay. The enveloped time histories are then band-pass filtered with corner frequencies at 0.5Hz and 12Hz. The filtered random time histories are used as the initial time histories in a computer iteration procedure to generate the acceleration time histories which are compatible with the NEBS 2% damped response spectrum. All of the resulted acceleration time histories are scaled such that the maximum acceleration is equal to  $1g$ .

The spectrum compatible acceleration time histories generated by the above procedures are shown in Fig.(6.3). The 2% damped response spectra computed from all five time histories are within  $\pm 20\%$  of the NEBS

spectrum. The average of the 2% damped response spectra for these five time histories is shown in Fig.(6.4). The average spectrum conforms very well to the NEBS spectrum except at around 12 Hz where the average spectrum is about 10% higher than the NEBS spectrum.

Using the 2% damped NEBS spectrum compatible time histories as input excitation, access floor response spectra are constructed. A typical ensemble average response spectrum can be seen in Fig.(6.5) for equipment with a 2% damping ratio. The equipment is supported on an access floor with an effective floor frequency  $\omega_f=6\text{Hz}$ , an effective floor damping  $\xi_f=2\%$  and a mass ratio  $\mu=0.8$ . The access floor response spectrum is in general larger than the 2% damped NEBS building floor spectrum. At a frequency below 2.0Hz (i.e.  $\Omega_e \leq 0.333$ ) the access floor response spectrum is essentially the same as the building floor spectrum. This behaviour qualitatively agrees with the results in chapter 5 which indicate that when the supporting access floor is much stiffer than the equipment, the equipment would behave as if it is supported on a fixed base. As a result, the dynamic response of the equipment on such access floor is the same as that on the building floor. For this particular case where the equipment is supported on an access floor with  $\omega_f=6\text{Hz}$ , the NEBS criteria are, therefore, applicable without modification to equipment having a natural frequency  $\omega_e < 2\text{Hz}$ .

It can be seen from Fig.(6.5) that for equipment frequencies greater than 24Hz (or  $\Omega_e \geq 4$ ), the access floor response spectrum asymptotically approaches a spectral acceleration of 3.1g. This behaviour also agrees with the results in chapter 5 which show that when the equipment is much stiffer than the access floor, the equipment would

behave as a rigid body on the access floor. Hence, the combined equipment-access floor can be treated as a single degree of freedom lumped mass system having a frequency equal to  $\omega_f$  and a damping ratio equal to  $\xi_f$ . For this particular case, a maximum acceleration response of 3.1g is obtained from the 2% damped NEBS spectrum at a frequency of 6Hz.

For equipment with frequencies between 2Hz and 24Hz on an access floor with  $\omega_f=6\text{Hz}$ , Fig.(6.5) indicates that neither treating the equipment as supported on a fixed base nor as a rigid body on the access floor would produce conservative results. Based on similar studies for equipment-access floor system of other  $\omega_f$ 's, it is concluded that in general within the interaction range defined by  $0.25 \leq \Omega_e \leq 4$  (or  $0.25\omega_f \leq \omega_e \leq 4\omega_f$ ) the dynamic response of the equipment on an access floor is needed to be determined from an analysis using the two degree of freedom model given here.

To study the effect of the mass ratio  $\mu$  on the seismic response of equipment supported on access floors, the average access floor response spectra for mass ratios of 0.8 and 0.95 are plotted in Fig.(6.6). The two graphs shown in this figure correspond to effective floor frequencies of 3Hz and 9Hz. The damping ratios for both the equipment and the access floor are assumed to be 2%. It is evident that in the range between 0.8 and 0.95 the effect of mass ratio on the response of the equipment under NEBS excitation is insignificant throughout the entire equipment frequency range. The response spectrum corresponding to  $\mu=0.8$  is in general slightly higher than that of  $\mu=0.95$ .

To investigate the effect of the effective floor damping ratios  $\xi_f$  on the response of the equipment under NEBS excitation, access floor response spectra for different  $\xi_f$  are plotted in Fig.(6.7). The three

graphs shown in the figure correspond to effective floor frequencies  $\omega_f$  of 3Hz, 9Hz and 15Hz and a mass ratio  $\mu$  of 0.8. The two curves in each of the three graphs correspond to  $\xi_f$  of 2% and 5%. In general, the effective floor damping ratio  $\xi_f$  has no effect on the response of the equipment when it is supported on an access floor such that  $\Omega_e < 0.5$  (i.e.  $\omega_e < 0.5\omega_f$ ). The effect of the access floor damping decreases as  $\omega_f$  increases.

In order to generate only a limited number of access floor response spectra which are relevant to the whole range of mass ratio and effective floor damping ratio, it is necessary to choose these parameters such that conservative response spectra would be obtained. Based on the above discussions, a mass ratio  $\mu$  of 0.8 and an effective floor damping ratio  $\xi_f$  of 2% are deemed to be appropriate.

#### 6.4 Design Spectra for Equipment Supported on Access Floors in Telecommunications Central Offices

To generate design spectra which are applicable to equipment supported on any access floor, it is necessary to first determine the access floor system which would cause the highest response for the equipment supported on it. Plotted in Fig.(6.8) are the access floor response spectra covering a range of effective floor frequencies  $\omega_f$  between 3 and 15Hz. Each spectrum is the ensemble average of spectra calculated using the five time histories as input excitation. The spectra correspond to  $\omega_f = 3, 4$  and 6Hz envelop all the other spectra. Plotted in Fig.(6.9), is the envelope of the average spectra in Fig.(6.8). Also plotted in this graph are the envelope of the average plus one standard deviation spectra and the NEBS 2% damped response spectrum. The average plus one standard

deviation spectral envelope is in general less than 10% higher than the average envelope. Since the NEBS criteria is already a conservative estimate of the earthquake induced motion on a building floor, it is sufficiently conservative to use the average instead of the average plus one standard deviation envelope for design applications. The mean spectral envelope shown in Fig.(6.9) can be approximated by straight lines as shown in Fig.(6.10). Similar straight-line envelopes are also obtained for equipment with damping ratios of 5% and 10% and are shown in the same figure. The three envelopes converge at a frequency of 10Hz. These envelopes are proposed to be the access floor response spectra representing the upper bound design criteria for equipment supported on access floors in telecommunications central offices.

For any response spectrum compatible time history, the maximum acceleration in the time history is defined by the spectral acceleration value at the high frequency end of the spectrum. As a result, an excitation time history compatible with the upper bound access floor response spectra in Fig.(6.10) must have a maximum acceleration of 5g. This is a very large acceleration compared to the 1g maximum acceleration of the excitation time histories defined by the NEBS spectra for equipment installed on building floors. For situations where the effective frequency of the access floor to be used is unknown, one has little choice but to consider the worst cases. However, bearing in mind that these spectra are governed by cases where the effective floor frequencies are low (i.e. between 3 to 6Hz), it would be overconservative to use these global upper bound spectra for equipment which is supported on access floor with  $\omega_f > 6\text{Hz}$ . Therefore, it is necessary to provide additional design spectra for

equipment supported on access floors with  $\omega_f > 6\text{Hz}$ .

To generate design spectra for cases where  $\omega_f \geq 6\text{Hz}$ , a new parameter termed as "access floor amplification factor" (denoted as " $a_f$ ") is introduced. It is computed by normalizing the access floor response spectrum of a given  $\omega_f$  with the NEBS spectrum of the same equipment damping ratio. Four sets of access floor amplification curves are shown in Fig.(6.11) for  $\omega_f$  of 6, 9, 12 and 15Hz. The three curves shown in each of the four graphs correspond to equipment damping ratios  $\xi_e$  of 2, 5 and 10%. The differences among the three curves are small. In other words, the access floor amplification curves are insensitive to the equipment damping ratio. Two other significant trends should be noted. First, for a given  $\omega_f$ , the amplification increases from a value of unity at low equipment frequencies to a maximum at an equipment frequency between 10 and 12Hz. Second, the amplification is reduced with the increase of effective access floor frequency. The amplification curves shown in Fig.(6.11) are approximated by curves consisting of straight line segments as shown in Fig.(6.12). For  $\omega_f \geq 6\text{Hz}$ , access floor response spectra for different equipment damping ratios can be generated by multiplying the appropriate NEBS spectra by the values of these amplification curves. The coordinates which define these amplification curves are also shown in the figure.

To illustrate the use of the amplification curves, consider a piece of equipment which has already been seismically qualified up to a 100% NEBS intensity shaking on a fixed base. The equipment has a frequency of 6Hz in the side-to-side direction and a frequency of 9Hz in the back-to-front direction. The equipment is now to be installed on an access floor at a location of lower seismicity where the building floor response

spectrum is only 50% of that of NEBS. Fig.(6.12) would provide useful guidelines in the choice of access floor system to be used. Any access floor system having an amplification larger than 2 at a frequency equal to 6 or 9Hz in Fig.(6.12) would not be suitable unless one is willing to seismically re-qualify the equipment for a higher level of shaking. Referring to Fig.(6.12), any access floor system with  $\omega_f \geq 9\text{Hz}$  would be an acceptable system to be used to support the equipment.

## 6.6 Summary and Conclusions

In this chapter, the seismic response of telecommunications central office equipment supported on access floor is studied. Access floor response spectra which may be used as the upper bound design criteria for equipment supported on any access floors are established. Useful guidelines are provided for the selection of a proper access floor system to ensure that the equipment supported on it would not be exposed to a seismic environment more severe than that used for the seismic qualification of the equipment.

Based on the results presented in this chapter, the following conclusions can be drawn:

1. For equipment supported on access floor system where  $\omega_e < 0.25\omega_f$ , the dynamic responses of the equipment is similar to that on a fixed base. For equipment-access floor system where  $\omega_e > 4.0\omega_f$ , the dynamic response of the equipment can be determined by treating the equipment as a rigid body attached on the access floor.

2. For an access floor system with a given  $\omega_f$ , the amplification of the equipment response due to the access floor increases as the

equipment frequency increases.

3. The amplification of the equipment response due to the access floor is reduced for stiffer access floor.

4. Access floor systems with  $\omega_f$  between 3 and 6Hz represent the most severe conditions for telecommunications equipment. To seismically qualify equipment which is to be supported on such access floors, the equipment is needed to be shaken by a time history having a 5g maximum acceleration.

Although the result presented in this chapter is applicable for any access floor system with an  $\omega_f$  between 3 and 15Hz, it is not practical to support equipment on access floor systems with  $\omega_f$  less than 6Hz in buildings located in area of high seismic risk. There are three reasons that lead to this reservation. First, the equipment supported on such access floor systems has to be able to withstand a maximum base excitation of 5g. Such large excitation would impose a severe requirement on the design of the equipment and its anchorage. Second, experiments carried out in this study indicates that access floor systems with  $\omega_f$  less than 6Hz are prone to be damaged even at excitation as small as 25% NEBS. Finally, it was observed in the experimental setup for the D20 access floor ( $\omega_f=4.8\text{Hz}$ ) that noticeable lateral vibrations were caused by people walking on the access floor. This could pose problems under day-to-day service conditions, apart from any seismic loading on the equipment

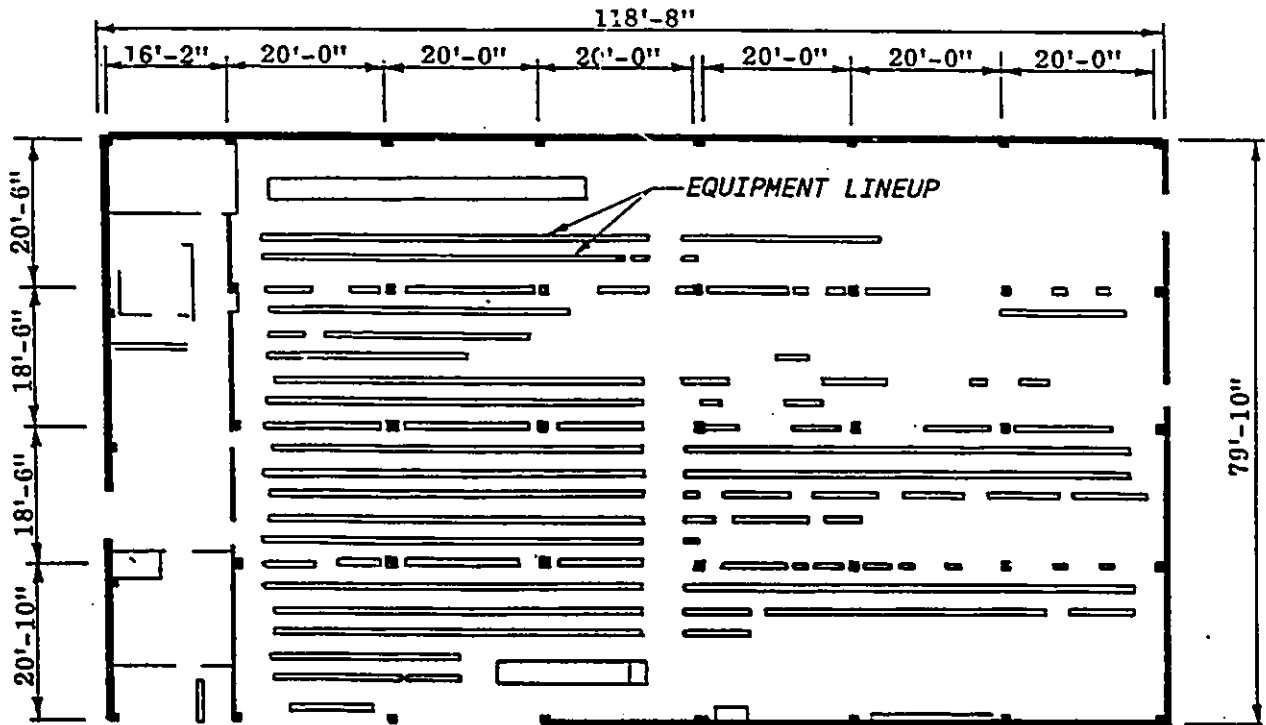
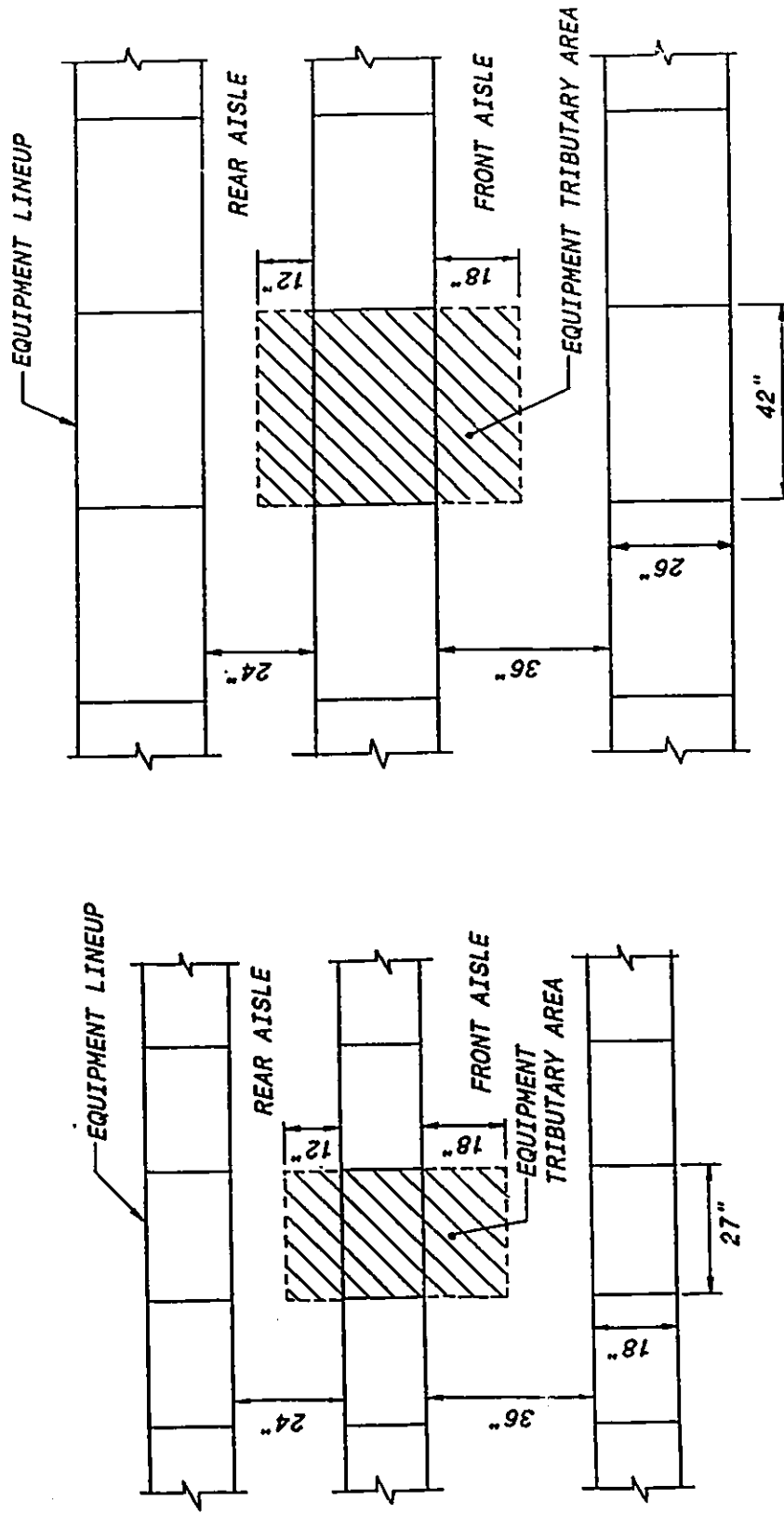
$1' = 0.305m$ 

Fig. 6.1 Equipment floor plan in typical telecommunications central offices



1" = 2.54cm

Fig. 6.2 Two typical telecommunications equipment lineup arrangements

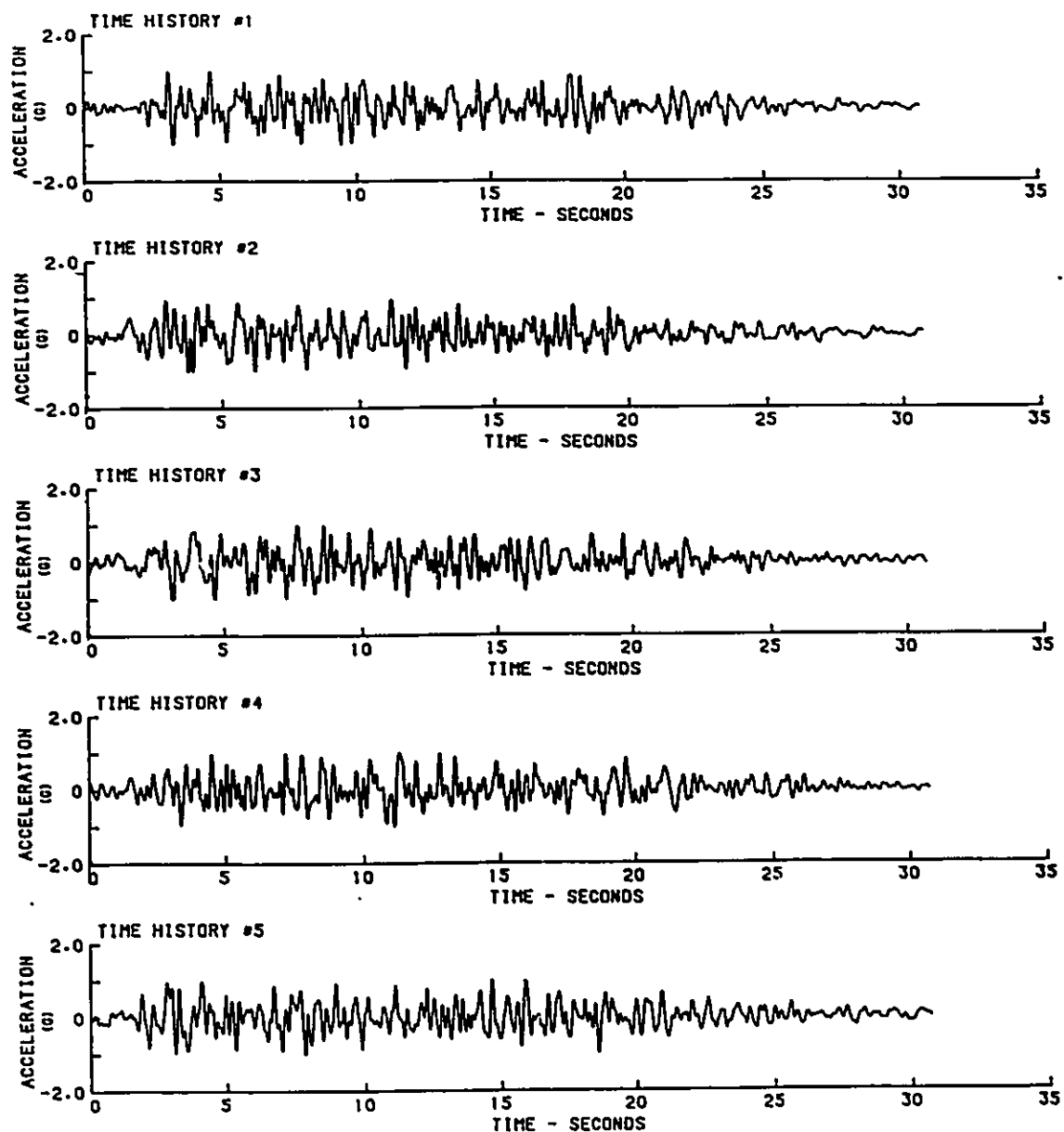


Fig. 6.3 Artificially generated NEBS 2% damped spectrum compatible acceleration time histories

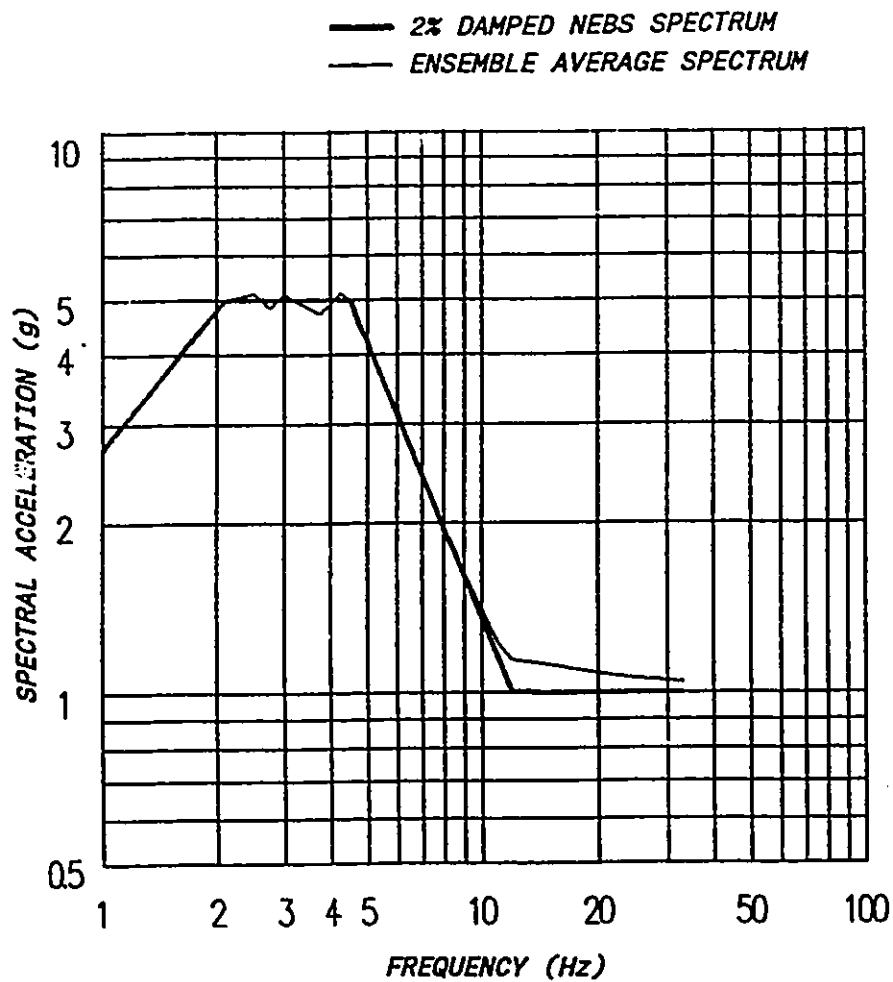


Fig. 6.4 Ensemble average 2% damped response spectrum for the artificially generated time histories

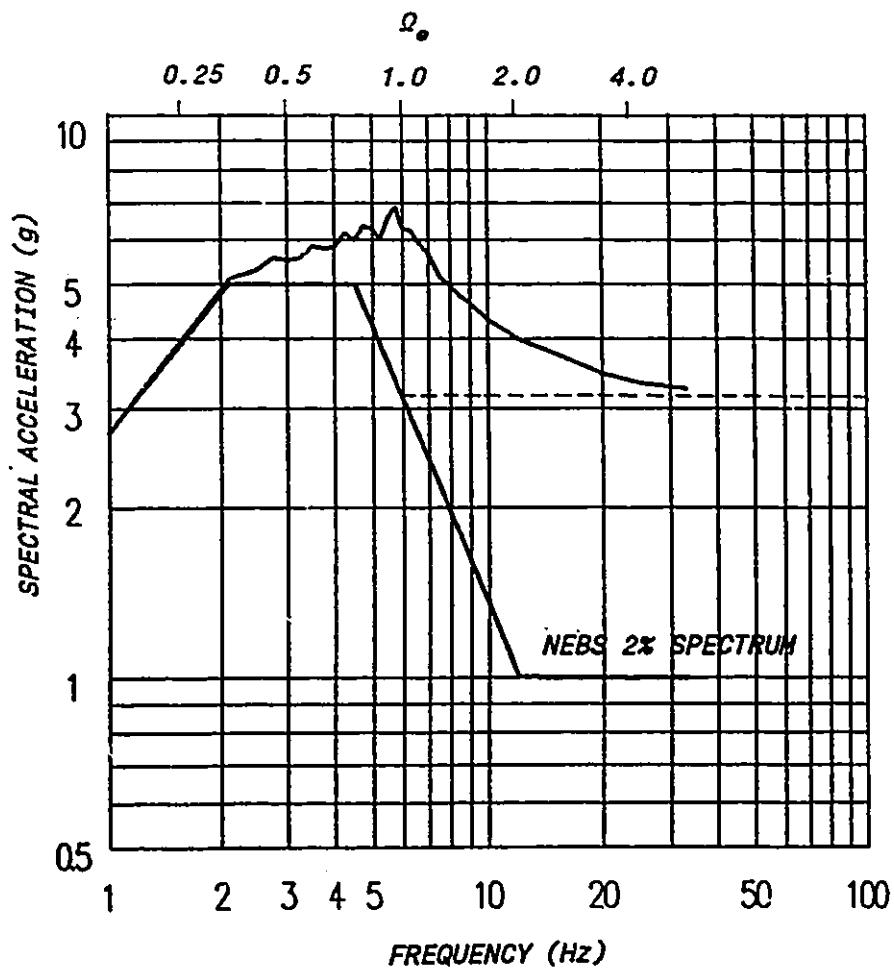


Fig. 6.5 Ensemble average 2% damped access floor response spectrum,  $\mu=0.8$ ,  $\omega_f=6\text{Hz}$  and  $\xi_f=2\%$

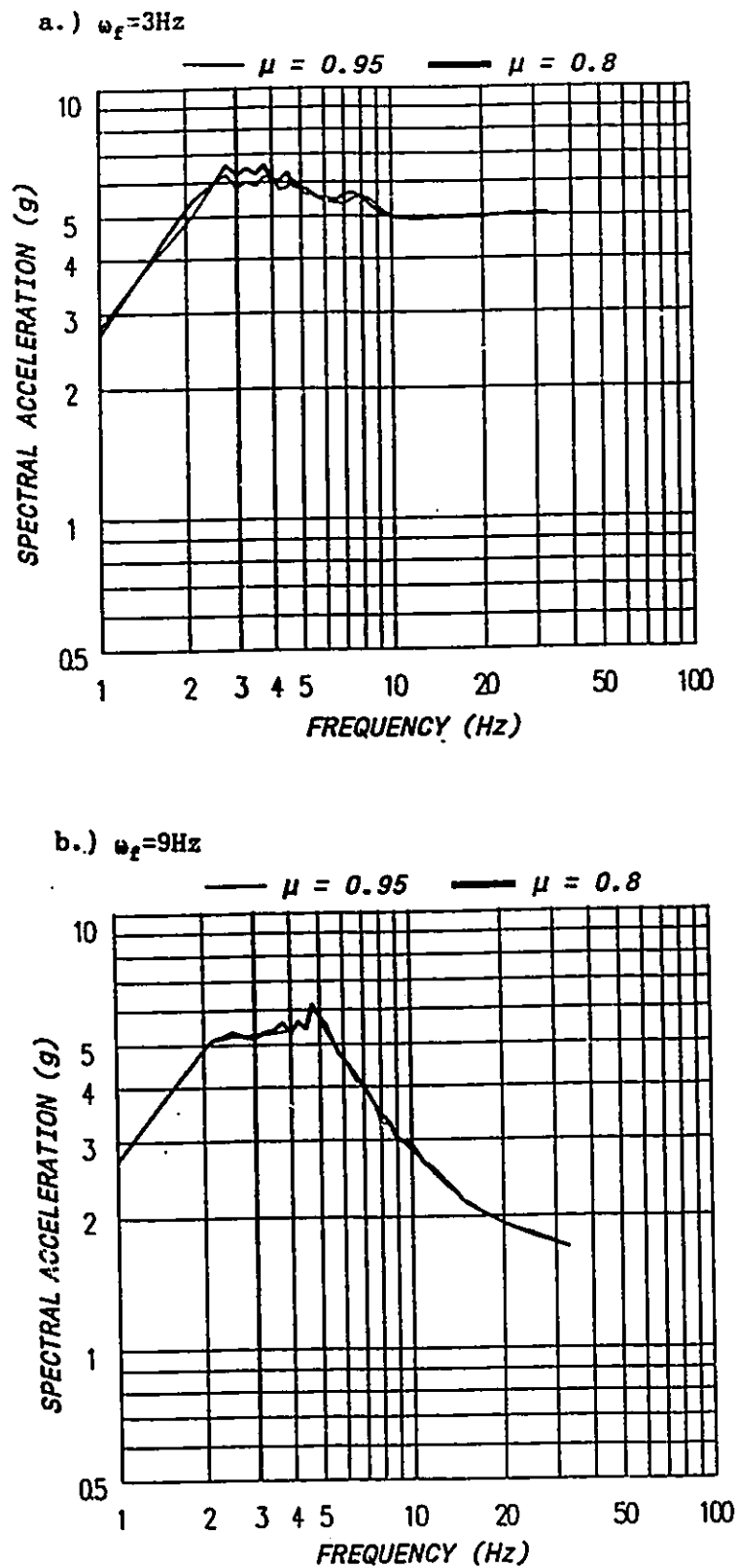


Fig. 6.6 Ensemble average 2% damped access floor response spectra for different mass ratios:  $\xi_f = 2\%$ : a.)  $\omega_f = 3\text{Hz}$  and b.)  $\omega_f = 9\text{Hz}$

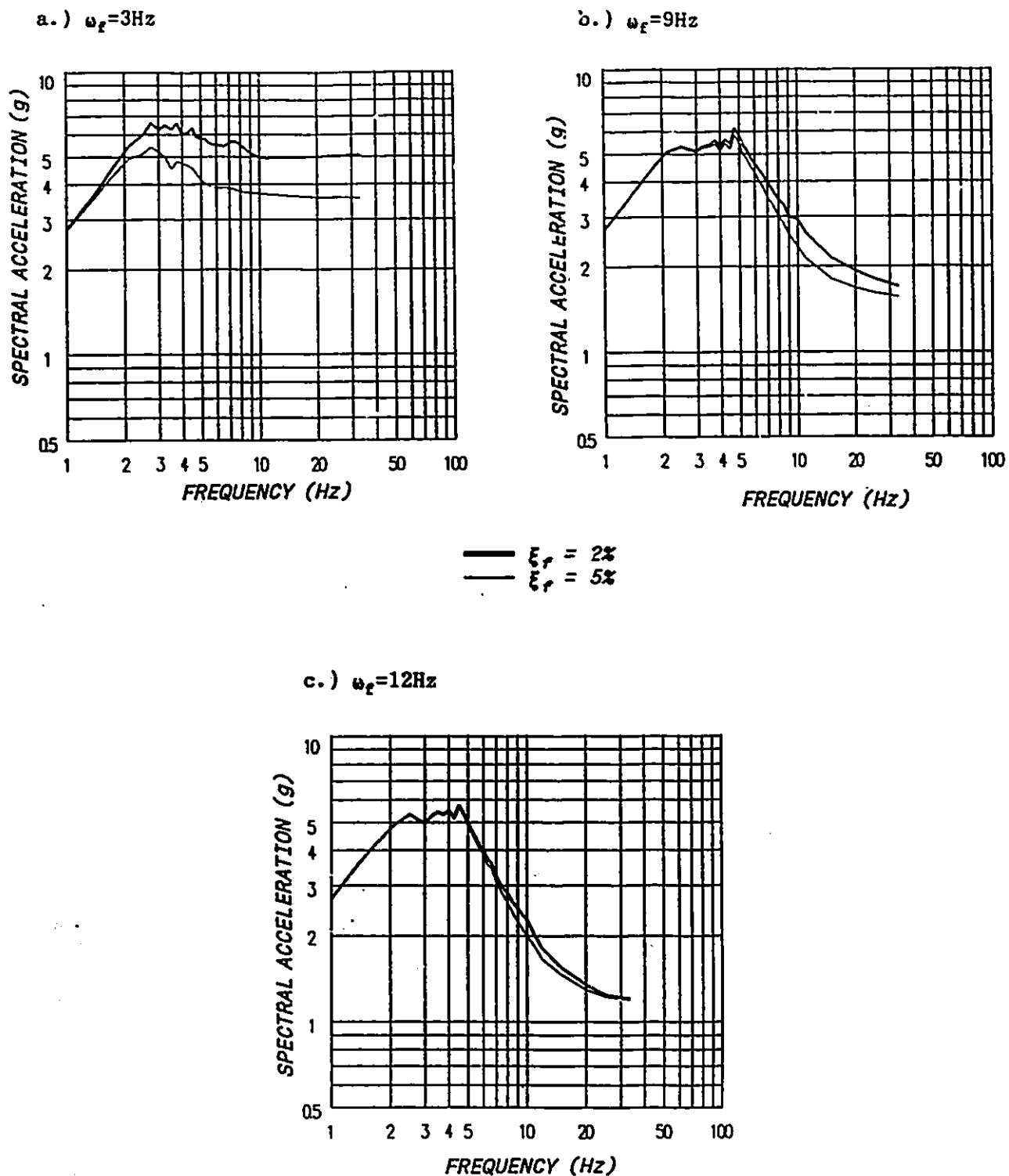


Fig. 6.7 Ensemble average 2% damped access floor response spectra for different access floor damping ratios  $\xi_f=2\%$ : a.)  $\omega_f=3\text{Hz}$ , b.)  $\omega_f=9\text{Hz}$  and c.)  $\omega_f=12\text{Hz}$

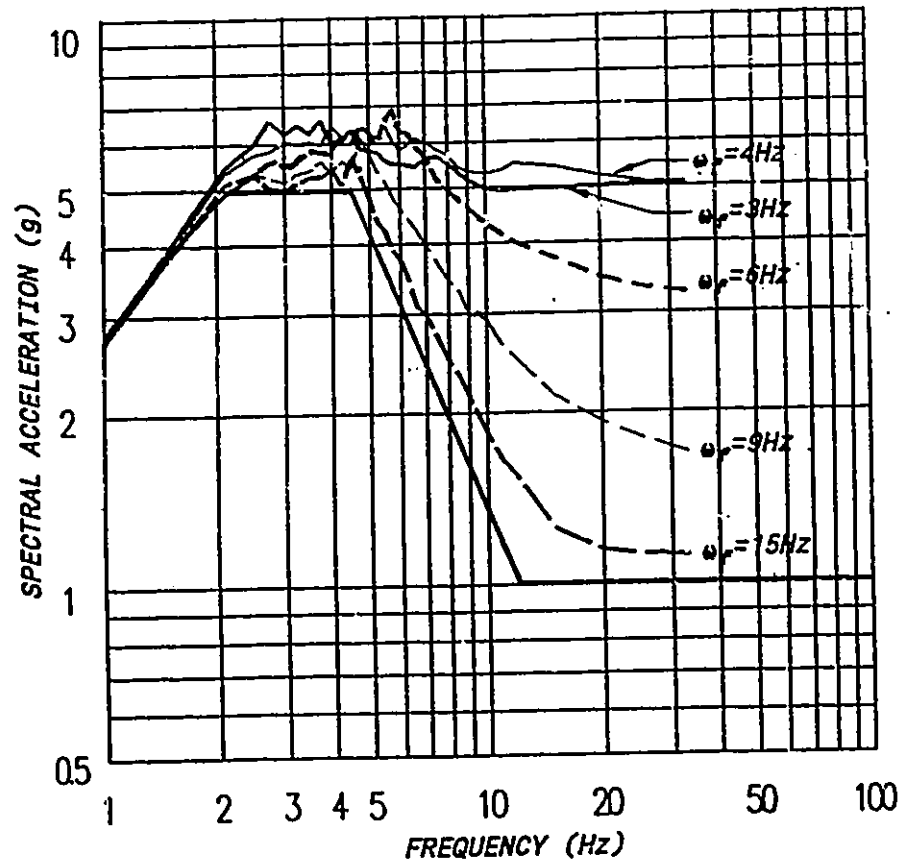


Fig. 6.8 Ensemble average 2% damped access floor response spectra for different effective floor frequencies,  $\xi_f=2\%$  and  $\mu=0.8$

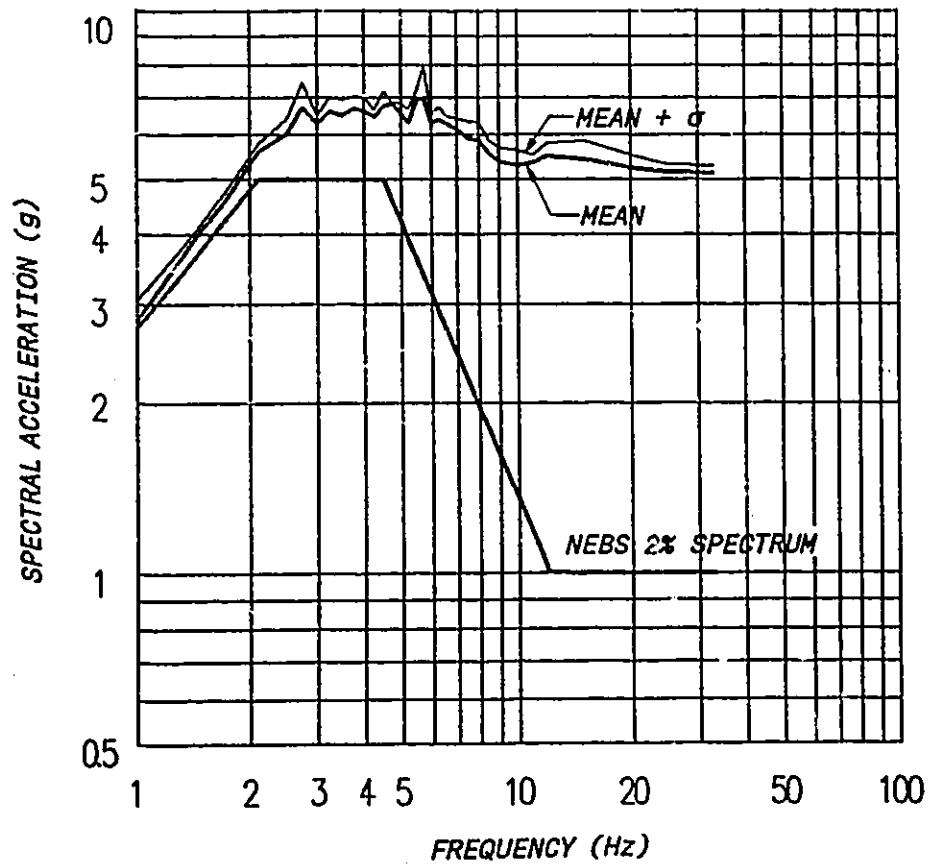


Fig. 6.9 Average and average plus one standard deviation spectral envelopes,  $\xi_f=2\%$  and  $\mu=0.8$

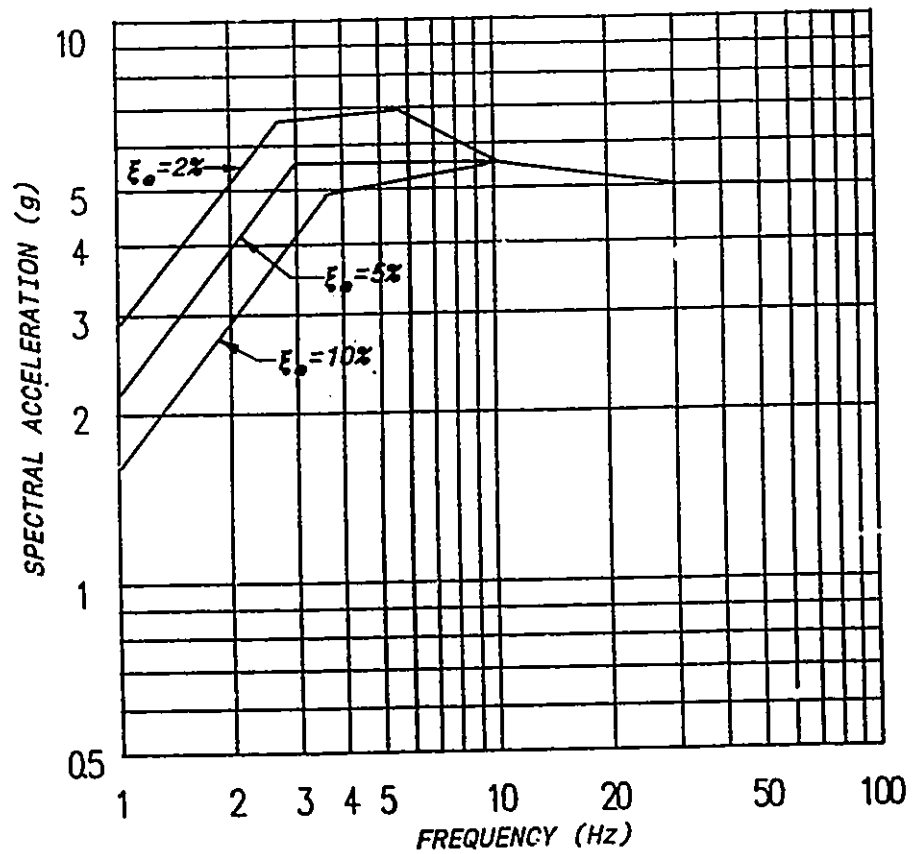


Fig. 6.10 Upper bound design spectra for equipment on access floor in telecommunications central offices

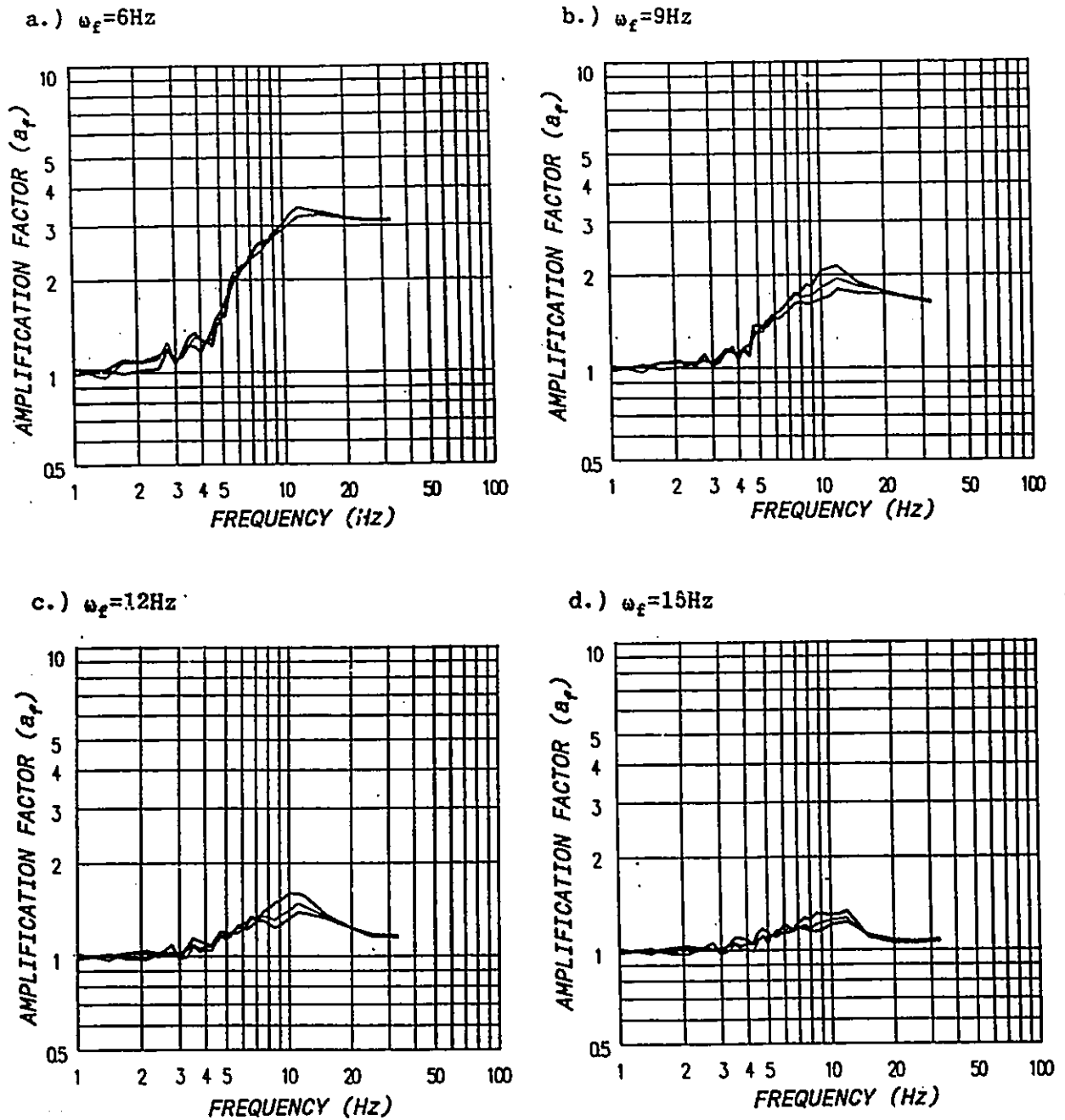
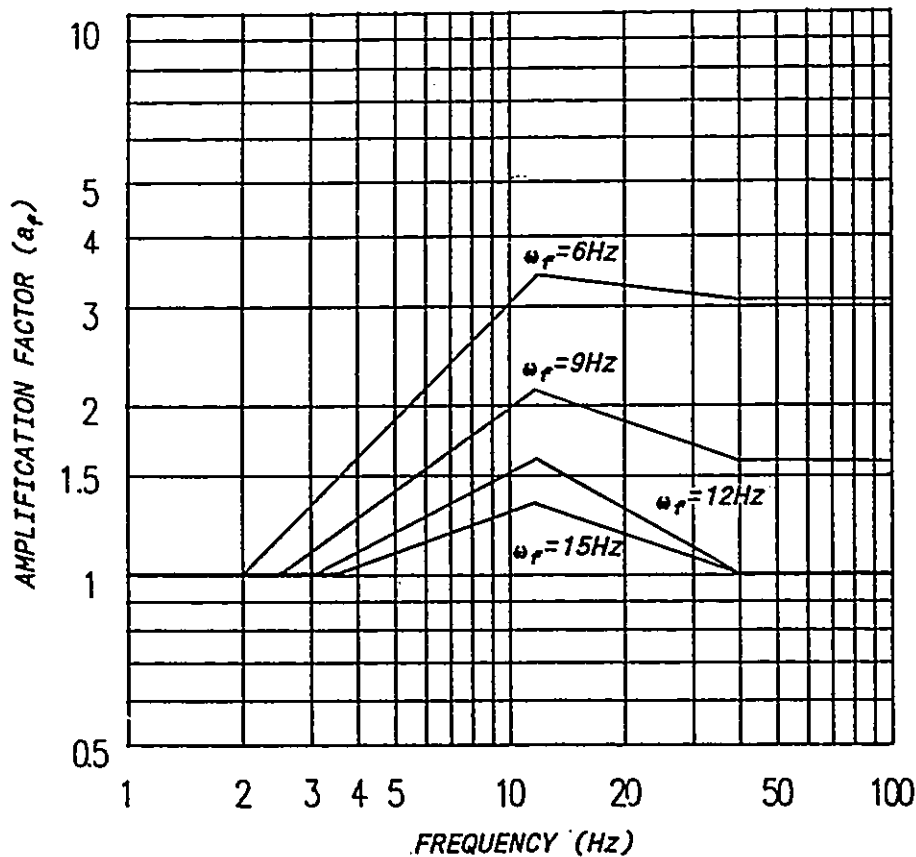
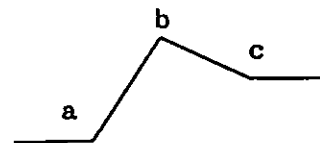


Fig. 6.11 Access floor amplification curves for different equipment damping ratios: a.)  $\omega_f = 6\text{Hz}$ , b.)  $\omega_f = 9\text{Hz}$ , c.)  $\omega_f = 12\text{Hz}$  and d.)  $\omega_f = 15\text{Hz}$

Fig. 6.12 Straight line approximation of amplification curves for different effective floor frequencies



	Coordinates		
	a	b	c
$\omega_f=6\text{Hz}$	1 (2.0Hz)	3.4 (12Hz)	3.1 (40Hz)
$\omega_f=9\text{Hz}$	1 (2.5Hz)	2.1 (12Hz)	1.6 (40Hz)
$\omega_f=12\text{Hz}$	1 (3.0Hz)	1.6 (12Hz)	1.0 (40Hz)
$\omega_f=15\text{Hz}$	1 (3.5Hz)	1.4 (12Hz)	1.0 (40Hz)



## CHAPTER 7

### CONCLUSIONS

In this thesis, a systematic in-depth study on the seismic response of telecommunications equipment supported on access floors has been presented. The objective of the study has been to provide guidelines for the seismic analysis, design and qualification of telecommunications equipment supported on access floors. The study was undertaken by both experiment and analysis. The significant conclusions of this thesis are summarized as follows:

1. A two degree of freedom (2DOF) system is necessary in general to analytically model a combined equipment-access floor system. In this 2DOF system, the access floor can be represented as a single degree of freedom (SDOF) lumped mass system. The stiffness property of this SDOF lumped mass system can be determined based on the effective pedestal stiffness obtained from the static test of a 1-panel access floor module. For typical telecommunications equipment, a generalized single degree of freedom system model is needed to represent the equipment in the 2DOF equipment-access floor model.

2. For equipment-access floor systems where the access floor is

much stiffer than the equipment or vice versa, they can be treated as single degree of freedom systems. In the first case, the access floor may be treated as a fixed base, and in the second case, the equipment may be treated as a rigid body attached on the access floor. In these two cases, the NEBS (Network Equipment Building System) criteria remain applicable in estimating the upper bound response of equipment on access floors. The NEBS criteria, however, are in general not applicable for most equipment-access floor systems because the dynamic interaction of the equipment and the access floors is usually significant. In these cases, the criteria developed in this study (Section 6.4) based on a 2DOF model provide guidelines for purposes of seismic design, analysis and qualification for telecommunications equipment supported on access floors.

3. The dynamic response of equipment can be amplified significantly by an access floor. In general, the amplification is higher for a more flexible access floor, and for a given access floor, the amplification is larger for equipment with higher frequency.

4. Access floor systems with effective floor frequencies between 3Hz and 6Hz represent the most severe shaking environment for telecommunications equipment in a central office setting. The intensity of the earthquake-induced shaking for equipment on these access floors is of the order of 5 times of that on the building floor.

5. It is shown by experiment that rigid diaphragm action cannot be achieved in access floors regardless of whether the floor panels

are bolted to the access floor understructure or not. By leaving the floor panels not bolted, the in-plane stiffness of the access floor is reduced, but the damping of the access floor is increased significantly.

## APPENDIX I

### DETERMINATION OF DAMPING RATIOS FROM TRANSFER FUNCTIONS

Eqn.(3.1) is derived by first determining the frequency ratios  $\beta_1$  and  $\beta_r$  which correspond to the two peaks of the real part of the transfer function  $\text{Re}[H(\beta)]$  where  $\text{Re}[H(\beta)]$  is written as:

$$\text{Re}[H(\beta)] = \frac{1 - \beta^2 + (2\xi\beta)^2}{(1 - \beta^2)^2 + (2\xi\beta)^2}$$

$\beta_1$  and  $\beta_r$  is determined by setting the derivative of  $\text{Re}[H(\beta)]$  with respect to  $\beta$  to zero as:

$$\frac{d\{\text{Re}[H(\beta)]\}}{d\beta} = (1 - 4\xi^2)\beta^4 - 2\beta^2 + 1 = 0$$

Solving the above quadratic equation for  $\beta^2$ ,  $\beta_1^2$  and  $\beta_r^2$  are determined as follows:

$$\beta_1^2 = \frac{1 - 2\xi}{1 + 4\xi^2} \quad \text{and} \quad \beta_r^2 = \frac{1 + 2\xi}{1 + 4\xi^2}$$

Hence,  $\xi$  can be expressed in terms of  $\beta_1$  and  $\beta_r$  as

$$\xi = \frac{1}{2} \cdot \frac{(\beta_r/\beta_1)^2 - 1}{(\beta_r/\beta_1)^2 + 1}$$

## APPENDIX II

### DERIVATION OF EQUATIONS OF MOTION

For the equipment-access floor system shown in Fig.(5.1) in a state of dynamic equilibrium, the virtual work expression is written as

$$\int_0^L \mathcal{Q}[z(x,t)] \delta z dx + \int_0^L m(x) [\ddot{z}(x,t) + \ddot{u}_g(t) + \ddot{u}_f(t)] \delta z dx + \int_0^L c(x) \dot{z}(x,t) \delta z dx + \int_0^L m(x) [\ddot{z}(x,t) + \ddot{u}_g(t) + \ddot{u}_f(t)] \delta u_f dx + M_f \ddot{u}_f(t) \delta u_f + C_f \dot{u}_f(t) \delta u_f + K_f u_f(t) \delta u_f = 0$$

where  $\delta z$ ,  $\delta u_f$  are virtual displacements compatible with the boundary conditions of the system. By assuming the equipment as a generalized SDOF system having a shape function  $\phi(x)$ ,

$$z(x,t) = \phi(x) u_e(t)$$

and  $\delta z = \phi(x) \delta u_e$

where  $u_e$  is the displacement at the top of the equipment-frame.

By substituting the above expressions for  $z(x,t)$  and  $\delta z$ , the virtual work expression can be written as

$$\left\{ \int_0^L m(x) \phi^2(x) dx \ddot{u}_e(t) + \int_0^L m(x) \phi(x) dx [\ddot{u}_f(t) + \ddot{u}_g(t)] + \int_0^L c(x) \phi^2(x) dx \dot{u}_e(t) + \int_0^L \mathcal{Q}[\phi(x)] \phi(x) dx u_e(t) \right\} \delta u_e + \left\{ \int_0^L m(x) \phi(x) dx \ddot{u}_e(t) + \int_0^L m(x) dx [\ddot{u}_g(t) + \ddot{u}_f(t)] + M_f \ddot{u}_f(t) + C_f \dot{u}_f(t) + K_f u_f(t) \right\} \delta u_f = 0$$

In order to satisfy the above expression in general, the two terms

enclosed by braces must vanish. This leads to the equations of motion in matrix form as:

$$[ M ] \{\ddot{u}\} + [ C ] \{\dot{u}\} + [ K ] \{u\} = \{P\} \ddot{u}_g$$

where

$$[ M ] = \begin{bmatrix} M_f + \int_0^L m(x) dx & \int_0^L \phi(x) m(x) dx \\ \int_0^L \phi(x) m(x) dx & \int_0^L \phi^2(x) m(x) dx \end{bmatrix}$$

$$[ C ] = \begin{bmatrix} C_f & 0 \\ 0 & \int_0^L \phi^2(x) c(x) dx \end{bmatrix}$$

$$[ K ] = \begin{bmatrix} K_f & 0 \\ 0 & \int_0^L g[\phi(x)] \phi(x) dx \end{bmatrix}$$

$$\{ P \} = \begin{bmatrix} M_f + \int_0^L m(x) dx \\ \int_0^L \phi(x) m(x) dx \end{bmatrix}$$

and  $\{ u \} = \begin{bmatrix} u_f \\ u_e \end{bmatrix}$

## REFERENCES

1. Bell Communications Research, "Network Equipment Building System (NEBS) - General Equipment Requirements", Technical Reference TR-EOP-000063, Issue 3, Morristown, New Jersey, March 1988.
2. Bendat, Piersol, Measurement and Analysis of Random Data. New York: John Wiley & Sons, 1966.
3. Bendat, Piersol, Engineering Applications of Correlation and Spectral Analysis. New York: John Wiley & Sons, 1980.
4. Chang, I.K., Liu, S.C. and Shah, H.C. "Seismic Support of Electronic and Computer Equipment on Raised Floor", Soil Dynamics and Earthquake Engineering, Vol.5, No.3, 1986, pp. 159-169.
5. Clough, R.W. and Penzien, J., Dynamics of Structures. McGraw-Hill Book Co., 1975.
6. FIMS, Data Processing Facilities: Guidelines for Earthquake Hazard Mitigation. Sacramento, California: VSP Associates, 1987.
7. Forell, N.F. "Earthquake Damage Mitigation for Computer Systems: Structural Engineering Considerations", Proceedings of Workshop on Earthquake Damage Mitigation for Computer Systems, July 1983, pp 109-118.
8. Foss, J.W., "Protecting Communications Equipment Against Earthquake", Proceedings of US Japan Seminar on Earthquake Engineering Lifeline Systems, November 1976, pp 237-255.
9. Foss, J.W., and Nikolakopoulou, G.A. "Electronic Data Processing Equipment Braced to Resist Seismic Loading", Proceedings of Seventh World Conference on Earthquake Engineering, Istanbul, Turkey, September 1980, pp. 477-480
10. Foss, J.W., and Scobee, J.D. "Telecommunications after Earthquake", Proceedings Social and Economic Impact of Earthquakes on Utility Lifelines, New York, ASCE, 1980, pp. 134-149.
11. Heidebrecht, A.C. and Tso, W.K. "Seismic Behaviour of Access Floor System Supporting Telecommunications Equipment", Proceedings of Fourth Canadian Conference on Earthquake Engineering, Vancouver, Canada, June 1983, pp. 174-184.

12. Liu, S.C., Fagel, L.W. and Dougherty, M.R. "Earthquake-Induced In-Building Motion Criteria", *Journal of Structural Division, ASCE*, Vol.103, No.ST1, January 1977, pp. 133-152
13. Mehraian, M., Clayton, M. and Stuart, J. "Seismic Testing and Design of Raised Computer Floors", Proceedings of Ninth World Conference on Earthquake Engineering, Vol.VI, Tokyo, Japan, August 1988, pp. 225-230.
14. Tso, W.K., Seismic Testing of DMS-100E Telecommunication System, McMaster University Earthquake Engineering Research Group, 1986.
15. Tso, W.K. and Naumoski, N., Periods and Damping of Telecommunications Equipment in Buildings During Strong Earthquake Shaking, Fourth U.S. National Conference on Earthquake Engineering, Palm Spring, Calif., May 1990.
16. Uniform Building Code, International Conference of Building Officials, Whittier, Calif., 1985.